Universidad Autónoma de Madrid
Facultad de Ciencias
Departamento de Biología Molecular

Analysis of the role of Arid3b in cardiac development

Tesis Doctoral

Verónica Uribe Sokolov

Madrid 2014

Universidad Autónoma de Madrid
Facultad de Ciencias
Departamento de Biología Molecular

Tesis Doctoral

Analysis of the role of Arid3b in cardiac development

Verónica Uribe Sokolov
Mayo 2014

Director: Dr. Juan José Sanz Ezquerro
Tutor: Dr. Federico Mayor Menéndez

This work was performed in Dr. Juan José Sanz Ezquerro's laboratory in the Cardiovascular Development and Repair Department at the National Center for Cardiovascular Research (CNIC-ISCIII). Verónica Uribe Sokolov was supported by a PhD fellowship from the Spanish Ministry of Education (FPU Programme).

The cat only grinned when it saw Alice. It looked good-natured, she thought: still it had VERY long claws and a great many teeth, so she felt that it ought to be treated with respect.

‘Cheshire Puss,’ she began, rather timidly, as she did not at all know whether it would like the name: however, it only grinned a little wider. ‘Come, its pleased so far,’ thought Alice, and she went on. ‘Would you tell me, please, which way I ought to go from here?’

‘That depends a good deal on where you want to get to,’ said the Cat.

‘I don’t much care where -- ’ said Alice.

‘Then it doesn’t matter which way you go,’ said the Cat.

‘-- so long as I get SOMEWHERE,’ Alice added as an explanation.

‘Oh, you’re sure to do that,’ said the Cat, ‘if you only walk long enough.’

Alice’s adventures in Wonderland
Lewis Carroll (1832-1898)

INDEX

INDEX OF FIGURES AND TABLES

FIGURES

TABLES

ABBREVIATIONS

AVC: Atrioventricular canal
Bmp: Bone Morphogenetic Protein
Delta4: Delta-like 4
EMT: Epithelial to Mesenchymal Transition
ESC: Embryonic stem cells
Fgf: Fibroblast growth factor
FHF: First heart field
GAPDH: Glyceraldehyde 3-phosphate dehydrogenase
Hey: Hairy Related genes
HFR: Heart forming region
HIF-1α: Hypoxic Inducible Factor-1α
HPRT: Hypoxanthine-guanine phosphoribosyltransferase
IFT: Inflow tract
iPC: induced pluripotent cells
LV: Left ventricle
NICD: Notch Intracellular Domain
NLS: Nuclear localization signal
OFT: Outflow tract
RA: Retinoic acid
RBPJK: Recombination Signal-Binding Protein 1 for J-Kappa sequence
RBPKO: Recombination Signal-Binding Protein 1 for J-Kappa mutant
RV: Right ventricle
SMA: Smooth muscle actin
SHF: Secondary Heart Field
Shh: Sonic-Hedgehog
Tgf-β: Transforming Growth Factor-β
WT: Wild type

SUMMARY

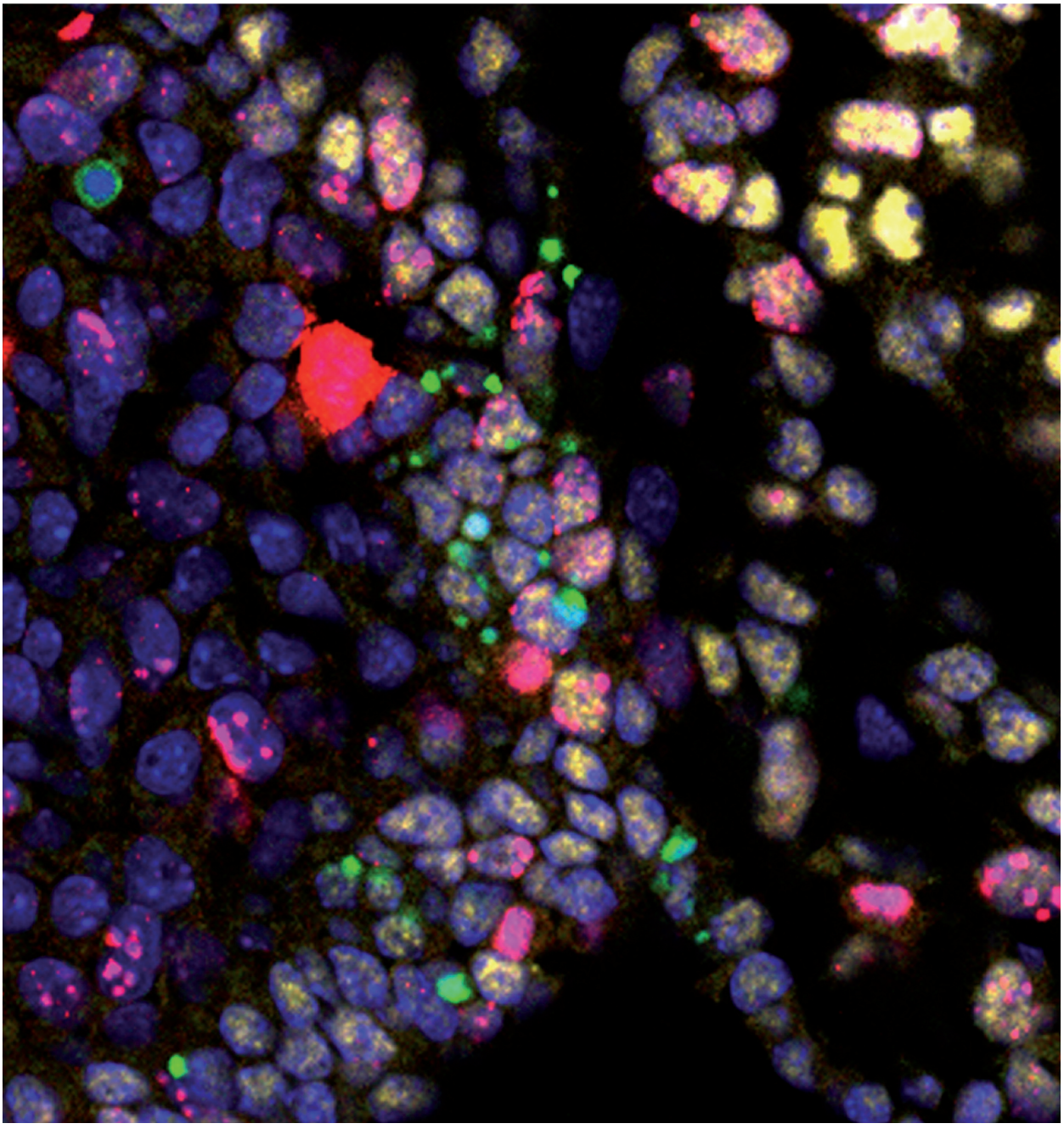

Understanding heart development is important for identifying the origin of congenital heart malformations, the most common birth defects. The heart is the first functional organ in the developing embryo. The early heart tube elongates by addition of cells from a pool of progenitors, called the second heart field (SHF), from which most regions of the heart are derived. After heart looping is completed, the formation of the chambers starts, as well as valvulogenesis in the atrioventricular canal (AVC) and in the outflow tract (OFT). A complex network of signalling molecules and transcription factors regulates heart morphogenesis and although different aspects of heart formation have been extensively studied, some of the processes are still not fully understood. For instance, the cellular mechanism of cell deployment from the SHF to the heart tube is unknown; also, later events in valve formation remain poorly understood.

Arid3b, a member of the conserved ARID family, was identified in the course of a candidate gene screen for factors important in vertebrate organogenesis. Based on its initial expression pattern, we decided to study its possible role in heart development. *Arid3b* expression can be detected in the early heart tube and in the SHF cells. When looping starts, the expression in the chambers diminishes but is maintained strong in the poles. Later, expression can be detected in the endocardium and in the epicardium. We used a gene-trap loss of function mouse line to analyse Arid3b function in heart development. Three main defects were observed: shortening of the poles of the heart, loss of normal patterning of the AVC and lack of epithelial-to-mesenchimal transition (EMT) in the AVC. The patterning defect in the myocardium seems to be responsible for EMT disruption, since in AVC explants *in vitro*, the invasion capacity of mesenchymal cells can be rescued by addition of Bmp2, a factor reduced in the mutant myocardium by the stage EMT starts. An RNA microarray analysis of wild type versus mutant embryos revealed a set of differentially expressed genes related to cell morphology and cell movement, suggesting that Arid3b might be involved in the regulation of these processes. The motility defect observed in mouse embryonic fibroblast derived from *Arid3b*-null embryos further supports this hypothesis. Moreover, while the balance of cell proliferation and cell death was normal in the SHF of mutant embryos, normal architecture was disrupted. DiI labelling of precursors from the SHF showed that in *Arid3b*-null embryos cells fail to properly ingress into the heart tube, pointing again to a role of this gene in cell motility. Precursors entering the heart tube also failed to differentiate properly and one of the candidate genes from the microarray, *Bhlhb2* (upregulated in the mutant heart), might be involved in this process. On the other hand, conditional deletion of *Arid3b* in the Nkx2.5 positive population using a floxed line, leads to defective valve remodelling, pointing to a later role of the gene in valve maturation.

This work uncovers an unsuspected role for Arid3b in heart formation, provides new mechanistic insight to heart development and reveals Arid3b as a candidate gene of human cardiac congenital malformations.

INTRODUCTION

Embryonic development is the sum of biological processes that lead to the formation of a mature complex organism from an unicellular zygote. Although important variations in development exist between different species, common mechanisms are present in all of them. Multicellular organisms arise by progressive changes driven by an increase in cell number, differentiation and specification into different cell types and their organization in tissues and organs. Disruption of any of the tightly regulated steps of development leads to malformations, a major issue in human health, as about 3% of live births occur with some kind of congenital defects, according to the Centres for Disease Control and Prevention (http://www.cdc.gov/mmwr/preview/mmwrhtml/mm5701a2.htm) (Parker S.E. *et al*., 2010).

The heart is the first organ to function during embryonic development. Even at very early developmental stages, as soon as the heart tube is formed, a peristaltic contraction pattern can be detected. In mammals, the mature heart is a four-chambered muscular organ with separated pulmonary and systemic circulatory pathways, which pumps blood through blood vessels (**Figure 1**). Before the definitive structure is achieved, the heartbeat has to be maintained and modified through development, while the organ grows and suffers morphogenetic changes. The primitive heart tube, which is first formed only by two layers, the myocardium and the endocardium, undergoes a stage of elongation by addition of cells from the pharingeal mesoderm and looping, followed by chamber specification, valvulogenesis, trabeculation, formation of the third layer, the epicardium, and septation. A large set of structural and functional defects that arise during cardiac embryogenesis lead to congenital heart disease (CHD), the most common congenital anomaly in new-borns (Fahed A.C. *et al*., 2013).

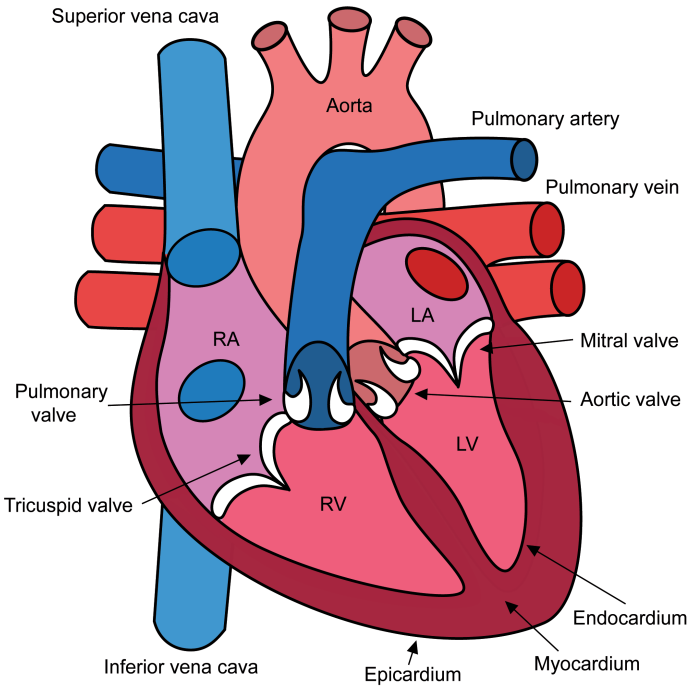

Figure 1. Anterior view of a mature mammalian heart. It is formed by four chambers: the left ventricle (LV) connected to the aorta; the right ventricle (RV), from which the pulmonary artery emerges; the right atrium (RA) connected to the caval veins; the left atrium (LA), in contact with the pulmonary artery. The heart also contains four valves: the aortic valve, the pulmonary valve, the tricuspid valve and the mitral or bicuspid valve. The wall of the heart is formed by three layers: the myocardium, the endocardium and the epicardium.

The use of mice as a model organism has proven to be very useful to address normal heart development, as well as the aetiology of human cardiac diseases. Mice are closely related to humans and show great similarities in anatomy, physiology and genetics; moreover, our ability to manipulate the mouse genome provides a powerful tool to study gene function and model human disease.

HEART DEVELOPMENT

Early steps in heart formation

The heart derives from the lateral plate mesoderm. During gastrulation epiblast cells ingress through the primitive streak and form the mesodermal layer. The trunk mesoderm of a neurula-stage embryo can be subdivided in four regions: the chordamesoderm, the paraxial or somatic mesoderm, the intermediate mesoderm and the lateral plate mesoderm. The lateral plate mesoderm is located farthest away from the notochord and gives rise to the heart, blood vessels and blood cells and the lining of the body cavities, including the pericardial cavity which envelops the heart.

In the early gastrula heart progenitor cells ingress at the rostral and middle segments of the primitive streak along with other cells destined for rostral structures, such as head mesoderm. Heart precursors get established in the lateral plate mesoderm where they form two bilateral cardiogenic fields. In the chick myocardial specification is induced by the hypoblast through transforming growth factor family β (TGF-β) factors, while in the mouse this function might be taken by the anterior visceral endoderm (Nijmeijer R.M. *et al*., 2009). Mesp1 (mesoderm posterior1) is expressed in the early mesodermal cells that ingress into the primitive streak and, as shown by genetic lineage tracing, almost all cardiac cells derive form Mesp1 positive population (Saga Y. *et al*., 1999) (Saga Y. *et al*., 2000). Together with Mesp2 it controls the exit of the mesoderm precursors of the primitive streak by regulating epithelial to mesenchymal transition (EMT) and cell migration (Kitajima S. *et al*., 2000) (Lindsley R.C. *et al*., 2008). It also acts as a key regulator of cardiovascular lineage commitment promoting the expression of the majority of cardiovascular transcription factors, such as Gata4, Nkx2.5, Hand2, Mef2c, Tbx20, myocardin (Bondue A. *et al*., 2008) (Bondue A. and Blanpain, 2010).

Once located in the lateral plate mesoderm the heart progenitors form a region called the cardiac crescent where promyocardial and endothelial cells are intermingled. The future myocardial cells express Nkx2.5, a master gene essential for integration of patterning information (Prall O.W.J. *et al*., 2007). At the same time, the neural plate starts to fold to become the neural tube, a process coupled with the invagination of the endoderm to produce the foregut. The heart forming regions move to the midline of the embryo in close proximity to the endoderm and fuse to form the initial heart tube (Moorman A. *et al*., 2003) (Wagner M. and Siddiqui, 2007). Together with Nkx2.5, Gata4 is one of the earliest genes expressed in the cardiac crescent and it regulates the expression of a number of myocardium-specific factors. Other genes, such as Tbx5, Mef2c (MADS-box) and

basic helix-loop-helix Hand1/2 are also implicated in the differentiation of myocardial cells in the crescent. Recently, important cardiogenic induction properties have been discovered for chromatin remodelling component Baf60c/Smarcd3. Non-cardiogenic mesoderm can be differentiated into contracting cardiomyocytes in the presence of Gata4, Tbx5 and Baf60c; Baf60c seems to recruit BAF chromatin remodelling complexes to heart-specific enhancers (Takeuchi J.K. and Bruneau, 2009).

The heart fields

Classically, it was considered that cardiac precursor cells were pre-patterned in terms of their contribution to the heart tube along the anterior-posterior axis, a pre-patterning which was present in the cardiac crescent and retained in the heart tube. This led to the proposal of the segmental model of heart formation where each region of the heart was composed of a separate unit and derived from a pre-patterned pool of progenitor cells, as well as supported the idea that all the heart forming cells were contained in the early heart tube (reviewed in (Buckingham M. *et al*., 2005)). However, for many years, studies from both chick and mouse appreciated that the heart tube continues to elongate through addition of cells to the poles. In their work in chick embryos, de la Cruz and colleagues observed that iron oxide particles placed in the cephalic end of the cardiac tube were observed at later stages inside the heart. In other series of experiments, the heart tube was separated from its anterior attachment and, as a consequence, failed to form the cephalic region. Their work led them to propose that not all parts of the heart are present in the pre-looped stage, but are added at different developmental moments (Argüello C. *et al*., 1975) (de la Cruz M.V. *et al*., 1977). However, it was not until 2001 when three independent studies, two in chick and one in mouse, confirmed the existence of a source of arterial progenitors through molecular and labelling techniques (Waldo K.L. *et al*., 2001) (Mjaatvedt C.H. *et al*., 2001) (Kelly R.G. *et al*., 2001) (reviewed in (Kelly, 2012)). The elongation and looping of the heart is driven by the addition to the poles of a highly proliferative population of cardiac precursor cells. They are located in the pharyngeal mesoderm beneath the heart tube and were termed the second heart field (SHF), as opposite to the first heart field which forms the tube (Buckingham M. *et al*., 2005) (**Figure 2**). The SHF cells express LIM homeodomain transcription factor Islet1 and lineage tracing experiments showed that the right ventricle, outflow tract (OFT) and the inflow region of the heart are derived from these Islet1 positive progenitors located in the pharyngeal mesoderm. Mutation of this gene leads to the formation of a linear heart tube unable to loop and elongate (Cai C.L. *et al*., 2003). Islet1+ progenitors are multipotent, as they are able to differentiate to cardiomyocytes, endothelial and smooth muscle cells (Moretti A. *et al*., 2006).

Subdomains within the SHF: the AHF and the pSHF

Inside the SHF, different subdomains can be distinguished, depending on the expression profile and the regions they form (**Figure 2**) (Vincent S.D. and Buckingham, 2010). The anterior region of the SHF (anterior heart field, AHF) provides cells to the arterial pole of the heart and gives rise to

the right ventricle and OFT (Kelly R.G. *et al*., 2001) (Zaffran S. *et al*., 2004). The AHF is marked by expression of several factors, such as Fgf8, Fgf10, Tbx1, Mef2c SHF enhancer. On the other hand, cells that contribute to the inflow region of the heart express Islet1 but not AHF markers and can be defined as the posterior SHF (pSHF). It has been shown that the atrioventricular canal (AVC), large proportion of the atria and the systemic venous inflow are derived from pSHF.

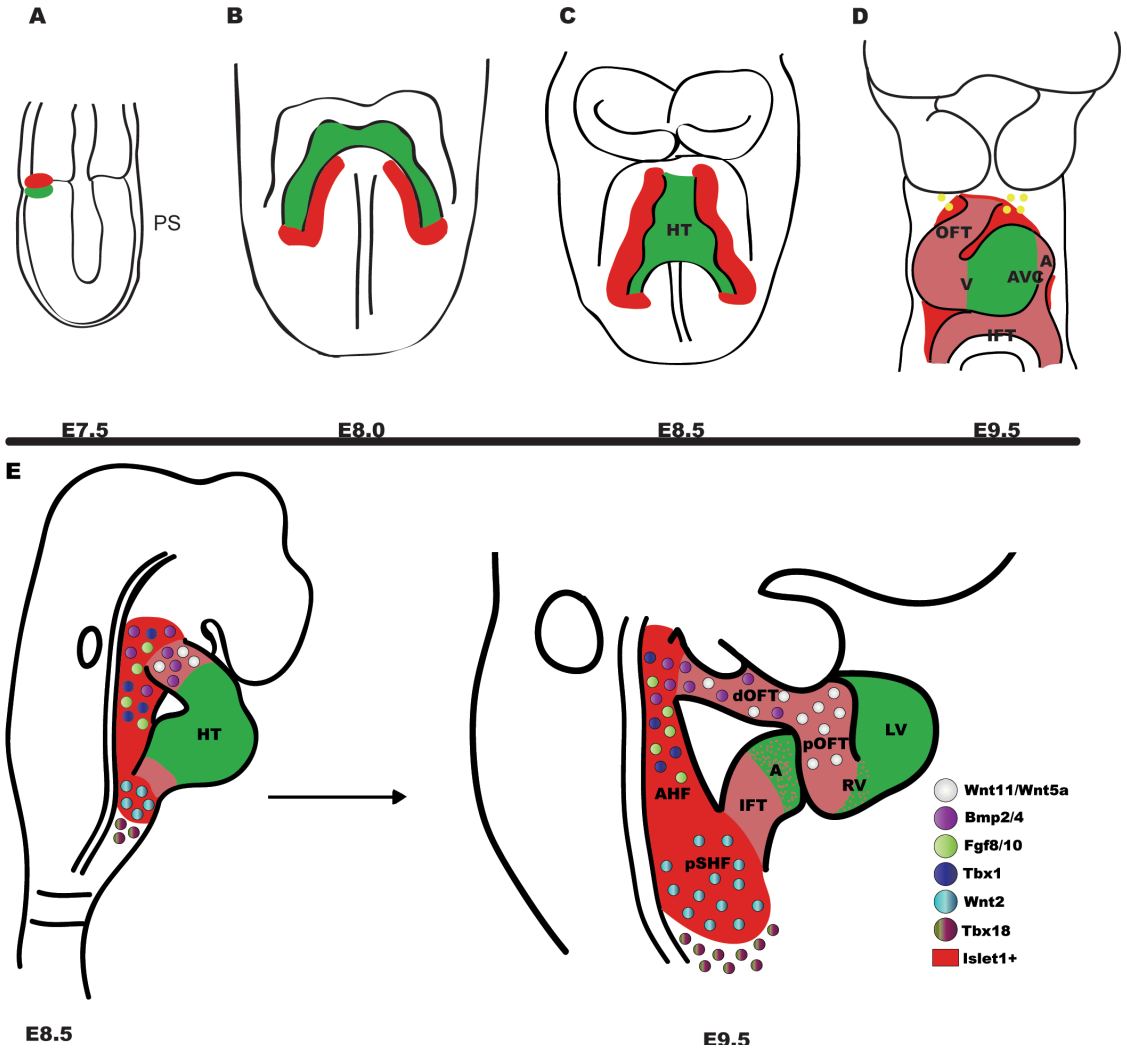

Figure 2. Overview of early heart development. (A) Schematic representation of mouse embryo at E7.5 when cardiac precursors migrate anteriorly from the primitive streak (PS). **(B)** Frontal view of an E8.0 embryo, the cardiac crescent is formed with cells from the first heart field (FHF, green). Precursor cells from the second heart field (SHF, red) lie medially to the cardiac crescent. **(C)** By E8.5, the cardiac tube is formed by fusion of the heart forming regions in the midline of the embryo; at this stage the heart starts to loop. **(D)** Frontal view of an E9.5 embryo where already a common ventricle (V) and atria (A) can be distinguished, as well as the atrioventricular canal (AVC) and the outflow tract (OFT). Contribution of SHF to the OFT, right ventricle, inflow region (IFT) and AVC can be observed depicted in pink. Also at this stage the neural crest cells (yellow) migrate from the pharyngeal arches to the arterial pole of the heart. Adapted from (Vincent S.D. and Buckingham, 2010). **(E)** Lateral view of an E8.5 and E9.5 embryos showing the elongation of the poles of the heart. Some of the molecules important for the development of both anterior heart field (AHF) and posterior SHF (pSHF) are depicted. Already the right and left ventricles can be distinguished (RV and LV), as well as two regions in the OFT, the proximal (pOFT) and distal (dOFT).

biosynthesis, causes a severe embryonic RA deficiency. Mutants for this enzyme present a posterior expansion of AHF markers, such as Tbx1 and Fgf8, fail to undergo heart looping and to form normal atria and sinus venosus (Ryckebusch L. *et al*., 2008). Islet1 expression is also expanded caudally when RA signalling is disrupted, suggesting that RA controls the posterior limits of the SHF (Sirbu I.O. *et al*., 2008). Hox genes are some of the important targets of RA. Their expression characterize distinct subdomains along the antero-posterior axis in the SHF and expressing cells contribute both to the atria and future myocardium at the base of the aorta (Bertrand N. *et al*., 2011).

Different studies have described a set of transcriptional and growth factors expressed in the AHF and involved in proper OFT and right ventricle formation, as their deletion gives rise to defects in the formation of these structures. For instance, ablation of *Fgf8* from the pharyngeal mesoderm leads to truncation of OFT and right ventricle, as a result of decreased cell proliferation and increased cell death of the AHF population (Ilagan R. *et al*., 2006) (Park E.J. *et al*., 2006). Tbx1, a T-box-containing transcription factor responsible for many defects observed in 22q11 deletion syndrome, is also expressed in the AHF and its ablation leads to OFT defects related to decrease in cell proliferation (Zhang Z. *et al*., 2006). Canonical Wnt/β-catenin signalling is also active in the pharyngeal mesoderm. β-catenin ablation leads to decrease in proliferation of Islet1+ progenitors and loss of FGF signalling, and, as a consequence, the OFT appears shortened and the right ventricle is reduced. On the other hand, stabilization of β-catenin in the nucleus produces the opposite effect: expansion of Islet1+ cells, enlarged OFT, abnormal right ventricle and defects in differentiation of Islet1+ cells in the OFT (Cohen E.D *et al*., 2007) (Qyang Y. *et al*., 2007) (Ai D. *et al*., 2007). Bmp2 and 4 are expressed in the OFT and promote myocardial differentiation of SHF cells: deletion of both of these genes leads to an expanded progenitor gene expression (Islet1 and Tbx1) and reduction of myocardial markers, such as sarcomeric myosin, in the proximal OFT (Wang J. *et al*., 2010).

Development of the posterior pole of the heart is poorly understood in comparison with the AHF region. It has been shown that more cranial cells in the pSHF contribute to the AVC and atria, while more caudal regions give rise to the sinus venosus. The contribution is symmetric from the distal portion, but the fate of cranial pSHF is asymmetrical, with the right region contributing to the ventral left atrium (Domínguez J.N. *et al*., 2012). The Wnt/β-catenin pathway plays an important role in the regulation of the posterior cardiac mesoderm; Wnt2, an activator of the pathway, is expressed in the posterior pole of the heart and in the inflow region from E8.5. In *Wnt2* mutant embryos formation of the atria and AVC is compromised. Signalling by Wnt2 proved to be necessary for the expansion of SHF progenitors and the later myocardial proliferation and differentiation, partially through activation of Gata6 (Tian Y. *et al*., 2010). The sinus horns of the systemic venous return are derived from a population of cells positioned ventral-caudal-lateral to the SHF. These cells fail to express Nkx2.5 and Islet1, but are marked by Tbx18 expression and form a myocardium distinguished from the atria myocardium by its Nkx2.5- Cx40- expression

profile (Christoffels V.M. *et al*., 2006). This lateral rim of cardiogenic mesoderm also contains the precursors of the proepicardium, which will give rise to the epicardium, coronary vessels and fibroblasts.

SHF proliferation and deployment

One of the obvious changes occurring in the early heart tube is its growth and increase in the number of cardiomyocytes. Strikingly, proliferation of the heart precursors decreases dramatically when they differentiate and incorporate into the heart tube. Consequently, cardiomyocytes within the early heart tube proliferate at a very slow rate. Both in chick and in mouse early cardiac growth occurs through the recruitment of cells to the poles of the heart from the SHF pool of progenitors (Soufan A.T. *et al*., 2006) (de Boer B.A. *et al*., 2012). As has been shown above, a number of signalling pathways that impact SHF promote proliferation. Recent results in the chick indicate that the heart elongates gradually at both poles from a single bilateral caudal growth centre located in the caudomedial pericardial wall and positive for Islet1. Moreover, cells from this region can be traced as they move cranially to differentiate into myocardium in the arterial pole (van den Berg G. *et al*., 2009) (van den Berg G. and Moorman, 2009). However, although it is clear that SHF precursors contribute to the poles, the cellular mechanism by which progenitors move from the SHF into the growing heart tube is unknown. In the chick, the SHF is described as a pseudostratified columnar layer of epithelial cells (Waldo K.L. *et al*., 2005). Non-canonical Wnt signalling seems to be important for OFT development. *Wnt11* mutants show early OFT defects and cytoskeletal rearrangements and polarized cell movement required for proper OFT morphogenesis are affected (Zhou W. *et al*., 2007). Disheveled (Dvl) is a regulator of both the canonical Wnt/β-catenin and the planar cell polarity (PCP) pathways. *Dvl1/2* mutants display OFT shortening, similarly to those observed in *Vangl2* (the core PCP gene) mutants and in the absence of non-canonical Wnt gene *Wnt5a*. Both in *Dvl1*/2 and *Wnt5a* mutants the caudal splachnic mesoderm presents aberrant cell packing and reduced filopodia formation. It was proposed that PCP signalling induces a mesenchymal to epithelial conversion, promoting SHF contribution to the OFT by a cell intercalation process (Sinha T. *et al*., 2012). Deletion of both *Wnt5a* and *Wnt11* showed their requirement to inhibit the canonical Wnt/β-catenin pathway, but no analysis were done of other possible SHF defects in these double mutants (Cohen E.D. *et al*., 2012).

Interaction of SHF with the pharyngeal endoderm and neural crest cells

SHF development, proliferation and deployment are also dependent on the interaction with other cell types. For instance, the ventral pharyngeal endoderm remains in close contact with the SHF precursors and generates some molecular cues important for the maintenance of this pool of progenitors. Fgf8, apart of being expressed in the SHF, is also expressed in the pharyngeal endoderm and its function in this tissue is required for proper OFT septation (Park E.J. *et al*., 2006). Shh is also expressed in the pharyngeal endoderm and its disruption gives rise to defects in both the arterial and venous poles. The AHF requires Shh signalling for proper septation of the OFT (Goddeeris M.M. *et al*., 2007). Shh signalling is also necessary for atrial septation (Hoffmann

A.D. *et al*., 2009).

The cardiac neural crest (CNC) is a subpopulation of neural crest cells that contribute to the smooth muscle of the pharyngeal arch arteries and also migrate through the AHF into the OFT to contribute to the endocardial cushions. However, CNC ablation leads not only to septation defects, but also to reduction in OFT myocardium and arterial pole defects. In chick it has been shown that cells destined to form the OFT myocardium fail to migrate and are retained at the base of the arterial pole after elimination of CNC (Waldo K.L. *et al*., 2005). Ablation of the CNC leads to increased levels of Fgf8 (otherwise, buffered by these cells) in the caudal pharynx, which disrupts SHF cells deployment (Hutson M.R. *et al*., 2006). In the mouse, mutation of *Tbx3*, which is expressed in the CNC, leads to OFT shortening; in this case, impaired CNC cells function seems to affect proliferation and deployment of the SHF cells (Mesbah K. *et al*., 2008). BMP pathway also plays an important role in the crosstalk between CNC and SHF, as deletion of *Smad4* from the CNC leads to increased apoptosis in these cells, but also to alteration in the expression of some factors in the SHF and in OFT elongation defect (Jia Q. *et al*., 2007).

Multiple heart fields?

The identification of a second mesodermal region as a source of cardiac cells changed the view on the formation of the heart. However, controversy exists on whether the so-called FHF and SHF represent two separate lineages or reflect a gradual contribution and differentiation of the precursors. Islet1 was considered a marker for the SHF, but later studies showed that expression of Islet1 is broader and it can be detected in the cardiac crescent, in the FHF and partially in the left ventricle (Prall O.W.J. *et al*., 2007) (Ma Q. *et al*., 2008) (Sun Y. *et al*., 2007). So, rather than marking a distinct lineage, expression of Islet1 seems to be related to the differentiation state of the precursors. However, it is interesting to notice that deletion of *Islet1* does not affect the formation of the primary heart tube and the phenotype mainly reflects a problem of SHF contribution to the heart tube (Cai C.L. *et al*., 2003). To address the question of lineage relationship between different regions of the heart in a gene expression-independent manner, a retrospective clonal analysis, where low frequency recombination events produce random clones in the myocardium, was carried out. The authors observed some clones in two or more adjacent cardiac compartments, other clones present exclusively in the left ventricle or in the poles of the heart and clones extending through all the cardiac compartments. The authors concluded that the results point to the existence of two lineages that segregate early from a common progenitor and, while most regions of the heart are colonized by both, there is an exclusive contribution of the first lineage to the left ventricle and of the second to the OFT (Meilhac S.M. *et al*., 2004). However, another interpretation can be given to these results. The distribution of clones over the heart reflects the gradual formation of this organ. In this case, early recombination events will give rise to clones in the left ventricle and in contiguous compartments, which are the first to be formed, while later recombination will take place in the precursors of the poles of the heart, which are formed later (Moorman A.F.M. *et al*., 2007). Recently, a distinct, tertiary field was proposed to exist in the chick embryo. Pacemaker cells

arise from a discrete region of mesoderm outside the classical FHF and SHF and are recruited by canonical Wnt signalling (Bressan M. *et al*., 2013). The proposal of distinct fields existing inside the heart-forming region (HFR) would imply a specific fate commitment to each of these fields. Classical experiments performed in early chick embryos that transplanted tissue within the HFR showed that relocated cells are able to adapt to their new location, arguing against an irreversible commitment of these cells (Satin J. *et al*., 1988). It would be interesting to repeat these studies with the current knowledge of heart formation to add new evidence about the nature of the HFR.

Differentiation of the heart tube

Shortly after its emergence, the heart tube starts to loop, while cells are added to its poles and Islet1+ cells differentiate into cardiomyocytes and start expressing muscular markers. The newly formed myocardium displays characteristics of a primary or embryonic myocardium with slow proliferation, slow conduction, slow contraction and the ability to depolarize spontaneously. But shortly after looping, ventricular and atrial chambers are formed and the myocardial phenotype of these regions changes: now, it is characterized by formation of gap junctions consistent of Cx40/Cx43 for fast conduction and an increase in the proliferation rate. The remaining regions – the inflow tract (IFT), the AVC and the OFT - retain the characteristics of the embryonic myocardium (Christoffels V.M. *et al*., 2000). The primary myocardium plays important roles in the developing heart. The myocardium of the AVC and the OFT signals to the endocardium to form the cushion mesenchyme which would later give rise to the valves (Eisenberg L.M. and Markwald, 1995). Also, the primary myocardium protects against the backflow of blood before the valves are formed and provides progenitors for the nodes of the conduction system.

The regionalization of the myocardium is driven by differential gene expression. The nascent chamber myocardium is characterized by expression of Anf, Cited1, Cx40, Cx43 and Chisel, while Tbx2 and Tbx3 are present exclusively in regions of primary myocardium. Deletion of *Tbx5* in the developing heart leads to decreased levels of Anf and Cx40 in the chambers (Bruneau B.G. *et al*., 2001). Tbx5 associates synergistically with Nkx2.5 to promote cardiomyocyte differentiation; they both bind to the *Anf* promoter and activate its expression (Hiroi Y. *et al*., 2001). At the same time, Tbx2 is expressed in regions of primary myocardium (IFT, AVC and OFT) where it forms a complex with Nkx2.5 and represses the expression of Anf (Habets P.E.M.H. *et al*., 2002). Overexpression of Tbx2 through the whole myocardium inhibits chamber formation and represses Cx40 and Cx43 promoter activity and Anf expression, confirming the role of Tbx2 as a determinant factor in the repression of chamber specific genes (Christoffels V.M. *et al*., 2004). Interestingly, genetic lineage tracing showed that Tbx2+ primary myocardium contributes to both ventricles; in the AVC, Tbx2 represses differentiation and proliferation of the myocardium, but switching off Tbx2 expression allows these cells to initiate differentiation into chamber myocardium and to proliferate (Aanhaanen W.T.J. *et al*., 2009). Tbx20, another T-box factor, is expressed through the whole myocardium and is necessary to ensure the progression from the linear heart tube to multi-

chambered heart by repressing Tbx2. In *Tbx20* mutant embryos chamber myocardium is not formed and Tbx2 is ectopically expressed in the linear heart tube (Singh M.K. *et al*., 2005). Another factor controlling multiple aspects of AVC morphogenesis is Bmp2. Apart from its role in early cardiac formation, Bmp2 is also expressed at high levels in the AVC and at lower in the OFT. Deletion of *Bmp2* from the AVC leads to downregulation of Tbx2 and expansion of chamber-specific genes to the AVC (Ma L. *et al*., 2005). Bmp2 has been shown to regulate directly the expression of Tbx2 through pSmad1/5/8 binding to a *Tbx2* enhancer that confers AVC specific expression to *Tbx2*. Tbx20 competes with Smad4 for binding Smad1 and 5 and thus supresses Tbx2 expression in the chambers (Singh R. *et al*., 2009). Tbx20 has been also proposed to regulate positively Hey1 and Hey2. Hey1 and Hey2, expressed in atrium and ventricle, respectively, regulate the AVC boundary and repress Tbx2 expression in the chambers (Kokubo H. *et al*., 2007).

Tbx3 is yet another member of the T-box family implicated in the regulation of heart development. At early stages of embryonic development, Tbx3 is expressed in a continuous way in a myocardial domain that extends from the sinoatrial node to the atrioventricular region. Similarly to Tbx2, Tbx3 represses Anf and Cx40 expression and disrupts their activation by the Nkx2.5-Tbx5 complex (Hoogaars W.M. *et al*., 2004). Tbx3 expression also delineates the sinoatrial node region, which controls the rate and rhythm of contraction and serves as the pacemaker of the heart. Ectopic expression of Tbx3 represses the atrial phenotype and imposes a pacemaker phenotype on atrial cells. Tbx3 is also required for molecular specification of the atrioventricular bundle and proximal bundle branches through repression of differentiation and proliferation, imposing the conduction system phenotype (Hoogaars W.M.H. *et al*., 2007) (Bakker M.L. *et al*., 2008). Although a direct regulation as in the case of Tbx2 has not been shown, Bmp2 is upstream of Tbx3 expression, as Bmp2 inactivation in myocardium leads to loss of Tbx3 in the AVC (Singh R. *et al*., 2012).

Valve formation.

The first step in heart septation is the formation of endocardial cushions, which later will be remodelled into atrioventricular cardiac valves (the ones formed in the AVC) and conoventricular cardiac valves (formed in the OFT). The myocardial and endocardial layers of the early heart tube are separated by an extracellular matrix, known as cardiac jelly, which expands focally to form endocardial cushions in the AVC and in the OFT. Later, endocardial cells that line these cushions undergo epithelial-to-mesenchymal transition (EMT) and the formed mesenchymal cells, precursors of the future valves, populate the cushions. Next steps involve their proliferation and expansion and elongation and remodelling of the valves to form mature leaflets (von Gise A. and Pu, 2012). Endocardial EMT occurs in both AVC and OFT, but in the last case valve formation starts later in gestation and involves important contribution from the cardiac neural crest, so the two processes will be discussed separately.

AVC cushions

Endocardial EMT depends on both the specialized AVC myocardium and cushion endocardium and the signal exchange between them (**Figure 3**). Bmp2, although expressed only in the myocardium and not in the endocardium, is required to enhance the formation of the cardiac jelly and to induce endocardial EMT (Ma L. *et al*., 2005). A feedback loop exists between Bmp2-Tbx2/3; while Bmp2 induces the expression of these two transcription factors, their expression is needed to maintain Bmp2 levels in the myocardium, as in double Tbx2/3 mutants Bmp2 expression is reduced. Moreover, misexpression of either Tbx2 or Tbx3 in the heart leads to ectopic expression of Bmp2 in the chamber myocardium and of EMT markers, such as Snail1 and Has2, in the underlying endocardium, with consequent cardiac jelly expansion and cushion formation. This induction is dependent on Bmp2, as inhibition of the BMP receptor down-regulates EMT markers and cushion formation (Singh R. *et al*., 2012) (Shirai M. *et al*., 2009). Indeed, Bmp2 can substitute for AVC myocardium in AVC explant cultures, supporting its role as a key myocardial EMT-inducing factor (Sugi Y. *et al*., 2004) (Rivera-Feliciano J. *et al*., 2006). Bmp2 activates the expression of some EMT genes in the endocardium, like Twist1, which acts upstream of Tbx20 in the endocardium and promotes mesenchymal cell proliferation and migration, while inhibiting valve cell differentiating (Shelton E.L. and Yutzey, 2007) (Shelton E.L. and Yutzey, 2008). Tgf-β2 is another important factor for EMT that acts downstream of Bmp2. *Tgf-β2* mutants show reduced number of mesenchymal cells, and it is also required to conclude the later stages of EMT (Sugi Y. *et al*., 2004) (Azhar M. *et al*., 2009). Tgf-β2 also has a role in valve remodelling and differentiation by inducing matrix organization and repressing the differentiation of the cushion mesenchyme into the cartilage cell lineage (Azhar M. *et al*., 2011).

The Notch pathway is also required for several steps in valve development. The Notch receptor is a single-pass transmembrane protein with an extracellular domain through which it binds to its ligands (Delta or Jagged), and a Notch intracellular domain (NICD), which is released after activation by the ligand and translocates into the nucleus to activate gene expression (Andersson E.R. *et al*., 2011). N1ICD (the active form of Notch1) is expressed in the endocardium lining the AVC and the OFT (del Monte G. *et al*., 2007), indicating that, contrary to Bmp2, it promotes endocardial EMT directly from the endocardium. Deletion of Notch activity in the endocardium leads to downregulation of Tgf-β2 and Snail1, a key promoter of EMT, and absence of EMT both *in vivo* and *in vitro* (Timmerman L.A. *et al*., 2004). Contrarily, overexpression of N1ICD through out the endocardium leads to ectopical activation of the mesenchymal gene program. Notch confines Bmp2 expression to the AVC myocardium, as Hey1 and Hey2, targets of Notch, repress Bmp2 expression in the endocardium. Bmp2 and Notch1 signalling pathways converge in Snail1 activation and promote a valve-forming field in the developing heart (Luna-Zurita L. *et al*., 2010) (de la Pompa J.L. and Epstein, 2012).

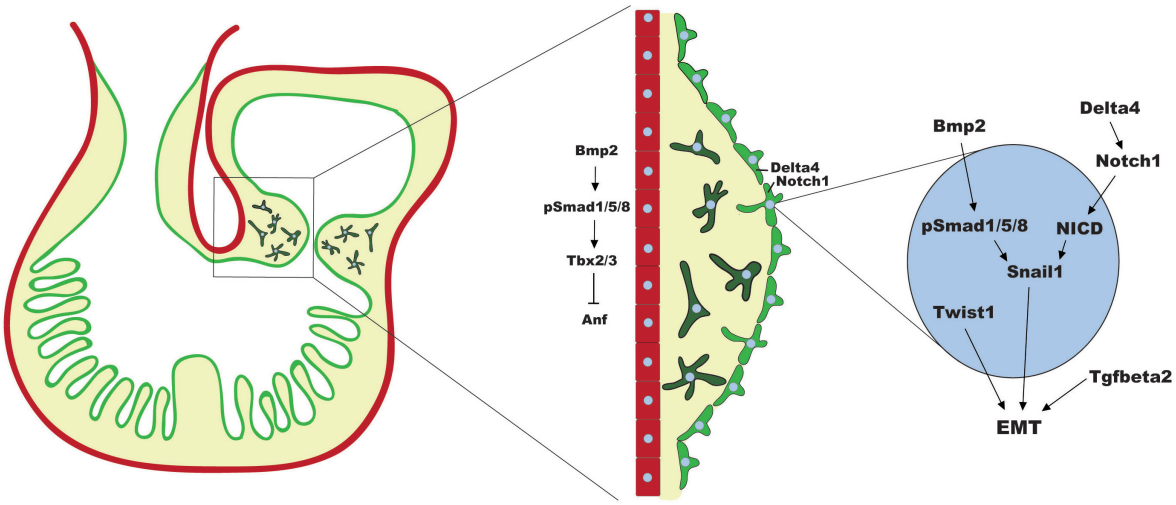

Figure 3. Schematic presentation of early steps of valve formation. AVC myocardium expresses Bmp2 that acts both on the myocardium (red) and on the endocardium (green). In the myocardium, Bmp2 induces the expression of Tbx2 and Tbx3 through pSmad1/5/8 signalling. Tbx2/3 repress the expression of chamber markers, such as Anf. In the AVC endocardium, part of the endothelial cells undergo epithelial-to-mesenchymal transition (EMT) and invade the underlying cardiac jelly (yellow). Notch1 and its ligands are expressed in the endocardium and activated Notch intracellular domain (NICD) together with pSmad1/5/8 activated by myocardial Bmp2 promote the expression of genes involved in EMT, such as Snail1/2, Tgfβ2 and Twist1.

OFT cushions and neural crest cells (NCCs)

OFT cushion development implies interaction between endocardium, endocardial-derived mesenchyme and cardiac neural crest. At the same time as the OFT is remodelled and separates into two vessels, the aorta and the pulmonary trunk, it rotates and aligns with the ventricles, so that the aorta emerges from the left ventricle and the pulmonary trunk from the right ventricle. The OFT contains two pairs of cushions: the conal cushions that form the conal septum when they fuse and separate the proximal OFT into right and left ventricular outlets; the truncal cushions which form the aortopulmonary septum, dividing the distal OFT into the aorta and pulmonary trunk. Adjacent to the conotruncal cushions, the intercalated cushions are formed and together they form the aortic and pulmonar valves (Lin C.J. *et al*., 2012). Deletion of both BMP6 and BMP7 from the myocardium disrupts the invasion of the cushions by endocardial cells (Kim R.Y. *et al*., 2001). At the same time, the SHF provides a source of Bmp4, which is necessary for cushion expansion and remodelling (Liu W. *et al*., 2004) (McCulley D.J. *et al*., 2008). On the other hand, Tbx2, which is expressed in the OFT myocardium, has been shown to activate directly the expression of Tgf-β2 in the myocardium, ultimately responsible for the induction of EMT in OFT cushions (Sakabe M. *et al*., 2012).

The NCCs migrate from their original location in the rhombomeres 6-8 and invade the OFT to form the aortopulmonary septum. The OFT myocardium secretes Sema3c to attract the NCCs and promote the invasion of the truncal cushions where they turn into mesenchymal cells (Toyofuku

T. *et al*., 2008). The truncal mesenchyme later differentiates into smooth muscle septum. Fgf8 signalling is important for the surviving of migrating NCCs, as reduction of Fgf8 levels leads to massive cell death when NCCs delaminate from the neural tube or when they reach the pharynx (Abu-Issa R. *et al*., 2002). FGF has been also shown to upregulate Bmp4, which enhances smooth muscle differentiation of NCCs (Zhang J. *et al*., 2010). Also, Notch in the NCCs is necessary for their differentiation into smooth muscle cells (High F.A et al., 2009).

Maturation of the cardiac valves

Post-EMT valve remodelling, where mesenchymal cells differentiate into interstitial fibroblasts and remodel their environment into a mature valve, is poorly understood. The expansion of the cushions is driven by proliferation of mesenchymal cells controlled by multiple signals such as Wnt/β-catenin pathway, BMPs and Fgf4 (Combs M.D. and Yutzey, 2009). It has been proposed that two distinct zones exist within the developing cushion tissue: a zone of proliferation close to the endocardium and a zone of differentiation adjacent to the myocardium, although the mechanisms for this regionalization are unknown (de Vlaming A. *et al*., 2012). During fetal stages the valve elongates to form a thin valve leaflets. This is accomplished by an increase of cellular density and reorganization of extracellular matrix (Kruithof B.P. *et al*., 2007). Differentiation of mesenchymal cells and appropriate deposition and ordering of the extracellular matrix are two processes essential for the formation of a functional valve. Periostin, a protein of the extracellular matrix, plays an important role in stimulating a valvulogenic signalling pathway. Periostin is secreted by cushion cells into the extracellular matrix and via β-integrin/FAK/ERK pathway promotes cell adhesion, migration and survival, as well as regulates the expression of hyaluronan and collagen I and activates collagen compaction (Norris R.A. *et al*., 2009) (Ghatak S. *et al*., 2014).

ARID FAMILY

The ARID family is a family of transcriptional factors characterized by a highly conserved DNA binding domain called ARID domain. The name stands for *AT rich interaction domain*, and derives from the first study where the founding member of the family, Bright (B cell regulator of IgH transcription) was described. In this work, the authors observed a previously unknown DNA binding domain with affinity for AT-rich DNA (Herrscher R.F. *et al*., 1995). Briefly after that, the *dead ringer* (*dri*) gene was described in *Drosophila*, identified in a screen as a gene with similar DNA-binding characteristics of homeodomain proteins. The newly described gene lacked any homology to the homeobox, but its ARID domain was closely related to other genes, including Bright. A novel, highly conserved family of DNA-binding proteins was established (Gregory S.L. *et al*., 1996). Later, members of the ARID family were found in a wide range of species, from yeasts to nematodes, insects and mammals, as well as in plants and fungi (Zhu H. *et al*., 2008) (Hansen F.T. *et al*., 2008). There are 15 proteins described in humans and 6 in *Drosophila* and members of the family have been shown to be involved in chromatin remodelling, cell differentiation, control

of cell cycle and embryonic development (Kortschak R.D. *et al*., 2000) (Wilsker D. *et al*., 2002).

Since the number of members of the ARID family grew, a tighter consensus sequence for the ARID domain emerged. This consensus sequence extends across around 100 residues; outside the ARID domain, the proteins of the family show diversity of sequence, structure and functions (Wilsker D. *et al*., 2002). The ARID domain codifies for six α-helices that form a non-canonical helix-turn-helix motif. The 3D structure of the minimal ARID domain-DNA complex, together with the poor conservation of aminoacids which dictate binding specificity to the DNA, suggests that most ARIDs bind DNA less tightly and with no AT-specificity, as was supposed earlier (Iwahara J. *et al*., 2002) (Cai S. *et al*., 2007). Indeed, recombinant GST-fusion proteins that included the ARID domain of each protein of the family showed that most of the ARID subfamilies bind DNA without any sequence preference (Patsialou A. *et al*., 2005). Some members of the family, which include Bright and Dri, present an "extended ARID (eARID)" domain with a 40 extra aminoacids, which forms one extra N-terminal and one extra C-terminal helix. This extra C-terminal helix might increase DNA affinity.

The ARID family can be subdivided in seven subfamilies based on the degree of sequence identity between individual proteins (**Figure 4**). Some of the main characteristics of these subfamilies are discussed below.

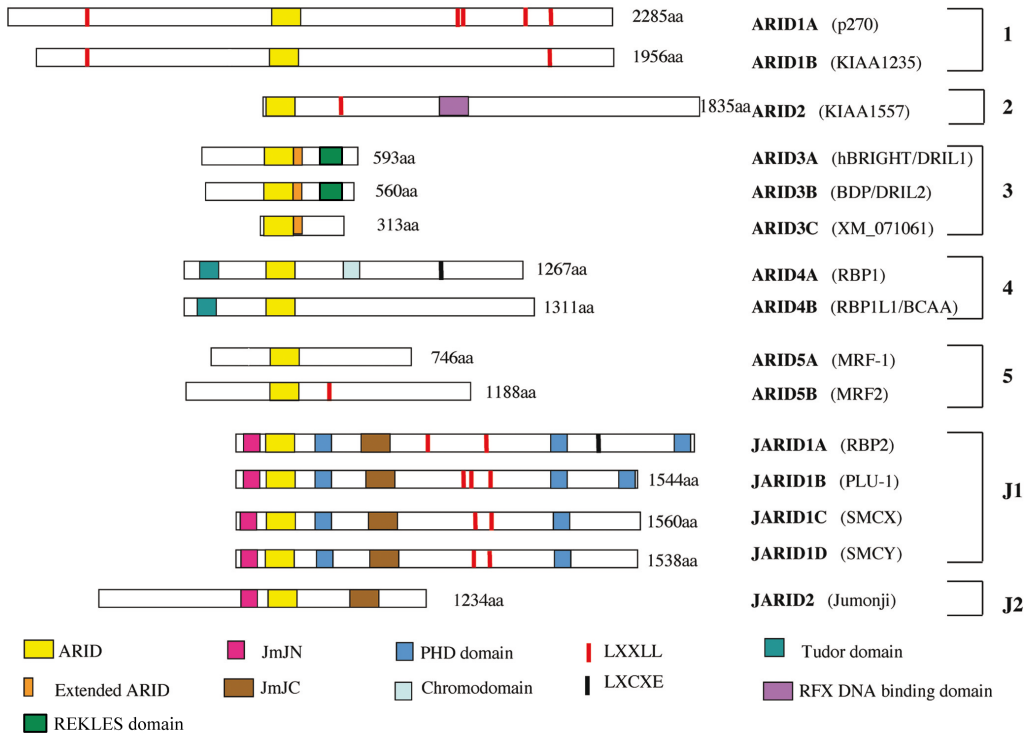

Figure 4. The human ARID family of proteins grouped in subfamilies according to their similarities within the ARID domain and the presence of other conserved domains; adapted from (Patsialou A. *et al*., 2005).

ARID1: includes Arid1a and Arid1b, the two largest and mutually exclusive subunits of SWI/SNF complexes, which are ATP-dependent chromatin remodelling complexes. The presence of one or the other protein in a SWI/SNF complex determines whether complexes would be further formed with activators or repressors (Nagl N.G.Jr. *et al*., 2007). Arid1a is expressed through embryonic development at higher levels than Arid1b and the levels of both proteins are regulated during different cell cycle phases (Flores-Alcantar A. *et al*., 2011).

ARID2: Arid2 has been shown to form part of the PBAF SWI/SNF complexes; inside this complex, Arid2 is required to mediate the expression of an interferon-responsive gene (Yan Z. *et al*., 2005).

ARID4: includes Arid4a (RBP1) and Arid4b (RBP1L1). Arid4a was cloned in search for pRb binding partners. The authors showed that pRb represses transcription by binding Arid4a, which serves as a bridging molecule to recruit histone deacetylases (HDACs), as well as functions at an additional HDAC-independent level as a repressor (Lai A. *et al*., 1999) (Lai A. *et al*., 2001). Moreover, the class III deacetylase SIRT1 associates with HDAC1 complexes through Arid4a/b and regulates the HDAC1-mediated transcriptional silencing (Binda O. *et al*., 2008).

ARID5: includes Arid5a (MRF-1) and Arid5b (MRF2). Arid5b is implicated in different processes. It has been shown to regulate smooth muscle cell differentiation and proliferation in cell culture (Watanabe M. *et al*., 2002). Targeted mutation in this gene in mice leads to reduced viability, delayed growth, abnormalities in the reproductive organs, as well as alterations in the T and B cell compartments of primary lymphoid organs (Lahoud M.H. *et al*., 2001). At the molecular level, Arid5b together with Phf2, a jmjC demethylase, forms a histone lysine demethylase complex, which is a signal-sensing modulator of histone methylation and gene transcription (Baba A. *et al*., 2011). By facilitating Phf2-mediated histone demethylation of Sox9-regulated chondrogenic gene promoters, Arid5b facilitates chondrogenesis (Hata K. *et al*., 2013). Recent genome-wide screens have identified genetic variations in ARID5B associated with susceptibility to childhood acute lymphoblastic leukemia (ALL) and these polymorphisms are determinant of ALL susceptibility and treatment outcome (Healy J. *et al*., 2010) (Xu H. *et al*., 2012).

JARID1: this subfamily includes four members: Jarid1a (RBP2), Jarid1b (PLU-1), Jarid1c (SMCX), Jarid1d (SMCY). Apart from the ARID domain, these proteins present two conserved jumonji (jmj) domains – jmjC (domain with histone demethylse activity) and jmjN, and a PHD finger domain (Takeuchi T. *et al*., 2006). Jarid1a-c proteins regulate histone demethylation *in vivo* and contribute to transcriptional silencing by keeping the levels of H3K4me3 low (Christensen J. *et al*., 2007). Jarid1a repression promotes differentiation; on the other hand, in the presence of pRb, it can also act as a coactivator and drive differentiation (Benevolenskaya E.V. *et al*., 2005). Jarid1b is expressed in some restricted tissues during embryonic development, including brain, mammary bud, thymus, limb, olfactory epithelium, teeth, eye and stomach (Madsen B. *et al*., 2002). Deletion of Jarid1b leads to early embryonic lethality, while Jarid1a knock-outs are viable and fertile (Catchpole S. *et al*., 2011). Jarid1c plays important roles in brain development and its

mutations in humans cause X-linked mental retardation. In accordance with the human pathology, in zebrafish and primary mammalian neurons it is involved in neuronal survival and dendritic development (Jensen L.R. *et al*., 2005) (Iwase S. *et al*., 2007).

JARID2: also known as Jumonji (Jmj). It presents the jmjC and jmjN domains, but lacks the PHD domain. It is involved in heart development, as its deletion leads to neonatal birth due to heart defects, such as ventricular septal defect, non-compaction of the ventricular wall, double-outlet right ventricle and dilated atria (Lee Y. *et al*., 2000). Jmj represses Anf expression by directly binding to Nkx2.5 and Gata4 (Kim T.G. *et al*., 2004), and its own expression is repressed by Nkx2.5 in the SHF (Barth J.L. *et al*., 2010). Several studies point to a major role for Jarid2 in mediating the recruitment of histone methylase-containing PRC2 repressor complexes to target genes. Jmj deletion leads to impaired differentiation in *Xenopus laevis* and in mouse embryonic stem cells, consistent with the essential role of PRC2 proteins in early development (Peng J.C. *et al*., 2009) (Li G. *et al*., 2010) (Pasini D. *et al*., 2010) (Landeira D. *et al*., 2010).

ARID3 subfamily

The Arid3 subfamily, as mentioned above, presents an extended ARID domain with two extra α-helices, possibly implicated in the specificity of DNA recognition (Iwahara J. and Clubb, 1999) (Iwahara J. *et al*., 2002). Members of the subfamily include the *Drosophila* Dead ringer and its three mammalian homologous - Arid3a/Bright, Arid3b/BDP and Arid3c – and are present specifically in metazoans (Kortschak R.D. *et al*., 2000). Apart from the ARID domain, the subfamily presents two domains in the C-terminal region called REKLES-α and REKLES-β, which have not been found in any non-Arid protein. These two domains contain nuclear import and export signals (Kim D. and Tucker, 2006). It has been proposed that REKLES-β is required for self-association of Arid3 proteins or association with other proteins, as well as for nuclear matrix interaction (Kim D. *et al*., 2007). However, controversy exists regarding this function, since a previous report claimed that REKLES-β is not required for self-association (Shandala T. *et al*., 2002).

Dead ringer/Retained in Drosophila development

The Dead ringer/Retained (Dri/Retn) protein can be detected from the first hours of development of *Drosophila* expressed nuclearly and ubiquitously until after gastrulation. After germ band extension it localizes predominantly in the mesoderm and during embryogenesis it can be detected in the pharyngeal muscles, in different regions of the brain and the digestive tube, as well as in the extraembryonic amnioserosa (Gregory S.L. *et al*., 1996). *Dri* mutants die during embryonic development. It is essential for early embryonic patterning and expression of some terminal genes, such as *argos* and *buttonhead*, as well as *even-skipped*, a gene required for segment formation, is disrupted in *Dri* mutants. Also, somatic musculature development is impaired. Interestingly, the more dramatic phenotypes, involving patterning defects, arise when the *dri* maternal component is removed, while *dri* deletion in the embryo yields only muscular and digestive defects (Shandala T. *et al*., 1999). The use of hypomorphic mutants enables the study of the role of Dri in late

development of longitudinal glia where it is involved in differentiation and migration to their final destination (Shandala T. *et al*., 2003). Dri is also involved in dorso-ventral patterning. Dri-depended recruitment of Groucho to Dorsal (Dl) binding sites switches Dl into a repressor and enables the restriction of *Zernüllt* (*Zen*) to the dorsal region of the embryo and supresses *Huckbein* (*Hkb*) expression in the ventral region (Häder T. *et al*., 2000). Together, these data suggest that Dri can act as a co-activator or co-repressor depending on the cellular context.

Arid3a and Arid3c

Arid3a/Bright is the most studied gene of the three mammalian Dri homologs. During adulthood it is expressed specifically in the B-lymphocytes in both mice and humans and its most known function is the regulation of the immunoglobulin heavy chain expression (Herrscher R.F. *et al*., 1995) (Nixon J.C. *et al*., 2004). Arid3a-DNA binding complexes are observed in the nucleus of activated murine B cells (Webb C.F. *et al*., 2000). It has been also suggested that Bright contributes to increased gene expression by remodelling the immunoglobulin locus (Kaplan M.H. *et al*., 2001). During embryonic development, deletion of *Arid3a* leads to midgestational death from failed hematopoiesis, as hematopoietic stem cells fail to differentiate into mature erythrocytes (Webb C.F. *et al*., 2011). Recently, a role for Arid3a in pluripotency and differentiation was proposed. *Arid3a*-deficient cells from adult tissues express a number of pluripotency-associated gene products, expand indefinitely and spontaneously differentiate into cells of multiple lineages, suggesting its role in pluripotency suppression (An G. *et al*., 2010). It appears as an Oct4 binding partner in mouse embryonic stem cells, although further studies are needed to confirm the *in vivo* importance of this interaction (Pardo M. *et al*., 2010) (van den Berg D.L.C. *et al*., 2010). It also appears, together with Arid3b, as one of the most upregulated genes upon ES cells differentiation (Wang J. *et al*., 2006).

Arid3c is the less known member of the Arid3 subfamily. Only recently it has been reported that this gene encodes for two alternatively spliced forms, one of which lacks the REKLES domain. The largest isoform co-activates Arid3a-dependent immunoglobulin transcription (Tidwell J.A. *et al*., 2011).

Arid3b

Arid3b was discovered in a screen of a human testis library and found as being expressed in some other adult tissues, like placenta and leukocytes. It was named Bdp (Bright-derived protein) and was confirmed its homology to Bright and Dri. The same report addressed its capacity to bind pRb *in vitro* (Numata S. *et al*., 1999). In the field of cancer research, some studies point to the important role of this protein in different cancer types. Arid3b is expressed in different neuroblastoma-derived lines and their growth ceases after suppression of Arid3b by siRNA. Moreover, it is also expressed in some human neuroblastoma stage IV tumours. Overexpression of Arid3b in mouse embryonic fibroblasts (MEFs) leads to the immortalization of these cells. Co-transfection with MYCN enhances MYCN oncogenic activity by supressing MYCN-induced

apoptosis in both MEFs and neural stem cells (Kobayashi K. *et al*., 2006) (Kobayashi K. *et al*., 2013). On the other hand, Arid3b is also overexpressed in malignant ovarian cancers and involved in the mesenchymal transformation of the ovarian epithelium (Cowden Dahl K.D. *et al*., 2009). Similarly, in breast cancer cells Arid3b has been described as a miR-125b target with roles in cell motility, as its transient silencing leads to decreased cell migration (Akhavantabasi S. *et al*., 2012). More recently, an alternative splicing form of Arid3b has been described in different cancer cell lines, including ovarian cancer. The full-length form and short form of Arid3b show different intracellular distribution and different capacity to induce apoptosis (Joseph S. *et al*., 2012). Additionally, Chip-seq experiments suggest that Arid3b might be a direct target of p53; consistent with it, the gene is deregulated in different cancers where p53 appears mutated (Garritano S. *et al*., 2013).

Less is known about Arid3b function during embryonic development. A first report described a dynamic pattern of expression of the gene in different structures, mostly the branchial arches, neural crest, rombomeres, OFT of the heart, otic vesicle, caudal neural tube and mesoderm and nascent somites. It also described a loss-of-function mutant, which dies at midgestation (E11.5-12.5) with growth delay and cardiovascular and craneofascial defects. The most striking phenotype observed was the massive death of cranial mesenchyme, which the authors pointed as the cause of embryonic death, as well as the cause of the cardiovascular phenotype (Takebe A. *et al*., 2006).

Arid3b is also involved in limb development. Its expression can be detected in the apical ectodermal ridge (AER). While signalling pathways involved in AER formation remain unaltered in both mutant mouse and loss-of-function assays in chick, AER maturation and structuring are affected. AER compaction is not achieved and *in vivo* DiI labelling of pre-AER cells in chick embryos shows reduced movement of these cells and defective contribution to the AER in the absence of Arid3b. The results point to a role of Arid3b in the regulation of cell motility and rearrangements that lead to AER maturation (Casanova J.C. *et al*., 2011).

Some recent studies have identified Arid3b as a protein involved in stem cells maintenance and differentiation. Indeed, similarly to what happens in tumours, Arid3b protects ES mouse cells from MYCN-induced apoptosis and both genes are upregulated in induced pluripotent cells (iPC) from neural stem cells (Kobayashi K. *et al*., 2013). Interestingly, in other study Arid3b appears as one of the most upregulated genes in differentiating ES mouse cells (Wang J. *et al*., 2006). Also, Arid3b was identified in several screens as a possible Oct4-binding partner in mouse ES cells and, additionally, as a possible target of Oct4, but no biological confirmation was obtained so far (Wang J. *et al*., 2006) (Wang J. and Orkin, 2008) (Sharov A.A. *et al*., 2008). Still, the specific roles of Arid3b remain elusive.

INTRODUCCIÓN

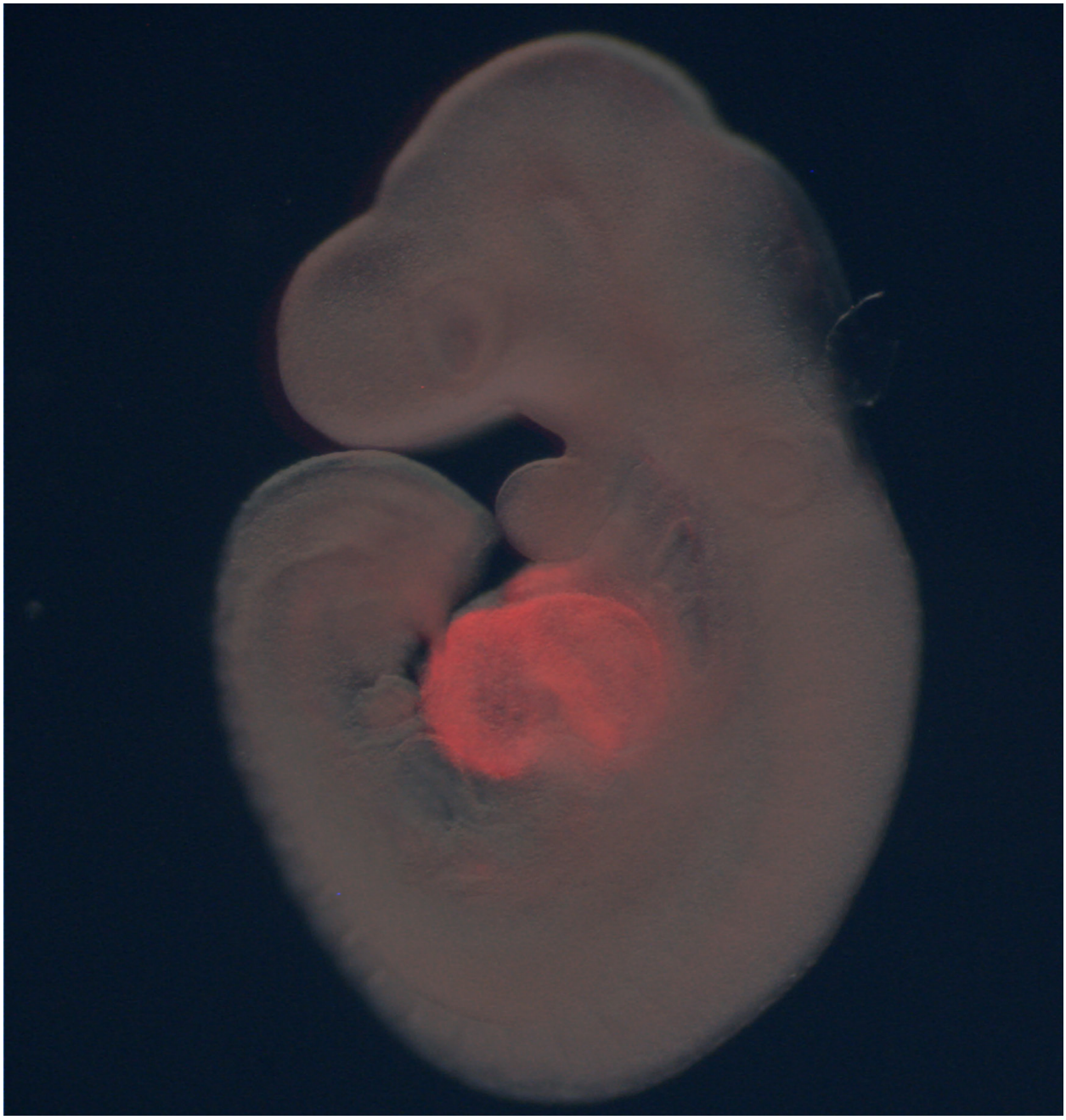

El desarrollo embrionario es la suma de los procesos biológicos que llevan a la formación de un organismo maduro y complejo a partir de un cigoto unicelular. A pesar de que existen variaciones sustanciales entre diferentes especies, algunos mecanismos comunes están presentes en todas. Los organismos pluricelulares se desarrollan a través de cambios progresivos que comprenden un aumento en el número de células, la diferenciación y especificación hacia diferentes tipos celulares y su organización en tejidos y órganos. La alteración de cualquiera de los pasos del desarrollo embrionario produce malformaciones, un tema importante en el campo de la salud humana, ya que hasta el 3% de los recién nacidos presentan algún defecto congénito, según el Centro de Control y Prevención de Enfermedades de Estados Unidos (Parker S.E. *et al*., 2010).

El corazón es el primer órgano en funcionar durante el desarrollo embrionario. En mamíferos, el corazón maduro es un órgano muscular de cuatro cámaras que permite una circulación de sangre cerrada y separada en circulación sistémica y pulmonar. Antes de se adquiera la estructura definitiva, el latido cardiaco se tiene que mantener y modificar mientras el órgano crece y sufre cambios morfogenéticos. El tubo cardiaco temprano pasa por una fase de elongación a través de la adición de células desde el mesodermo faríngeo y por una fase de giro, seguidas de la especificación de cámaras, valvulogénesis, trabeculación, formación de la tercera capa –epicardio– y septación. Defectos estructurales y funcionales pueden dar lugar a patologías congénitas cardiacas, las anomalías más comunes en los recién nacidos (Fahed A.C. *et al*., 2013).

El uso del ratón como organismo modelo ha demostrado ser muy útil para el estudio del desarrollo embrionario del corazón, así como de la etiología de patologías cardiacas humanas. El ratón guarda grandes similitudes con los humanos en cuanto a anatomía, fisiología y genética se refiere; además, la posibilidad de manipular el genoma murino proporciona una potente herramienta para el estudio de la función de genes y para modelar enfermedades humanas.

DESARROLLO CARDIACO

Procesos tempranos en la formación del corazón

El corazón deriva del mesodermo lateral. Durante la gastrulación, las células del epiblasto ingresan a través de la línea primitiva y forman la capa mesodérmica. El mesodermo del embrión en el estado de neurula se puede subdividir en cuatro regiones: el cordamesodermo, el mesodermo paraxial o somático, el mesodermo intermedio y el mesodermo lateral. El mesodermo lateral es el que se encuentra más alejado de la notocorda y origina el corazón, los vasos y las células sanguíneas, así como los recubrimientos de las cavidades del cuerpo, incluida la cavidad pericárdica que envuelve el corazón.

Durante la gastrulación, los progenitores cardiacos ingresan en los segmentos rostrales y medios de la línea primitiva junto con las células destinadas a dar lugar a estructuras rostrales, como el mesodermo cefálico. Los precursores del corazón se establecen en el mesodermo lateral,

donde forman campos cardiogénicos. En el embrión de pollo la especificación del miocardio se produce a través del factor TGFβ secretado por el hipoblasto, mientras que en el ratón esta función posiblemente le corresponde al endodermo visceral anterior (Nijmeijer R.M. *et al*., 2009). Mesp1 se expresa en las células mesodérmicas tempranas que ingresan a través de la línea primitiva y, según trazados de linaje genéticos, prácticamente todas las células cardiacas derivan de la población Mesp1+ (Saga Y. *et al*., 1999) (Saga Y. *et al*., 2000). Junto con Mesp2, controla la salida de los precursores mesodérmicos de la línea primitiva a través de la regulación de la transición epitelio-mesénquima (EMT) y la migración celular (Kitajima S. *et al*., 2000) (Lindsley R.C. *et al*., 2008). Además, es un factor clave en el compromiso hacia linajes cardiovasculares, ya que promueve la expresión de la mayoría de los factores de transcripción cardiacos, como Gata4, Nkx2.5, Hand2, Mef2c, Tbx20, myocardin (Bondue A. *et al*., 2008) (Bondue A. and Blanpain, 2010).

Una vez localizados en el mesodermo lateral, los precursores cardiacos forman una región denominada cresta cardiaca, donde las células pre-miocárdicas y endoteliales están entremezcladas. Las futuras células del miocardio expresan Nkx2.5, un gen esencial para la integración de la información del establecimiento de patrón (Prall O.W.J. *et al*., 2007). Al mismo tiempo, la placa neuronal empieza a plegarse para formar el tubo neural, proceso que va acoplado con la invaginación del endodermo para formar el intestino embrionario anterior. Las regiones cardiogénicas se mueven hacia la línea media del embrión en íntimo contacto con el endodermo y se fusionan para dar lugar al tubo cardiaco primitivo (Moorman A. *et al*., 2003) (Wagner M. and Siddiqui, 2007). Junto con Nkx2.5, Gata4 es uno de los genes más tempranos de la cresta cardiaca, responsable de la expresión de una serie de factores miocardio-específicos. Otros genes, como Tbx5, Mef2c y Hand1/2 también están implicados en la diferenciación de células miocárdicas en la cresta. Recientemente, se han demostrado importantes propiedades de inducción cardiogénica del componente de complejos de remodelación cromatínica Baf60c/Smarcd3. Mesodermo no cardiogénico se puede diferenciar a cardiomiocitos contráctiles en presencia de Gata4, Tbx5 y Baf60c; el último parece reclutar complejos de remodelación de cromatina BAF a *enhancers* cardio-específicos (Takeuchi J.K. and Bruneau, 2009).

Los campos cardiacos

Tradicionalmente se ha considerado que los precursores cardiacos estaban predestinados a contribuir a las diferentes regiones del tubo cardiaco en función de su posición a lo largo del eje antero-posterior, un pre-establecimiento de patrón presente tanto en la cresta cardiaca como en el tubo. Ello llevó a proponer el modelo segmental de la formación del corazón, según el cual cada región de este órgano era una unidad separada y derivada de un grupo de progenitores predestinados, además de apoyar la idea de que todas las células formadoras de corazón estaban contenidas en el tubo cardiaco temprano (revisado en (Buckingham M. *et al*., 2005)). Sin embargo, durante muchos años, varios estudios realizados tanto en pollo como en ratón apuntaban a que el tubo cardiaco seguía alargándose por los polos. En su trabajo en embriones de pollo, de la Cruz y colaboradores

pudieron apreciar que partículas de óxido de hierro depositadas en el extremo cefálico del tubo cardiaco acababan desplazándose al interior del mismo en estadios más tardíos. En otra serie de experimentos, la separación del tubo cardiaco de su anclaje anterior conllevaba la formación de un corazón carente de la región cefálica. Sus resultados les llevaron a proponer que no todas las partes del corazón están presentes en el tubo del estadio previo al giro, sino que se añadían en diferentes momentos del desarrollo (Argüello C. *et al*., 1975) (de la Cruz M.V. *et al*., 1977). Aun así, no fue hasta el año 2001 cuando tres grupos independientes, uno con el modelo de ratón y los otros dos con el modelo de pollo, confirmaron la existencia de una fuente adicional de progenitores a través de técnicas genéticas y de marcaje (Waldo K.L. *et al*., 2001) (Mjaatvedt C.H. *et al*., 2001) (Kelly R.G. *et al*., 2001) (revisado en (Kelly, 2012)). La elongación y el giro del corazón son promovidos por la incorporación de una población de progenitores altamente proliferativa. Se localizan en el mesodermo faríngeo detrás del tubo cardiaco y se denominan campo secundario cardiaco (SHF), como contraposición al campo cardiaco primario (FHF) que forma el tubo (Buckingham M. *et al*., 2005). El SHF expresa el factor de transcripción con homeodominio LIM Islet1, y experimentos de trazado de linaje han mostrado que el ventrículo derecho, el tracto de salida (OFT) y la región de entrada (IFT) derivan de estos progenitores Islet1+ localizados en el mesodermo faríngeo. La mutación de este gen conlleva a la formación de un tubo cardiaco lineal que no puede girar y alargarse (Cai C.L. *et al*., 2003). Los progenitores Islet1+ son multipotentes, dada su capacidad para diferenciarse a cardiomiocitos, células endoteliales y células de músculo liso (Moretti A. *et al*., 2006).

Subdominios dentro del SHF: el AHF y el pSHF

Dentro del SHF se pueden distinguir subdominios, dependiendo de la expresión génica y de las regiones a las que contribuyen (Vincent S.D. and Buckingham, 2010). La región anterior del SHF (AHF) proporciona células al polo arterial del corazón y forma el ventrículo derecho y el OFT (Kelly R.G. *et al*., 2001) (Zaffran S. *et al*., 2004). El AHF se caracteriza por la expresión de algunos factores, como Fgf8, Fgf10, Tbx1, Mef2c SHF *enhancer*. Por otro lado, células que contribuyen a la región de entrada expresan Islet1, pero no los demás marcadores de AHF y se conforman el SHF posterior (pSHF). Se pudo comprobar que el canal atrioventricular (AVC), gran parte de los atrios y la afluencia sistémica venosa derivan del pSHF.

El establecimiento de patrón antero-posterior se regula por el ácido retinoico (RA). La mutación de retinaldehido dehidrogensa 2 (RALDH2), que cataliza el segundo paso de oxidación de la biosíntesis de RA, causa una severa deficiencia embrionaria en RA. Mutantes para esta enzima presentan una expansión posterior de marcadores de AHF, como Tbx1 y Fgf8, el tubo cardiaco no es capaz de girar y la formación de las atrios y el IFT es deficiente (Ryckebusch L. *et al*., 2008). La expresión de Islet1 también se expande caudalmente, sugiriendo que el RA controla los límites posteriores del SHF (Sirbu I.O. *et al*., 2008). Los genes Hox son una de las importantes dianas del RA. Su expresión define distintos subdominios a lo largo del eje antero-posterior del SHF que contribuyen tanto al atrio como al futuro miocardio de la base de la aorta (Bertrand N. *et al*., 2011).

Diferentes estudios han descrito una serie de factores de transcripción y de crecimiento que se expresan en el AHF y que están involucrados en la formación correcta del OFT y del ventrículo derecho, ya que su deleción genera defectos en la formación de estas estructuras. Así, la ablación de *Fgf8* del mesodermo faríngeo produce OFT y ventrículo derecho truncados, como consecuencia de la disminución de la proliferación celular y un aumento de la apoptosis en el AHF (Ilagan R. *et al*., 2006) (Park E.J. *et al*., 2006). Tbx1, un factor de transcripción T-box, responsable de muchos de los defectos del síndrome de delección de 22q11, también se expresa en el AHF y su ablación produce defectos de formación de OFT relacionados con una disminución de la proliferación celular (Zhang Z. *et al*., 2006). La vía canónica de Wnt/β-catenina también está activa en el mesodermo faríngeo. La deleción de β-catenina tiene como consecuencia la disminución de la proliferación de células Islet1+ y pérdida de señalización por Fgf8, lo cual produce un acortamiento de OFT y reducción del ventrículo derecho. Por otro lado, la estabilización de β-catenina en el núcleo produce un efecto opuesto: expansión de las células Islet1+, excesivo alargamiento del OFT, ventrículo derecho anormal y defecto en la diferenciación de células Islet1+ en el OFT (Cohen E.D *et al*., 2007) (Qyang Y. *et al*., 2007) (Ai D. *et al*., 2007). Bmp2 y 4 se expresan en el OFT y promueven la diferenciación a miocardio de las células del SHF: la deleción de ambos produce un aumento en la expresión de genes de progenitores (Islet1 y Tbx1) y la reducción de los niveles de marcadores de miocardio, como la miosina sarcmérica, en el OFT proximal (Wang J. *et al*., 2010).

El desarrollo del polo posterior del corazón es menos conocido que el de la región AHF. Se ha visto que las células más craneales del pSHF contribuyen al AVC y a los atrios, mientras que regiones más caudales dan lugar al seno venoso. La contribución es simétrica desde la porción distal, pero el destino de la región craneal del pSHF es asimétrico, pues la región derecha contribuye a la parte ventral del atrio izquierdo (Domínguez J.N. *et al*., 2012). La vía Wnt/β-catenina desempeña un papel importante en la regulación del mesodermo cardiaco posterior; Wnt2, un activador de la vía, se expresa en el polo posterior del corazón y en la región de entrada desde el estadio E8.5. En embriones mutantes de Wnt2 la formación de los atrios y el AVC está comprometida, ya que su señalización es necesaria para la expansión de los progenitores del SHF y, más tarde, para la proliferación y diferenciación del miocardio, parcialmente a través de la activación de Gata6 (Tian Y. *et al*., 2010). Los cuernos del seno venoso derivan de una población de células posicionada ventro-caudo-lateral con respecto al SHF. Estas células no expresan Nkx2.5 o Islet1, pero están marcadas por la expresión de Tbx18 y dan lugar a un miocardio distinguible del miocardio de los atrios por su perfil de expresión Nkx2.5- Cx40- (Christoffels V.M. *et al*., 2006). Este borde lateral de mesodermo cardiogénico también contiene a los precursores del proepicardio que va a dar lugar al epicardio, vasos coronarios y fibroblastos.

Proliferación e incorporación del SHF

Uno de los cambios obvios que tiene lugar en el tubo cardiaco temprano es su crecimiento y el aumento del número de cardiomiocitos. Curiosamente, la proliferación de los precursores cardiacos decae drásticamente cuando se diferencian e incorporan al tubo cardiaco. De esta manera, los

cardiomiocitos del corazón temprano presentan un índice de proliferación muy bajo. Tanto en el pollo como en el ratón, el crecimiento temprano del corazón tiene lugar a través del reclutamiento de células a los polos del conjunto de progenitores de SHF (Soufan A.T. *et al*., 2006) (de Boer B.A. *et al*., 2012). Como se menciona arriba, varias vías de señalización importantes para el desarrollo del SHF promueven la proliferación. Recientes resultados en el pollo indican que el corazón se alarga gradualmente por los dos polos desde un único centro de crecimiento Islet1+ caudal bilateral, localizado en la pared pericárdica. Además, células de esta región se pueden rastrear conforme se desplazan cranealmente para diferenciarse en miocardio en el polo arterial (van den Berg G. *et al*., 2009) (van den Berg G. and Moorman, 2009). Sin embargo, aunque está claro que los precursores del SHF contribuyen a los polos, el mecanismo celular, por el cual los progenitores ingresan en el tubo cardiaco desde el SHF, se desconoce. En embriones de pollo, el SHF se ha descrito como una capa de epitelio columnar pseudoestratificado (Waldo K.L. *et al*., 2005). La vía no canónica de Wnt parece importante para el desarrollo del OFT. Mutantes de *Wnt11* muestran defectos tempranos en el OFT, donde aparecen afectados la reorganización del citoesqueleto y el movimiento celular polarizado, necesario para una morfogénesis normal del OFT. (Zhou W. *et al*., 2007). Disheveled (Dvl) actúa como regulador, tanto de la vía canónica Wnt/β-catenina, como de la vía PCP. Mutantes dobles de *Dvl1/2* presentan un acortamiento del OFT, similar al que se observa en mutantes de *Vangl2* y en los mutantes del activador de la vía no canónica, Wnt5a. Tanto en mutantes de *Dvl1/2*, como en los de *Wnt5a* el mesodermo visceral caudal presenta una aberrante compactación celular y una disminución en el número de filopodios. Se ha propuesto que las señalización por PCP induce una conversión mesénquimo-epitelial, promoviendo de esta manera la contribución del SHF al OFT por un proceso de intercalación (Sinha T. *et al*., 2012). Una doble delección de *Wnt5a* y *Wnt11* ha mostrado el requerimiento de estos factores para inhibir la vía canónica de Wnt/b-catenina, pero no se han analizado otros posibles defectos de SHF en estos dobles mutantes (Cohen E.D. *et al*., 2012).

Interacción del SHF con el endodermo faríngeo y las células de la cresta neuronal

El desarrollo, proliferación y reclutamiento del SHF dependen también de la interacción con otros tejidos. Así, el endodermo faríngeo ventral permanece en íntimo contacto con los precursores del SHF y genera algunas moléculas importantes para el mantenimiento del grupo de progenitores. Fgf8, aparte de expresarse en el SHF, también se expresa en el endodermo faríngeo, y su función en este tejido se requiere para una correcta septación del OFT (Park E.J. *et al*., 2006). Shh se expresa igualmente en el endodermo faríngeo y su deleción produce defectos en los dos polos. El AHF necesita Shh para la septación del OFT (Goddeeris M.M. *et al*., 2007) y la señalización por Shh es también requerida para la septación de los atrios (Hoffmann A.D. *et al*., 2009).

La cresta neural cardiaca (CNC) es una subpoblación de las células de la cresta neural que contribuye al músculo liso del arco aórtico faríngeo y que también migra a través del AHF hacia el OFT para contribuir a los cojinetes endocárdicos. Sin embargo, la ablación de la CNC produce no sólo defectos de septación, sino que conlleva una reducción del miocardio de OFT y defectos

en el polo arterial. En embriones de pollo se ha visto que células destinadas a formar el miocardio del OFT no son capaces de migrar correctamente y se quedan retenidas en la base del polo arterial (Waldo K.L. *et al*., 2005). La ablación de CNC produce un aumento de los niveles de Fgf8 en la faringe caudal, lo que interrumpe el ingreso de SHF en el corazón (Hutson M.R. *et al*., 2006). En el ratón, la mutación en *Tbx3*, que se expresa en la CNC, produce un acortamiento del OFT; en este caso, la incorrecta función de la CNC parece afectar la proliferación y el reclutamiento de las células del SHF (Mesbah K. *et al*., 2008). La señalización por BMPs parece también tener un papel importante en la comunicación entre CNC y SHF, ya que la deleción de *Smad4* de la CNC produce un aumento de apoptosis en estas células, pero además altera la expresión de algunos factores en el SHF y da lugar a defectos en elongación del OFT (Jia Q. *et al*., 2007).

¿Múltiples campos cardiacos?

La identificación de una segunda región mesodérmica como fuente de células cardiacas cambió la visión sobre la formación del corazón. Sin embargo, existe cierta controversia sobre si los llamados FHF y SHF representan dos linajes separados o reflejan una contribución y diferenciación graduales de los precursores. Islet1 fue considerado un marcador del SHF, pero estudios posteriores mostraron que la expresión de Islet1 es más amplia y que se puede detectar en la cresta cardiaca, en el FHF y, parcialmente, en el ventrículo izquierdo (Prall O.W.J. *et al*., 2007) (Ma Q. *et al*., 2008) (Sun Y. *et al*., 2007). De esta manera, más que marcar un linaje, la expresión de Islet1 parece estar relacionada con el estado de diferenciación de los precursores. Es interesante destacar que la deleción de *Islet1* no afecta la formación del tubo cardiaco primario y el fenotipo del mutante refleja principalmente un problema en la contribución del SHF al corazón (Cai C.L. *et al*., 2003). Para resolver la cuestión de la relación de linajes entre diferentes regiones cardiacas de manera independiente de la expresión génica, se llevó a cabo un trazado de linajes retrospectivo, donde recombinaciones de baja frecuencia producían clones aleatorios en el miocardio. Los autores han podido observar algunos clones en dos o más regiones contiguas del corazón, otros clones presentes exclusivamente en el ventrículo izquierdo o en los polos, y clones que se extendían a través de todo el tubo cardiaco. Los autores concluyen que el resultado apunta a la existencia de dos linajes que segregan temprano en desarrollo de un progenitor común y, mientras que la mayoría de las partes del corazón son colonizadas por los dos, existe una contribución exclusiva del primer linaje al ventrículo izquierdo y del segundo al OFT (Meilhac S.M. *et al*., 2004). Sin embargo, se puede dar una interpretación alternativa a estos resultados, según la cual la distribución de los clones en el corazón refleja la formación gradual de este órgano. En este caso, la recombinación en estadios más tempranos va a dar lugar a clones posicionados en el ventrículo izquierdo y en compartimentos cercanos, mientras la recombinación más tardía se da en precursores de los polos cardiacos, que se añaden más tarde (Moorman A.F.M. *et al*., 2007). Recientemente, se ha propuesto la existencia de un campo cardiaco terciario en el embrión de pollo. Según este estudio, las células generadoras del impulso eléctrico derivan de una región discreta del mesodermo localizada fuera de los clásicos FHF y SHF y reclutadas por señalización canónica de Wnt/b-catenina (Bressan M. *et al*., 2013). La

proposición de la existencia de distintos campos dentro de la región formadora de corazón (HFR) implica un específico compromiso de las células a cada uno de los diferentes campos. Experimentos clásicos llevados a cabo en embriones de pollo tempranos en los que se trasplantaban tejidos dentro del HFR, mostraron que las células recolocadas eran capaces de adaptarse a su nueva localización, contradiciendo, por lo tanto, una irreversible determinación de estas células (Satin J. *et al*., 1988). Sería interesante repetir estos experimentos con los conocimientos actuales sobre la formación cardiaca para obtener más evidencias sobre la naturaleza del HFR.

Diferenciación del tubo cardiaco

Una vez formado, el primitivo tubo cardiaco empieza a girar, mientras células Islet1+ se van añadiendo a sus polos y diferenciando a cardiomiocitos. El miocardio recién formado presenta características de un miocardio primario o embrionario, como son la baja tasa de proliferación, la baja conductividad, la baja contracción y la capacidad de despolarizarse espontáneamente. Pero, inmediatamente después del giro, se forman las cámaras (ventrículo y atrio) y el fenotipo del miocardio cambia: ahora, sus uniones *gap* están formadas por Cx40/Cx43 para una rápida conductividad y el índice de proliferación aumenta. Las otras regiones – el IFT, el AVC y el OFT – retienen las características de miocardio embrionario, hecho que desempeña un papel importante en el desarrollo del corazón (Christoffels V.M. *et al*., 2000). El miocardio del OFT y del AVC señaliza hacia el endocardio para formar los cojinetes endocárdicos, que en estadios más avanzados se remodelan para dar lugar a las válvulas cardiacas (Eisenberg L.M. and Markwald, 1995). Además, protege frente al reflujo de sangre antes de que se formen las válvulas y proporciona progenitores para el nodo del sistema conductor.

La regionalización del miocardio se consigue gracias a la expresión diferencial de genes. El miocardio naciente de las cámaras se caracteriza por la expresión de Anf, Cited1, Cx40, Cx43 y Chisel, mientras que Tbx2 y Tbx3 están presentes exclusivamente en regiones de miocardio primario. La deleción de Tbx5 del corazón embrionario produce una bajada en los niveles de Anf y Cx40 en las cámaras (Bruneau B.G. *et al*., 2001). Se ha visto que Tbx5 se asocia sinérgicamente con Nkx2.5 para promover la diferenciación de los cardiomiocitos; juntos se unen al promotor de Anf y activan su expresión (Hiroi Y. *et al*., 2001). Al mismo tiempo, Tbx2 se expresa en regiones de miocardio embrionario (IFT, AVC y OFT), donde también forma un complejo con Nkx2.5 y reprime la expresión de Anf (Habets P.E.M.H. *et al*., 2002). De esta manera, si se sobreexpresa Tbx2 en todo el miocardio, se inhibe la formación de cámaras y la expresión de Cx40/43 y de Anf; ello confirma la función de Tbx2 como un factor determinante en la represión de genes específicos de cámaras (Christoffels V.M. *et al*., 2004). Por otro lado, trazados de linaje genéticos mostraron que miocardio primario marcado por Tbx2 contribuye a los dos ventrículos: mientras está en el AVC y expresa Tbx2, la proliferación y diferenciación del miocardio están inhibidas, pero, una vez apagada la expresión de Tbx2, las células pueden iniciar la diferenciación a miocardio de cámara y empezar a proliferar (Aanhaanen W.T.J. *et al*., 2009). Tbx20, también un factor T-box, se expresa

a través de todo el miocardio y es esencial para asegurar la transición desde el tubo cardiaco a un corazón multicameral, ya que reprime la expresión de Tbx2. En mutantes de Tbx20, el miocardio de cámaras no se forma y se detecta expresión ectópica de Tbx2 en el corazón lineal (Singh M.K. *et al*., 2005). Otro gen que controla múltiples aspectos de morfogénesis de AVC es Bmp2. Además de tener un papel en la formación temprana del corazón, Bmp2 también se expresa a altos niveles en el AVC y más débilmente en el OFT. La deleción de Bmp2 del miocardio produce una reducción de los niveles de Tbx2 y la expansión de marcadores de cámaras al AVC (Ma L. *et al*., 2005). Se ha visto que Bmp2 regula directamente la expresión de Tbx2 a través de las pSmad1/5/8, que se unen a un *enhancer* de *Tbx2* capaz de conferir una expresión específica de canal a Tbx2. Tbx20 compite con Smad4 por la unión a Smad1 y Smad5 y, de esta manera, suprime la expresión de Tbx2 en las cámaras (Singh R. *et al*., 2009). Tbx20 también podría regular positivamente a Hey1 y Hey2. Estos dos genes, expresados en el atrio y en el ventrículo, respectivamente, regulan la frontera del AVC y reprimen la expresión de Tbx2 en las cámaras (Kokubo H. *et al*., 2007).

Tbx3 también pertenece a la familia T-box de factores de transcripción y, como los anteriores, está implicado en la regulación del desarrollo cardiaco. A estadios tempranos, Tbx3 se expresa de manera continua en un dominio del miocardio que se extiende del nodo sinoatrial a la región atrioventricular. De manera similar a Tbx2, Tbx3 reprime la expresión de Anf y Cx40 e impide su activación por el complejo Nkx2.5-Tbx5 (Hoogaars W.M. *et al*., 2004). La expresión de Tbx3 también delinea la región del nodo sinoatrial, responsable del control de la frecuencia y del ritmo de las contracciones cardiacas, y que funciona como el marcapasos del corazón. La sobreexpresión ectópica de Tbx3 produce una inhibición del fenotipo atrial en las células de dicha cámara e impone un fenotipo de células de marcapaso. Además, Tbx3 también es necesario para la especificación del fascículo atrioventricular y de las ramas próximas del fascículo, ya que reprime la proliferación y diferenciación y promueve el fenotipo de sistema conductor (Hoogaars W.M.H. *et al*., 2007) (Bakker M.L. *et al*., 2008). Aunque no se ha demostrado una regulación directa como en el caso de Tbx2, Bmp2 parece estar controlando la expresión de Tbx3, ya que su inactivación en el miocardio conlleva la pérdida de Tbx3 en el AVC (Singh R. *et al*., 2012).

Formación de válvulas

El primer paso en la septación del corazón es la formación de cojinetes endocárdicos, que más tarde son remodelados para dar lugar a válvulas atrioventriculares (las que se forman en el AVC) y válvulas conoventriculares (formadas en el OFT). Las capas de miocardio y endocardio del corazón temprano están separadas por una matriz extracelular, denominada gelatina cardiaca, que se expande focalmente para formar los cojinetes endocárdicos en el AVC y en el OFT. Más tarde, las células del endocardio que envuelven estos cojinetes sufren una transición epitelio-mesénquima (EMT) y las células mesenquimales formadas, precursoras de las futuras válvulas, invaden los cojinetes. Los siguientes pasos implican su proliferación y expansión, así como la elongación y remodelación de la válvula para formar las valvas maduras (von Gise A. and Pu, 2012). La EMT

endocárdica ocurre tanto en el AVC, como en el OFT, pero en el último caso empieza más tarde en el desarrollo embrionario e implica una importante contribución de las células de la cresta neural cardiaca; por ello, los dos procesos se discuten por separado.

Cojinetes del AVC

La EMT endocárdica depende tanto del miocardio especializado del AVC como del endocardio de los cojinetes y del intercambio de señales entre ellos. Bmp2, secretado desde el miocardio, se requiere para potenciar la formación de la gelatina cardiaca e inducir la EMT del endocardio (Ma L. *et al*., 2005). Existe un bucle de retroalimentación positiva entre Bmp2 y Tbx2/3; mientras que Bmp2 es necesario para inducir la expresión de estos factores de transcripción, lo cuales, a su vez, son necesarios para mantener los niveles de expresión de Bmp2, ya que en mutantes dobles de Tbx2/3 Bmp2 está reducido. Más aún, la incorrecta expresión de Tbx2 o Tbx3 en el corazón produce una expresión ectópica de Bmp2 en el miocardio de las cámaras, así como de marcadores de EMT, como Snail1 y Has2, en el endocardio que lo recubre, con la consecuente expansión de la gelatina cardiaca y la formación de cojinetes. Esta inducción es dependiente de Bmp2, ya que la inhibición del receptor de BMPs regula a la baja los marcadores de EMT y la formación de cojinetes (Singh R. *et al*., 2012) (Shirai M. *et al*., 2009). Ciertamente, Bmp2 puede sustituir el miocardio del AVC en cultivos de explantes de AVC, apoyando de esta manera su función como factor clave en la inducción de EMT (Sugi Y. *et al*., 2004) (Rivera-Feliciano J. *et al*., 2006). Algunos genes de EMT son activados por Bmp2, como, por ejemplo, Twist1, un activador de Tbx20 en el endocardio y promotor de la proliferación y migración de células mesenquimales, a la vez que inhibe la diferenciación de células de la válvula (Shelton E.L. and Yutzey, 2007) (Shelton E.L. and Yutzey, 2008). Tgf-β2 es otro factor importante para la EMT que actúa por debajo de la cascada de Bmp2. Los mutantes de Tgf-β2 presentan un número reducido de células mesenquimales; además, se requiere para completar estadios más tardíos de la EMT (Sugi Y. *et al*., 2004) (Azhar M. *et al*., 2009). Una función adicional de Tgf-β2 tiene que ver con la remodelación y diferenciación de la válvula, ya que induce la organización de la matriz extracelular y reprime la diferenciación del mesénquima de los cojinetes hacia el linaje de células de cartílago (Azhar M. *et al*., 2011).

La vía de señalización de Notch también está implicada en varios pasos de la formación de la válvulas. El receptor de Notch es una proteína transmembranal con un dominio extracelular, con el cual se une a sus ligandos (Delta o Jagged), y un dominio intracelular (NICD), que se libera después de la activación por los ligandos y se transloca al núcleo, donde activa la expresión de genes (Andersson E.R. *et al*., 2011). N1ICD (la forma activa de Notch1) se expresa en el endocardio que recubre el AVC y el OFT (del Monte G. *et al*., 2007), indicando que, a diferencia de Bmp2, promueve la EMT directamente desde el endocardio. La deleción de la actividad de Notch en el endocardio produce una reducción de los niveles de Tgf-β2 y de Snail1, factor clave para la EMT, y la ausencia de este proceso tanto *in vivo* como *in vitro* (Timmerman L.A. *et al*., 2004). Al contrario, si se sobreexpresa N1ICD a través de todo el endocardio, se produce una activación ectópica de genes mesenquimales. Notch, además, confina la expresión de Bmp2 al

miocardio del AVC, ya que Hey1 y Hey2, dianas de Notch, reprimen la expresión de Bmp2 en el endocardio. Las rutas de Bmp2 y de Notch1 convergen en la activación de Snail1 y promueven la formación de un campo valvulogénico en el corazón embrionario (de la Pompa J.L. and Epstein, 2012; Luna-Zurita L. *et al*., 2010).

Los cojinetes del OFT y las células de la cresta neural (NCCs)

El desarrollo de los cojinetes del OFT implica la interacción entre el endocardio, el mesénquima derivado del endocardio y las células de la cresta neural. Al mismo tiempo que el OFT se remodela y se separa en dos grandes vasos (la aorta y la arteria pulmonar), gira y se alinea con los ventrículos, de tal manera que la aorta salga del ventrículo izquierdo y la arteria pulmonar del derecho. El OFT contiene dos pares de cojinetes: los proximales, que forman el septo conal y separan el OFT proximal en las salidas derecha e izquierda del ventrículo; los distales, que forman el septo aortopulmonar necesario para dividir el OFT distal en aorta y arteria pulmonar. Al lado a estos cojinetes se forman los cojinetes intercalados y, juntos, forman las válvulas aórtica y pulmonar (Lin C.J. *et al*., 2012). La deleción de Bmp6 y Bmp7 del miocardio impide la invasión de los cojinetes por parte de las células del endocardio (Kim R.Y. *et al*., 2001). Al mismo tiempo, el SHF proporciona una fuente de Bmp4, necesario para la expansión de los cojinetes y su remodelación (Liu W. *et al*., 2004) (McCulley D.J. *et al*., 2008). Por otro lado, se ha demostrado que Tbx2, expresado en el miocardio del OFT, activa directamente la expresión de Tgf-β2 en el miocardio, el efector real de la inducción de EMT en los cojinetes del OFT (Sakabe M. *et al*., 2012).

Las células de la CNC migran de su posición original en los rombómeros 6-8 e invaden el OFT para formar el septo aortopulmonar. El miocardio del OFT secreta Sema3c para atraer a las células de la CNC y promueve la invasión de los cojinetes distales, donde se transforman en células mesenquimales (Toyofuku T. *et al*., 2008). Este mesénquima más tarde se diferencia en septo de músculo liso. Fgf8 juega un papel importante en la supervivencia de las NCCs durante su migración, ya que la reducción de sus niveles produce una muerte masiva de estas células, bien cuando se delaminan del tubo nervioso o bien cuando alcanzan la faringe (Abu-Issa R. *et al*., 2002). Se ha demostrado que, además, FGF estimula la expresión de Bmp4, el cual, a su vez, potencia la diferenciación de las NCCs a músculo liso (Zhang J. *et al*., 2010). Notch expresado en las NCCs también es necesario para su diferenciación (High F.A *et al*., 2009).

Maduración de las válvulas cardiacas

La remodelación posterior a la EMT, donde las células mesenquimales se diferencian a fibroblastos intersticiales y remodelan su entorno para formar una válvula madura, es un proceso poco conocido. La expansión de los cojinetes es promovida por la proliferación de células mesenquimales, controlada por múltiples señales, como la vía de Wnt/β-catenina, BMPs y Fgf4 (Combs M.D. and Yutzey, 2009). Se ha propuesto que existen dos zonas distintas en el cojinete en desarrollo: una zona de proliferación cercana al endocardio y una zona de diferenciación adyacente al miocardio, aunque los mecanismos para esta regionalización se desconocen (de

Vlaming A. *et al*., 2012). Durante los estadios fetales, la válvula se alarga para formar las finas valvas. Ello se consiguen gracias a un aumento en la densidad celular y a la reorganización de la matriz extracellular (Kruithof B.P. *et al*., 2007). La diferenciación de las células mesenquimales y la correcta distribución y ordenamiento de la matriz extracelular son dos procesos fundamentales para la formación de una válvula funcional. Periostina, una de las proteínas de la matriz extracelular, desempeña un papel importante en la estimulación de la ruta valvulogénica. Es secretada por las células de los cojinetes hacia la matriz extracelular y desde ahí, a través de la ruta β-integrina/FAK/ERK, promueve la adhesión, migración y supervivencia celulares, además de regular la expresión de hialuronano y del colágeno I, y de activar la compactación del colágeno (Norris R.A. *et al*., 2009) (Ghatak S. *et al*., 2014).

FAMILIA ARID

La familia ARID es una familia de factores de transcripción caracterizados por un dominio de unión a ADN muy conservado, denominado ARID. El nombre proviene de *AT rich interaction domain*, y se debe al primer estudio donde se describió el miembro fundador de la familia, Bright. En este trabajo, los autores localizaron un dominio de unión a ADN previamente desconocido, con afinidad a regiones ricas en AT (Herrscher R.F. *et al*., 1995). No mucho tiempo después, se describió el gen *dead ringer* (*dri*) en *Drosophila*, en un *screening* donde se intentaban localizar genes con propiedades de unión a ADN similares a las proteínas con homeodominio. El gen descrito carecía de cualquier homología al homeobox, pero su dominio ARID estaba relacionado con otros genes, como Bright. De esta manera, se estableció una nueva familia de proteínas de unión a ADN altamente conservada (Gregory S.L. *et al*., 1996). Más tarde, miembros de la familia ARID se encontraron en un amplio rango de especies, desde ~~las~~ levaduras hasta nematodos, insectos y mamíferos, así como en plantas y hongos (Zhu H. *et al*., 2008) (Hansen F.T. *et al*., 2008). Hay 15 proteínas descritas en humanos y 6 en *Drosophila*; miembros de esta familia participan en multitud de procesos, como la remodelación de cromatina, diferenciación celular, control del ciclo celular y desarrollo embrionario (Kortschak R.D. *et al*., 2000) (Wilsker D. *et al*., 2002).

Como el número de miembros de la familia ARID crecía, surgió la necesidad de definir con mayor precisión la secuencia consenso del dominio ARID. Esta secuencia comprende alrededor de 100 aminoácidos; fuera del dominio ARID, las proteínas de la familia muestran diversidad de secuencias, estructuras y funciones (Wilsker D. *et al*., 2002). El dominio ARID codifica para seis hélices a que forman un motivo no canónico de hélice-giro-hélice. La estructura 3D del complejo ADN con el dominio ARID mínimo, junto a la poca conservación de los aminoácidos responsables de la especificidad de unión al ADN, sugieren que la mayoría de los ARIDs se unen al ADN sin mucha fuerza y sin especificidad de secuencia, al contrario de lo que se pensaba antes (Iwahara J. *et al*., 2002) (Cai S. *et al*., 2007). De hecho, proteínas GST de fusión que incluían el dominio ARID de cada miembro de la familia han mostrado que la mayoría de las subfamilias ARID se unen al

ADN sin preferencia por ninguna secuencia (Patsialou A. *et al*., 2005). Algunos miembros de la familia, incluyendo a Bright y a Dri, presentan un dominio "ARID extendido (eARID)" con 40 aminoácidos más, que forman dos hélices extra, una en el N-terminal y otra en el C-terminal. Esta hélice C-terminal extra podría aumentar la afinidad de unión al ADN.

La familia ARID se puede subdividir en 7 subfamilias basándose en el grado de conservación de secuencia entre proteínas individuales. Algunas de las principales características de estas subfamilias se discuten a continuación:

ARID1: incluye a Arid1a y Arid1b, las dos mayores y mutuamente excluyentes subunidades de los complejos SWI/SNF, que son complejos remodeladores de cromatina dependientes de ATP. La presencia de uno u otro Arid1 en estos complejos determina la consiguiente asociación con activadores o supresores (Nagl N.G.Jr. *et al*., 2007). Arid1a se expresa más significativamente durante el desarrollo embrionario que Arid1b; los niveles de las dos proteínas se regulan durante las diferentes fases del ciclo celular (Flores-Alcantar A. *et al*., 2011).

ARID2: Arid2 forma parte de los complejos PBAF SWI/SNF; dentro del complejo, se requiere para mediar la expresión de genes en respuesta a interferón (Yan Z. *et al*., 2005).

ARID4: incluye a Arid4a (RBP1) y Arid4b (RBP1L1). Arid4a se clonó en un estudio donde se buscaban proteínas de unión a pRb. Se ha visto que pRb reprime la transcripción a través de la unión a Arid4a, que actúa como molécula puente para reclutar histona deacetilasas (HDACs), además de funcionar a otro nivel independiente de HDACs como represor (Lai A. *et al*., 1999) (Lai A. *et al*., 2001). Más aún, la deacetilasa de clase III SIRT1 se asocia con los complejos HDACs a través de Arid4a/b y de esta manera regula el silenciamiento de transcripción mediado por HDACs (Binda O. *et al*., 2008).

ARID5: incluye a Arid5a (MRF-1) y a Arid5b (MRF2). Arid5b está implicado en diferentes procesos. En cultivos celulares se ha visto que regula diferenciación y proliferación de células de músculo liso (Watanabe M. *et al*., 2002). Mutaciones de este gen en el ratón producen una reducción de la viabilidad, retraso en el crecimiento, anormalidades en los órganos reproductivos, así como defectos en los compartimentos de células T y B en los órganos limfáticos primarios (Lahoud M.H. *et al*., 2001). A nivel celular, Arid5b junto con Phf2, una jmjC demetilasa, forma un complejo de histona lisina demetilasa que actúa como modulador del estado de metilación de las histonas y de la transcripción génica en respuesta a señales (Baba A. *et al*., 2011). Este complejo actúa sobre los promotores de genes condrogénicos regulados por Sox9, consiguiendo así facilitar la condrogénesis (Hata K. *et al*., 2013). Recientes *screens* del genoma identificaron que las variaciones en ARID5B están asociadas con la susceptibilidad a la leucemia limfoblástica aguda infantil (ALL); estos polimorfismos son determinantes tanto para susceptibilidad a la ALL, así como para predecir el efecto del tratamiento (Healy J. *et al*., 2010) (Xu H. *et al*., 2012).

JARID1: esta subfamilia contiene cuatro miembros: Jarid1a (RBP2), Jarid1b (PLU-1), Jarid1c (SMCX) y Jarid1d (SMCY). Además del dominio ARID, estas proteínas poseen dos dominios

conservados jumonji (jmj) –jmjC (dominio con actividad histona demetilasa) y jmjN, además de un dominio PHD (Takeuchi T. *et al*., 2006). Las proteínas Jarid1a-c regulan la demetilación de histonas en vivo y contribuyen al silenciamiento transcripcional manteniendo los niveles de H3K4me3 bajos (Christensen J. *et al*., 2007). El silenciamiento de Jarid1a promueve la diferenciación; por otro lado, en presencia de pRb puede actuar como un co-activador y favorecer la diferenciación (Benevolenskaya E.V. *et al*., 2005). Jarid1b se expresa en algunos tejidos durante el desarrollo embrionario, como cerebro, primordio mamario, timo, pata, epitelio olfativo, dientes, ojos y estómago (Madsen B. *et al*., 2002). La delección de Jarid1b produce mortalidad embrionaria, mientras que mutantes de Jarid1a son viables y fértiles (Catchpole S. *et al*., 2011). Jarid1c juega un papel importante en el desarrollo del cerebro y su mutación en humanos produce en retraso mental asociado al cromosoma X. En sintonía con la patología humana, en el pez cebra y en neuronas primarias de mamíferos Jarid1c está involucrado en supervivencia neuronal y desarrollo de las dendritas (Jensen L.R. *et al*., 2005) (Iwase S. *et al*., 2007).

JARID2: también conocido como Jumonji. También contiene los dominios jmjC y jmjN, pero carece del dominio PHD. Está involucrado en el desarrollo cardiaco, ya que su deleción produce muerte neonatal debida a anomalías en el corazón, como defectos en el septo interventricular, no-compactación de la pared ventricular, ventrículo derecho con doble salida y atrio dilatado (Lee Y. *et al*., 2000). Jumonji reprime la expresión de Anf a través de la unión directa a Nkx2.5 y Gata4 (Kim T.G. *et al*., 2004); su propia expresión se inhibe por Nkx2.5 en el SHF (Barth J.L. *et al*., 2010). Varios estudios apuntan a una función importante de Jarid2 en el reclutamiento de complejos represores PRC2, que presentan acción histona metilasa, a sus genes diana. La delección de Jmj impide una correcta diferenciación en embriones de *Xenopus laevis* y en células de ratón embrionarias, consistente con el papel esencial de proteínas PRC2 en desarrollo temprano (Peng J.C. *et al*., 2009) (Li G. *et al*., 2010) (Pasini D. *et al*., 2010) (Landeira D. *et al*., 2010).

Subfamilia ARID3

La subfamilia Arid3, como ya se mencionó arriba, presenta un dominio ARID extendido con dos hélices extra, y que podría estar implicado en la especificidad de reconocimiento del ADN (Iwahara J. and Clubb, 1999) (Iwahara J. *et al*., 2002). La subfamilia incluye a Dead ringer de *Drosophila* y a sus tres homólogos mamíferos –Arid3a/Bright, Arid3b/BDP y Arid3c– y están presentes específicamente en los metazoos (Kortschak R.D. *et al*., 2000). Aparte del dominio ARID, esta subfamilia se caracteriza por dos dominios en la región C-terminal denominados REKLES-α y REKLES-β, no presentes en ninguna proteína no-Arid. Estos dominios contienen una señal de localización nuclear (Kim D. and Tucker, 2006). Se ha propuesto que REKLES-β se requiere para la homedimerización de las proteínas Arid3 y su unión a otras proteínas, así como la interacción con la matriz nuclear (Kim D. *et al*., 2007). Sin embargo, existe cierta controversia sobre esta función, ya que un estudio anterior indica que REKLES-β no es necesario para la homodimerización (Shandala T. *et al*., 2002).

Dead ringer/Retained en el desarrollo de Drosophila

Dead ringer/Retained (Dri/Retn) se puede detectar desde las primera horas del desarrollo de *Drosophila*, expresado en el núcleo ubicuamente hasta después de la gastrulación. Después de la extensión de la banda germinal, se localiza predominantemente en el mesodermo, y durante la embriogénesis se puede detectar en los músculos de la faringe, en diferentes regiones del cerebro y del tubo digestivo, y en la amnioserosa extraembrionaria (Gregory S.L. *et al*., 1996). Los mutantes de *Dri* mueren durante el desarrollo embrionario. Es esencial para el establecimiento de patrón temprano, y la expresión de algunos genes de clase Terminal, como *argos* y *buttonhead*, así como *even-skipped*, un gen requerido para la segmentación, está alterada en los mutantes de *Dri*. Además, está afectado el desarrollo de la musculatura somática. Curiosamente, el fenotipo más drástico, incluyendo defectos en el establecimiento de patrón, se da cuando el *Dri* de origen materno es eliminado, mientras que la deleción exclusiva del *Dri* embrionario produce sólo defectos musculares y digestivos (Shandala T. *et al*., 1999). El uso de mutantes hipomorfos para *Dri* permite el estudio de la función del gen en el desarrollo más tardío de la glía longitudinal, donde está involucrado en su diferenciación y migración a su lugar de destino (Shandala T. *et al*., 2003). Dri también está implicado en el establecimiento de patrón dorso-ventral. El reclutamiento de Groucho, dependiente de Dri, a los sitios de unión de Dorsal (Dl), produce un cambio en la función de Dl a represor, lo cual permite la restricción de la expresión de *Zernült* (*Zen*) a la región dorsal, además de suprimir la expresión de *Huckbein* (*Hkb*) en la región ventral (Häder T. *et al*., 2000). Los datos obtenidos hasta el momento sobre Dri sugieren que este gen puede actuar tanto como co-activador como co-represor, dependiendo del contexto celular.

Arid3a y Arid3c

Arid3a/Bright es el gen más estudiado de los tres homólogos mamíferos de Dri. En adultos se expresa específicamente en los linfocitos B, tanto en humanos como en ratón, y su función más conocida es la regulación de la expresión de la cadena pesada de la inmunoglobulina (Herrscher R.F. *et al*., 1995) (Nixon J.C. *et al*., 2004). Se pueden observar complejos Arid3a-ADN en los núcleos de células B activadas (Webb C.F. *et al*., 2000). También se ha sugerido que Bright contribuye a un aumento de la expresión génica a través de la remodelación del locus de la inmunoglobulina (Kaplan M.H. *et al*., 2001). Durante el desarrollo embrionario, la deleción de Arid3a produce una muerte a mitad de la gestación por un fallo en la hematopoyesis, ya que las células madre hematopoyéticas no consiguen diferenciarse a eritrocitos maduros (Webb C.F. *et al*., 2011). Recientemente, se ha propuesto la implicación de Arid3a en pluripotencia y diferenciación. Células deficientes en Arid3a de tejidos adultos expresan algunos genes asociados a la pluripotencia, se expanden indefinidamente y se diferencian espontáneamente a células de múltiples linajes, sugiriendo así su función en la supresión de la pluripotencia (An G. *et al*., 2010). Además, aparece como proteína de unión a Oct4 en células madre de ratón, aunque son necesarios estudios más específicos para confirmar la importancia de esta unión en vivo (Pardo M. *et al*.,

2010) (van den Berg D.L.C. *et al*., 2010). También aparece, junto a Arid3b, como uno de los genes más expresados después de la diferenciación de la células madre (Wang J. *et al*., 2006).

Arid3c es el miembro menos conocido de la subfamilia Arid3. Sólo recientemente se ha descrito que su gen codifica para dos formas de *splicing* alternativas, una de las cuales carece del dominio REKLES. La isoforma más larga co-activa la transcripción de inmunoglobulinas dependiente de Arid3a (Tidwell J.A. *et al*., 2011).

Arid3b

Arid3b había sido descubierto a través de un *screen* de una biblioteca de testículo humano y se vio que también se expresa en otros tejidos adultos, como placenta y leucocitos. Se denominó Bdp (Bright-derived protein) y se confirmó su homología a Bright y a Dri. Además, se detectó su capacidad de unirse a pRb *in vitro* (Numata S. *et al*., 1999). En el campo del cáncer, algunos estudios apuntan a una importante función de esta proteína en diferentes tipos de tumores. Arid3b se expresa en varias líneas celulares derivadas de neuroblastomas y su crecimiento se detiene si la expresión de Arid3b se inhibe por siRNA. Además, también se ha detectado en algunos neuroblastomas humanos en la fase IV del tumor. La sobreexpresión de Arid3b en fibroblastos embrionarios de ratón (MEFs) produce la inmortalización de estas células. La co-transfección con MYCN amplifica su actividad oncogénica al inhibir la apoptosis que induce MYCN, tanto en MEFs, como en células madre neuronales (Kobayashi K. *et al*., 2006) (Kobayashi K. *et al*., 2013). Por otro lado, Arid3b se encuentra sobreexpresado en cánceres de ovario malignos donde está involucrado en la transformación mesenquimal del epitelio ovárico (Cowden Dahl K.D. *et al*., 2009). De manera similar, en células de cáncer de pecho, Arid3b se ha descrito como una diana de miR-125b con una función en motilidad celular, ya que su silenciamiento transitorio disminuye la migración celular (Akhavantabasi S. *et al*., 2012). Más recientemente, se ha detectado una forma de *splicing* alternativa de Arid3b en diferentes líneas tumorales, incluyendo cáncer ovárico. Las formas larga y corta muestran distintas distribuciones intracelulares y distinta capacidad de inducir apoptosis (Joseph S. *et al*., 2012). Adicionalmente, experimentos de Chip-seq sugieren que Arid3b podría ser una diana directa de p53; precisamente, su expresión está desregulada en diferentes cánceres donde p53 está mutado (Garritano S. *et al*., 2013).

Menos se sabe sobre la función de Arid3b durante el desarrollo embrionario. El primer trabajo publicado describe un patrón dinámico de expresión del gen en diferentes estructuras, sobre todo arcos branquiales, cresta neural, rombómeros, OFT del corazón, vesícula ótica y somitos nacientes. También describe un mutante de pérdida de función que muere a mitad de gestación (E11.5-12.5) con retraso de crecimiento y defectos craneofaciales y cardiovasculares. El fenotipo más destacado es una muerte masiva del mesénquima craneal que los autores señalan como la causa de la muerte embrionaria, así como la causa del fenotipo cardiovascular (Takebe A. *et al*., 2006).

Arid3b también está involucrado en el desarrollo de la extremidad. Su expresión se puede detectar en la cresta ectodérmica apical (AER). Mientras que rutas de señalización importantes

para la formación del AER están inalteradas, tanto en ratón como en ensayos de pérdida de función en el pollo, la maduración y estructura del AER están afectadas. No se produce la compactación del AER y marcajes con DiI en vivo de células de pre-AER en embriones de pollo muestran una reducción en la motilidad de estas células y una aberrante contribución al AER en ausencia de Arid3b. Los resultados apuntan a un papel de Arid3b en la regulación de movimientos y reorganizaciones celulares que permiten la maduración del AER (Casanova J.C. *et al*., 2011).

Algunos estudios recientes identifican a Arid3b como una proteína con funciones en el mantenimiento y diferenciación de células madre. Ciertamente, de manera similar a lo que ocurre en los tumores, Arid3b protege células ES de ratón de la apoptosis inducida por MYCN; los dos genes aumentan su expresión cuando células madre neuronales se desdiferencian a células pluripotentes inducidas (iPC) (Kobayashi K. *et al*., 2013). Curiosamente, en otro estudio Arid3b aparece como uno de los genes más abundantes después de la diferenciación de las células ES (Wang J. *et al*., 2006). Además, Arid3b se identificó en varios *screens* como una posible proteína de unión a Oct4 en células ES de ratón y como una posible diana de Oct4, aunque no se ha obtenido ninguna confirmación biológica al respecto (Wang J. *et al*., 2006) (Wang J. and Orkin, 2008) (Sharov A.A. *et al*., 2008). Aún ahora las funciones específicas de Arid3b siguen sin estar claras.

OBJECTIVES

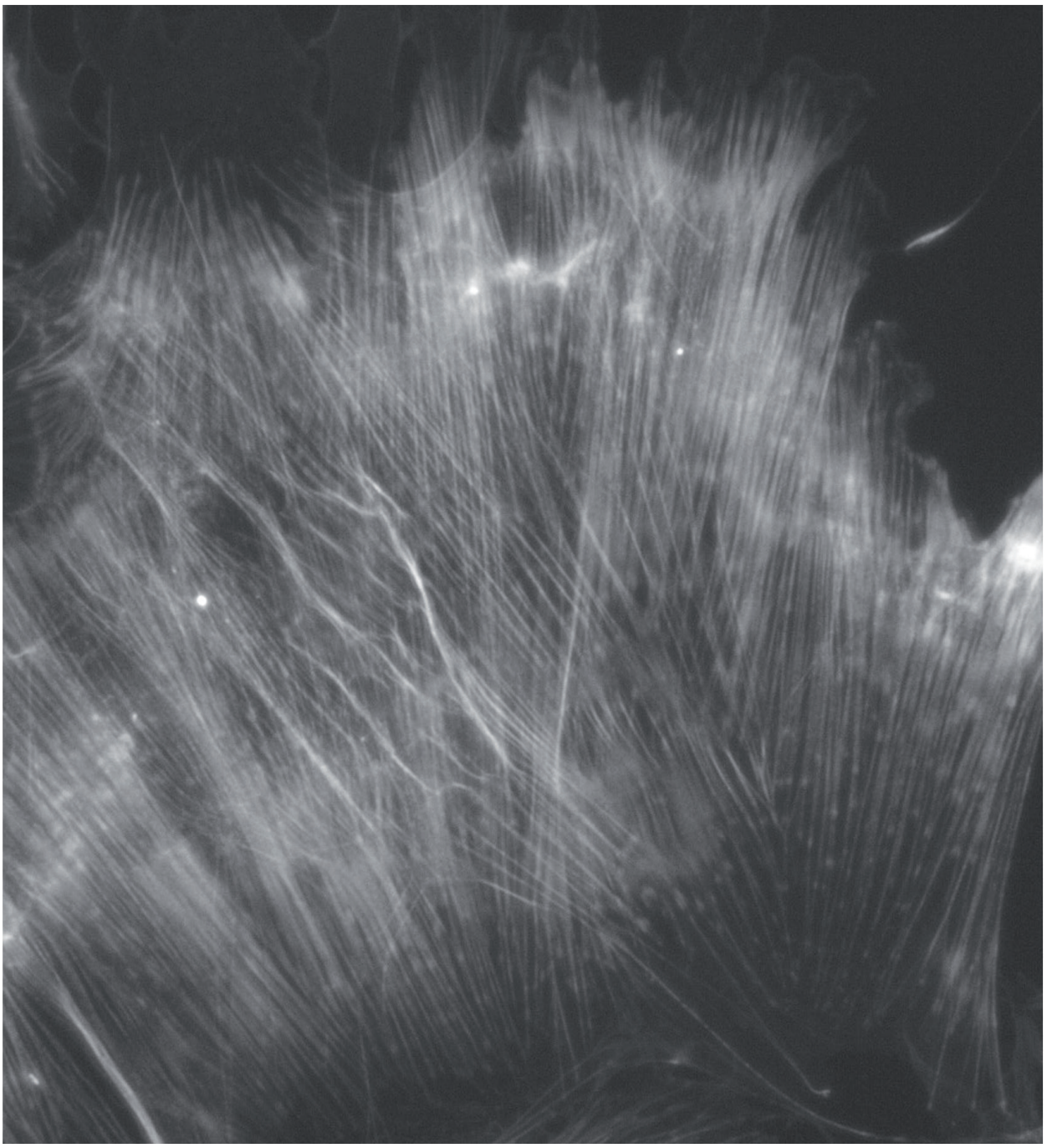

In the course of a candidate gene screen looking for new genes potentially involved in vertebrate limb development, the pattern of expression of *Arid3b* was analysed in mouse embryos. Although a previous study dismissed a direct role of Arid3b in heart development, we could detect expression in different regions of the heart and wondered whether it might be directly involved in its embryonic development. To address this question we decided to propose the following objectives.

1. To describe in detail the expression pattern of *Arid3b* in the heart

2. To analyse the role of Arid3b in early heart development using a mouse genetic model of loss-of-function of *Arid3b*

3. To search for Arid3b molecular targets and to understand the mechanisms of its function

4. To generate a conditional *Arid3b* floxed mouse line to determine tissue-specific functions of the gene during development

MATERIALS AND METHODS

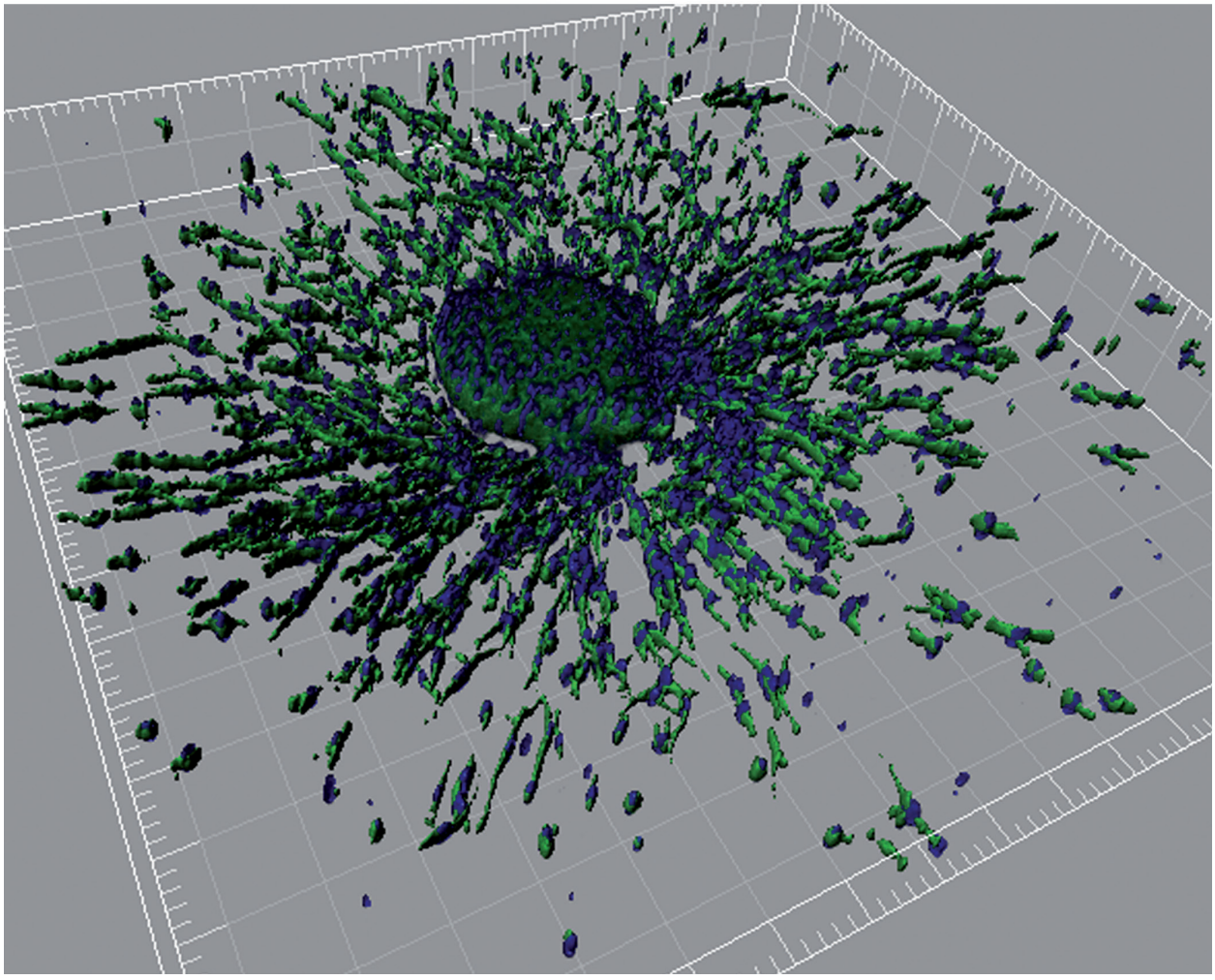

Embryo staging

Mouse embryos were collected at the indicated gestational stages, with E0.5 defined as noon on the day on which a vaginal plug was detected. For a more precise staging, pairs of somites (ps) were counted and groups were assigned as follows: E8.5 (8-12 ps), E9.0 (13-16 ps), E9.25 (17-23 ps), E9.5 (24-26 ps). Embryos were dissected in cold PBS and fixed overnight in 4% PFA at 4°C.

Mouse lines

Mouse Arid3b gene-trap line

A mouse line (CD1;129P2-Arid3bGt(RRJ028) Byg) was generated as previously described from a Baygenomics gene trap ES cell line: (http://www.genetrap.org/cgi-bin/annotation.py?cellline=RRJ028), which has an insertion of vector pGT0lxf in the intron after the first coding exon of *Arid3b*. This produces a fusion protein between the N-terminal of Arid3b and β-galactosidase enzyme, which lacks all the functional domains of Arid3b (**Figure 5**). Adult mice were genotyped by PCR from tail DNA, based on amplification of the first coding Arid3b exon (wt and heterozygous) and the presence of the β-Geo cassette in the gene-trap vector (heterozygous). Mutant (*Arid3b*$^{gt/gt}$) embryos were obtained by mating heterozygous animals. Embryos were genotyped by β-Gal activity, measured as the clear different intensity of staining due to different lacZ dose (**Figure 6**). Heterozygous mice were viable and fertile and both wild type and heterozygous embryos were used as controls; for simplicity, we always use the term wild type for the control.

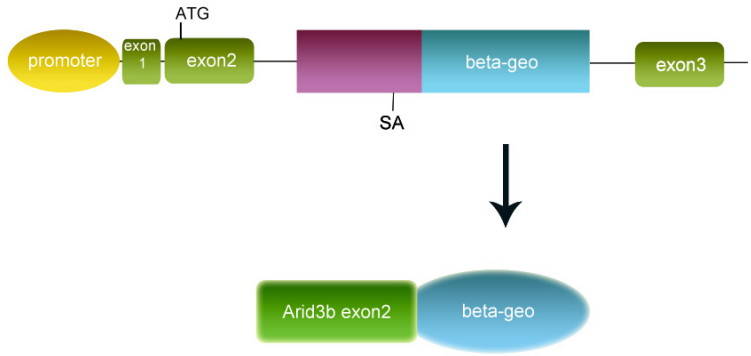

Figure 5. Scheme representing the *Arid3b* locus in the gene-trap mouse line. The β-geo cassette is located somewhere in the intron$_{2\text{-}3}$ and has a splice acceptor site (SA) and stop codon after the β-galactosidase sequence. The resulting product of translation is a fusion protein between the N-terminal region of Arid3b (which lacks functional domains) and the β-geo.

For genotyping adult mice the following set of primers were used:

Forward primer wild type: 5'-CAGCAGAAGCAGCCACAGCAG-3'

Reverse primer wild type: 5'-AGTTCGCACCCATCCTACACC-3'

Fragment size: 589 pb

Forward primer heterozygous: 5'-ACTATCCCGACCGCCTTACT-3'

Reverse primer heterozygous: 5'-ATACTTTCTCGGCAGGAGCA-3'

Fragment size: 720 pb

PCR programme for genotyping:

94ºC	3'30''		
94ºC	30''	}	x30 cycles
60ºC	30''		
72ºC	2'30''		
72ºC	5'		
4ºC	…		

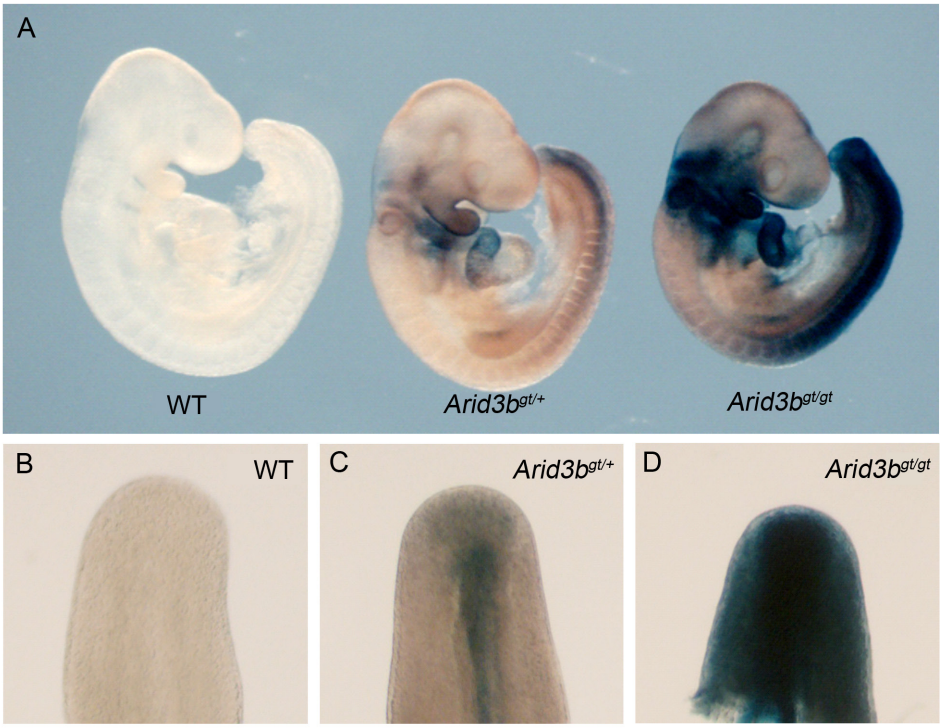

Figure 6. β-Gal activity in wild type, *Arid3b*$^{gt/+}$ and *Arid3b*$^{gt/gt}$ embryos enables to distinguish between different genotypes. Whole embryos (**A**) and tails (**B-D**) stained with Lac-Z in parallel; the difference in intensity between embryos allowed us to use this technique to genotype the embryos.

Arid3b floxed mice line

The Arid3b floxed line was generated by Gene Bridges Inc. The target floxed sequence was *Arid3b* second exon, which contains the ATG (**Figure 7**). Briefly, the PKG-gb2-*neo*/*km* cassette was inserted into the subcloned *Arid3b* sequence, containing the homology arms, and the whole construction was cloned into pMV vector (**Figure 8)** and electroporated into ES cells. Neomicin

(G-418) treatment was used to select electroporated clones, DNA was extracted and homologous recombination checked by Southern blot. Positive clones were injected into wild type blastocysts and implanted into foster mother to generate chimaeric mice. The ES cells used were from R1 (129sv x129/sv-CP) background, while the blastocysts used were from C57BL/6 background. This enabled the selection of chimaeric mice by the colour of their fur. One chimaeric male form the first injections was able to transmit the colour to its progeny, suggesting germ line transmission of the floxed allele and, indeed, we confirmed by genotyping that his offsprings were genetically modified. To eliminate the neo cassette, *Arid3b*$^{flox/flox;Neo\ cassette}$ mice were crossed with mice carrying a Flp transgene which acts on FRT sites and liberates the cassette (Schaft J. *et al*., 2001) (**Figure 7**).

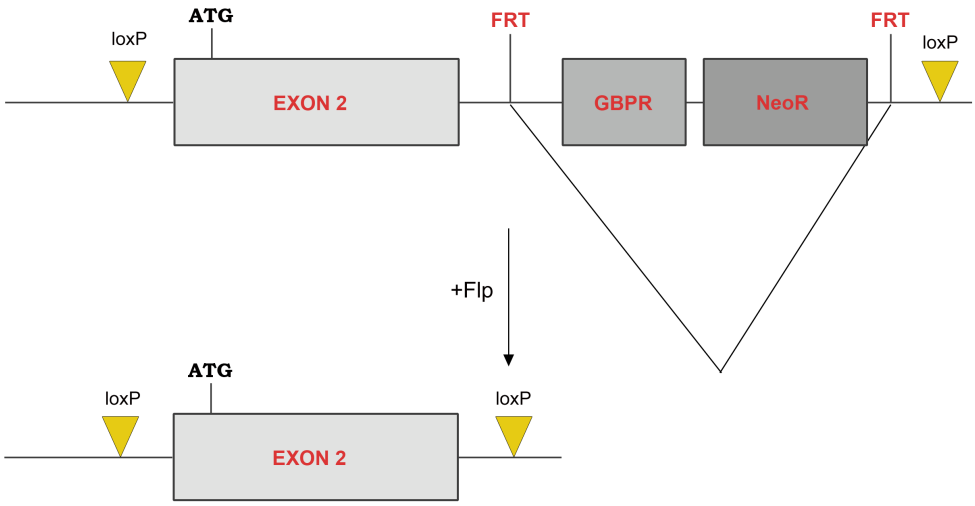

Figure 7. Schematic representation of the *Arid3b* floxed allele. The construction contains a resistance cassette flanked by FRT sites and the whole construction is flanked by loxP sites. The targeting sequence is the second exon where the ATG is located. Addition of Flp liberates the resistance cassette and now the second exon appears flanked by the loxP sites.

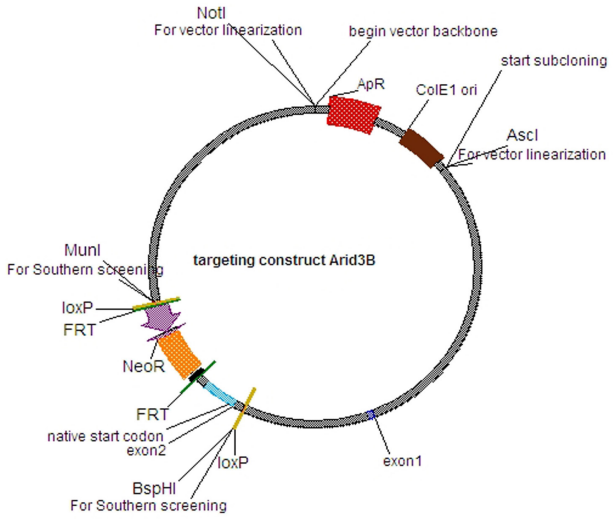

Figure 8. Targeting construct used for generation of *Arid3b* floxed line.

For genotyping adult mice and embryos, two pair of primers were used. The first surrounds the 3' loxP site and produces a 323 pb PCR product by wild-type allele and 365 pb band when the loxP site is present (**Figure 9**):

Forward primer 5'-TCTGCAGCCACTGAGATTTG-3'

Reverse primer 5'-GCTGCAGAGGCTCCATTACT-3'

The second pair of primers amplifies the region flanked by loxP sites. It produces a 1320 bp fragment by wild-type allele, 1446 bp in the presence of the loxP sites and a 383 pb fragment after Cre deletion (**Figure 9**).

Forward primer 5'-TCTGCAGCCACTGAGATTTG-3'

Reverse primer 5'-CTTGCTATCATCTTCAGCTTTTTG-3'

PCR program for genotyping:

94ºC	5'	
94ºC	30''	} x30 cycles
60ºC	45''	
72ºC	2'	
72ºC	10'	
4ºC	…	

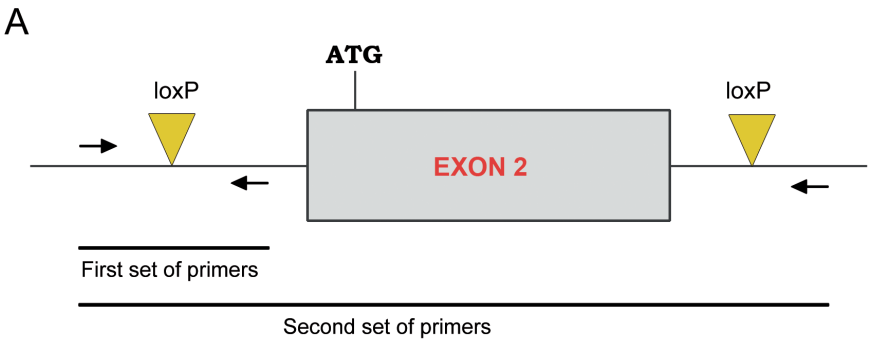

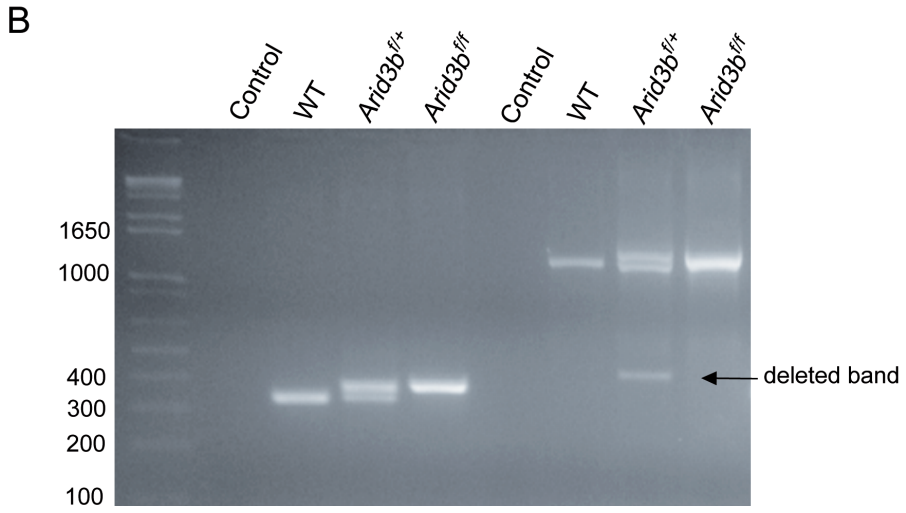

Figure 9. PCRs used to genotype *Arid3b*$^{flox/flox}$ embryos and adult mice. A. Schematic representation of the localization of the primers used for genotyping in the *Arid3b* gene. **B.** PCR with genomic DNA extracted from yolk sacs of E9.5 *Arid3b*$^{flox/flox}$*/Nkx2.5-Cre* embryos. The first set of primers, which flank the 3' loxP site, produces a PCR product of 323 pb in wild type alleles and a 365 pb in presence of a loxP site (right). The second set of primers are located upstream and downstream the two loxP sites. A 1320 pb band is synthetized in a wild type allele and a 1446 pb fragment when the second exon is flanked by loxP sites. In the presence of Cre, the second exon is deleted and a remaining 383 bp fragment is amplified.

The Arid3b flox/flox line was crossed with the following Cre-lines:

- Sox2-Cre (Hayashi S. *et al*., 2002) genotyping conditions to detect the Cre:

Forward primer: 5'-TGACGGTGGGAGAATGTTAA T-3'

Reverse primer: 5'-GCCGTAAATCAATCGATGAGT-3'

94ºC	4'	
94ºC	30''	} x32 cycles
56ºC	30''	
72ºC	1'	
72ºC	10'	
4ºC	…	

Expected PCR fragment: 286 pb

- Nkx2.5-Cre (Stanley E.G. *et al*., 2002) genotyping conditions:

Nkx2.5Cre Antisense: 5´ GCGCACTCACTTTAATGGGAAGAG 3´

Nkx2.5Cre Sense: 5´ GCCCTGTCCCTCAGATTTCACACC 3´

Nkx2.5Cre: 5´ GATGACTCTGGTCAGAGATACCTG 3´

94ºC	5'	
94ºC	30''	} x30 cycles
60ºC	30''	
72ºC	1'	
72ºC	10'	
4ºC	…	

Expected PCR fragment: a 264 pb fragment for the wild type allele and 583 pb fragment when a cre allele is present.

Embryo extraction and dehydration for whole-mount staining

Embryos were dissected in cold PBS (10 mM $Na_2HPO_4 \cdot 2H_2O$, 2 mM KH_2PO_4, 2.7 mM KCl, 137 mM NaCl at pH 7.4) and fixed in 4% paraformaldehyde in PBS (PFA) overnight at 4ºC. Next day they were washed twice in PBT (0.1% Triton X-100 in PBS) and dehydrated through methanol:PBT (50%, 75%, 100%) series and finally stored in methanol 100% at -20ºC untill used.

Paraffin embedding

Embryos were dissected in PBS and fixed overnight in 4% PFA at 4ºC. After two rinses in PBS, embryos were dehydrated through ethanol:water series (30%, 50%, 70%, 85%, 90%, 96%, 100%) at room temperature. Then they were washed twice in xylol and two times in paraffin wax at 65ºC. Embryos were oriented in warm paraffin and the blocks left solidify overnight.

Gelatin-sucrose embedding for cryostat sectioning

Embryos were dissected in PBS and fixed overnight in 4% PFA at 4ºC. They were washed twice in PBS at 4ºC and transferred into a sucrose 15% in PBS at 4ºC till the samples went to the botton of the tube. Next they were incubated in sucrose 15% in PBS, gelatin 7.5% in PBS for 30-60 minutes at 37ºC and embedded at room temperature. The blocks were left to cool at 4ºC and then frozen in isopentane at -72ºC for 1 minute and stored at -80ºC until cryostat sectioning.

Digoxigenin-labelled riboprobe synthesis

Total RNA from E9.5 and E10.5 mouse embryos was extracted with Qiagen extraction Rneasy Mini Kit (Qiagen, ref. 74106); cDNA was synthesized with High Capacity cDNA Reverse Transcription Kit (Applied Biosystems, ref. 4368814). Specific PCR primers usually located in the 3' UTR were designed for each probe with primer 3 software. Sp6 or T7 promoter sequences were added to the 5' of the reverse primer to generate anti-sense probes or to the 5' of the forward primer to generate sense probes. Alternatively, plasmids containing the required DNA fragment were linearised and purified with Qiagen gel extraction kit. Digoxigenin-labelled riboprobe synthesis was performed according to manufacturer's protocol (Roche). **Table 1** depicts the riboprobes used in this thesis. In (**Figure 10**) the two riboprobes designed against *Arid3b* are depicted.

GENE	CUT	Transcrition of a-probe	Origin
Anf	BamHI	T7	Robert Kelly
β-galactosidase	PstI	T7	Primers used for genotyping heterozygous mice (this thesis)
Bmp2	EagI	T3	Ángela Nieto
Bmp4	EcoRI	Sp6	Ángela Nieto
Cx40	XhoI	T3	Robert Kelly
Fgf8	HindIII	T7	Marián Ros
Fgf10	BgIII	Sp6	Robert Kelly
Hand1	NotI	T7	Robert Kelly
Hand2	EcoRI	T7	Robert Kelly
Has2	SalI	T3	J.L. de la Pompa
Hey1	EcoRI	T3	J.L. de la Pompa
Hey2	SalI	T3	J.L. de la Pompa
HeyL	EcoRI	T3	J.L. de la Pompa
Islet1	SacII	Sp6	This thesis
Mef2c	NotI	T7	J.L. de la Pompa
Mlc2a	BanHI	T7	J.L. de la Pompa
Mlc2v	SmaI	T7	J.L. de la Pompa
Nkx2.5	XbaI	T7	J.L. de la Pompa
Snail1	XbaI	T3	J.L. de la Pompa
Tbx1	KpnI	T3	Robert Kelly
Tbx2	EcoRI	T3	J.L. de la Pompa
Tbx3	PstI	T3	Robert Kelly
Tbx5	EcoRV	T7	J.L. de la Pompa
Tbx20	NotI	T3	J.L. de la Pompa
Tbx18	HindIII	T7	J.L. de la Pompa
Tgfb2	HindIII	T7	J.L. de la Pompa
Twist1	SalI	Sp6	J.L. de la Pompa

Table 1.1. List of probes used during the thesis cloned in plasmids.

GENE	PRIMERS	Length	Origin
Arid3b	5'-CAAGAACCCAGAGCAACACC-3' 5'-GAGTAGAGCCCGCAATGAGG-3'	1209 pb	Casanova *et al.*, 2011
Arid3b ex2	5'-GTTGAGAGCCATGCCAGTCT-3' 5'-AAGCTGCTCATCCAGACTCC-3'	460 pb	This thesis
Bhlhb2	5'-GGATTTTGCCCACATGTACC-3' 5'-CCTTCTCCAATTCACCTCCA-3'	671 pb	This thesis
Dkk3	5'-TTGGCTTCATAGGGGAAGTG-3' 5'-TTGTGTAGCCACTGCCTCAG-3'	537 pb	Witte *et al.*, 2009
Gata4	5'-GTGATCCTAGAGTGGCTGTAG-3' 5'- GTCCTGGGAACAGTATTGTGC -3'	546 pb	Robert Kelly
Insc	5'-GCAGGTAGACTCGGTTCAGC-3' 5'-AGCTCAATCAGGCGAGACAT-3'	1347 pb	This thesis
Kcne3	5'-TTTCTGTCTGTGCCCATTTG-3' 5'-GGGCCTATCAGTCCCTCTTC-3'	644 pb	This thesis
Kdm3a	5'-CCTGCAGACCATGACCCTAT-3' 5'-TTGAATGAGCTGTCCAGACG-3'	676 pb	This thesis
Lims2	5'-CCGGCACTATGAGAAGAAGG-3' 5'-AGAGGTGGGTTTGCTGACAC-3'	784 pb	This thesis
Nox4	5'-GGATTTCTGGACCTTTGTG-3' 5'-CAGATAAAGTACAGTCTTCTTA-3'	525 pb	This thesis
Smyd1/BOP	5'-TCAGCATTGCATCAGAGGTC-3' 5'-ATGGTGGGATCTAGCACCTG-3'	569 pb	This thesis
Sox7	5'-GCACAGCTGCTACCGCGAAGG-3' 5'-AATCCTACTGCAAACAGCTCCCAAGG-3'	859 pb	Takash *et al.*, 2001
Unc45b	5'-TACGGCAGGCAGCCACCGAATGCATGTG-3' 5'-CAGTCTACAGCCCGTTATCTGGCCTGC-3'	755 pb	Price *et al.*, 2002
Vggl2	5'-TACTTCCAGGGGGACATCAG-3' 5'-AAGGCTCAGTAGTCGCGTGT-3'	605 pb	This thesis

Table 1.2. List of probes used during the thesis obtained by PCR.

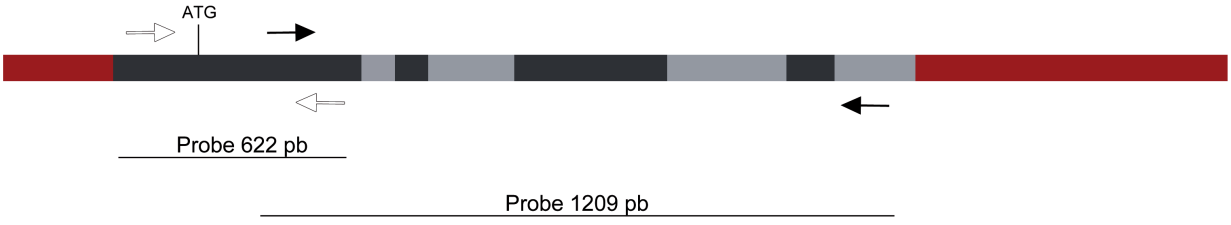

Figure 10. Schematic representation of the localization of the probes used. The largest probe (black arrows) covers almost the whole length of the mRNA and was used to describe the pattern of expressión of Arid3b. The short probe (white arrows) is located in the second exon where the ATG is located and was used to check for its deletion.

In situ hybridisation in whole mount embryos and on paraffin sections

Whole-mount *in situ* hybridisation was performed as previously described (Wilkinson D.G. and Nieto, 1993). Whole embryos were rehydrated and digested with proteinase K 10 µg/ml for 4 minutes (E8.5-9.0) or 7 minutes (E9.5). The incubation with the probes was performed at 65ºC overnight. *In situ* hybridisation on sections (7 µm) was performed in paraffin-embedded embryos according to previously described protocols with some modifications (Jostarndt K. et al., 1994) (Kanzler B. et al., 1998). Sections were rehydrated and digested with proteinase K 10 µg/ml at 37ºC for 10 minutes. Overnight hybridisation was performed at 65ºC. Both embryos and sections were washed next day, incubated with anti-DIG antibody and developed with BM-purple (Roche, ref. 11442074001). Images were acquired with a Nikon Eclipse 90i microscope and in a Leica MZ-12 dissecting microscope.

Lac- Z staining

Tails and embryos from E7.5-E12.5 were dissected in PBS and fixed with 0.125 % glutaraldehide in PBS for 15 minutes. Samples were washed twice in PBS for 10 minutes each time and incubated in LacZ buffer (0.08 mM $Na_2HPO_4 \cdot 2H_2O$, 0.03 mM $NaH_2PO_4 \cdot H_2O$, 2 mM $MgCl_2$, 0.11% sodium deoxicholate, 0.0035 mM igepal, 0.02 mM TrisHCl pH=7.3 in water) for another 10 minutes. The developing solution contained 5% X-gal as substrate, $K_4[Fe(CN)_6] \cdot 3H_2O$ 500 mM and $K_3[Fe(CN)_6] \cdot 3H_2O$ 500 mM and the enzymatic reaction was let to develop for 30-40 minutes for tails or several hours for embryos. Samples were washed twice in PBS, fixed in 4% PFA and kept at 4ºC.

Immunohistochemistry

Embryos were collected and fixed in 4% PFA at 4ºC overnight, dehydrated and embebedded in paraffin. Alternatively, embryos were included in gelatine-sucrose and frozen for cryostate sections. Immunochemistry was performed on 5 µm paraffin sections and on 8 µm cryostate sections. Images were acquired on a Leica TCS SP-5 confocal microscope or on a Nikon Eclipse 90i microscope.

Immunostaining for Troponin T, smooth muscle actin (SMA), sarcomeric myosin heavy chain, Islet1, Delta4 and periostin on paraffin sections

Slides were dewaxed and rehydrated, washed in distilled water and antigens retrieved by microwave heating for 15 minutes in 10mM citrate buffer, pH 6.0. They were left to cool at room temperature for another 15 minutes, washed in PBS and permeabilized with Triton X-100 0.5% for

10 minutes. Samples were washed twice in PBS and blocked for 1 hour in either 10% goat serum (Islet1, MF20) or in histoblock (3% BSA, 20 mM MgCl2, 0.3% Tween 20, 5% FBS in PBS). Slides were incubated overnight at 4ºC with the next primary antibodies:

Protein	Troponin T	Sarcomeric myosin heavy chain	Islet1	Delta4	Periostin	Smooth muscle actin (SMA)
Dilution	1:20	1:20	1:100	1:100	1:10	1:100
Species	Mouse monoclonal	Mouse monoclonal	Mouse monoclonal	Rabbit polyclonal	Rabbit polyclonal	Mouse monoclonal
Source	Hybridoma bank	Hybridoma bank	Hybridoma bank	Santa Cruz	Novuls Biologicals	Sigma
Reference	Ref. CT3 supernatant	Ref. MF20 supernatant	Ref. 39.4D5 supernatant	Ref. sc-28915	Ref. NBP1-30042	Ref. C6198

After washing in PBS, slides were incubated with secondary antibody for 1 hour at room temprature: biotin goat anti-mouse (1:500, Jackson, ref. 115-066-071) or biotin goat anti-rabbit (1:500, Jackson, ref. 111-066-003) and for another hour with streptavidin-DyLight594 (1/500, Jackson, ref. 016-510-084), streptavidin-Cy3 (1/500, Jackson, ref. 016-160-084) or streptavidin-Alexa-488 (1:500, Invitrogen, S-11223) (except SMA, which is directly conjugated to Cy3). Finally, samples were washed in PBS and mounted with Vectashield containing DAPI (Vector Laboratories, H-1200). Alternativelly, they were incubated for 10 minutes with Dapi in PBS (1:1000, Invitrogen, ref. D1306), washed in PBS and mounted with Vectashield (Vector Laboratories, H-1000).

Immunostaining for Jagged1, phospho-SMAD1/5/8 (pSMAD1/5/8) and Islet1 on paraffin sections

Slides were dewaxed and rehydrated, washed in distilled water and antigens retrieved by microwave heating for 15 minutes in 10mM citrate buffer, pH 6.0. They were left to cool at room temperature for another 15 minutes, washed in distilled water and incubated for 40 minutes in 1% H_2O_2 in methanol to block the endogenous peroxidase activity. Following two washes in PBS, samples were permeabilized in Triton X-100 0.5% in PBS for 10 minutes, washed in PBS again and blocked with histoblock for 1 hour at room temperature. Samples were incubated overnight with primary antibodies at 4ºC:

Jagged1	pSMAD1/5/8	Islet1
1:100	1:200	1:100
Rabbit polyclonal	Rabbit polyclonal	Mouse monoclonal
Cell Signalling	Cell Signalling	Hybridoma bank
Ref. 2620	Ref. 9511	Ref. 39.4D5 supernatant

After washing in PBS, slides were incubated with secondary antibody HRP goat anti-rabbit (1:100, Dako, P0448) or anti-mouse (1:100, Dako, P0447) prepared in PBS-BSA 5% for 1 hour at room temperature. Following two washes in PBS, fluorescent detection was carried out and reaction was left to develop for 3.5 minutes in darkness at room temperature with TSA working solution (1:100 TSA-Cy3, TSA-488 or TSA-Cy5 Stock Solution diluted in 1X Plus Amplification Diluent) (Perkin Elmer, ref. NEL744001KT). Samples were washed and mounted with Vectashield containing Dapi.

Immunostaining for Notch1 intracellular domain (NICD) on paraffin sections

Embryos were collected and fixed in 4% PFA at 4ºC for 2 hours, dehydrated in ethanol series and embebedded in paraffin. Slides were dewaxed and rehydrated, washed in distilled water and antigens retrieved by microwave heating for 15 minutes in 10mM citrate buffer, pH 6.0. They were left to cool at room temperature for another 15 minutes, washed in distilled water and incubated for 40 minutes in 1% H2O2 in methanol to block the endogenous peroxidase activity. Following two washes in PBS, samples were permeabilized in Triton X-100 0.5% in PBS for 10 minutes, washed in PBS again and blocked with histoblock for 1 hour at room temperature. Samples were incubated overnight with primary antibody rabbit polyclonal anti-NICD (1:100, Cell Signalling, ref. 2421) at 4ºC. After washing in PBS, slides were incubated with secondary antibody biotin goat anti-rabbit (1:500, Jackson) diluted in PBS-BSA 5% for 1 hour at room temperature. After secondary antibody was washed with sequential PBS incubations, kit ABC (Vector labs, PK-6100) was added to the slides and left to reveal in darkness for 1 hour at room temperature. Following two washes in PBS samples were incubated in TSA working solution for 3.5 minutes in darkness at room temperature. Slides were washed again and mounted with Vectashield containing Dapi.

Detection of cell proliferation by BrdU immunstaining on paraffin sections

Embryos at E8.5 were dissected and incubated in culture medium (DMEM, 10% FBS) with 10 mg/ml BrdU for 1 hour at 37ºC 5% CO2. They were quickly transfered to ice cold PBS to stop the incorporation of BrdU and fixed overnight in 4% PFA at 4ºC. Embryos were embedded in paraffin and immunostaining was performed as described for Jagged1 and pSMAD1/5/8 with mouse anti-BrdU primary antibody (1:30, BD, ref. 347580).

Detection of cell proliferation by phospho-histone3 (PH3) immunostaining on paraffin sections

Slides were dewaxed and rehydrated, washed in distilled water and antigens retrieved by microwave heating for 15 minutes in 10mM citrate buffer, pH 6.0. They were left to cool at room temperature for another 15 minutes, washed in PBS and blocked for 1 hour in 10% goat serum in PBS. Slides were incubated for 1 hour at 37ºC with the primary antibody rabbit polyclonal anti-PH3 (1:200, Miliipore, 06-570). Samples were washed with PBS and incubated for 1 hour at room

temperature with secondary antibody Alexa488 goat anti-rabbit (1:200, Molecular Probes, ref. A11034). After a couple of washes with PBS, slides were mounted with Vectashield containing Dapi.

Detection of apoptosis by TUNEL on paraffin sections

Cell death was detected using a TUNEL kit from Roche (Ref. 03 333 574 001). Slides were dewaxed and rehydrated, washed in distilled water and permeabilazed with Triton X-100 0.5 % in PBS for 10 minutes. After two washes with PBS, samples were incubated for 15 minutes with TdT buffer 1x CoCl2 1mM at room temperature. Next, slides were incubated with TdT reaction mix, which contains the recombinant terminal transferase, at 37ºC for 1 hour. Next, they were incubated with TdT buffer 1x CoCl2 1mM for 10 minutes and the reaction was stopped with two washes in Tween 20 0.01% in PBS. After washing in PBS slides were incubated with streptavidin-DyLight594, streptavidin-Cy3 or streptavidin-Alexa-488 (1:500, Jackson) for 1 hour at room temperature. Samples were washed again in PBS and mounted with Vectashield containing Dapi.

Immunostaining for CD31, β-galactosidase and nuclear β-catenin on cryostate sections

Cryostate slides were left at room temperature for 20 minutes and gelatin was removed by 15 minutes incubation in PBS at 37ºC. Slides were washed twice in TBST (0.1% Tween 20 in TBS), permeabilized with Triton X-100 0.5% in PBS for 10 minutes, washed again and blocked for 1 hour in 10% goat serum in TBST. Slides were incubated overnight at 4ºC with the following primary antibodies:

CD31	β-galactosidase	Nuclear β-catenin
1:50	1:10	1:10
Rat monoclonal	Mouse monoclonal	Mouse monoclonal
BD	Hybridoma Bank	Hybridoma Bank
Ref. 553370	Ref. 40-1a supernatant	Ref. PY489 supernatant

Samples were washed with TBST and incubated with secondary antibodies: biotin goat anti-mouse for beta-galactosidase (1:500, Jackson), followed by an incubation of 1 hour with streptavidin-DyLight594, streptavidin-Cy3 or streptavidin-Alexa-488 (1:500, Jackson); with Alexa488 goat anti-rat for CD31 (1:500, Molecular Probes, ref. A11006) and with Alexa488 goat anti-mouse for nuclear beta-catenin (1:500, Jackson). Samples were washed in TBST and mounted with Vectashield containing Dapi.

Immunostaining of actin filaments with phalloidin on cryostate sections

Cryostate slides were left at room temperature for 20 minutes and gelatin was removed by 15 minutes incubation in PBS at 37ºC. Slides were washed twice in PBS, permeabilized with Triton X-100 0.5% in PBS for 10 minutes, washed again and blocked for 1 hour with PBS-BSA 1%.

Slides were incubated with Alexa 488 conjugated phalloidin (1:200, Molecular Probes, A12397) for 45 minutes at room temperature. Sections were washed with PBS and mounted with Vectashield containing Dapi.

Hypoxia detection

To detect hypoxia levels in embryos we used pimonidazole as previously described (Lee Y.M. et al., 2001) (Krohn K.A. et al., 2008). 1.5 mg of pimonidazol were injected in a pregnant mouse at the desired stage. 3 hours after the female was anesthetized with a mixture of xylacine (0.4 mg/gr mouse weight) and ketamine (7.5 mg/gr mouse weight). The embryos were extracted and fixed immediately in PFA 4% to avoid inespesific hypoxia. Embryos were embedded in paraffin and immunostaining against pimonidazole (1:500, HPI, HP3-200Kit) was done following the same protocol as for Jagged1 and pSMAD1/5/8 antibodies.

Ink injection

Indian ink was injected following a modified version of a previously described protocol (Winnier G.E. *et al*., 1999). Embryos at stage E9.25 were dissected in warm culture medium (DMEM, 10% FBS) and Pelikan India Ink diluted 1:40 in PBS was injected into the left ventricle. Embryos were fixed in 4% PFA overnight and dehydrated to methanol. To visualize the ink, embryos were cleared for several hours in 2 vol benzyl benzoate/1 vol benzyl alcohol.

Atrio ventricular canal (AVC) explants

AVC explants were prepared as described previously (Luna-Zurita L. *et al*., 2010). A 1.5 mg/ml solution of rat-tail collagen type I (BD Bioscience, 354236) was prepared and allowed to solidify on 4-well micro culture dishes at 37ºC and 5% CO2. Gels were washed several times with DMEM (Sigma, D5796) containing 10% FBS, antibiotics, fungizone and non-essential aminoacids and left for at least 4 hours in the same medium supplemented with 1% insulin-transferin-selenium (ITS; GIBCO, 51300-044). Hearts from E9.5 embryos were dissected in the same medium and AVCs were isolated, cut and placed with the endocardium facing the collagen gel. Explants were left to attach overnight at 37ºC and 5% CO2. Complete medium was added and explants were left to grow for three days. Explants were fixed with 4% PFA for 30 minutes at room temperature and stained with phalloidin-Alexa 488 (1:100, Molecular Probes) to reveal the actin cytoskeleton and with anti-SMA-Cy3 (1:80, Sigma) to detect mesenchymal cells. Explants were mounted with Vectashield medium containing DAPI to stain the nuclei. For treatment of explants with BMP2, collagen gels were incubated 30 minutes before explant culture with medium containing 500 ng/ml recombinant human BMP2 (R&D Biosciences, 355-BM) and the medium added to attached

explants was supplemented with the same concentration of BMP2. 2D migration (number of scattered cells) was counted with Imaris software. 3D migration (number of cells invading the gel) was determined by counting DAPI stained cells in the Z-stack using ImageJ. At least 17 explants were considered per condition.

DiI labelling and embryo culture

DiI labelling and embryo culture were performed as described previously (Franco D. *et al*., 2001) (Domínguez J.N. *et al*., 2012). Embryos ranging from 4 to 11 somites were dissected in Hank's solution (Sigma, H9269) without damaging the yolk sac. Long-chain carbocyanine dye (DiI, Molecular Probes) was dissolved in pure ethanol and diluted 1:9 in 0.3M sucrose containing 0.1% Nile Blue Sulfate after heating at 42ºC for 10 min. To track the contribution to the inflow region, embryos with 4-7 pairs of somites were injected in a caudal position within the left lateral mesenchyme positive for Islet1 (pSHF). The position was determined by using a grid centred on the midline of the embryo. To track the contribution to the outflow tract (OFT), embryos from 8 to 11 somites were injected beneath the heart tube in a rostral Islet1+ region (AHF). The time of injection was considered "t=0". Labelled embryos were photographed under a Leica MZ12F dissecting microscope fitted with a fluorescent lamp and cultured in rolling-bottles for 24 hours in 75% rat serum (Harlan, SR-0100D), 25% DMEM. For the first 12 hours a 5%CO2, 5%O2, 90%N2 mixture was used; from then on a 5%CO2, 20%O2, 75%N2 mixture was employed. Two embryos were cultured per bottle, and could be distinguished by DiI injection into the head (embryo 2) or no dye (embryo 1). After 24 hours in culture embryos were collected in PBS, the yolk sac was removed and embryos were fixed in 4% PFA overnight at 4ºC. From the total number of labelled embryos, 51 were excluded due to abnormal development. We also excluded 70 embryos due to inappropriate labelling (cases that presented leakage of DiI into the pericardial cavity or the heart lumen during injection and cases when labelling was too deep and DiI appeared mostly in the pharyngeal endoderm but not in the heart OFT). A total of 43 wild-type embryos and 21 Arid3b mutants were considered for the analysis of embryos marked for IFT contribution, and a total of 82 wild-type and 20 Arid3b-null embryos were analysed in the case of embryos labelled for OFT contribution. The contribution to the IFT was measured by determining whether DiI-labelled cells were observed in or outside of the heart tube (binomial distribution). The contribution to the OFT was classified into three regions: the length of the OFT was measured by ImageJ and divided into an upper half (distal OFT) and a lower half (proximal OFT). The third region was the right ventricle, defined using the outer curvature of the heart tube. The following analyses using R were used to assess the statistical significance of the results: A 2-sample test for equality of proportions with continuity correction was used to analyse the results of pSHF labelling, and a Fisher exact test was used to analyse the contribution to the OFT.

Whole mount immunochemistry

Embryos were extracted in warm Hank's medium and marked with DiI and image acquired as described above. Inmediately they were fixed in PFA 4% overnight. Next day they were dehydrated to methanol and left overnight at -20ºC. Whole mount immunochemistry was performed according to standard protocol. Embryos were rehydrated, permeabilized with TritonX, left 1 hour in blocking solution and incubated overnight at 4ºC with anti-Islet1 antibody (1:100, Hybridoma Bank). The next two days embryos were washed in PBT four times and incubated overnight with biotin Sp anti-mouse IgG (1:500, Jackson) first and then with streptavidin Alexa 488 (1:500, Invitrogen). Embryos were stored in Vectashield and images acquired in Leica fluorescent scope.

DNA Microarray

E9.5 embryos were dissected in cold PBS. Three regions were separated: head (including head and first branchial arch); heart (including the heart tube and the pharyngeal mesoderm and endoderm located beneath); and trunk (including the body from the otic vesicle to somite 15). Four wild type and four mutant embryos were collected for each of the microarray triplicates. For E9.0 whole embryo microarray, four wild type and four mutant samples consisting of 3-4 embryos each were used. RNA was extracted with the Qiagen extraction kit and RNA quality was checked by Nanodrop spectrophotometer measure and gel electrophoresis. Samples were labelled and hybridised to Agilent chips (Whole Mouse Genome Microarray 4 x 44K, G4112F and G4846A, Agilent Technologies). Functions were analysed with Ingenuity Pathway Analysis software (Ingenuity Systems®, www.ingenuity.com).

Sample labelling and microarray hybridisation.

RNA amplification and labelling

The One-Color Microarray-Based Gene Expression Analysis Protocol (Agilent Technologies, Palo Alto, CA, USA) was used to amplify and label RNA. Briefly, 200-800 ng of total RNA was reverse transcribed using T7 promoter Primer and MMLV-RT. cDNA was then converted to aRNA using T7 RNA polymerase, which simultaneously amplifies target material and incorporates cyanine 3-labeled CTP.

Hybridisation protocol

Samples were hybridised to Whole Mouse Genome Microarray 4 x 44K (G4112F and G4846A, Agilent Technologies). 1.65 mg of Cy3 labelled aRNA were hybridised for 17 hours at 65ºC in a hybridisation oven (G2545A, Agilent) set to 10 rpm in a final concentration of 1X GEx Hybridisation Buffer HI-RPM, according to the manufacturer's instructions (One-Color Microarray-Based Gene Expression Analysis, Agilent Technologies).

Washing protocol

Arrays were washed according to manufacturer's instructions (One-Color Microarray-Based Gene Expression Analysis, Agilent Technologies). Arrays were dried by centrifugation.

Scan protocol

Arrays were scanned at 5mm resolution on an Agilent DNA Microarray Scanner (G2565BA, Agilent Technologies) using the default settings for 4x44k format one-color arrays.

Image analysis

Images provided by the scanner were analysed using Feature Extraction software version 9.5.3.1 (Agilent Technologies).

Data analysis

Data files from Feature Extraction were imported into GeneSpring® GX software version 9.0 (Agilent Technologies). Quantile normalization was performed and expression values (log2 transformed) were obtained for each probe. Expression ratios (log2) were calculated using the wild type samples from each experiment as baseline.

Statistical analysis of differential gene expression between Arid3b mutant tissues and wild type tissues was assessed using two-class paired SAM 12.

Mouse embryonic fibroblasts, MEFs (RRJ028)

MEFs extraction

Mouse embryonic fibroblasts were obtained from E9.5 homozygous and control embryos due to the early mortality of this line. Dissection was performed in a tissue culture hood. Whole embryos were extracted in warm PBS and transferred to a cell strainer with 100 mm grid pore (BD Falcon, REF352360) on a 60 mm dish with complete culture medium (DMEM, FBS 20%, penicilin/streptavidin 1%) and gently smashed with a syringe piston. The mesh was washed with medium and all the liquid was collected into a Falcon and centrifuged 5 min at 1000 rpm. Cells coming from each embryo were cultured in a 24-well culture dish well individually to identify embryos by β-gal genotyping. The incubator where the cells were cultured was at 37ºC, 5% CO_2, 90% humidity.

Immunostaining of actin filaments with phalloidin on fixed MEFs

MEFs were fixed for 15 minutes at room temperature with 4% PFA. After two washes with

PBS, membranes were permeabilized with PBT (Triton-X 100 1% in PBS). Samples were blocked with PBS-BSA 1% for 30 minutes at room temperature. Next, cells were incubated for 30 minutes with Alexa 488 conjugated phalloidin (1:200, Molecular Probes) at 37ºC. Cells were washed with PBS and mounted with Vectashield mounting medium.

Migration assay

For video recording, cells were cultured in 6 well culture plates, left to attach overnight and recorded for a minimum of three hours with a Nikon time-lapse microscope. Cell tracking was made with MetaMorph software using three hours windows for the analysis.

MEFs (cKOArid3b)

MEFs extraction

MEFs were obtained from embryos at E12.5 coming from crosses between *Arid3b*$^{flox/+;Neo\ cassette}$ mice. Dissection was performed in a tissue culture hood. Head, limbs and viscera were removed in warm PBS. The rest of the body was transfered to a cell strainer with 40 mm grid pore (BD Falcon, REF352340) on a 60 mm dish with complete culture medium (FBS 10%) and gently smashed with a syringe piston. The mesh was washed with medium and all the liquid was collected into a Falcon and centrifuged 5 min at 1000 rpm. Cells from each embryo were cultured in 12-well culture dish well individually and tails were used to obtain DNA and genotype each embryo. The medium used contained DMEM enriched in glucose and glutamate, 10% FBS, 1% penicillin/streptavidin.

Alternatively, for MEFs extraction from the *Arid3b*$^{flox/flox}$ line, male and female mice with two copies of floxed Arid3b were crossed and embryos were extracted at E13.5. Embryos were dissected in a tissue culture hood. Head and viscera were removed in PBS 1% antibiotic and the rest of the body was transferred to a dish with 1 ml of trypsin per embryo (Gibco, 25200-07). The digestion was left for 5 minutes at 37ºC. Then a syringe was used to disaggregate the cells. Culture medium with 10% FBS and antibiotics was added to stop the digestion. Cells were centrifuged ar 1200 rpm for 5 minutes and cultured in p100 dishes (2-3 embryos per dish).

Adenovirus infection for Cre expression in vitro

Recombinant adenovirus expressing eGFP and Cre were second-generation vectors derived from Ad5ΔE1aΔE3 virus. Viral production was made by mid-scaling up stocks in HEK-293A cells as described (Palmer D.J. and Ng, 2008). Total IFU (infectious units) present in the eluate as purified virus was determined by infecting fresh HEK-293 cells with appropriated dilutions, and counting the cells positive for expression of the major capsid protein 48 hpi according to the Adeno-X Titer kit (Clontech). The viral titer (total IFU) from each pellet was determined.

For infection, MEFs extracted from *Arid3b*$^{flox/flox;Neo\ cassette}$ and *Arid3b*$^{flox/flox}$ lines were used. Both *Arid3b*$^{flox/flox}$ and *Arid3b*$^{flox/+}$ MEF were infected with virus either containing eGFP alone or eGFP and Cre. The infection was carried out when cells were around 50-70% confluent. Adenoviruses were added to cells to achieve a multiplicity of infection of 10. Infection efficiency was evaluated the next day by GFP expression. Cells were left to achieve confluency, then tripsinized and sorted by flow citometry. Sorted cells were seeded and grown for several days. Aliquots of the cells were frozen in complete medium, used for RNA extraction or seeded for wound healing assay.

Wond healing assay

For the wound healing assay, cells were left to grow until confluency. Mitomycin C (Sigma, M4287) was used to inhibit cell proliferation. Mitomycin C was diluted in PBS to a final concentration of 1mg/ml and added to the culture medium (1/10). Cells were left for 2.5 hours at 37ºC with the inactivation medium. The inhibition was stopped by PBS washes before the healing assay. The wound was done with a yellow tip, pictures were taken at "t=0" and cells were left in the incubator. Pictures were taken at the same point 24, 48 and 72 hours after the wound.

RT-PCR and qRT-PCR

To perform RT-PCR or qRT-PCR, total RNA was extracted either from embryos or from cells. Embryonic hearts at stage E9.0 were dissected in cold PBS in two regions: the first one containing the OFT with the pharyngeal endoderm and mesoderm located beneath and the second consistent of atria, ventricle and IFT. The dissected hearts were stored dry at -80ºC until the RNA extraction. A pool of 12 mutant and wild type embryos was used. For MEFs RNA extraction, p35, p60 or a third part of a p100 plates were lysated directly with the lysis buffer. The kit used for extraction was Rneasy Mini Kit (Qiagen, 74106). cDNA was synthetized with the High Capacity cDNA Transcription Kit (Applied Biosystems, 4368814). RT-PCR was performed on a standard thermal cycler, while qRT-PCR on a 7900HT Fast Real-Time PCR System (Applied Biosystems, 4329001) with SYBR green master mix (Life Technologies, 4309155). qBASE was used for data analysis. The following primers were used:

Gene	Primers	Product lenght	Reference
β-Actin	5'-GGCACCACACCTTCTACAATG-3' 5'-TGGATGGCTACGTACATGGCT-3'	196 pb	(Varona R. *et al*., 2005)
Arid3b exon7	5'-AAGGTGATGGAGTCCCAGTG-3' 5'-TGCTCCTCCTCTGACAACCT-3'	166 pb	This thesis
Arid3b exon2	5'-AGAGAGAAGCAGGGACCACA-3' 5'-GCTCATCCAGACTCCAGCTC-3'	460 pb	This thesis
Arid3b ARID domain	5'-AGAGAGGCACCCCAATCAAC-3' 5'-CACCAGGCCTCCTTTCTCTG-3'	98 pb	This thesis
Gapdh	5'-CATGGCCTTCCGTGTTCCTA-3' 5'-GCGGCACGTCAGATCCA-3'	55 pb	From RT PrimerDB
Hprt	5'-CTGGTGAAAAGGACCTCTCG-3' 5'-TGGCAACATCAACAGGACTC-3'	219 pb	This thesis

Human Arid3b cloning

Whole length human Arid3b was amplified with High Fidelity Phusion Polymerase (New England Biolabs, M0530S). The following primers were used:

5'-CTTGAGGCAAAAATGGAGCCAC-3'

5'-TGTGCATCAACTTCCTTCACTCTCG-3'

The following PCR program was used to amplify the fragment:

94ºC	5'	
94ºC	30''	} x35 cycles
66ºC	45''	
72ºC	1'	
72ºC	10'	
4ºC	…	

BamHI and EcoRI recognition sites were added at the ends to digest the PCR product. The PCR fragment was purified with Qiagen purification kit. EF-Flag plasmid and PCR fragment were digested with BamHI/EcoRI and purified with Qiagen purification kit. The plasmid was subjected to dephosphorilation with alcaline phosphotase to avoid self-ligations. A mixture of plasmid and digested PCR fragment was ligated overnight at 4ºC with T4 ligase. Thermo-competent bacteria DHα were transformed with this mixture and the next day minipreps were done from a few colonies. The insertion was checked by double-digestion with BamHI/EcoRI. The plasmids were sequenced and compared to NCBI database.

Cell transfection

Human Embryonic Kidney 293 cells (HEK293) were used for transfection with JetPei using a standard protocol. Cells were cultured in p100 plates and transfected when 60-80% confluency was achieved. 10 mg of each plasmid were dissolved in 500 µl of NaCl 150 mM and 20 µl of JetPei per 10 mg of DNA were also diluted in 500 µl of NaCl 150 mM. The two solutions were mixed, vortexed for 2 seconds and incubated at room temperature for 20-30 minutes. The solution was added to the culture plate by drop fall. Cells were left for 24 hours and than the medium was changed. GFP fluorescence started to be detected at 48 hours approximately. For protein extraction cells were lysed. The following plasmids were used for transfection:

Human Arid3b-EF-FLAG (as described above)

Mouse Smad1-MYC (Singh R. *et al*., 2009)

Mouse Smad5-FLAG (Singh R. *et a*l., 2009)

PCAGGS/GFP (Momose T. *et al*., 1999)

Protein extraction

Non-denaturalizing lysis buffer (ND-lysis buffer: 20 mM Tris HCl pH8, 137 mM NaCL, 10% glycerol, 1% NP-40, 2 mM EDTA) supplemented with proteinase inhibitors cocktail (cOmplete ULTRA Tablets, Roche 05892970001) and phosphatase inhibitors (NaF, NaVO4) were used to lysate the cells. Cells were trypsinized and centrifuged, washed in cool PBS and resuspended in ND-lysis buffer. Samples were kept on ice for 30 minutes, pipetting each 5-7 minutes for cell lysis, centrifuged for 15 minutes at 12000 rpm at 4ºC and stored at -80C till used. Dc protein assay kit (BioRad 500-0111) was used to measure protein concentration. For embryonic protein extract, three *Arid3b*$^{gt/gt}$ embryos and a mixture of 14 wild type and *Arid3b*$^{gt/+}$ embryos at E9.5 were used. The protocol for protein extraction was the same as for cells in culture and the amount of protein used for Western blot was the same for both wild type and mutant embryos.

Immunoprecipitation of Arid3b-Flag and Smad1-Myc

Beads directly conjugated to anti-FLAG antibody were used (anti-FLAG M2 affinity gel, Sigma A2220). 40 ul of beads were used for each immunoprecipitation experiment. They were washed in cold TBS 3 times and incubated with 400 mg of cell extracts on a wheel for 2 hours at 4ºC. The supernatant was collected and beads were washed 5 times with 1 ml of ND-lysis buffer for 8 minutes at 4ºC. Proteins were denaturalized with lysis buffer used for polyacrylamide gel electrophoresis at 95^{O}C for 5 minutes. The supernatant which contained the denaturalized proteins was collected and either freezed or ran directly in acrylamide gel for western blot detection. Immunoprecipitation

was carried out with four different types of protein extracts, including the experimental one and the controls. The first extract contained both Smad1-Myc and hArid3b-Flag proteins and was used for the experiment to check the co-immunoprecipitation. Samples containing only Smad1-Myc were used as a control of unspecific binding of Smad1-Myc to the beads; extracts containing only hArid3b-Flag, to confirm the antibodies specificity towards the antigen. And, finally, extracts transfected with GFP, as a control for unspecific protein binding to the beads.

Western blot protein detection

Western blot was carried out according to a standard protocol. 25 mg of protein were used per sample. The acrylamide concentration for the separating gels was 8-10%. While the gel was running, Immobilon®-P membrane (Millipore) was activated in methanol. The protein transference was carried out in Tris-Glycine 20% methanol at 100V for 1 hour at 4ºC. Next, the membrane was washed in TBST (Tween 20 1%), cut into pieces for the detection of different proteins and blocked for 1-2 hours in 3% milk/TBS. Overnight incubation was carried out with the following antibodies:

anti-ARID3b 1:5000 in TBST/2%BSA (Abcam, ab92328)

anti-β-actin 1:6000 in 5% BSA (Sigma, A5441)

anti-FLAG 1:1000 in TBST/2% BSA (Sigma, F7425)

anti-MYC 1:500 in TBST/2% BSA (Invitrogen, Clone 9E10)

anti-MYC 1:50 in TBST/2% BSA (A-14, Santa Cruz-789)

Next day membranes were washed in TBST and incubated with secondary antibodies (policlonal goat anti-mouse/rabbit inmmunoglobulin HRT; Dako, P0448/P0447) 1:5000 in 5% milk/TBS for 1 hour at room temperature. After several washes with TBST, membranes were subjected to chemiluminiscent assay with ECL™ Western Blotting Detection Reagents (GE Healthcare, RPN2106).

RESULTS

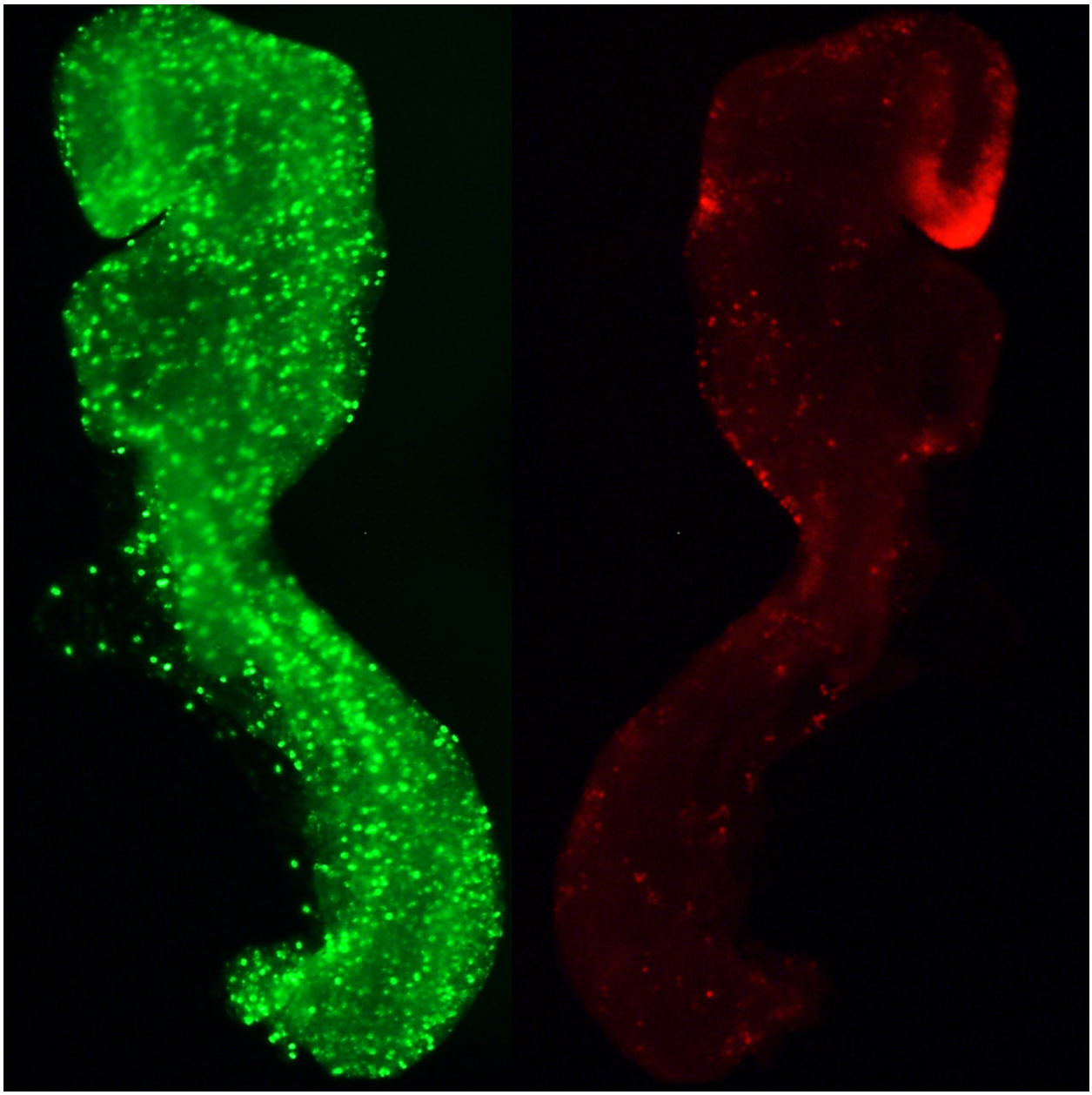

Arid3b is expressed in the heart from early stages of development

During embryonic development, Arid3b shows a broad tissue-specific and dynamic pattern of expression (Casanova J.C. *et al*., 2011) (Takebe A. *et al*., 2006). We used RNA *in situ* hybridisation and β-galactosidase staining to analyse the expression pattern of the gene (**Figure 11**). Expression could be detected at E7.5 (**Figure 11 A, a,b**) in the neural ectoderm (**Figure 11 B, d, arrow**) and in the extraembryonic endoderm of the visceral yolk sac (**Figure 11 B, d, arrowhead**). Already from E8.0, expression becomes restricted to posterior and anterior regions. The strongest signal could be detected in the unsegmented paraxial mesoderm and in the less mature somites (**Figure 11 A c-f).** While development progresses, the expression persists in the more caudal regions and in the tail bud (**Figure 11 A g-l, black arrowhead**). Expression is also detected in rostral structures, such as the branchial arches and pharingeal pouches, the rombenchepalon, the otic vesicle, the cranial neural crest and the heart (**Figure 11 A c-l, B e-l**). We also observed expression in the developing limbs in the apical ectodermal ridge (AER) and in the underlying mesenchyme (**Figure 11 A i-l, B i-l, arrows**). The signal detected by β-galactosidase staining was broader that the one measured by RNA *in situ* hybridisation and persisted for longer. For instance, at E10.5 β-galactosidase staining showed a strong signal throughout the heart, while by *in situ* hybridisation at the same stage expression was barely detected (**Figure 11, compare A k,l with B k,l**). At E9.0, most of the somites were stained, while by *in situ* hybridisation the signal was detected only in caudal somites, well posterior to the forelimb level (**Figure 11, compare A g,h with B g,h, white arrowheads**). To address whether the β-galactosidase staining reflects the real expression of *Arid3b* RNA, we designed a probe against the β-geo cassette with the primers used to genotype heterozygous animals and performed an *in situ* hybridisation on wild type, heterozygous and mutant embryos at E9.5. We observed an RNA signal distribution similar to the one observed with the probe against *Arid3b*, with low levels in heart chambers and a gradually reduced signal in the maturing somites (**Figure 12**). Thus, we confirm that the β-geo cassette expression reproduces the endogenous *Arid3b* RNA expression.

In order to characterize the role of Arid3b during heart development, we analysed in detail its expression pattern in the heart by RNA *in situ* hybridisation. *Arid3b* was expressed from early stages in the heart crescent and in the heart precursors (**Figure 13A**). At E8.0 expression was observed throughout the primary heart tube myocardium and also strongly in the second heart field (SHF) (**Figure 13 B-D**). At E8.5 expression in the heart tube was fainter but remains strong in the SHF and the heart poles (**Figure 13E**). At E9.0 high-level expression persisted in the heart poles (inflow and outflow tracts; IFT and OFT) and in the SHF (**Figure 13 F-J**). However, expression gradually decreases in the heart chambers, whereas it is clearly observed in the atrioventricular canal (AVC) (**Figure 13I**). At E9.5 expression was still strong in the sinus venosus, dorsal mesocardium and OFT (**Figure 13 K-O**). At E10.5, expression in the heart myocardium was much fainter, but a clear signal is still seen in the OFT (**Figure 13 P,Q**). From E11.0 expression in the myocardium was no longer detected. From E10.5 *Arid3b* expression was also detected in the endocardium

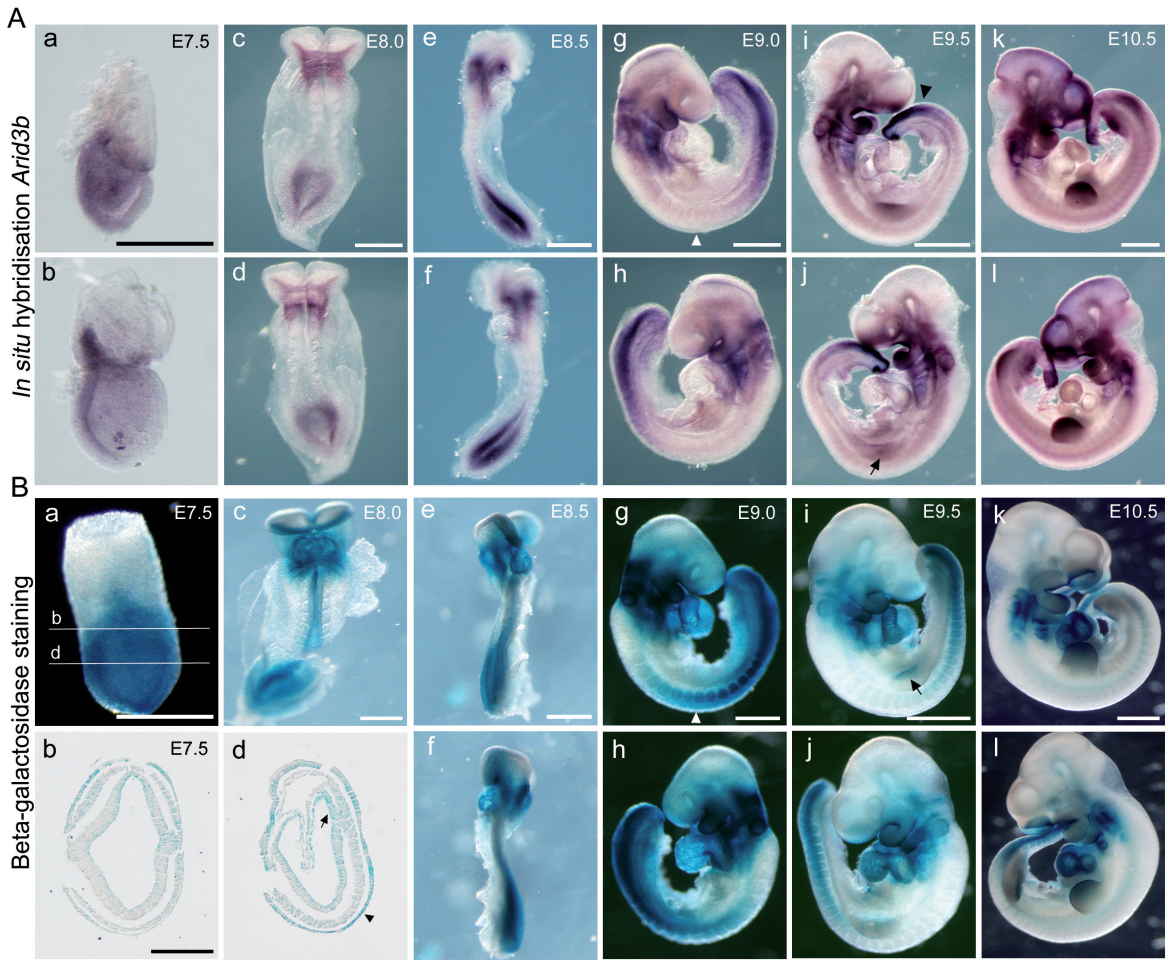

Figure 11. *Arid3b* is expressed in a broad tissue-specific and dynamic way during development. A. RNA *in situ* hybridisation showing *Arid3b* expression from stage E7.5 to E10.5. Strong expression could be detected in the caudal (unsegmented paraxial mesoderm and immature somites) and rostral (branchial arches and pouches) regions, as well as in the limb (arrows) **B.** Lac-Z staining in *Arid3b*$^{gt/+}$ embryos. Expression is observed in similar areas as by *in situ* hybridisation (in the caudal and rostral regions), but is stronger and is detected towards the middle region of the embryo, compared to the *in situ* hybridisation (arrowheads). Scale bars: panel A a-h, panel B a,c,e-h 500 μm; panel B b,d 150 μm; panel A i-l, panel B i-l 1 mm.

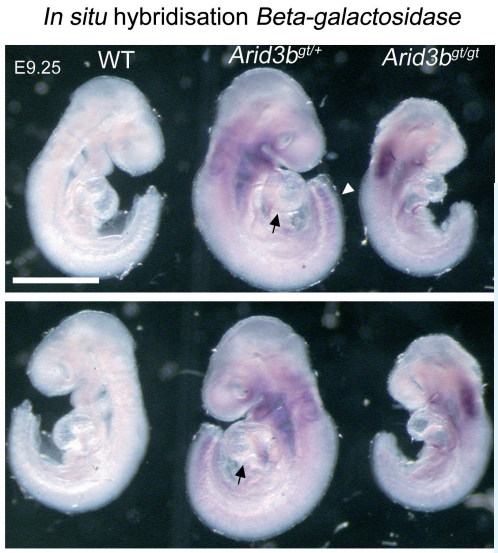

Figure 12. β-geo RNA shows a pattern of expression similar to *Arid3b* RNA. *In situ* hybridisation against the β-geo cassette in wild type, *Arid3b*$^{gt/+}$ and *Arid3b*$^{gt/gt}$ embryos. The expression is restricted to the posterior (white arrowhead) and anterior regions of the embryo, reproducing the expression of *Arid3b* mRNA, rather that the β-galactosidase staining. The expresión in the heart is also similar to the *Arid3b* probe (black arrow). Scale bar: 1 mm.

(Figure 13 P') and at E11.5-E12.5 there was an especially strong signal in the valve cushions of the AVC and OFT (**Figure 13 R-U**), although expression is also seen throughout the whole endocardium. At E14.5 strong expression was detected in the arterial trunk, as well as in the wall of the aorta (**Figure 13V**). Expression was also present in the epicardium at these stages (**Figure 13 R,T**).

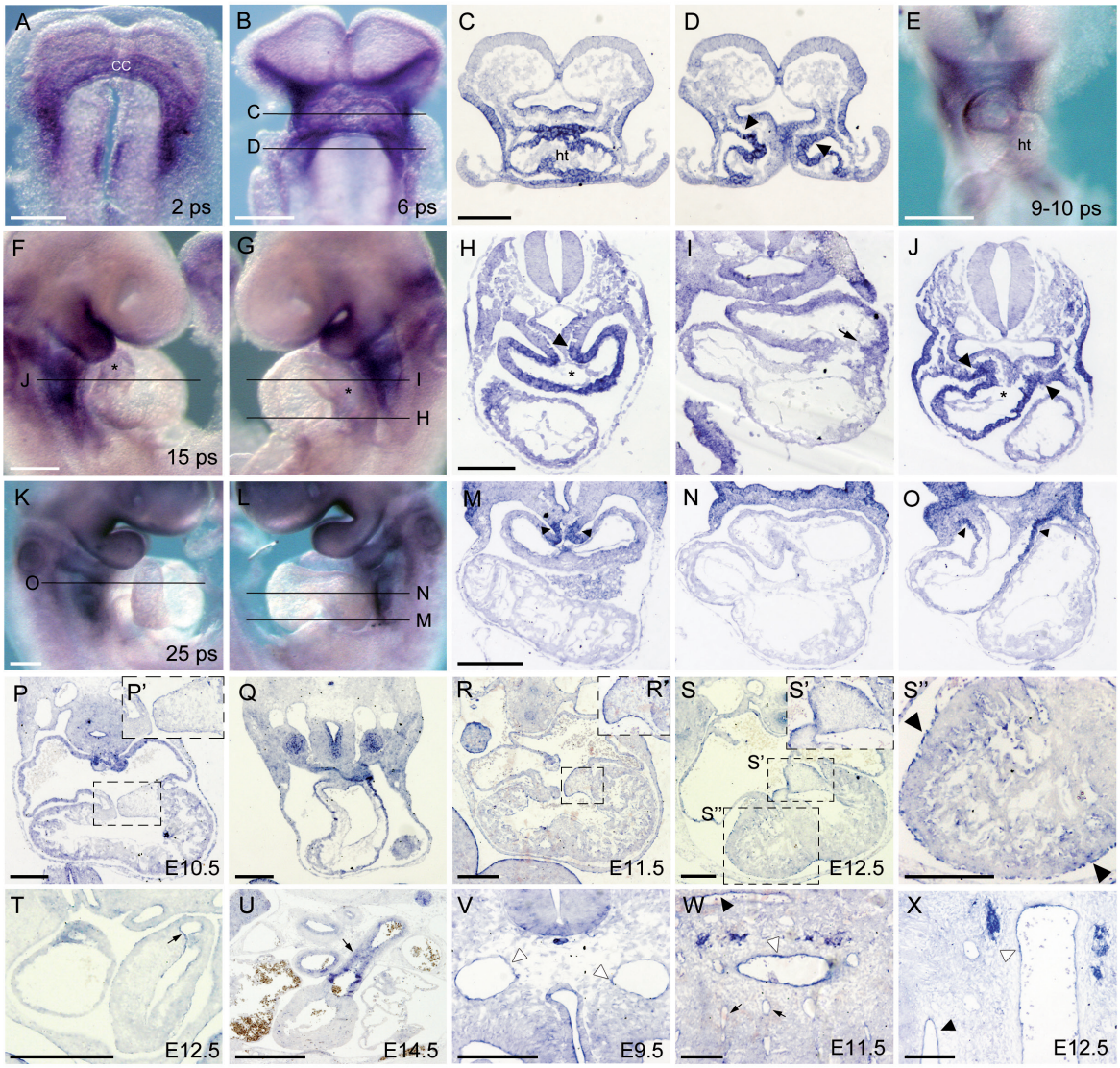

Figure 13. *Arid3b* is expressed in the heart from early stages of development. RNA *in situ* hybridisation showing *Arid3b* expression in the heart at different stages of mouse heart development in whole-mount embryos (**A,B,E-G,K,L**) and on paraffin sections (**C,D,H-J,M-X**). From early stages expression is observed throughout the heart tube and in the SHF (**A-D**, arrowheads). In the looping heart expression diminishes in the developing chambers but is maintained strong in the myocardium of the heart poles (asterisks: OFT in **F,J** and IFT in **G,H**) and in the SHF (**E-O,Q**, arrowheads in **H, J, M** and **O**). Expression can also be observed in the AVC myocardium at E9.0 (**I**, arrow), but not at E9.5. From E10.5 expression is observed in the endocardium, especially in the AVC cushions (**P,P',R,R',S,S',S"**) and later in the OFT cushions (**T,U**, arrows). We also observed expression in the epicardium at E12.5 (S" arrowheads). In the vessels *Arid3b* expression starts in the dorsal aorta at E9.5 (**V,W,X** white arrowheads) and later also appears in small vessels (arrows) and in veins (black arrowheads) (**W,X**). Scale bars: 150 µm C,D,H-J,M-O,V-X; 250 µm A,B,E,F,G,K,L,P-S"; 500 µm T,U. Stages are indicated as embryonic day (E10.5) or pairs of somites, ps.

In blood vessels, *Arid3b* was not expressed in the endothelium at early stages, neither in the embryo nor in the yolk sac, although expression was high in the yolk sac endoderm as detected by immunostaining against β-galactosidase (**Figure 14**). However, from E9.5, expression was readily seen in the vessels endothelium (**Figure 13X**). This expression was first seen in the aorta and great vessels, including veins, and later extended to smaller vessels (**Figure 13 V-X**).

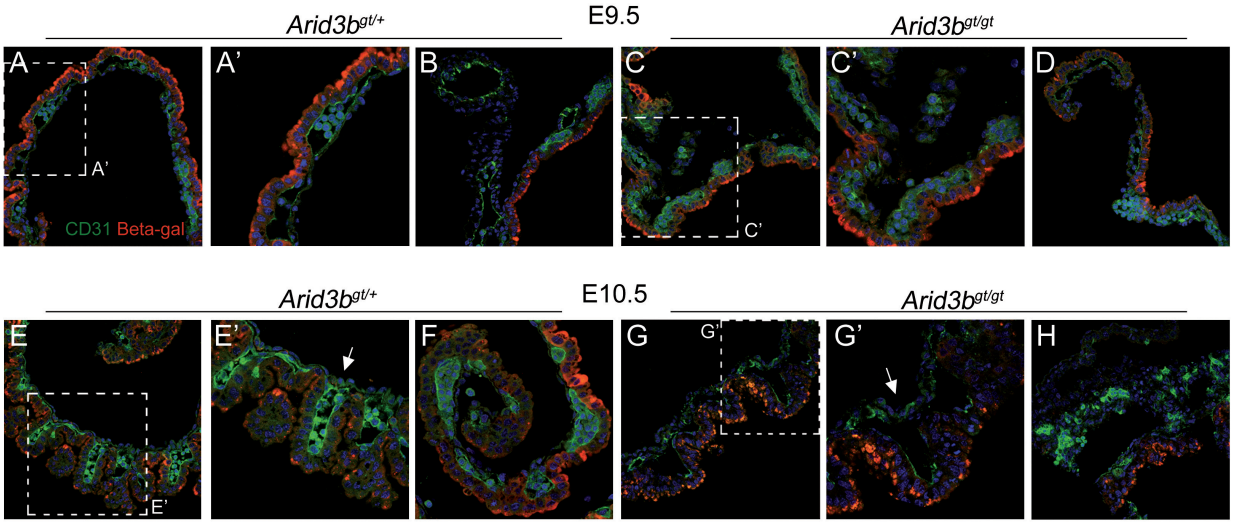

Figure 14. *Arid3b* is not expressed in the endothelium but mutants fail to form mature vessels in the yolk sac. Immunostaining against b-galactosidase (red, tracking Arid3b expression) and CD31 (green) in *Arid3b*$^{gt/+}$ and *Arid3b*$^{gt/gt}$ yolk sacs. (**A-H**) b-galactosidase could not be detected in the endothelium but was strongly expressed in the endoderm. Note that normal mature vessels (**E'**, arrows) are not observed in mutant yolk sac (**G'**, arrows).

Arid3b-null embryos show cardiac defects

Previous reports showed that Arid3b is essential during embryonic development and mouse embryos lacking *Arid3b* have severe cardiovascular defects and die at mid-gestation. To analyse the role of *Arid3b* in heart development we have used a mouse gene-trap line (see Materials and Methods). We first checked whether in our gene trap line, as expected from the insertion point, Arid3b lacked its known functional domains. *In situ* hybridisation with a probe against the whole length of *Arid3b* mRNA showed no signal in mutant embryos (**Figure 15A**); a RT-PCR with primers amplifying the whole length of the mRNA (**Figure 15B**), as well as a qRT-PCR with primers located in the exon 7 (**Figure 15C**) confirmed that in our gene-trap line the full length *Arid3b* is not transcribed. Thus, the line provided a good loss of function model to study the role of Arid3b.

Embryos deficient for *Arid3b* die at E10.5 with multiple developmental defects, especially severe craniofacial and cardiovascular malformations. Most of the structures affected are regions with strong *Arid3b* expression. From E9.25 *Arid3b*$^{gt/gt}$ embryos show reduced size and an arrest in somitogenesis, although newly formed somites look abnormal from earlier stages. The craniofacial defects include hypoplastic branchial arches and smaller heads (**Figure 16 A-B**).

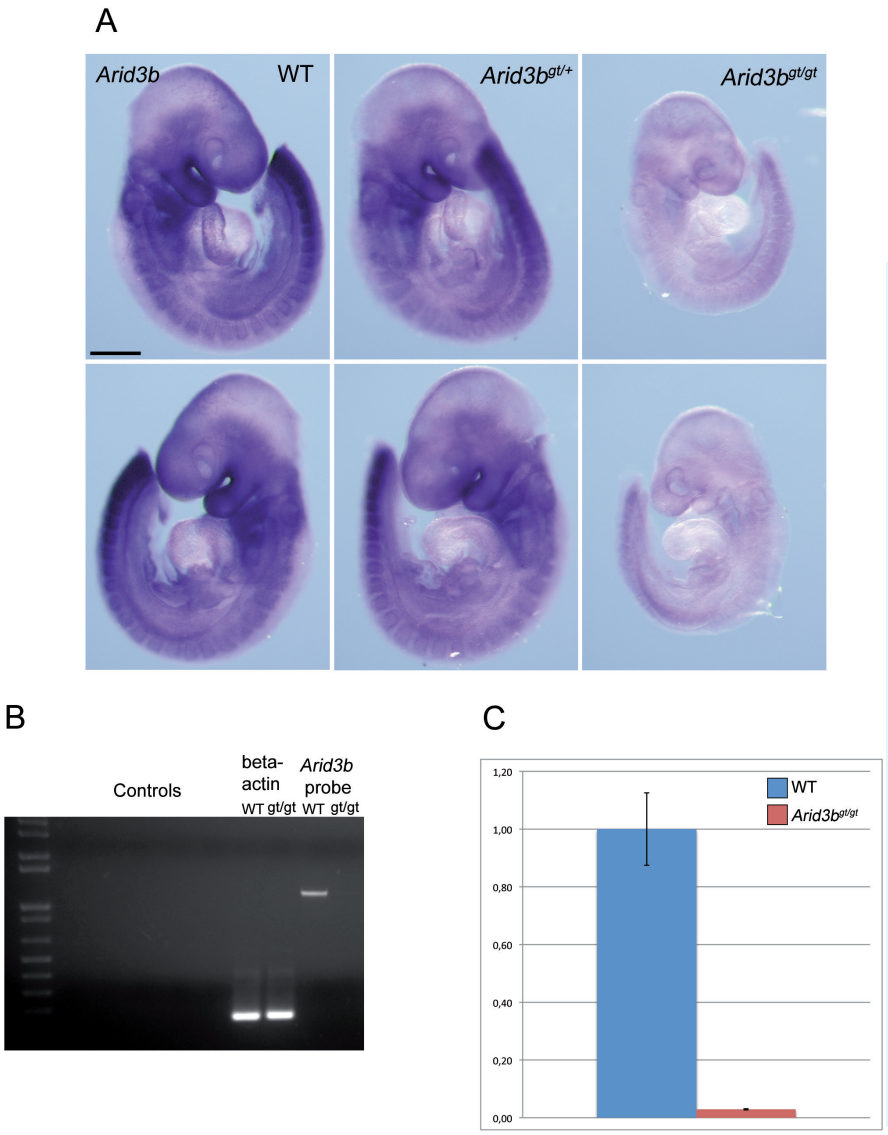

Figure 15.
The *Arid3b*$^{gt/gt}$ mice lack *Arid3b* functional domains. **A.** *In situ* hybridisation with *Arid3b* probe on wild type, *Arid3b*$^{gt/+}$ and *Arid3b*$^{gt/gt}$ embryos. A specific signal is detected in wild type and *Arid3b*$^{gt/+}$ embryos but not in the mutants. **B**. RT-PCR with RNA extracted from pools of 12 wild type and mutant OFTs; the PCR was performed with the primers used to generate the probe for *in situ* hybridisation **C.** qRT-PCR with pools of 12 wild type and mutant OFTs with primers against the exon 7 of Arid3b; no signal is detected in the mutant condition. Scale bar: 500 µm.

At E10.5 the cardiac defect was very pronounced with an abnormally dilated heart, altered looping and pericardial effusion (**Figure 16 A-B**). Moreover, the yolk sac lacked large mature blood vessels and presented haemorrhages, suggesting that appropriate vascular remodelling is impaired (**Figure 14 and 16C**). However, mutant hearts beat and Indian ink distributed to the body after injection into the heart at E9.25, confirming blood circulation (**Figure 16 J,O**), although vessels are smaller as shown by connexin 40 expression (**Figure 16 T,Y**). To determine whether earlier heart defects are observed before the development of the general severe cardiovascular phenotype, we closer examined mutant hearts at earlier stages. Already at E8.5 a shortening of the outflow and inflow tracts and defective looping could be detected (**Figure 16 D,E**). The defect in the elongation of the poles became more evident at E9.0 (**Figure 16 F,G,K,L**), and at E9.5 a severe hypoplasia of the OFT and IFT prevented the normal looping of the heart (**Figure 16 H,I,M,N**). To obtain a more precise information on the shortening of the poles, we measured OFT length along the inner curvature and IFT length along the outer curvature at E9.0 and E9.5, in both wild type and *Arid3b*$^{gt/gt}$ embryos (**Figure 17 A,C,E,G**). As can be observed, the reduction in length of both

poles of the heart is indeed evident from E9.0 (**Figure 17 B,F**), and, while in the wild type embryos both poles continue their growth (the OFT almost doubles its length), very little elongation is observed in the mutant embryos (**Figure 17 D,H**).

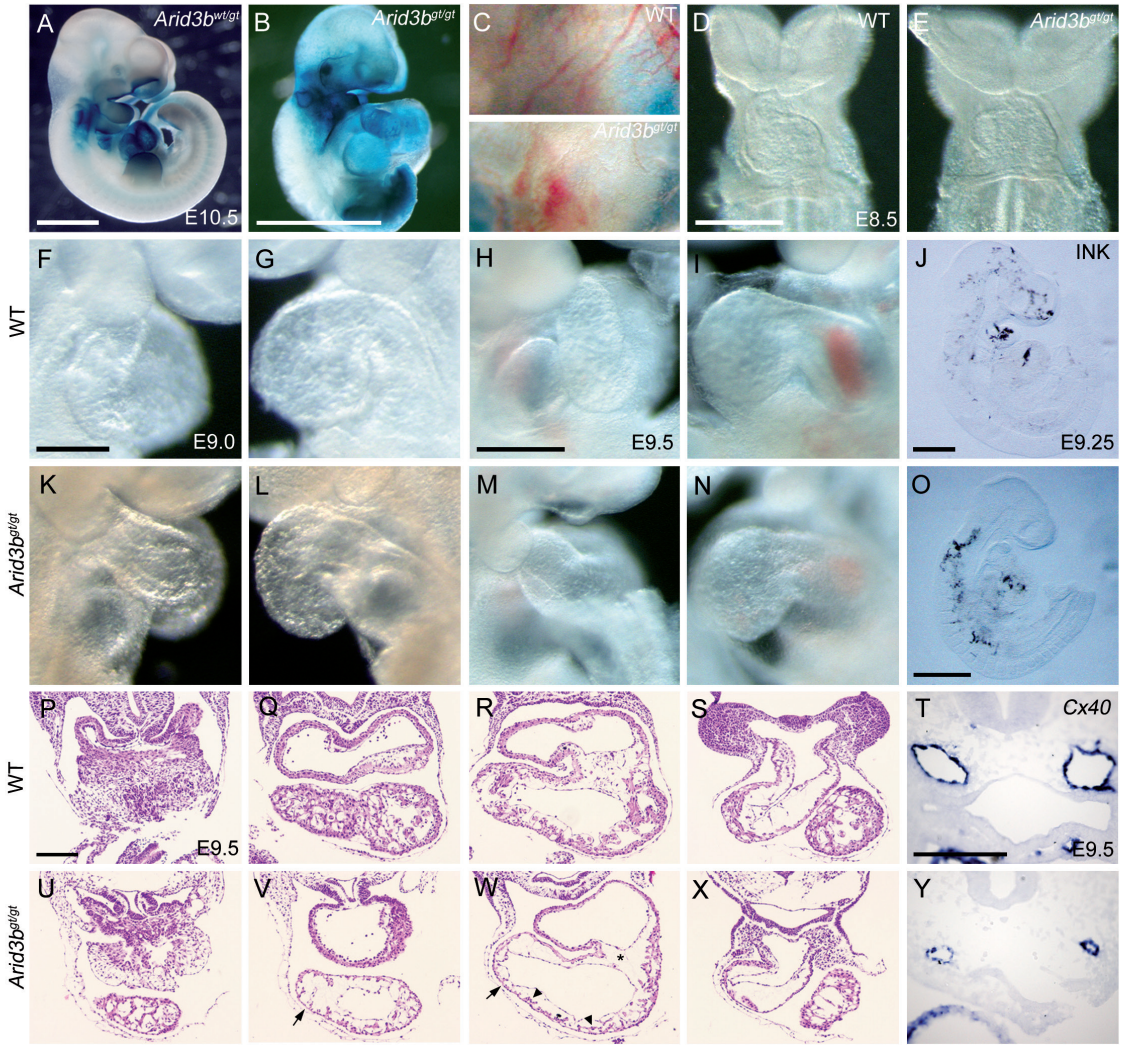

Figure 16. *Arid3b* mutant embryos show early cardiac defects. β-gal staining of *Arid3b*$^{gt/+}$ (**A**) and *Arid3b*$^{gt/gt}$ (**B**) embryos at E10.5. Major defects are seen in the mutant: smaller size (note the different scale), craniofacial and heart malformations. (**C**) Absence of normal vascular remodelling in the *Arid3b*$^{gt/gt}$ yolk sac at E10.5. (**D,E**) Defective looping and heart pole formation is seen as early as E8.5 in *Arid3b*-null embryos. (**F,G,K,L**) At stage E9.0, *Arid3b*$^{gt/gt}$ embryos show a substantial shortening of the OFT and IFT, which becomes more evident at E9.5 (**H,I,M,N**). (**J,O**) Injection of Indian ink into the heart confirms blood circulation in mutant embryos, although vessels are smaller than in wild type embryos, as shown by connexin40 expression (RNA in situ hybridisation in **T,Y**). (**P-S,U-X**) H&E staining on sections of E9.5 embryos, showing abnormal heart structure in *Arid3b*-null embryos. The poles appear disorganised (IFT, compare **U** with **P**; OFT, compare **X** with **S**). Note also the thinned myocardium (**V,W** arrows), reduced trabeculation in the ventricle (**W**, arrowheads) and absence of EMT in the AVC (**W**, asterisk). Scale bars: 150 µm P-Y; 250 µm F,G,K,L; 500 µm A,B,H-J,M-O.

On the other hand, in histological sections at E9.5, the mutant heart showed disorganized sinus horns, thinner myocardium walls in atria and ventricle and reduced trabeculation as compared with the wild type heart (**Figure 16 P-S,U-X**). Moreover, the mutant OFT was short and the

atrioventricular canal was narrow and did not show the epithelial-to-mesenchymal transition (EMT) of the endocardium that was already evident in wild-type hearts, where mesenchymal cells were conspicuous. The expression pattern of *Arid3b* and the heart defects in the mutant embryos suggest that Arid3b is directly required for proper early heart morphogenesis, although the defective vasculature, both in the embryo and in the yolk sac (**Figures 14 and 16 T,Y**), could contribute to cardiovascular failure and lethality.

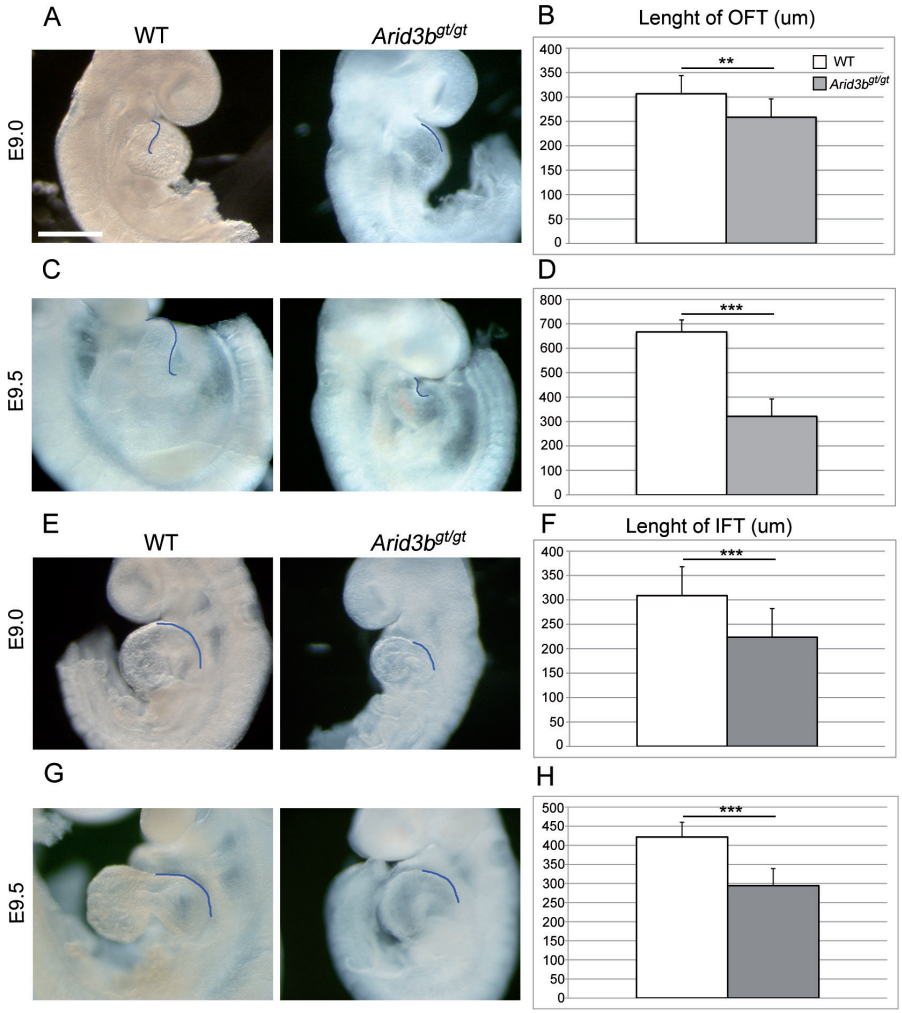

Figure 17. The poles of the heart are shortened in *Arid3b*$^{gt/gt}$ embryos. Pictures of the right side of wild type and mutant embryos at E9.0 (**A**) and E9.5 (**C**), where the blue line traces the measured inner curvature of the OFT. While already evident at E9.0 (**B**), the shortening is easier appreciated at E9.5 (**D**). Pictures of the left side of wild type and mutant embryos at E9.0 (**E**) and E9.5 (**G**), with the blue line following the outer curvature of the IFT. Note that the shortening is already strong at E9.0 (**F**) and the differences increased when stage E9.5 is achieved (**H**). Scale bar: 500 µm. Results are expressed as mean +/- SD. **p<0.01; ***p<0.001, Student's t-test.

The phenotype of *Arid3b* mutants is dependent on the genetic background of the mice

A previously published report showed that deletion of *Arid3b* during development leads to embryonic lethality but the phenotype observed is variable: at E10.5 40% of the embryos showed only growth retardation, while the rest displayed a severe phenotype similar to the one described above. On the other hand, they could recover mutant embryos at later stages (until E12.5) (Takebe A. *et al*., 2006). To elucidate whether the phenotype of *Arid3b* mutants might be dependent on the background, we backcrossed our *Arid3b*$^{gt/gt}$ line to C57BL/6 background, which was the one used in the previous report. We collected several embryos at different developmental stages and checked the phenotype. The results are depicted in **Table 2**. As can be observed, at E10.5 we obtained mutant embryos with no apparent developmental defects and could recover live embryos

till stage E12.5. No viable mutants were found after E12.5, similar to what was observed in the previous study.

Stage	Nº of litters	Total nº of embryos	Reabsor.	*gt/+*	WT	*gt/gt* with no apparent phenotype	*gt/gt* found dead	*gt/gt* with phenotype
E10.5	2	13	4	7	4	2	0	0
E11.5	3	17	3	7	5	0	4	1
E12.5	9	41	23	29	6	0	2	4
E13.5	4	21	0	14	7	0	0	0
E14.5	1	3	3	3	0	0	0	0

Table 2. Embryos from *Arid3b*$^{gt/+}$ crosses in C57BL/6 background collected at different developmental stages.

To elucidate whether mutant embryos found at E12.5 display any heart defects, we performed haematoxylin and eosin staining on an *Arid3b*$^{gt/gt}$ embryo and its *Arid3b*$^{gt/+}$ littermate recovered at E12.5 (**Figure 18**). The heart appeared smaller and a clear ventricular septum defect was observed (**Figure 18 C-D, arrow**). Curiously, the formation of endocardial cushions by EMT in the AVC, which is severely affected in the CD1 background, appeared normal in this mutant (**Figure 18 A,B**). Also, the septation of the OFT was delayed and formation of normal OFT valves was disrupted (**Figure 18 E-H, asterisk**). In conclusion, the results suggest that mouse background affects the severity of the phenotype derived from *Arid3b* mutation. All the following work was done using the gene-trap line on the CD1 background.

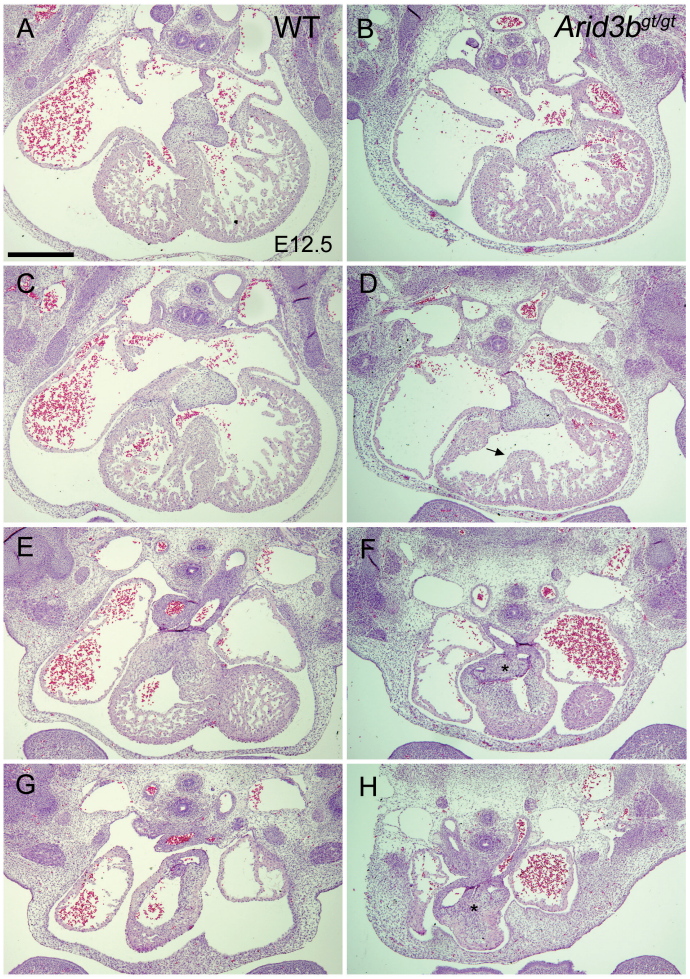

Figure 18. *Arid3b*$^{gt/gt}$ embryos on C57BL/6 background present a milder phenotype. Haematoxylin and eosin staining of E12.5 *Arid3b*$^{gt/+}$ and *Arid3b*$^{gt/gt}$ embryos. Contrary to what is observed in mutant embryos on CD1 background, the endocardial cells of the AVC undergo EMT (**A,B**). The mutant heart appears smaller and a ventricular septum defect can be observed (**C,D**, arrows). The septation of the OFT is delayed and no remodelling of the valves is observed, a process already taking place in a wild type situation (**E-H**, asterisk). Scale bar: 500 µm.

Chamber patterning and rates of proliferation and cell death are normal in the absence of *Arid3b*

To evaluate whether *Arid3b* deletion affects genes known to be important for heart formation, we performed *in situ* hybridisation to detect mRNA expression of cardiac transcription factors, signalling molecules and heart structural genes. We analysed hearts at E9.0 when the general appearance of the embryos is normal, but some cardiac defects, like heart poles shortening, are already visible. Two early cardiac master genes, later involved in the specification of chamber myocardium, *Nkx2.5* and *Gata4*, showed similar patterns and levels of expression in wild type and mutant hearts at E9.0 (**Figure 19 A-D**). Chamber patterning also appeared to be unaltered in mutant hearts, since normal expression was detected for several chamber markers: *Tbx5*, which activates chamber differentiation programme (**Figure 19 E,F**); *Mef2c*, involved in proper formation of the right ventricle (**Figure 19 G,H**), *Hand1* and *2*, with important roles in ventricular cardiomyocyte expansion and heart chamber morphogenesis (**Figure 19 I-L**), *Hey1* and *Hey2*, atrial and ventricular markers, respectively, which delimit the atrioventricular canal (**Figure 19 M-P**), *Mlc2v* and *Mlc2a*, expressed in the ventricle and atria (**Figure 19 Q-T**). These results suggest that the specification and patterning of different heart regions occur normally in *Arid3b*$^{gt/gt}$ embryos.

Because a correct balance of cell division and apoptosis is important for normal heart development, we also analysed proliferation and cell death in the heart tube and the forming heart chambers between stages E8.0 and E9.5. There were no significant differences in proliferation in any region at the stages analysed, as measured both by pH3 staining and by BrdU incorporation (**Figure 20A**). Apoptotic cell death assessed by TUNEL labelling was also similar, except for a significantly higher level in the atria of mutant hearts at E9.5 (**Figure 20B**). These results suggest that an imbalance in proliferation and cell death is not the cause of heart phenotype of *Arid3b*$^{gt/gt}$ embryos.

***Arid3b* is required for AVC patterning**

An important heart region affected in the mutant is the AVC, located between the forming chambers. Cells in this area are distinguished from atrial and ventricular neighbours by a distinct molecular code and will also undergo EMT to form the valves that separate the chambers. Expression of *Bmp2*, an upstream regulator of AVC fate, was similar in mutant and wild type hearts at E9.0 (**Figure 21A**). However, *Arid3b*-null hearts showed significantly below-normal expression of *Tbx2* and *Tbx3*, targets of Bmp signalling and determinants of AVC specification through the repression of chamber-specific genes (**Figure 21A**). Notably, expression of the chamber myocardium marker *Anf*, repressed by Tbx2/3, was expanded to the AVC region (**Figure 21A**). These altered expression patterns persisted at E9.5 (**Figure 21B**), where almost no expression of *Tbx3* could be detected in the inner curvature of the AVC and *Anf* signal was continuous through it. These alterations were now accompanied by a relative drop in the expression of *Bmp2* (**Figure 21B**), indicating

disruption of the regulatory feedback loop between Tbx2/3 and Bmp2 and leading to abnormal AVC formation. Not only *Anf*, but also other genes expressed in the chamber myocardium, like *Cx40*, were expanded into the AVC in mutant embryos (**Figure 21B**).

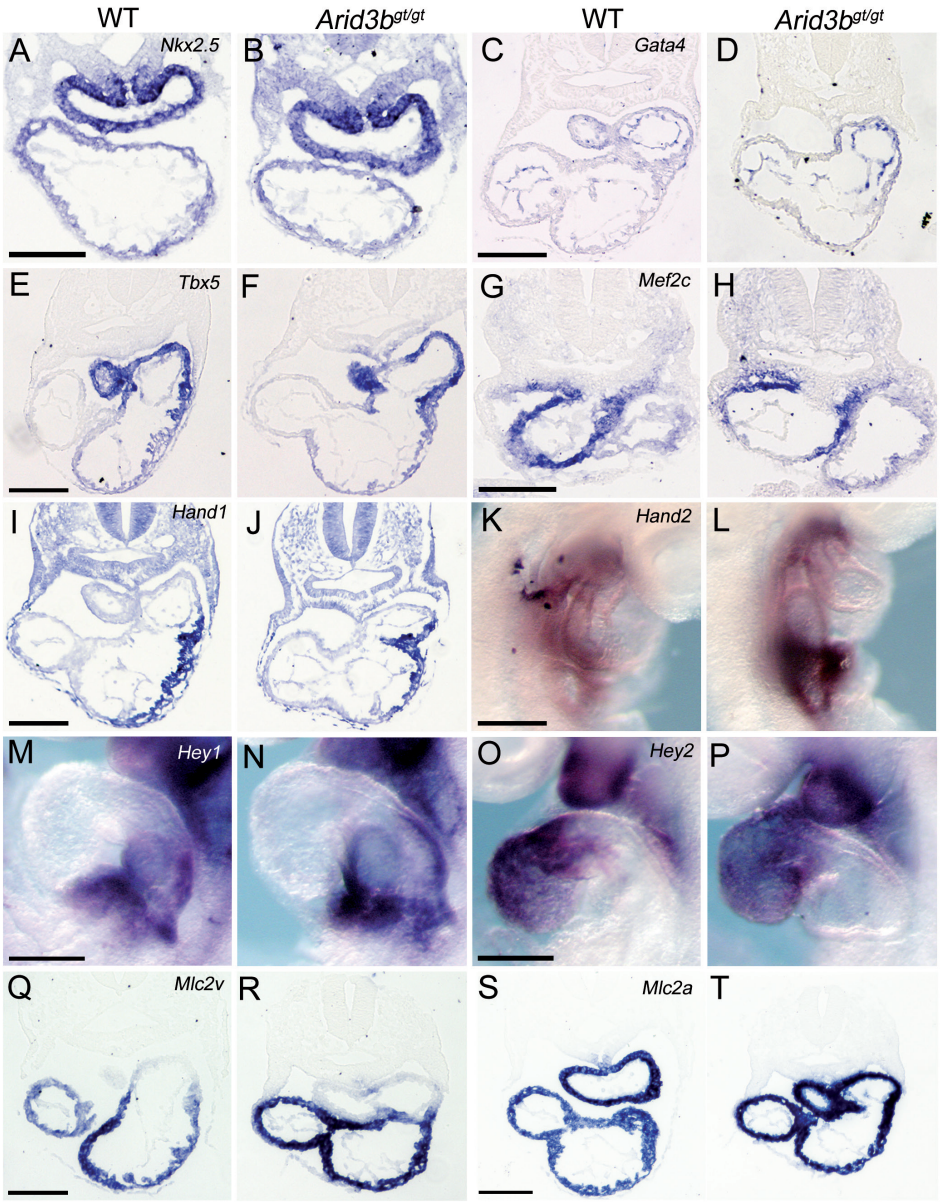

Figure 19. Patterning of the heart is not affected in *Arid3b*$^{gt/gt}$ embryos. Analysis of gene expression in E9.0 embryos by RNA *in situ* hybridisation. **A-D.** Expression of the cardiac master genes *Nkx2.5* and *Gata4* is normal in mutant embryos. **E-T.** Chamber patterning is not altered in *Arid3b* mutants, as shown by normal expression of *Tbx5* (**E,F**), *Mef2c* (**G,H**), *Hand1/2* (**I-L**), *Hey1/2* (**M-P**) and *Mlc2v/2a* (**Q-T**). Scale bars: 150 µm A-J, Q-T; 250 µm K-R.

Figure 20. Proliferation and cell death are not affected in the hearts of *Arid3b*$^{gt/gt}$ embryos. A. Cell proliferation measured by pH3 immunostaining at different stages and in different heart regions (**b,c,e,f**; **a** shows the quantification of the results) and by BrdU incorporation at E8.5 (**d,g**); no statistically significant differences were detected between mutant and wild-type embryos **B.** Cell death measured by TUNEL; statistically significant differences are only observed at E9.5 in the atria (**a,c,f**). Results are expressed as mean +/- SD. ***p<0.001, Student's t-test.

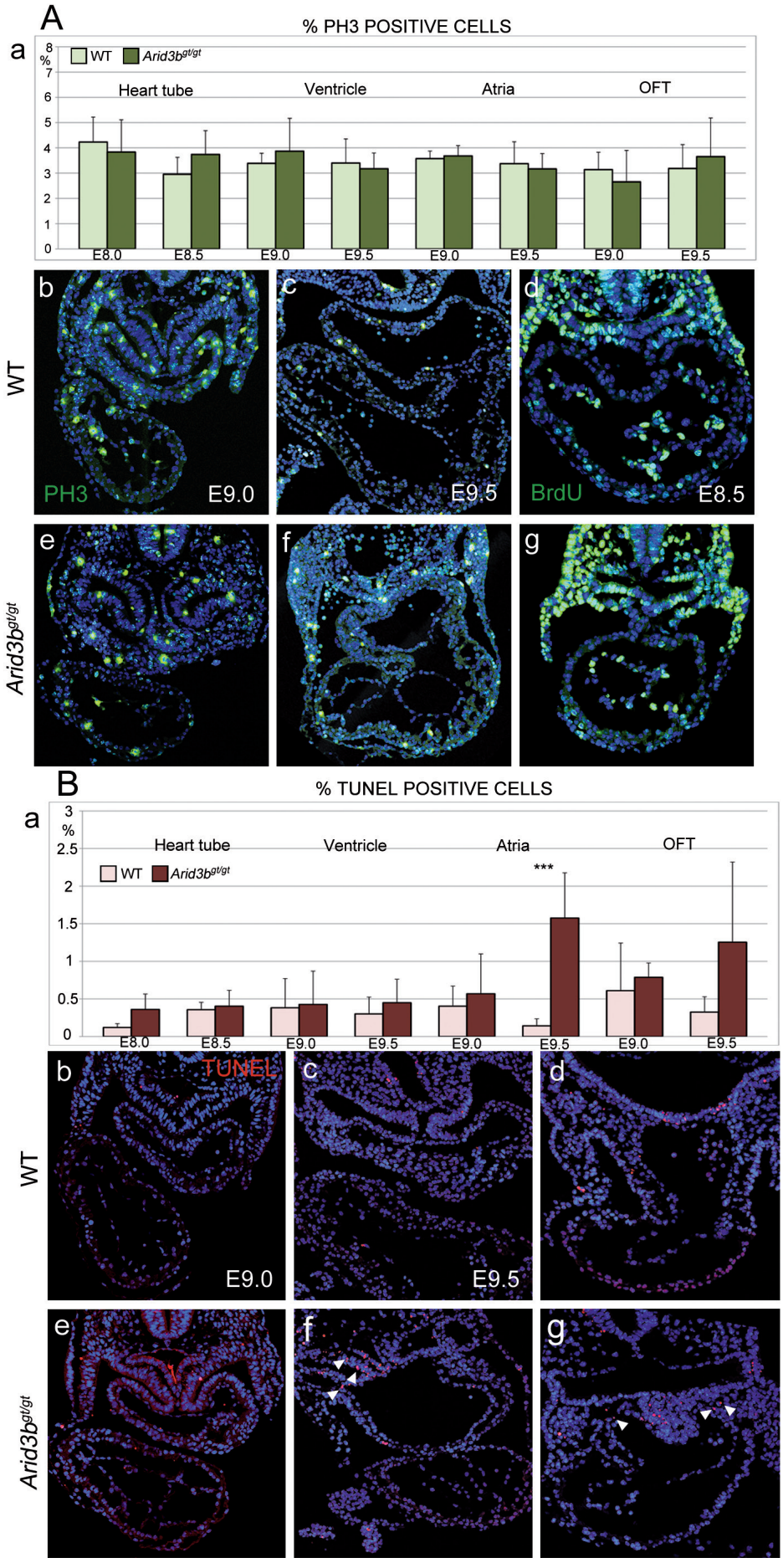
A
% PH3 POSITIVE CELLS
a
WT
Arid3b gt/gt
Heart tube
Ventricle
Atria
OFT
E8.0
E8.5
E9.0
E9.5
E9.0
E9.5
E9.0
E9.5
b
c
d
WT
PH3
E9.0
E9.5
BrdU
E8.5
e
f
g
Arid3b gt/gt
B
% TUNEL POSITIVE CELLS
a
Heart tube
Ventricle
Atria
OFT
***
WT
Arid3b gt/gt
b
TUNEL
c
d
E9.0
E9.5
e
f
g

To characterize the origin of the AVC alterations we analysed by immunostaining pSmad expression, which mediates BMP signalling. Consecutive sections were stained with *Bmp2* to define the AVC region. In the AVC myocardium, similar nuclear localization of pSmad, indicative of pathway activation, was observed in wild type and *Arid3b*$^{gt/gt}$ hearts at E9.0 (**Figure 22 C, D**) and E9.5 (**Figure 22 G-I**), despite the lower *Bmp2* expression in mutants at E9.5 as described above (**compare Figure 22 A, B with E, F**). On the other hand, pSmad nuclear localization was present in mutant AVC endocardium at E9.0 at a similar level then in wild type endocardium (**Figure 22 C,D**) but at E9.5 the number of pSmad-positive endocardial cells was lower in mutant than in wild type AVC (**Figure 22 G,H,J**). These results suggest that Arid3b acts in the myocardium downstream of pSmad nuclear translocation and that its absence disrupts the relay of Bmp2 signalling to the endocardium.

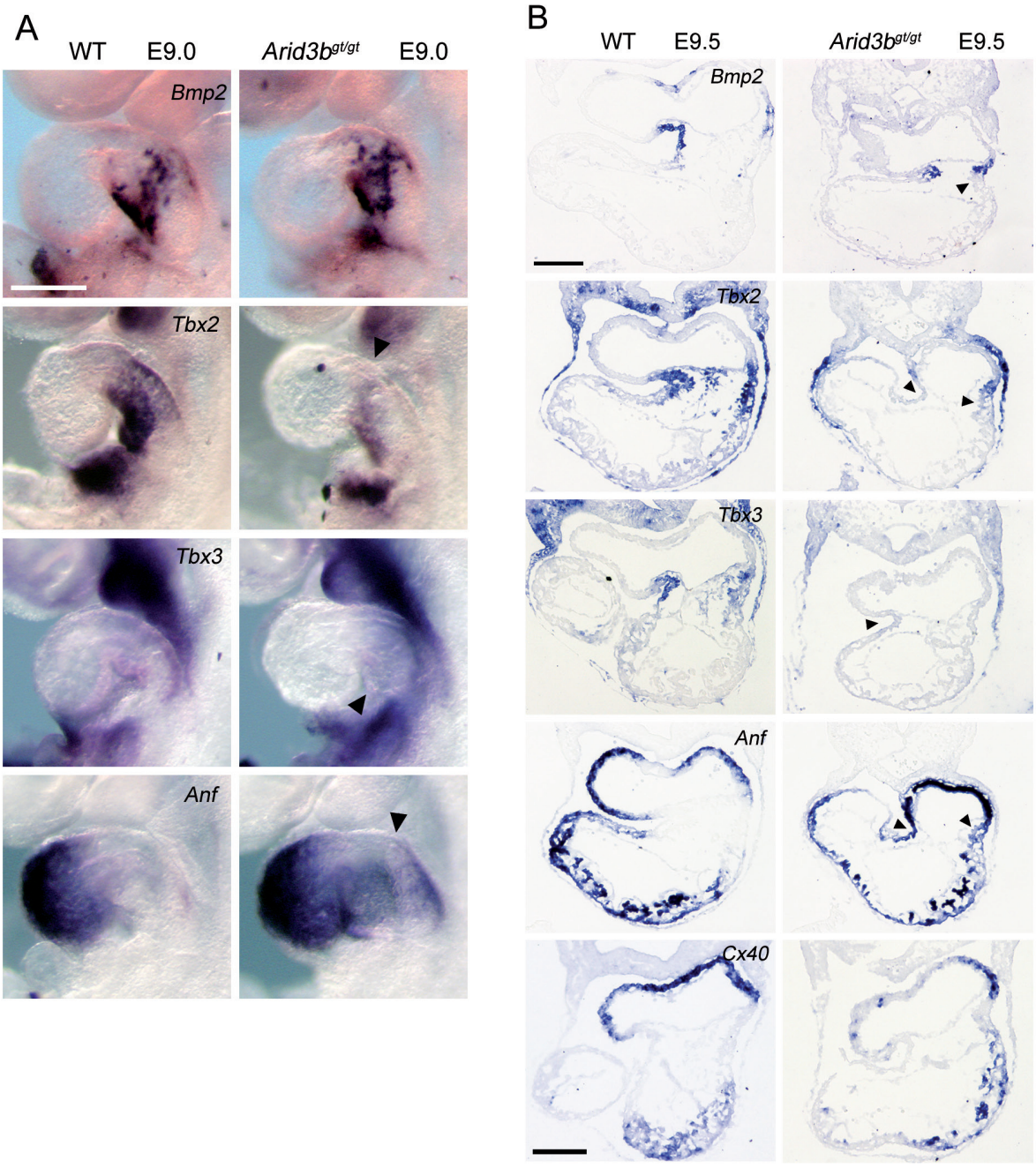

Figure 21. Arid3b is required for patterning of the AVC. A. *In situ* hybridisation of molecules important for AVC patterning at E9.0 in whole mount. *Bmp2* expression in E9.0 *Arid3b*$^{gt/gt}$ embryos is normal but *Tbx2* and *Tbx3* (arrowheads) are below-normal and expression of the chamber marker *Anf* is expanded (arrowhead). **B.** *In situ* hybridisation at E9.5 on paraffin sections. In E9.5 *Arid3b*$^{gt/gt}$ embryos *Bmp2* expression diminishes (arrowhead), *Tbx2* and *Tbx3* expression remains low (arrowhead), and expansion of *Anf* towards the AVC is more evident (arrowhead). *Cx40*, another marker of chamber myocardium, is also expanded towards AVC in the mutant. Scale bars: panel A 250 µm; panel B 150 µm.

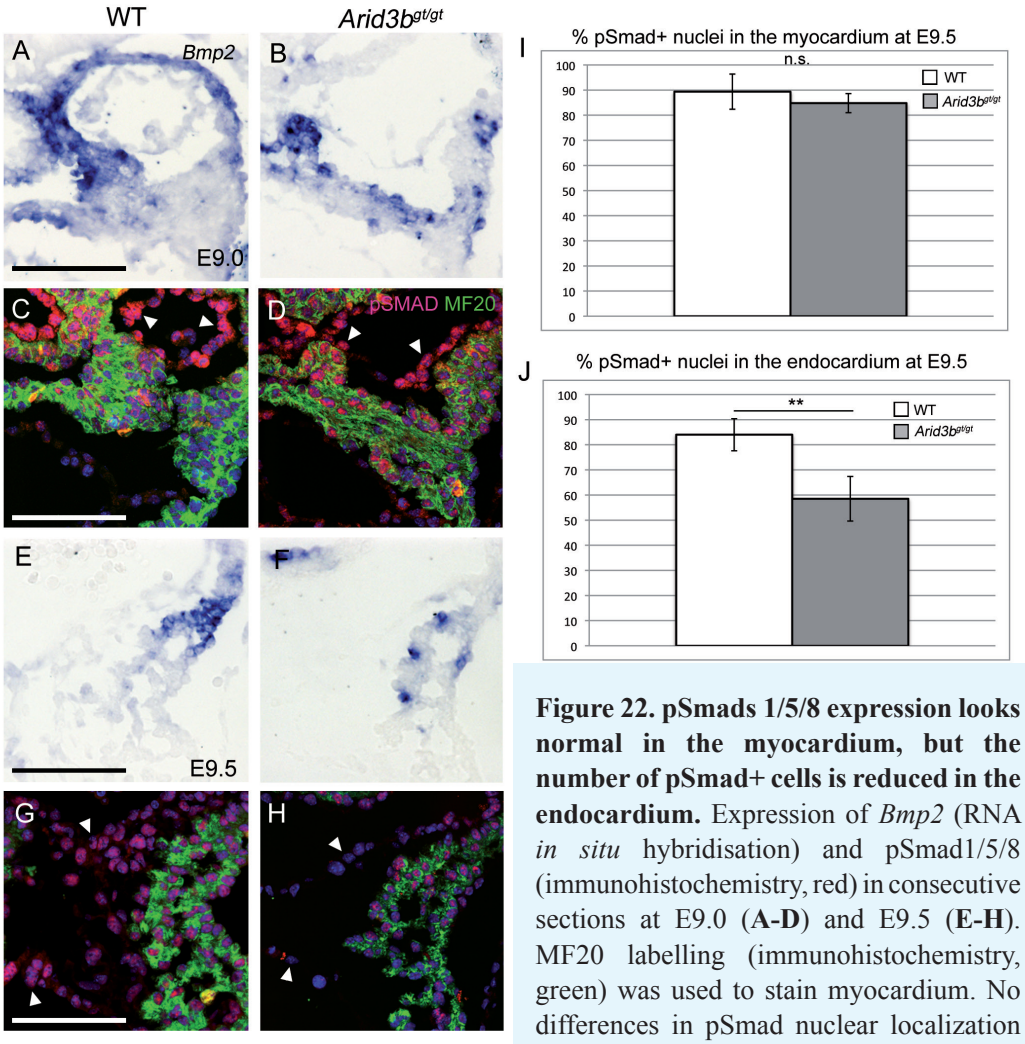

Figure 22. pSmads 1/5/8 expression looks normal in the myocardium, but the number of pSmad+ cells is reduced in the endocardium. Expression of *Bmp2* (RNA *in situ* hybridisation) and pSmad1/5/8 (immunohistochemistry, red) in consecutive sections at E9.0 (**A-D**) and E9.5 (**E-H**). MF20 labelling (immunohistochemistry, green) was used to stain myocardium. No differences in pSmad nuclear localization between wild type and *Arid3b*$^{gt/gt}$ embryos are seen in the myocardium at any stages analysed, but a much lower number of pSmad-positive nuclei is evident in *Arid3b*$^{gt/gt}$ endocardium at E9.5 (**G,H**, arrowheads), although not at E9.O (**C,D**, arrowheads). Graphs representing the per cent of pSmad+ nuclei in the myocardium (**I**) and in the endocardium (**J**) at E9.5 in wild type and *Arid3b*$^{gt/gt}$ embryos. While in the myocardium the proportion of pSmad+ cells is similar between the two conditions, in the endocardium there is a statistically significant reduction in the proportion of pSmad-expressing cells in the *Arid3b*-null embryos. Scale bars: 100 µm. Results are expressed as mean +/- SD. **p<0.01, Student's t-test.

Arid3b does not bind pSmad1 *in vitro*

The data shown above point to a normal activation of the Bmp2 pathway in the myocardium until the step of pSmad nuclear translocation; however, normal activation of *Tbx2* and *Tbx3* did not occur. Although it was recently shown that, at least in the case of Tbx2, a region located upstream Tbx2 promoter enriched in pSmad binding sites is sufficient to drive its expression, the regulation seems to be far more complex. For instance, Tbx20, also expressed in the myocardium, competes with Smad4 for binding to Smad1/5/8, thus inhibiting Tbx2 activation (Singh R. *et al*., 2009). On the other hand, pSmad DNA-binding is thought to be stabilized by other sequence specific DNA-binding proteins to ensure successful activation of its targets (Blitz I.L. and Cho, 2009). We wondered whether Arid3b could be involved in the proper activation of Tbx2 by directly interacting with pSmad proteins. To address this question we cloned human *Arid3b* into a Flag-vector and co-transfected it together with mouse Smad1-Myc (Singh R. *et al*., 2009) into HEK cells to test whether they co-immunoprecipitate.

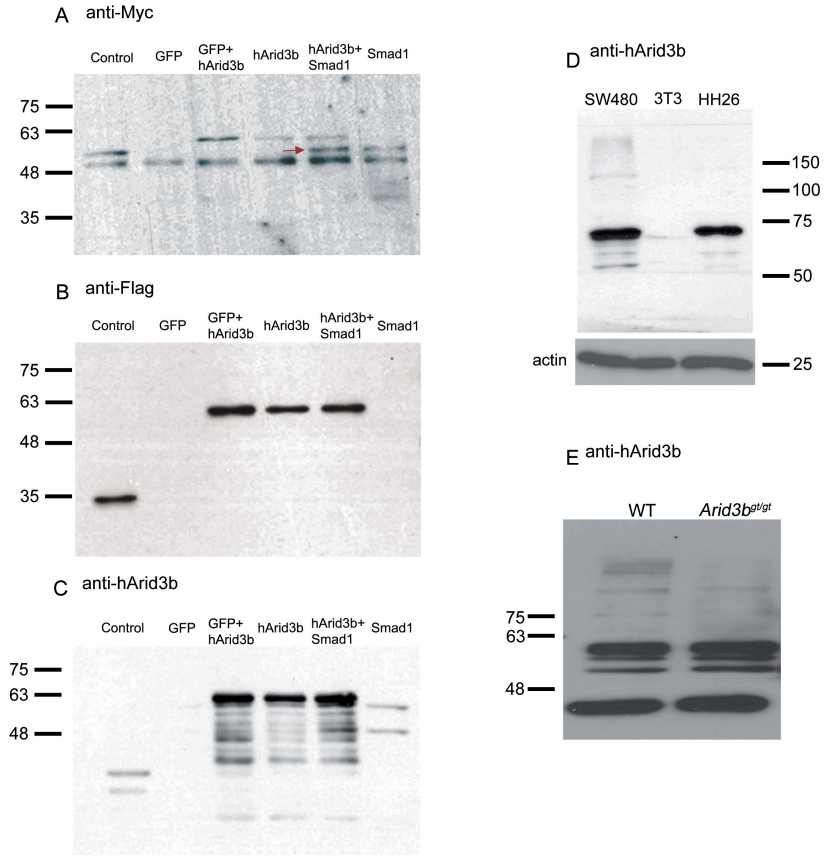

Figure 23. Successful overexpression of hArid3b-Flag and Smad1-Myc in HEK cells. A. Western blot with anti-Myc antibody to detect Smad1 overexpression in HEK293 cells. A specific band of 50-60 kDa is detected in samples transfected with Smad1-Myc plasmid (arrow). Smad1-Myc from previous transfections is used as a control for antibody **B.** Western blot with anti-Flag antibody to detect hArid3b overexpression in HEK293 cells. A unique band of around 60 kDa is visible in the three dishes that were transfected with the hArid3b-Flag plasmid. A truncated form of Arid3b of around 35kDa is used as a positive control for the antibody. **C.** Western blot with anti-hArid3b commercially available antibody. A distinct band is detected only when cells are transfected with hArid3b-Flag plasmid. A truncated form of Arid3b of around 35kDa is used as a positive control for the antibody. **D.** Western blot with anti-Arid3b antibody on protein extracts from the SW480 cell line (human colon adenocarcinoma cell line), 3T3 cell line (mouse fibroblast cell line) and chick embryos at stage HH26 (Hamburger V. and Hamilton, 1951). While in human and chick samples a band of expected size is detected, it does not appear in the mouse sample. **E.** Western blot with anti-Arid3b antibody on samples extracted from a pool of wild type and mutant embryos. Note that the pattern of bands is similar between the two samples and no specific band of the expected size is detected in the wild type extract.

We first checked whether overexpression was observed in cells by Western blot with anti-Myc-tag, anti-Flag-tag and anti-human Arid3b antibodies (**Figure 23 A-C**). Western blot against Myc-tag showed a specific band in the conditions where Smad1 was transfected (**Figure 23A, arrow**). Similarly, anti-Flag antibody detected a unique band of the expected size in cells transfected with hArid3b-containing plasmid (**Figure 23B**). Moreover, anti-hArid3b antibody recognizes a distinct band in cells transfected with hArid3b-Flag, a band not present in cells with only endogenous levels of Arid3b (**Figure 23C**). Indeed, it seems that endogenous levels of Arid3b in HEK cells are quite low, as we confirmed that the antibody recognized a band of the expected size for Arid3b in SW480 cells, where high levels of Arid3b have been detected in a previous study (Numata S. *et al*., 1999) (**Figure 23D**). However, the antibody did not recognize mouse Arid3b, since no specific band could be detected by Western blot in embryonic extracts from *Arid3b*$^{gt/gt}$ and wild type embryos (**Figure 23E**).

Subsequently, immunoprecipitation was carried out with beads attached to anti-Flag antibody in samples co-transfected with hArid3b-Flag and Smad1-Myc and in control samples. We confirmed that the transfected Arid3b-Flag was binding to the beads both when transfected alone or co-transfected with Smad1 (**Figure 24A**). Contrary, while a clear band was visible in the input, no band was detected with anti-Myc antibody in these samples (**Figure 24B**), suggesting that no co-immunoprecipitation took place between hArid3b-Flag and Smad1-Myc. The result suggests that under these experimental conditions Arid3b does not bind pSmad1.

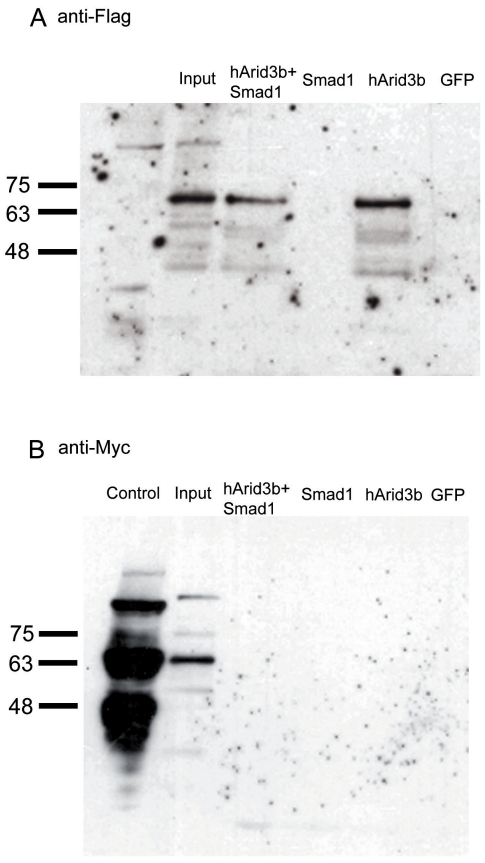

Figure 24. Arid3b and Smad1 do not co-immunoprecipitate *in vitro*. A. Western blot on samples immunoprecipitated with beads attached to anti-Flag antibody and revealed with a different anti-Flag antibody. As expected, in samples transfected with hArid3b-Flag plasmid a band of the hArid3b-Flag protein size (input) is detected. **B.** Western blot on samples immunoprecipitated with beads attached to anti-Flag antibody and revealed with anti-Myc antibody. Although present in the sample (input), Smad1-Myc does not co-immunoprecipitate with proteins recognized by anti-Flag beads. PAE-N1IC clone1 cell extract, which overexpress N1IC-Myc, is used as a positive control for the Myc antibody (Timmerman L.A. et al., 2004)

Defective EMT in *Arid3b*$^{gt/gt}$ AVC can be rescued by BMP2 *in vitro*

Bmp2 from the myocardium signals to the endocardium and through pSmad activation promotes EMT, an early step in valve formation. The reduction in the number of pSmad positive cells in the endocardium of the AVC in mutant embryos at E9.5 suggests that the process of EMT could be affected. To gain further insight into *Arid3b* function in the AVC, we analysed the expression of EMT markers, some of which are indeed known targets of Bmp signalling. Snail1 plays a central role in EMT by repressing cadherins necessary for cell adhesions, and is regulated by both Bmp2 and Notch pathway (Timmerman L.A. *et al*., 2004) (Luna-Zurita L. *et al*., 2010). Tgfβ2 is expressed in the myocardium, where it is a target of Bmp2 signalling and in the endocardium, where it is involved in EMT. Twist1 is also required for AVC EMT downstream of Bmp2 (Ma L. *et al*., 2005), while Tbx20 is strongly expressed in mesenchymal cells and is involved in later events of valve remodelling (Shelton E.L. and Yutzey, 2008). Has2 is a hyaluronic acid synthetase and its absence in the endocardium leads to decreased EMT (Camenisch T.D. *et al*., 2000). At E9.5 EMT is already detected in the wild type AVC, and transformed cells expressing the above mentioned mesenchymal markers are observed in the cardiac jelly (**Figure 25A**). In contrast, these cells are not present in *Arid3b*-deficient AVC (**Figure 25A**). Moreover, although *Tgf*β*2* expression was detected in wild type and *Arid3b*-null AVC myocardium (**Figure 25A**), its expression in the mutant AVC endocardium was undetectable, as well as the expression of *Snail1*, *Twist1* and *Tbx20*. By the contrary, *Has2* was expressed normally in the *Arid3b*$^{gt/gt}$ endocardium (**Figure 25A**).

Because the Notch pathway has been described as playing a crucial role in AVC EMT, we decided to check whether this pathway was disrupted in the mutant endocardium. We analysed the expression of two Notch ligands, Delta4 and Jagged1, which act as activators of the Notch pathway in the AVC. No differences between wild type and mutants were observed (**Figure 25B**). Moreover, we checked whether the active form of Notch1 translocates into the nucleus by immunostaining against NICD1 (**Figure 25B, arrowheads**). NICD1 positive nuclei could be detected in *Arid3b*$^{gt/gt}$ endocardium, suggesting that the observed EMT disruption is independent of the Notch pathway.

The reduction of the number of pSmad1/5/8 positive nuclei in the endocardium suggests that the primary defect in these mutants is the incorrect relay of myocardial Bmp2 signal to the endocardium. To test this possibility, we cultured AVC explants on collagen gels *in vitro*. In these conditions, endocardial cells undergo EMT and invade the collagen gel, a process which can be measured and quantified as the transformation index (% invading cells/total number of transformed cells, see Materials and Methods). Compared with wild type AVC explants, mutant explants generated significantly fewer transformed cells and, more importantly, a significantly lower transformation index (**Figure 26 A-C**). Because the *in vitro* system reproduced the results observed *in vivo*, we decided to check whether *Arid3b*$^{gt/gt}$ endocardium is responsive to Bmp2. Indeed, addition of Bmp2 to the culture medium rescued the defects restoring the total number of transformed cells and the transformation index to values similar to those of wild type explants (**Figure 26 A-C**). This result confirms that the EMT deficiency in *Arid3b* mutant AVC is caused by

inefficient BMP2 signalling from the myocardium to the endocardium.

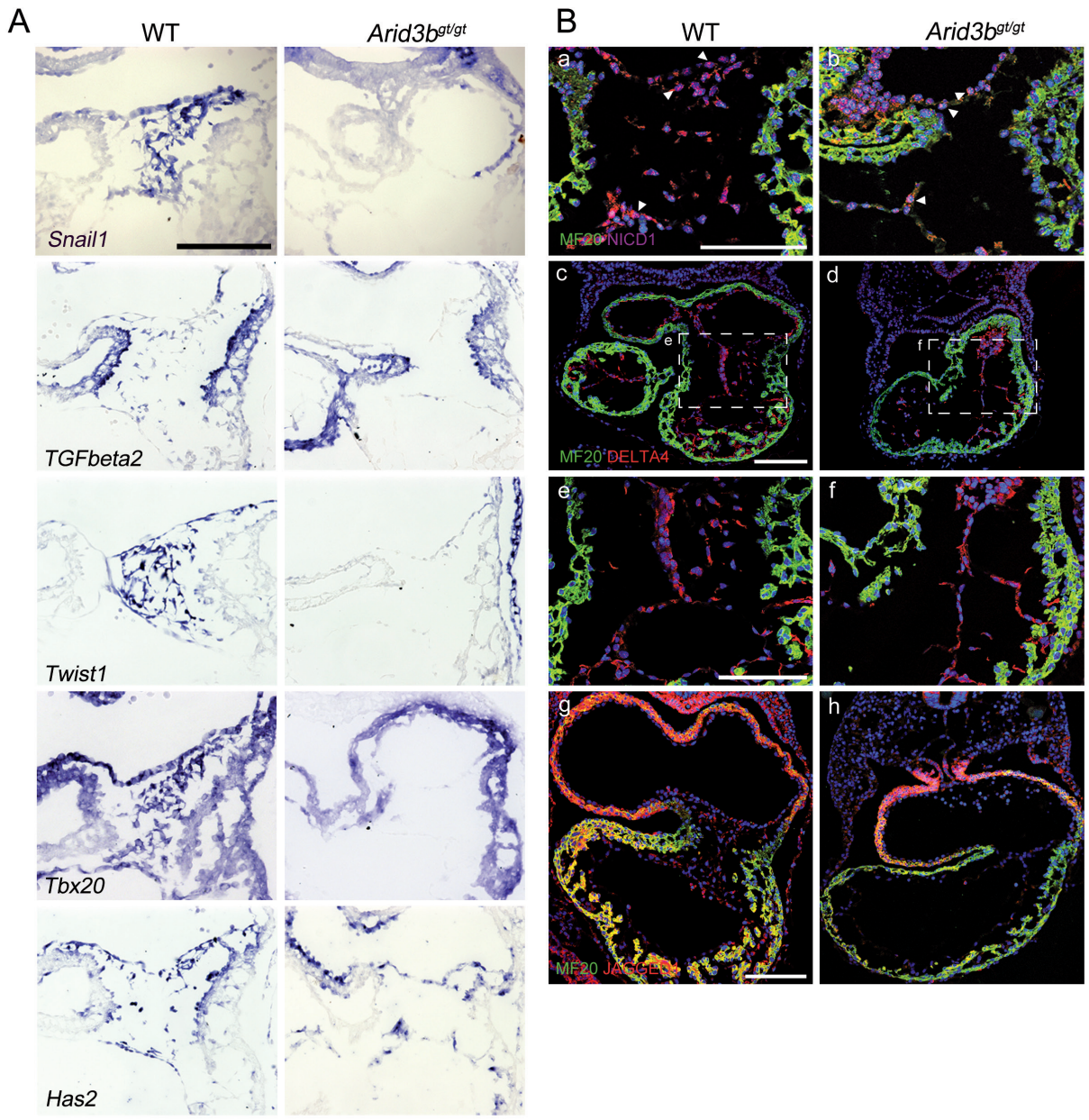

Figure 25. Disruption of EMT in *Arid3b* mutant hearts. A. *In situ* hybridisation of molecules involved in EMT in the AVC. Expression levels of *Snail1*, *TGFbeta2*, *Twist1* and *Tbx20* are significantly lower in the mutant AVC endocardium, whereas *Has2* is unaltered; note also the almost total absence of mesenchymal cells invading the cushions in the mutant. **B.** Immunostaining against Notch1 active form, NICD1 (**a,b**, red), and Notch1 ligands present in the heart at this stage, Delta4 (**c-f**, red) and Jagged1 (**g,h**,red). MF20 is used to stain myocardium (green). Expression of the ligands of Notch1 is similar between wild type and mutant embryos and, consistent with it, NICD1 positive nuclei are detected in the AVC endocardium (arrowheads). Scale bars: panel A, panel B c,d,g,h 150 μm; panel B a,b,e,f 100 μm.

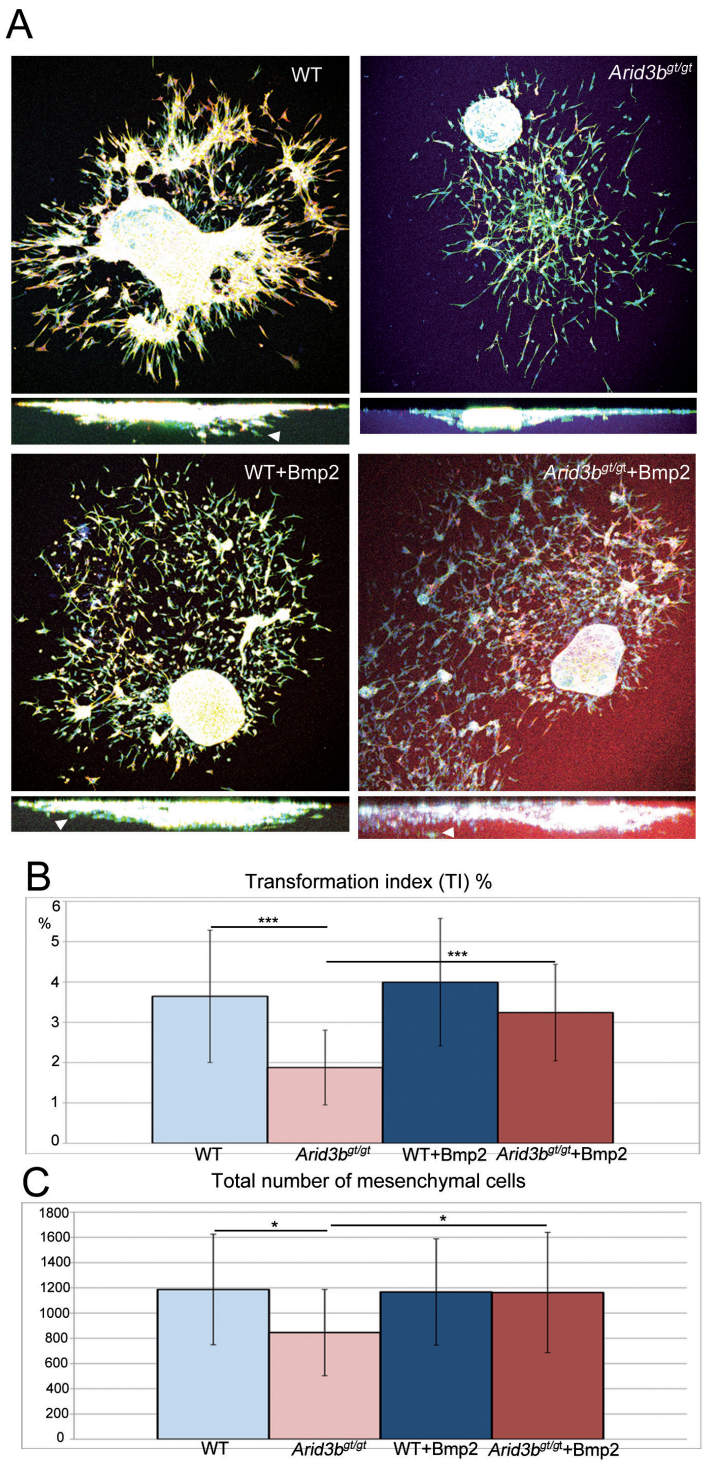

Figure 26. EMT can be rescued *in vitro* by addition of Bmp2. AVC explants on collagen gels stained for SMA (red) and phalloidin (green) (**A**). The bottom small panels show a confocal Z section to detect invasive cells (arrowheads). Both the total number of mesenchymal cells and the number of cells invading the gel (transformation index, TI in %; arrowheads) were lower significantly in mutant explants (**B,C** show quantification of the results). After addition of BMP2, the total number of mesenchymal cells and the TI were restored to the levels in wild-type explants (**B,C**). Results are expressed as mean +/- SD. * $p<0.05$; ***$p<0.001$, Student's t-test.

Microarray analysis identifies candidate genes and processes mediating Arid3b effects on heart development

To identify the genes regulated by Arid3b that mediate its effects on heart development, we performed a microarray comparison of mRNA expression between wild type and mutant embryos. In two separate experiments, RNA was extracted from whole E9.0 embryos or from E9.5 hearts, heads and trunks and expression compared between the samples using Agilent chips (**Figure 27**

A-C). As can be observed, if specific filters are applied (p value less than 0.05 and a fold change of <> +/-2), most of the differentially expressed genes are upregulated in whole E9.0 embryos. At E9.5, while not so dramatic, there are also more up-regulated genes in the three regions analysed. Of the genes showing differential expression in *Arid3b*-null embryos, 93 were altered in both E9.0 whole embryos and E9.5 hearts and 453 genes were common to the three tissues analysed in E9.5 embryos (**Figure 27 D-E** and **Supplementary Tables 1-2**). We used the Ingenuity software to analyse functionally the data and identify the top highly overrepresented functions in the sets of common genes, as well as in the separated regions. The results, shown in **Tables 3** and **4**, correspond to the five top molecular and cellular functions in each condition. As can be seen, cell morphology appears in all the conditions, while the top function in the common genes for heart, head and trunk at E9.5 is cellular movement. These results support a role for Arid3b in the control of cell motility and cellular rearrangements.

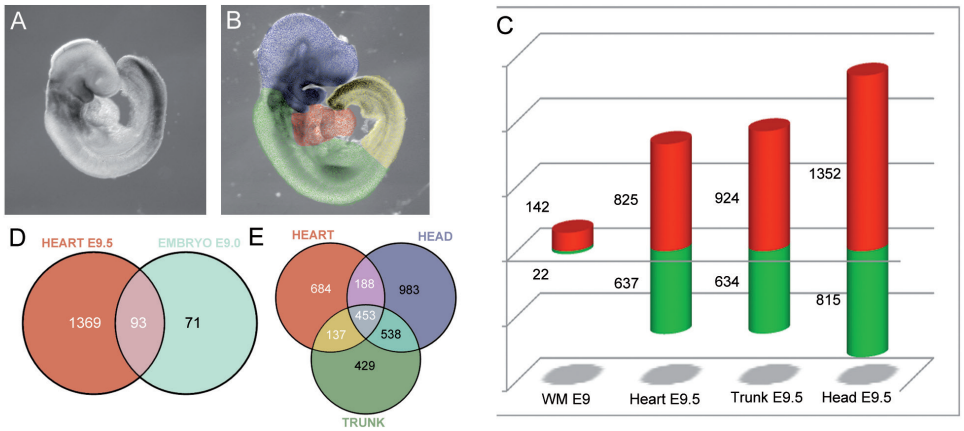

Figure 27. General information obtained from the microarray. Samples used for the microarrays. RNA was extracted from whole embryos at E9.0 (**A**) or from dissected heart, head and trunk regions of E9.5 embryos as shown in colours (**B**). **C**. Analysis of the microarray expression data, using a 2 fold-change threshold and an adjusted p-value of less than 0.05 for false discovery rate, identified a total of 164 genes in E.9 whole embryos, 1462 genes in E9.5 hearts, 1558 genes in E9.5 trunk regions and 2167 in E9.5 heads as differentially expressed between mutant and control embryos. **D-E**. The lists of genes were compared to identify genes similarly altered in the different conditions; 93 were common to E9.0 whole embryos and E9.5 hearts (**D**) and 453 genes were similarly altered in the three tissues analysed in E9.5 embryos (**E**).

To validate the microarray data, we performed mRNA *in situ* hybridisation analysis of the genes that showed high differential expression (**Figure 28**). Selected genes included members of important signalling pathways, genes described to play roles in embryonic development and genes involved in vessel or muscle differentiation. Clear up- or downregulation of these genes was observed in agreement with the microarray result. Among the genes analysed were *HeyL,* a downstream effector of the Notch pathway (Fischer A. *et al*., 2007), which appeared completely downregulated in the entire embryo (**Figure 28 E,J**). *Dkk3*, a Wnt antagonist (Witte F. *et al*., 2009), was upregulated in the heart (**Figure 28 K,L,P,Q**).

Heart E9.5		
Molecular and cellular functions		
Name	p-value	Num. Molecules
Cellular movement	1,48E-17-1,91E-04	258
Cell morphology	1,56E-16-2,32E-04	278
Cellular development	4,85E-16-2,34E-04	391
Cell death and survival	2,68E-14-2,11E-04	378
Cell-to-cell signalling and interaction	1,19E-12-2,24E-04	262

Head E9.5		
Molecular and cellular functions		
Name	p-value	Num. Molecules
Cellular development	1,99E-17-1,48E-03	506
Cell morphology	9,36E-17-1,41E-03	380
Cell death and survival	7,36E-12-1,46E-03	505
Molecular transport	8,96E-11-1,47E-03	349
Cellular growth and proliferation	9,48E-10-1,50E-03	498

Trunk E9.5		
Molecular and cellular functions		
Name	p-value	Num. Molecules
Cell morphology	1,17E-17-1,43E-03	321
Cellular development	1,65E-16-1,40E-03	418
Cellular movement	2,71E-12-1,38E-03	249
Cellular growth and proliferation	6,43E-12-1,34E-03	405
Cell death and survival	1,24E-11-1,44E-03	389

Embryo E9.0		
Molecular and cellular functions		
Name	p-value	Num. Molecules
Cellular growth and proliferation	3,26E-07-8,29E-03	65
Cell morphology	5,53E-07-9,90E-03	29
Cellular function and maintenance	5,53E-07-9,14E-03	42
Small molecule biochemistry	1,50E-05-9,71E-03	38
Carbohydrate metabolism	3,97E-05-1,02E-02	20

Table 3. Top molecular functions overrepresented in the four different samples as analysed by Ingenuity.

Intersection Heart E9.5 and whole embryo E9.0		
Molecular and cellular functions		
Name	p-value	Num. Molecules
Cell morphology	5,71E-08-2,03E-02	25
Cellular function and maintenance	5,71E-05-2,03E-02	32
Cellular growth and proliferation	2,00E-06-1,88E-02	42
Cell death and survival	1,07E-05-1,91E-02	37
Cellular assembly and organization	2,20E-05-1,53E-02	17

Intersection Heart, Head and Trunk at E9.5		
Molecular and cellular functions		
Name	p-value	Num. Molecules
Cellular movement	2,09E-10-5,03E-03	91
Cellular function and maintenance	5,39E-08-5,31E-03	112
Cell death and survival	6,16E-08-5,36E-03	124
Cell morphology	2,10E-07-4,69E-03	103
Cellular growth and proliferation	7,31E-07-5,36E-03	121

Intersection Heart, Head, Trunk E9.5 and embryo E9.0		
Molecular and cellular functions		
Name	p-value	Num. Molecules
Cellular function and maintenance	1,32E-08-2,03E-02	30
Cell morphology	3,18E-08-2,03E-02	22
Cellular growth and proliferation	5,24E-07-2,21E-02	39
Carbohydrate metabolism	1,46E-05-2,06E-02	13
Cell death and survival	1,65E-05-2,43E-02	33

Table 4. Top molecular functions overrepresented in the set of common genes between Heart E9.5 and whole embryos at E9.0, between Heart, Head and Trunk at E9.5 and between the four conditions.

Other genes, such as the potassium channel *Kcne3* (de Castro M.P. *et al*., 2006) or the transcription factor *Sox7* (Takash W. *et al*., 2001), were up regulated in the vasculature and the endocardium (**Figure 28 A-D, F-I**). The chromatin remodelling protein *Kdm3a*, which regulates smooth muscle cell differentiation (Lockman K. *et al*., 2007), was also upregulated in the heart (**Figure 28 M,N,R,S**), as was *Nox4*, a NAPDH oxidase involved in myocardial differentiation (Li J. *et al*., 2006) (**Figure 28 U,V,Z,A'**). Outside the heart, *Insc*, a key regulator of mitotic spindle orientation (Carmena A. *et al*., 1998) and neutrophil chemotaxis (Kamakura S. *et a*l., 2013), was practically absent in the dorsal root ganglia (**Figure 28 O,T**). The results of the microarray also point to a role of Arid3b in muscle differentiation, as genes related to this process were missexpressed in the mutant. In the somites, the expression of *Vgll2* and the chaperone *Unc45b*,

both involved in muscle formation (Bonnet A. *et al*., 2010) (Price M.G. *et al*., 2002), was severely reduced (**Figure 28 X,Y,C',D'**). However, levels of *Vgll2* appeared normal in the branchial arches, although the signal did not expand as caudally as in wild type embryos (**Figure 28 W,B'**).

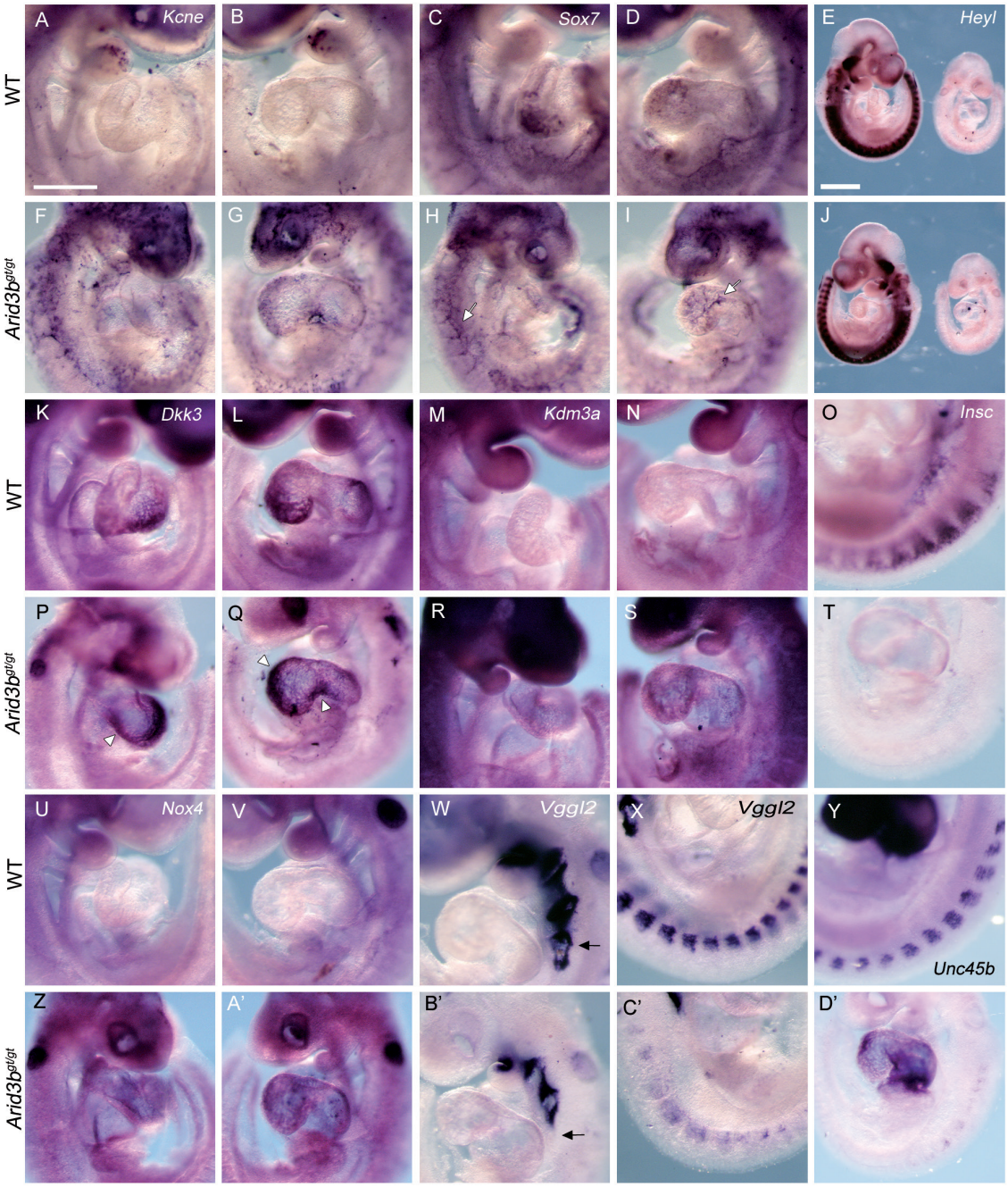

Figure 28. Validation of microarray gene-expression profiling by RNA *in situ* hybridisation at E9.5. Whole-mount RNA *in situ* hybridisation showing differential expression of selected genes in *Arid3b*$^{gt/gt}$ embryos at E9.5. *Kcne3* (**A,B,F,G**) *Sox7* (**C,D,H,I**, white arrowheads), *Dkk3* (**K,L,P,Q**, white arrowheads), *Kdm3a* (**M,N,R,S**) and *Nox4* (**U,V,Z,A'**) appeared upregulated in the mutant embryos. *HeyL* (**E,J**), *Insc* (**O,T**), *Vgll2* (**W,X,B',C'**) and *Unc45b* (**Y,D'**) were strongly downregulated in different regions of the embryo. Scale bar: 500 µm; E,J 1 mm.

For more in depth analysis, we focused on two up-regulated genes that could provide mechanistic insight into Arid3b function.

- Bhlhb2 (also known as Bhlhe40, Stra13, DEC1, Sharp2) is a transcription factor of the basic helix-loop-helix family expressed in a number of cell types during mouse embryogenesis. Several studies have revealed that it is involved in a variety of processes, such as cellular differentiation programs, cell cycle progression, senescence, apoptosis, immune responses, tissue regeneration and circadian rhythms (Sun H. and Taneja, 2000) (Honma S. *et al*., 2002) (Shen M. *et al*., 2002) (Miyazaki K. *et al*., 2002). It was also shown to be involved in muscular differentiation. Skeletal muscle stem cells express Bhlhb2 and its deletion leads to an increase in Notch activity and defective differentiation; *in vitro* Bhlhb2 antagonizes Notch activity (Sun H. *et al*., 2007). Interestingly, in heart progenitors, an up-regulation of Bhlhb2 was observed after β-catenin stabilization that led to repression of *Smyd1/BOP*, a histone methyltransferase essential for cardiomyocyte differentiation. Hence, it was proposed that Bhlhb2 regulates cardiac progenitor cell fate determination downstream of Wnt/β-catenin signalling (Kwon C. *et al*., 2009).

Bhlhb2 was one of the most strongly upregulated genes in our microarray analysis, both in E9.0 whole embryos and in all E9.5 regions. *In situ* hybridisation revealed much higher expression of *Bhlhb2* in *Arid3b*-null embryos than in wild type littermates (**Figure 29A**). Increased levels of *Bhlhb2* were observed in the somites, branchial arches, ventral region of the pharyngeal endoderm and in the forebrain. At the level of the heart, up-regulation could be observed in the SHF at E9.0 (**Figure 29A, c**) and in the OFT at E9.5 **(Figure 29A, d**). High levels could also be detected in the IFT at both stages (**Figure 29A, e-h**). *In situ* hybridisation on sections (**Figure 29B, a-h**) confirmed that expression was particularly strong in the heart poles, especially in the IFT (**Figure 29B e,f, arrowheads; compare with a,b**). As mentioned above, Wnt/β-catenin canonical pathway activates *Bhlhb2* expression. We performed an immunostaining against nucleus β-catenin, which reflects the activation of the pathway, to check whether an excessive stabilization of β-catenin in the nuclear leads to upregulation of *Bhlhb2* in $Arid3b^{gt/gt}$ embryos. We also performed an *in situ* hybridisation against *Axin2*, which is a target of the Wnt canonical pathway (**Figure 30A**). Nuclear β-catenin was indeed present in the nuclei of mutant embryos and the expression pattern looked similar to wild type hearts. *Axin2* expression was also normal in mutant embryos. We conclude that *Bhlhb2* overexpression does not seem to be caused by aberrant Wnt/β-catenin pathway activation in $Arid3b^{gt/gt}$ embryos.

Because of the previously described repressive role of Bhlhb2 on Smyd1, we checked its expression in our mutants. *Smyd1* levels were indeed reduced in mutant hearts, noticeably in the IFT, in the same area in which *Bhlhb2* was highly expressed (**Figure 29B, j-p, arrowhead**). *Unc45b*, a chaperone expressed specifically in muscle and in the heart, also appeared down-regulated in the heart microarray. Its expression was also reduced in the IFT of the heart at E9.5 (**Figure 29 B, i,m, arrowhead**), providing more evidence that the differentiation of the IFT is impaired.

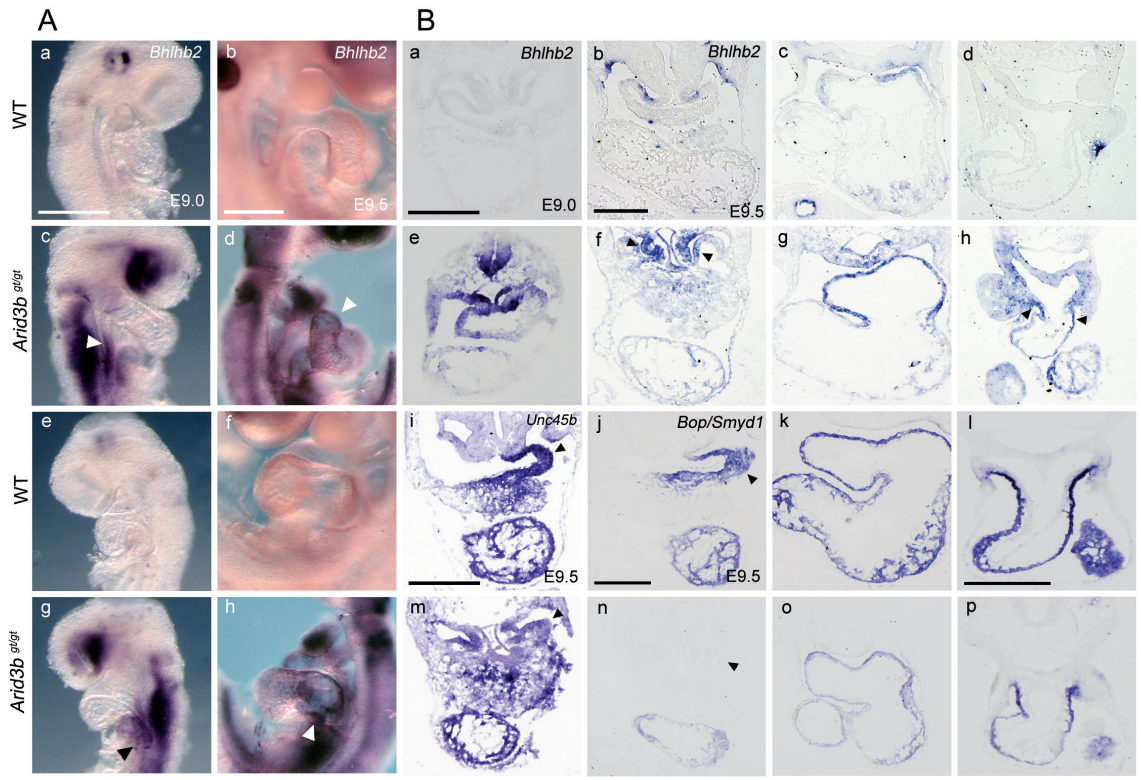

Figure 29. Microarray analysis reveals *Bhlhb2* and as Arid3b target gene. A. RNA *in situ* hybridisation of *Bhlhb2* in whole-mount embryos at E9.0 and E9.5. Upregulation of the gene can be observed in a wide range of tissues, including the head, the rombomeres, the branchial arches and the heart poles. **B.** Detection of *Bhlhb2* mRNA on paraffin sections at E9.0 (**a,e**) and E9.5 (**b-d**, **f-h**). High levels of expression in the heart poles are evident in the *Arid3b*$^{gt/gt}$ embryos (**f,h**, arrowheads). *In situ* hybridisation of *BOP/Smyd1*, a marker for cardiomyocyte differentiation, in wild type (**j-l**) and *Arid3b*$^{gt/gt}$ (**n-p**) embryos. The overall level of expression is lower in *Arid3b*$^{gt/gt}$ myocardium and OFT and absent in the IFT (**j,n**, arrowheads). *Unc45b*, another factor involved in muscular differentiation, is also reduced in the sinus horns (**i,m,** arrowheads).

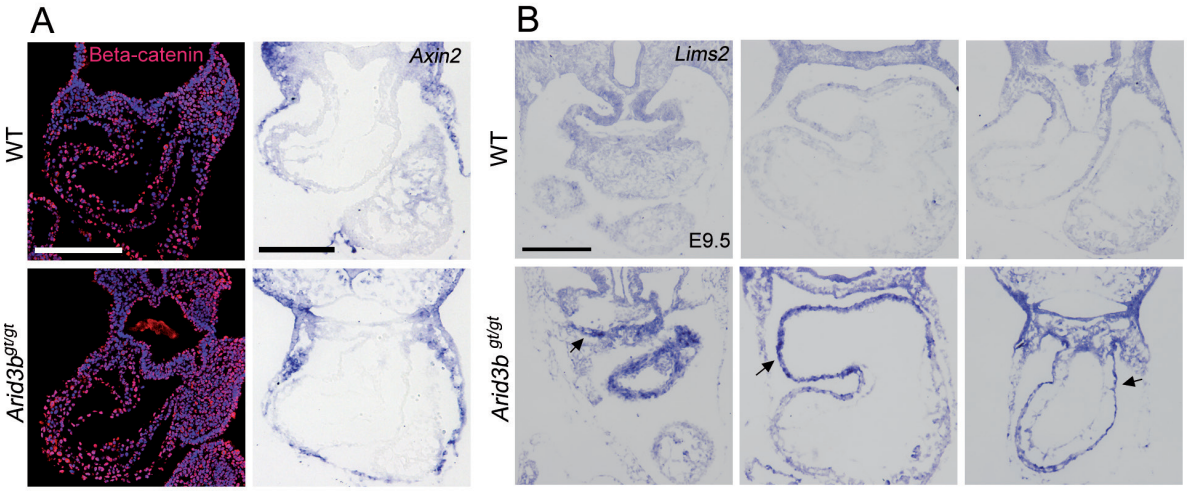

Figure 30. *Lims2* is upregulated in the heart poles. A. Immunostaining for nuclear b-catenin and RNA *in situ* hybridisation for *Axin2*, a target of Wnt/β-catenin pathway. Both nuclear localization of β-catenin and levels of expression of *Axin2* look normal in mutant embryos. **B.** Expression of *Lims2* in wild type and *Arid3b*$^{gt/gt}$ hearts; note the upregulation in the OFT and atria of the mutants (arrows). Scale bars: sections 200 µm, whole-mount 500 µm.

To further characterize the differentiation defect of the poles, expression of smooth muscle actin (SMA) and troponin T (TnT) was analysed. Expression of SMA and TnT was observed at the heart poles in wild type and mutant embryos (**Figure 31**). However, mutant embryos lacked expression in the distal regions closer to the SHF, both in the IFT (at E9.5, **Figure 31 A,B, e,f**) and in the OFT (at E9.0, **Figure 31 A,B, c,d** and at E9.5, **Figure 31 A,B g,h**), suggesting defective differentiation or delayed maturation of heart precursors. These results suggest that Arid3b regulates cardiac precursor differentiation at the heart poles indirectly through repression of Bhlhb2.

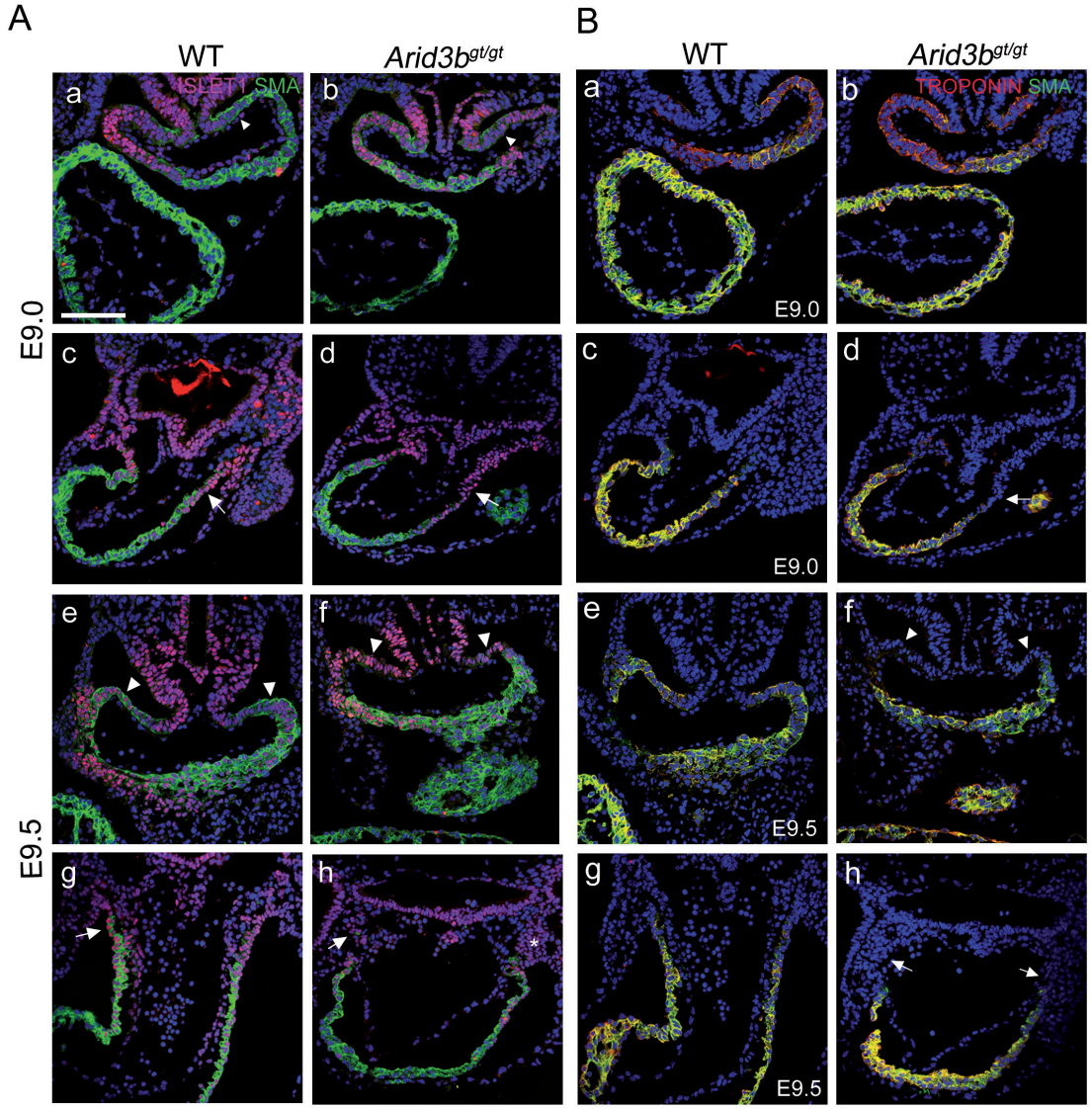

Figure 31. Differentiation of cardiomyocytes in the heart poles is impaired in *Arid3b*$^{gt/gt}$ hearts. A. Smooth muscle actin (SMA) (green) and Islet1 (red) immunostaining on paraffin sections of *Arid3b*$^{gt/gt}$ and wild type embryos. Expression of SMA is reduced in the most distal part of the OFT at E9.0 and E9.5 (white arrows, compare **d with c and h with g**). In the IFT, SMA expression in *Arid3b*$^{gt/gt}$ embryos is normal at E9.0, but at E9.5 less SMA positive cells are seen at the most dorsal region of the sinus horns (**e,f** white arrowheads). An accumulation of Islet1-positive cells can be observed at the entrance of the OFT of *Arid3b*$^{gt/gt}$ embryos (**h**, asterisks). **B.** Immunostaining for SMA (green) and troponin T (red) reveals defective differentiation of the distal-most cardiomyocytes added to the poles of the heart in the OFT at stage E9.0, as well as E9.5 (**c,d,g,h**, arrows) and in the IFT at E9.5 (**a,b,e,f**, arrowheads). Scale bar: 100 µm.

- Lims2 (also known as Pinch2) is a LIM-domain adaptor protein involved in protein recruitment, assembly of protein complexes and their subcellular localization. Together with the integrin-linked kinase (ILK) and parvin it forms IPP complexes, localized in focal adhesions, which serve as a link between integrins and the actin cytoskeleton and diverse signalling pathways. Along with Lims1, Lims2 is expressed during development and they both regulate proper cytoskeletal organization and adhesion (Legate K.R. *et al*., 2006) (Kovalevich J. *et al*., 2011). Interestingly, when Lims2 is overexpressed in HEK293 cells, it competes with Lims1 for ILK binding, blocking the transduction of integrin-mediated signals that control cell spreading (Zhang Y. *et al*., 2002). Similarly, in myoblasts, upregulation of Lims2 leads to decreased motility (Boudoukha S. *et al*., 2010). Deletion of both Lims1/2 in the myocardium results in dilated cardiomyopathy and early death from heart failure, pointing to an important role of these proteins in heart development (Liang X. *et al*., 2009).

Lims2 appeared upregulated in the E9.5 heart microarray. Although *in situ* hybridisation of *Lims2* at E9.0 did not show a clear result, at E9.5 a noticeable upregulation was observed in *Arid3b* mutants. High levels of *Lims2* were detected in the atria, OFT and SHF cells close to OFT in *Arid3b*$^{gt/gt}$ embryos (**Figure 30D, arrows**). Because of the above-mentioned role of Lims2 in cell adhesion and motility, the results suggest that its upregulation may also contribute to the heart defects observed in *Arid3b* mutants, interfering with proper cell movements and rearrangements.

Specification of SHF and number of precursors are normal in *Arid3b*$^{gt/gt}$ embryos

As has been shown above, some of the most striking defects in *Arid3b*$^{gt/gt}$ embryos are related to the poles of the heart, which derive from the SHF. We decided to look in more detail at this population of cells. Islet1 is the best known marker for SHF precursors and its absence leads to severe shortening of the poles of the heart (Cai C.L. *et al*., 2003). The expression of Islet1, as analysed by immunohistochemistry, revealed no differences between wild type and mutant hearts. Moreover, wild type and mutant hearts contained similar total numbers of Islet1+ precursors (**Figure 32C**). Also, no significant differences in proliferation of Islet1+ cells could be detected, as measured both by pH3 staining and by BrdU incorporation (**Figure 32A**). Cell death assayed by TUNEL, showed an increase at E9.5, which coincided with the only moment where we detected a reduction in the total number of Islet1+ cells in *Arid3b* mutants in the SHF (**Figure 32 B,C**) but could not explain the earlier defects observed in the poles of the heart. Expression of other genes reported to regulate SHF cardiac precursors and normal OFT formation, such as *Fgf8* and *Tbx1*, was also unaltered (**Figure 32D**). These results suggest that the absence of *Arid3b* does not alter the specification of heart precursors in the SHF and that a difference in precursor cell number is not the primary cause of the observed defects in mutant hearts.

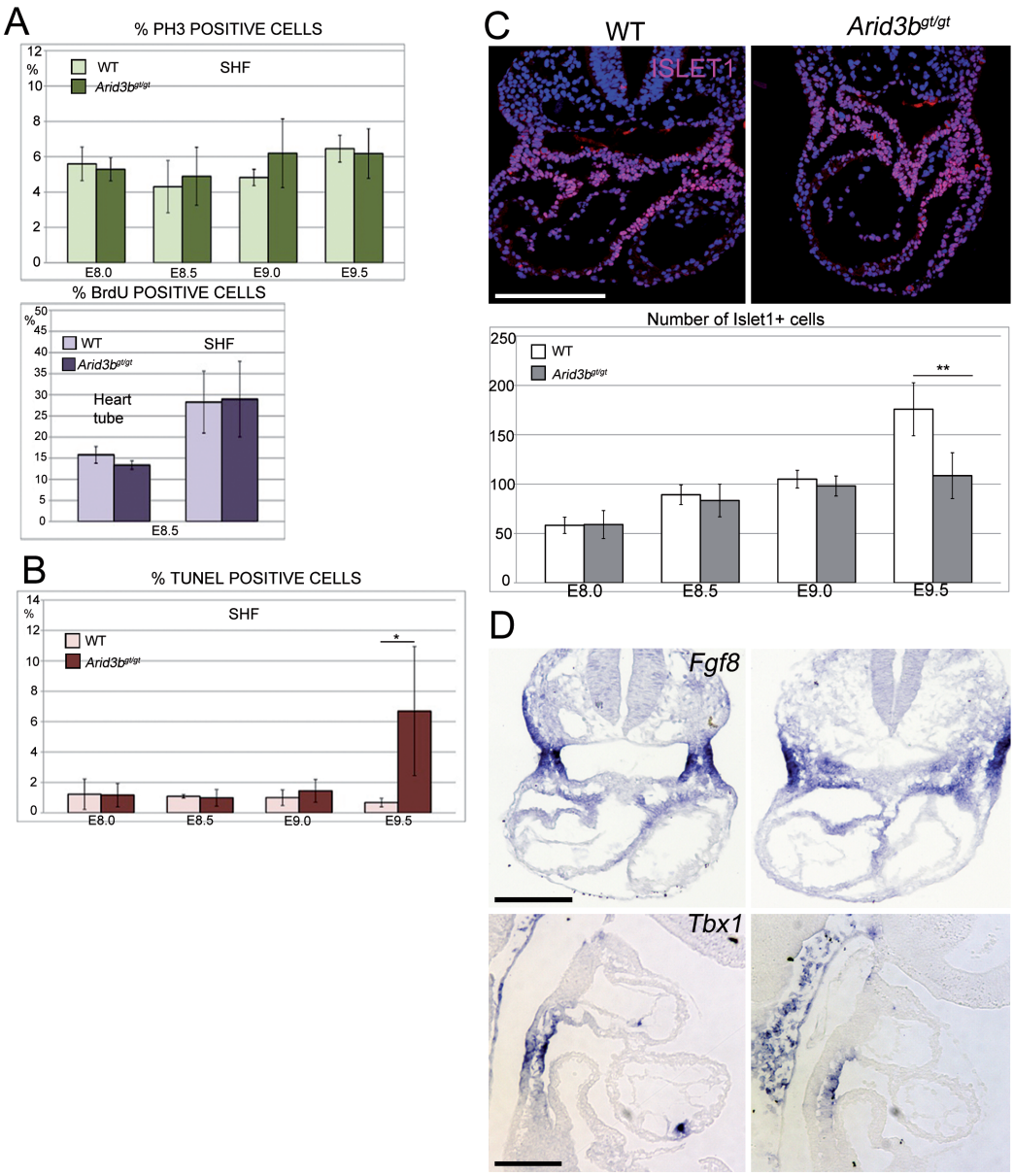

Figure 32. Expression of SHF markers and proliferation and cell death of the precursors are not affected. A, B. Graphs showing cell proliferation (PH3 immunostaining and BrdU incorporation) and cell death (TUNEL staining) in the SHF, defined as Islet1+ population, of wild type and *Arid3b*-null embryos. No differences are observed except for an increase in cell death in mutant SHF at E9.5. Results are expressed as mean+/- SD. (*p<0.05, Student's t test). **C.** Immunohistochemistry against Islet1 in wild type and *Arid3b*$^{gt/gt}$ embryos at E9.0. Islet1 is expressed in cardiac precursors and the quantification of total number of Islet1 positive cells shows that their number only decreases at E9.5 when an increase in cell death is observed. Results are expressed as mean+/- SD. (*p<0.01, Student's t test). **D.** Analysis of gene expression in E9.0 embryos by RNA *in situ* hybridisation. Expression of genes involved in the regulation of SHF precursors (*Fgf8* and *Tbx1*) showed no differences between *Arid3b*$^{gt/gt}$ and wild-type embryos. Scale bars: 150 µm.

As already mentioned, Islet1 is a marker of cardiac precursors in the SHF and Islet1-positive cells were indeed observed in the mutant SHF next to the heart poles, at both E9.0 and E9.5. Noticeably at this later stage, an accumulation of Islet1+ precursors was seen in the SHF in the OFT region (**Fig 31A h asterisk**). Additionally, the actin cytoskeleton of Islet1+ cells in the SHF and the overall tissue architecture of this region were abnormal in mutants. SHF cells in wild type hearts had a wide band of actin on the pericardial cavity side (which is thicker at the IFT region), suggestive of a polarized epithelium (**Figure 33 A-D**). In contrast, mutant SHF cells did not show such a clear actin band (**Figure 33 E-H**). Moreover, cells dorsal to the wall epithelium, which appear loose and mesenchyme-like in the wild type (**Figure 33D**), appeared more compact and epithelial-like in the mutant (**Figure 33F,H**). The disposition of the cells in the pharyngeal mesoderm also appeared more disorganised in the mutant embryos as compared to the wild type (**Figure 33 G,H, arrows**).

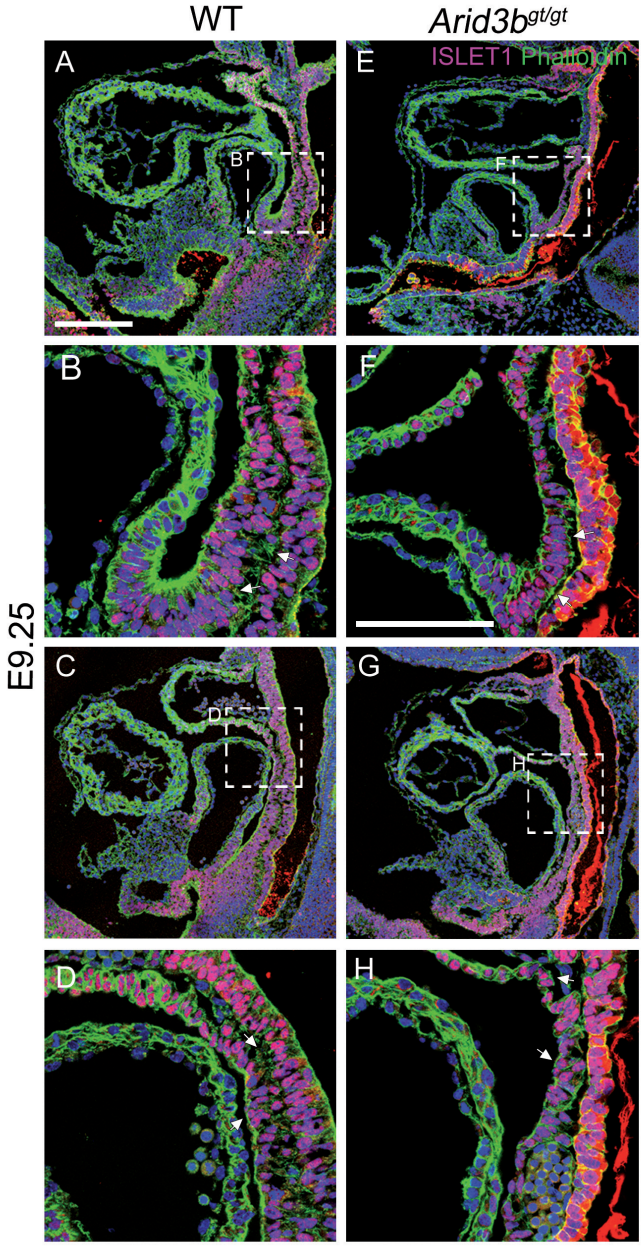

Figure 33. SHF shows abnormal architecture. Phalloidin (green) and Islet1 (red) staining on longitudinal sections in E9.25 embryos. Mutant cells (**F,H**) appear more compact and epithelial-like than wild-type cells (**B,D**, arrows). Also, the actin band facing the pericardial cavity, very conspicuous in wild type embryos (**D**, arrow), is less prominent in the mutant (**H**). Scale bars: 200 µm (A,C,E,G), 100 µm (B,D,F,H).

The results presented so far show that Islet1+ precursors are correctly specified in the mutant SHF, that proliferation and cell death are unaltered and that the early patterning of the heart is normal. However, the cellular architecture and tissue organization in the SHF are disrupted and eventually the poles of the heart are malformed. Moreover, *Lims2*, which regulates cell motility, is upregulated in the heart poles of *Arid3b* mutants. This suggests that abnormal incorporation of Islet1+ progenitors into the heart, probably due to defective cellular movements or cell rearrangements, is the cause of the phenotype at the heart poles.

Addition of SHF precursors to the heart poles is impaired in *Arid3b* mutant embryos

In order to directly analyse the fate of mutant SHF cells we DiI-labelled Islet1+ precursors, both in ventro-caudal positions at E8.0 (6 ps), which will contribute to the IFT (**Figure 34**) and in rostro-lateral positions at E8.5 (10 ps), which will contribute to the OFT and right ventricle (**Figure 35**). Cells were labelled, embryos cultured *in vitro* for 24 hours, and the position of DiI-positive cells was recorded.

In the case of DiI labelling to track the contribution to the IFT, a more caudal population of Islet1+ region was labelled, so that contribution was observed mostly in the sinus horns (**Figure 34 B-D**). Labelling of IFT precursors led to the presence of DiI-positive cells in the IFT in 91% of wild type embryos, but in only 48% of Arid3b mutant embryos (**Figure 34, E-T, summarised in U**), thus showing that cardiac precursors in the absence of *Arid3b* do not reach the heart as efficiently as in the wild type situation.

To track SHF contribution to the OFT, Islet1+ cells located beneath the heart tube were labelled (**Figure 35 A-D**). In this case, three regions derived from the SHF precursors were differentiated: the right ventricle, the proximal OFT and the distal OFT (**Figure 35E**). Cryostat sections of cultured embryos showed an accumulation of DiI-labelled cells at the entrance of the OFT in *Arid3b*$^{gt/gt}$ embryos (**Figure 35 F-G, arrow**), consistent with Islet1+ cell accumulations observed previously (**Figure 31A, h asterisk**). Labelling of these precursors led to the presence of DiI-positive cells in the proximal OFT in most wild type embryos (66%), with a significant proportion showing cells in the right ventricle (13%); in contrast, in most mutant embryos (55%), DiI-positive cells were found in the distal OFT close to the SHF, and only reached the right ventricle in one embryo (5%) (**Figure 35 H-M, summarised in N**).

Taken together these results suggest that Islet1+ precursors, although present in *Arid3b* mutant SHF, have an impaired capacity to contribute to the heart poles, which eventually causes the observed cardiac defects.

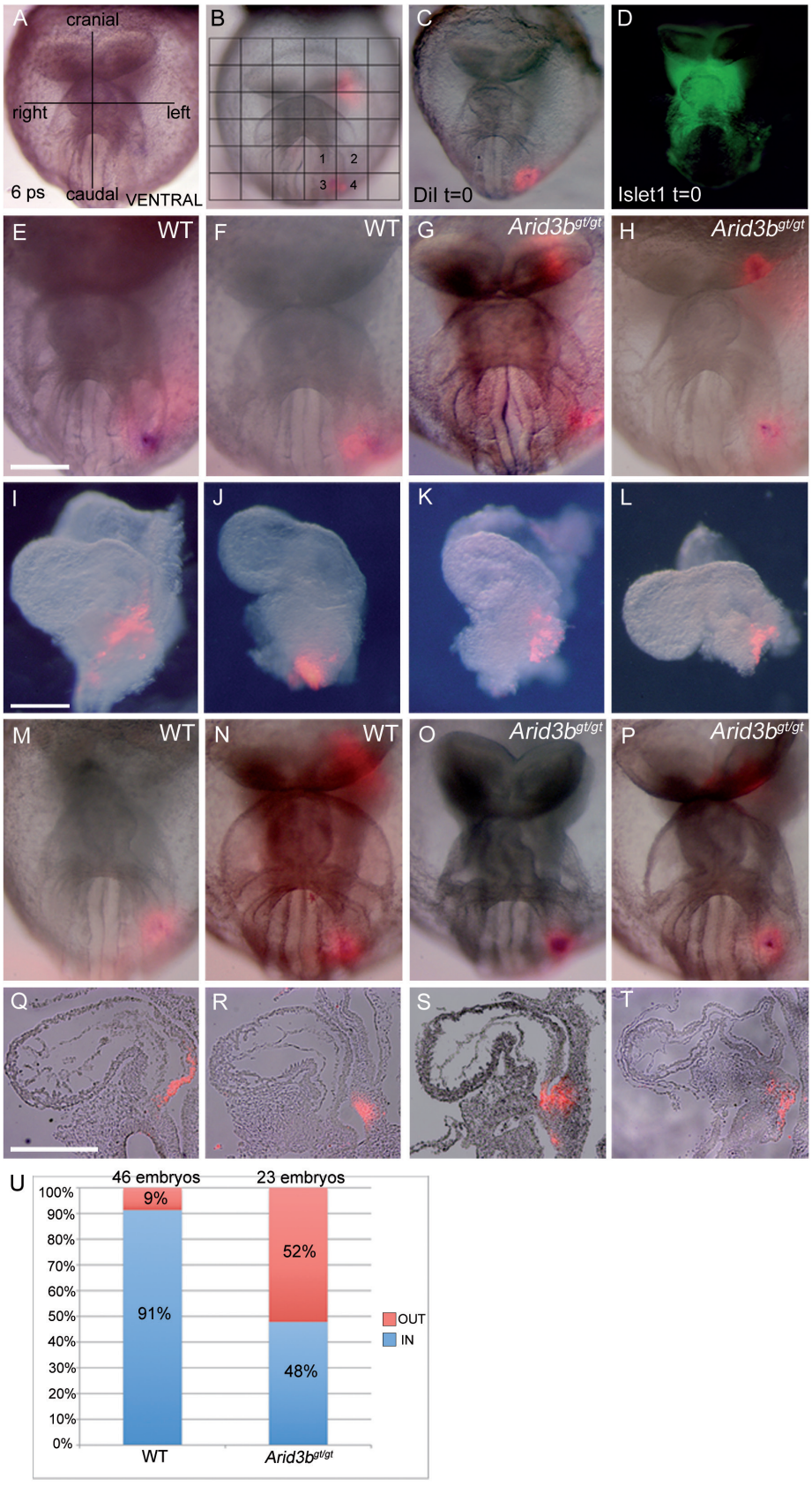
A
cranial
right
left
6 ps
caudal
VENTRAL
B
1
2
3
4
C
DiI t=0
D
Islet1 t=0
E
WT
F
WT
G
Arid3b gt/gt
H
Arid3b gt/gt
I
J
K
L
M
WT
N
WT
O
Arid3b gt/gt
P
Arid3b gt/gt
Q
R
S
T
U
46 embryos
23 embryos
100%
90%
80%
70%
60%
50%
40%
30%
20%
10%
0%
9%
91%
52%
48%
OUT
IN
WT
Arid3b gt/gt

Figure 34. Addition of Islet1-positive precursors to the IFT is impaired in *Arid3b*$^{gt/gt}$ embryos. A. Ventral view of a 6 somite embryo, as used in DiI fate-mapping experiments, showing the left-right and cranial-caudal axes for orientation. **B.** Example of DiI labelling of the pSHF to study the contribution of Islet1+ cells to the IFT. A grid was used to map the position of the injection; for the analysis shown here, positions 3 and 4 (caudo-lateral) were considered. DiI (red fluorescence, **B,C**) was injected into the region known to contain Islet1+ cells, later detected by whole-mount immunochemistry (**D**, green). (**E-H**) *Arid3b*$^{gt/gt}$ and wild-type embryos labelled with DiI at similar positions (t=0) and (**I-L**) the resulting label seen in whole dissected hearts after 24 hours of in vitro culture. Images show wild type (**E,F,I,J**) and *Arid3b*$^{gt/gt}$ (**G,H,K,L**) embryos. Those with DiI-labelled cells in the heart IFT (**I,K**) were recorded as "IN" and those with labelled cells outside the heart (**J,L**) recorded as "OUT". (**M-P**) Additional examples of DiI labelling in the pSHF at t=0; in this case, 24 hours after labelling embryos were cryosectioned and DiI staining observed on longitudinal sections (**Q-T**). DiI labelled cells could be detected in the heart IFT in some wild-type (**Q**) and *Arid3b*$^{gt/gt}$ (**S**) embryos. In other cases DiI labelled cells appear outside the IFT (**R**, wild type; **T**, Arid3b$^{gt/gt}$). **U**. Summary of the contributions of the pSHF to the IFT in normal and *Arid3b*$^{gt/gt}$ embryos expressed as the percentage of embryos with labelling in or out of the IFT. A 2-sample test for equality of proportions was used to compare the two groups. The percentage of embryos with labelling in the IFT is significantly higher in the wild-type than the *Arid3b*$^{gt/gt}$ group (p value= 0.0001903).

Mouse embryonic fibroblasts (MEFs) have reduced motility *in vitro*

To address the migratory and adhesive behaviour of *Arid3b*$^{gt/gt}$ cells, we obtained MEFs from wild type and mutant E9.5 embryos. While wild-type MEFs grew normally and filled the culture plate within days, *Arid3b*$^{gt/gt}$ MEFs failed to increase their number and never formed a confluent monolayer. Their general appearance was abnormal, with fewer protrusions and a more compact shape than wild-type MEFs. Staining for actin revealed an increase in stress fibres and an aberrant distribution of actin filaments (**Figure 36A**). To analyse their migratory behaviour, we performed time-lapse video microscopy, where individual cells were tracked in a time window of at least 3 hours. Wild-type MEFs travelled extensively, changed the direction of their migration and explored the medium by producing filopodia. On the contrary, *Arid3b*$^{gt/gt}$ MEFs moved slower and the total distance covered in the same timespan was smaller than in the wild-type situation (**Figure 36 B,C**). Some cells did not move at all, or did not advance, but stayed in the same position moving backwards and forwards. The number of protrusions emitted was lower than in the wild type MEFs and they were smaller than normal filopodia (**Figure 36D**). In some cases, migrating mutant cells left behind cell fragments, adhered to the plate; also, transient blebs protruding from the membrane could be observed. In summary, these results point to defective cell migration and alteration of the cytoskeleton in the absence of *Arid3b*.

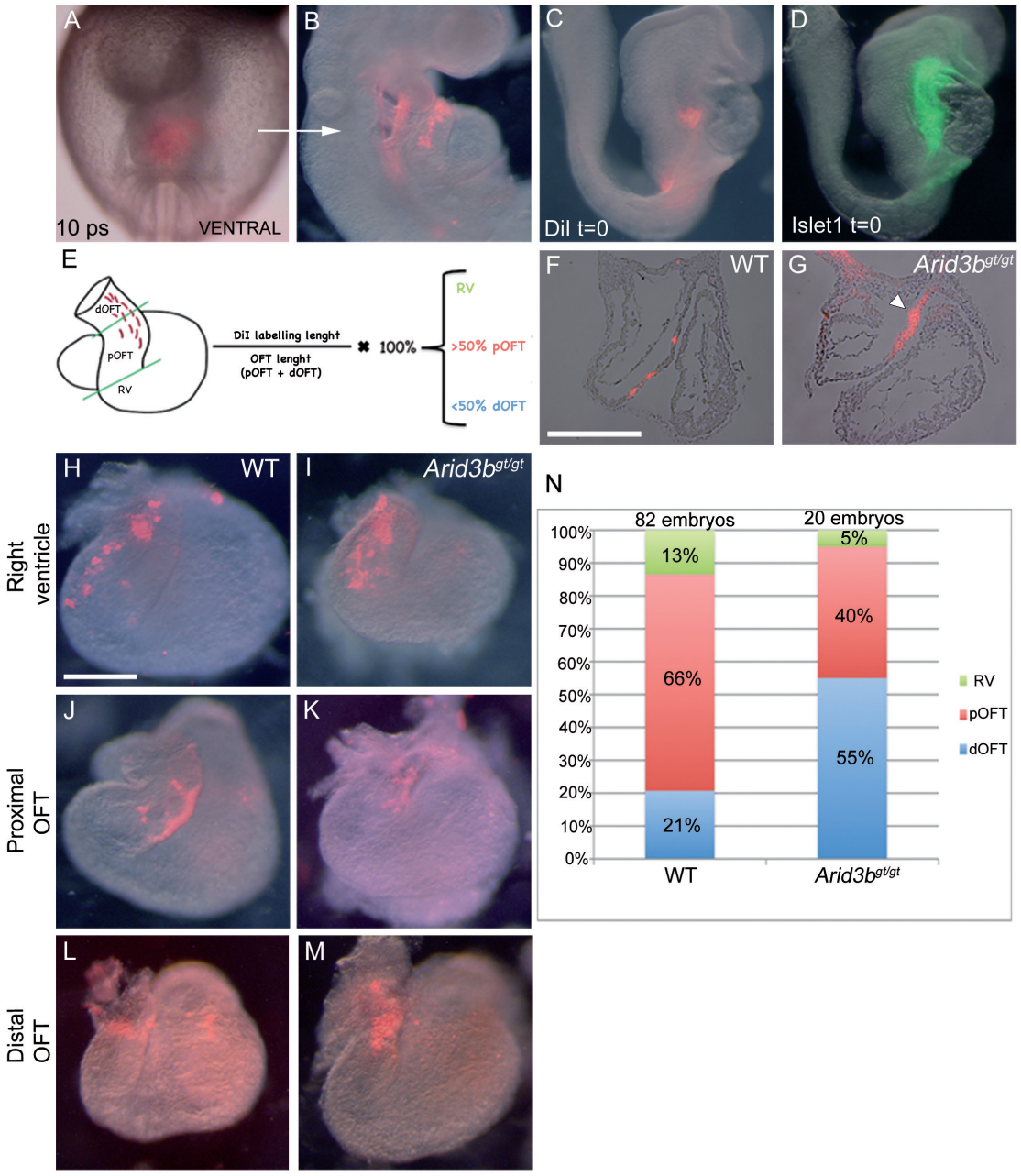

Figure 35. Normal contribution of precursors to the OFT is altered in *Arid3b*$^{gt/gt}$. A. Ventral view of DiI labelling in a representative embryo at t=0. **B.** Lateral view after 24 hours in vitro culture. **C-D.** DiI labelling is performed in the Islet1 positive region (**D**, immunostaining with Islet1 antibody). **E.** Scheme illustrating the three regions in which the heart was subdivided for data analysis. **F-G.** Cryosections of wild type and mutant embryos 24 hours after labelling; note the accumulation of DiI-labelled cells at the entrance of the heart in the mutant (arrowhead). **H-M.** Examples of the three locations of the DiI staining 24 hours after labelling in wild-type and mutant embryos. **N.** Summary of the contributions of the AHF to the heart in *Arid3b*$^{gt/gt}$ and normal embryos expressed as the percentage of embryos with labelled cells in each of the regions. Fisher's test was used to compare the two groups. The difference in the distribution between wild type and *Arid3b*$^{gt/gt}$ embryos is statistically significant (p value= 0.01149). Scale bar: 250 µm

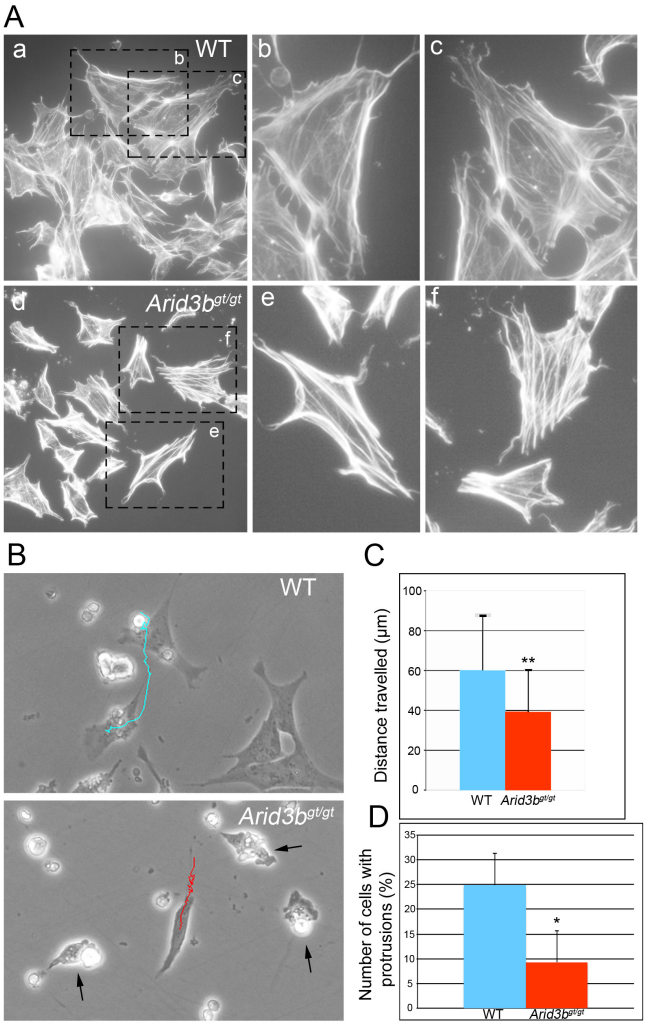

Figure 36. Mouse embryonic fibroblasts (MEFs) have reduced mobility *in vitro*. **A.** Phalloidin staining of actin cytoskeleton of wild type and mutants MEFs isolated from E9.5 embryos. Note the shortening and aberrant distribution of the actin filaments in *Arid3b*$^{gt/gt}$ MEFs. **B.** Cell trajectory and travelled distance were determined by a time-lapse filming of MEFs cells. Representative recording and cell trajectories for both wild type and mutant cells are shown. Blebbing cells could be observed in mutant fibroblasts (arrows) **C.** Quantification of travelled distance; 48 wild-type and 54 *Arid3b*-null cells were used. Results are expressed as mean +/- SD. **p<0.01, Student's t-test. **D.** Quantification of the number of cells with lamelipodia in wild type and mutant MEFs. A total number of 198 wild type and 133 mutant cells were analysed. Results are expressed as mean +/- SD. *p<0.05, Student's t-test.

Generation of an *Arid3b*$^{flox/flox}$ line

The early lethality of *Arid3b*$^{gt/gt}$ embryos prevented the study of the potential roles of *Arid3b* in some later developmental processes. Besides, part of the phenotype observed in the gene-trap line can be secondary to the general cardiovascular failure of the embryo and we might miss some defects directly dependent on Arid3b function. In order to address more precisely tissue-specific functions of Arid3b, we decided to generate a line with the *Arid3b* allele flanked by *loxP* sites, recognition sites for Cre-mediated recombination (a *floxed* line). Thus, crosses with mouse driver lines with tissue-specific expression of a *cre* transgene would result in *Arid3b* loss in that particular tissue. Cre activity can also be controlled temporally by using a fusion protein of Cre and a mutant ligand-binding domain of the estrogen receptor (CreER or CreER^{T2}), which only translocates to the nucleus in the presence of 4-hydroxytamoxifen administrated by food, water or intraperitoneal injection (Doetschman T. and Azhar, 2012). These strategies could enable us to study Arid3b functions not only in specific cardiac populations but also determine the critical developmental stages in which its function is required.

The *Arid3b*$^{flox/flox;Neo\ cassette}$ construct was generated by Gene Bridges and the transgenic

mouse line was generated at CNIC by the gene targeting and transgenesis facilities. When the first germ line transmission was detected, we crossed *Arid3b*$^{flox/+;\ Neo\ cassette}$ offsprings to obtain *Arid3b*$^{flox/flox;\ Neo\ cassette}$ mice. Unexpectedly, almost no viable double homozygous floxed mice were obtained. To determine whether *Arid3b*$^{flox/flox;Neo\ cassette}$ mice died before birth, we collected embryos at different developmental stages. We could recover *Arid3b*$^{flox/flox;Neo\ cassette}$ embryos, but already at E10.5 the number of mutants was half of the expected and at E11.5 only one *Arid3b*$^{flox/flox;\ Neo\ cassette}$ embryo could be recovered. Some embryos showed developmental defects, although most of them looked normal (**Figure 37 A,B**). We also found some reabsorbed embryos in these litters. As a possible explanation of the reduced number of homozygous embryos, we wondered whether *Arid3b* expression was normal and to address this question we performed *in situ* hybridisation against *Arid3b* at E10.5 in *Arid3b*$^{flox/flox;Neo\ cassette}$, *Arid3b*$^{flox/+;Neo\ cassette}$ and wild type littermates. As can be seen in (**Figure 37C**) *Arid3b* levels are gradually reduced as the number of *Arid3b*^{flox} copies increased. We confirmed this result by RT-PCR against the Arid3b exon 7 (**Figure 37D**). The low levels of *Arid3b* in *Arid3b*$^{flox/flox;Neo\ cassette}$ embryos might explain the observed embryonic lethality.

A

Number of embryos recovered

E10.5	WT	Flox/WT	Flox/Flox	TOTAL
Expected	25%	50%	25%	43
Real	30% (13)	56% (24)	14% (6)	43
E11.5	WT	Flox/WT	Flox/Flox	TOTAL
Expected	25%	50%	25%	22
Real	23% (5)	73% (16)	4% (1)	22

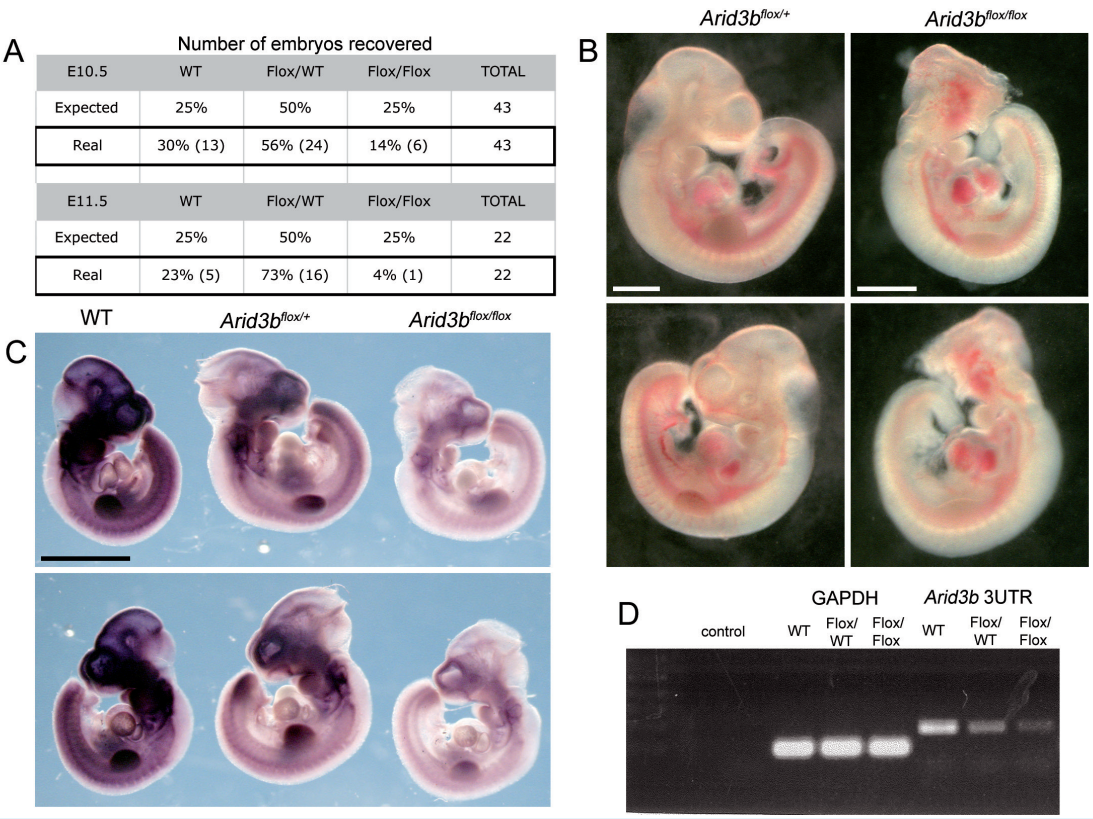

Figure 37. ***Arid3b*$^{flox/flox;Neo\ cassette}$ mice are embryonically lethal because of reduced levels of *Arid3b*. A.** Table depicting the number of embryos recovered at different stages after crossing Arid3b$^{flox/+}$ mice. **B.** Example of *Arid3b*$^{flox/+}$ and *Arid3b*$^{flox/flox}$ E10.5 embryo with developmental defects. **C.** Whole-mount RNA *in situ* hybridisation against *Arid3b* in wild type, *Arid3b*$^{flox/+}$and *Arid3b*$^{flox/flox}$ embryos. Note the gradual reduction of the levels of expression. **D.** RT-PCR with RNA extracted from wild type, *Arid3b*$^{flox/+}$ and *Arid3b*$^{flox/flox}$ embryos showing the reduction of *Arid3b* levels correlating with the increase in the number of the floxed copies. Scale bars: B 1 mm; C 1.5 mm.

Because it has been reported that the Neo cassette might interfere with normal gene expression (Chen L. *et al*., 1999) (Rucker E.B. *et al*., 2000) (Xu X. *et al*., 2001), we crossed *Arid3b*$^{flox/flox;Neo\ cassette}$ females with males carrying the flipase transgene, which recognizes the Flp sites (Schaft J. *et al*., 2001). In this way, the resistance cassette is eliminated and we can expect to obtain viable *Arid3b*$^{flox/flox}$ mice. In the absence of the Neo cassette normal proportions of viable and fertile double flox mice were obtained (**Table 5**), suggesting that the presence of the Neo cassette indeed interfered with normal *Arid3b* expression. These mice were used to cross with specific Cre lines.

Arid3b$^{flox/+}$ x *Arid3b*$^{flox/+}$	WT	*Arid3b*$^{flox/+}$	*Arid3b*$^{flox/flox}$	TOTAL
Expected numbers	25%	50%	25%	38
Observed numbers	31% (12)	45% (17)	24% (9)	38

Table 5. Number of embryos of different genotypes obtained from crosses between *Arid3b*$^{flox/+}$ mice after the deletion of the resistance cassette.

Analysis of the phenotype of the *Arid3b*$^{flox/flox}$*/Sox2-Cre* line

To confirm the lethal phenotype of *Arid3b* deficient embryos, produced in a conditional manner, we crossed our *Arid3b*$^{flox/flox}$ line with *Sox2-Cre* line, which deletes genes from the epiblast stage (Hayashi S. *et al*., 2002). We collected embryos at different points of development to determine the stage of embryonic death (**Table 6**). We could detect some variability in the phenotype: while some mutant embryos looked normal at E10.5, others were already necrotic at this stage. No *Arid3b*$^{flox/flox}$*/Sox2-Cre* live embryos were recovered on day E12.5. This phenotype was similar to the described for *Arid3b* knockout in C57BL/6 strain background described previously (Takebe A. *et al*., 2006) and to the phenotype we observed with our gene-trap line on C57BL/6 background.

E10.5	*Arid3b*$^{flox/+}$/*Sox2*$^{+}$	*Arid3b*$^{flox/+}$/*Sox2*^{Cre}	*Arid3b*$^{flox/flox}$/*Sox2*$^{+}$	*Arid3b*$^{flox/flox}$/*Sox2*^{Cre}	Reabsortions	TOTAL
Expected	25%	25%	25%	25%	-	35
Observed	28% (10)	26% (9)	26% (9)	20% (7)	3	35

Table 6. The expected and observed ratios of embryos collected at E10.5 from crosses between *Arid3b*$^{flox/+}$*/Sox2-Cre* and *Arid3b*$^{flox/flox}$ mice.

To confirm the deletion, we performed an *in situ* hybridisation with an *Arid3b* probe against the coding mRNA (starting from the second exon, where the ATG is located to the ninth exon which codifies partially for the REKLES domain). Strikingly, using this probe, we could detect robust expression of *Arid3b* in the mutant embryos similar to the control (**Figure 38**). Because the flox sites flank the second exon of *Arid3b* (**Figure 7**), we designed a probe against this exon. *In situ* hybridisation in wild type and mutant embryos confirmed a total deletion of this region in *Arid3b*$^{flox/flox}$*/Sox2-Cre* embryos (**Figure 38**). Together, these data suggests that a successful deletion of the ATG region of Arid3b occurs in *Arid3b*$^{flox/flox}$*/Sox2-Cre line*, and the consequent

mid-gestational lethality of the embryos supports the idea that no functional protein is synthetized, although we can detect *Arid3b* mRNA.

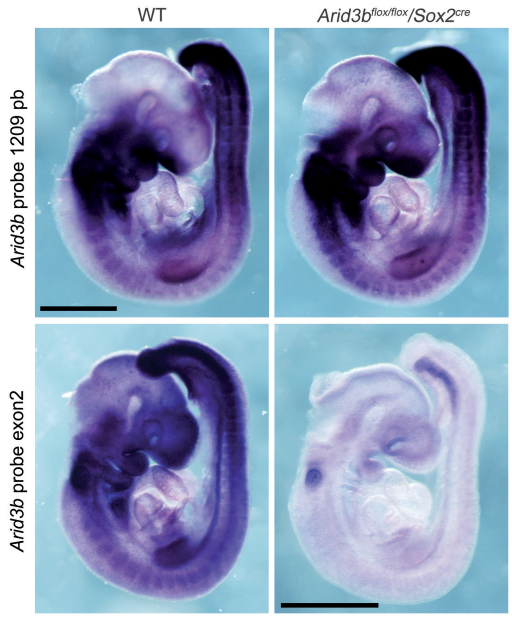

Figure 38.
Expression of *Arid3b* RNA in *Arid3b*$^{flox/flox}$/*Sox2-Cre* embryos. RNA *in situ* hybridisation in wild type and *Arid3b*$^{flox/flox}$/*Sox2-Cre* embryos with two different probes against *Arid3b*. Expression was similar when a probe against the whole mRNA was used, while no expression was detected in *Arid3b*$^{flox/flox}$/*Sox2-Cre* embryos with a probe against the second exon, which is the floxed region. Scale bar: 1 mm.

Analysis of the phenotype of *Arid3b*$^{flox/flox}$ and *Arid3b*$^{flox/flox;Neo\ cassette}$ derived MEFs

We isolated MEFs from E12.5 *Arid3b*$^{flox/+}$ and *Arid3b*$^{flox/flox}$ embryos from two different lines: from embryos that still carried the Neo cassette and from embryos in which the cassette was deleted by crossing the line with a flipase transgenic line. Both types of cells, independently of the genotype, grew normally. Part of the *Arid3b*$^{flox/flox}$ MEFs was infected with an adenovirus expressing Cre and the infected cells were sorted based on GFP expression from the viral vector. We confirmed a successful deletion by RT-PCR with primers against the second exon; however, when the RT-PCR was done with primers located in the 3'-region (exon 7) or in the ARID domain (exon 5), a band still could be detected in cells infected with adenovirus with cre (**Figure 39 A,B**). This is consistent with the results observed in the *in situ* hybridisation performed in *Arid3b*$^{flox/flox}$/*Sox2-Cre* embryos. The phenotype of the *Arid3b*$^{flox/flox;Neo\ cassette}$ and *Arid3b*$^{flox/flox}$ MEFs was different after the addition of Cre and deletion of the second exon. While *Arid3b*$^{flox/flox;Neo\text{-}cassette}$ +Cre MEFs were still able to grow and fill the plate, *Arid3b*$^{flox/flox}$ +Cre MEFs did not expand and no increase in the number of cells could be detected after several days on the culture dish. This is reminiscent on the phenotype obtained in *Arid3b*$^{gt/gt}$ MEFs. Because of this limitation, we used *Arid3b*$^{flox/flox;Neo\text{-}cassette}$ MEFs for further experiments.

An *in vitro* wound-healing assay was performed with those MEFs to test whether a motility phenotype is present, similarly to MEFs from *Arid3b*$^{gt/gt}$ embryos (**Figure 39C**). Mitomycin C was used to inhibit proliferation. When plates were examined 48 hours after the wound, control *Arid3b*$^{flox/flox;Neo\text{-}cassette}$ MEFs showed almost complete closure of the gap, confirming that cells migrated and covered the free space. On the contrary, when *Arid3b* was deleted from the cells, the wound looked very similar to the starting moment of the experiment, t=0 (**Figure 39C**). Cells

extended protrusions towards the gap, but failed to cover the cell-free surface, as they did in the absence of Cre. Because proliferation was inhibited in both conditions, disruption of normal cell motility and/or adhesion looks as the main reason for the phenotype observed. Thus, we confirm that MEFs isolated from our *Arid3b*$^{flox/flox;Neo\text{-}cassette}$ mice line, after *Arid3b* deletion, display similar defects to the ones observed in MEFs from *Arid3b*$^{gt/gt}$ embryos, including a migration capacity impairment.

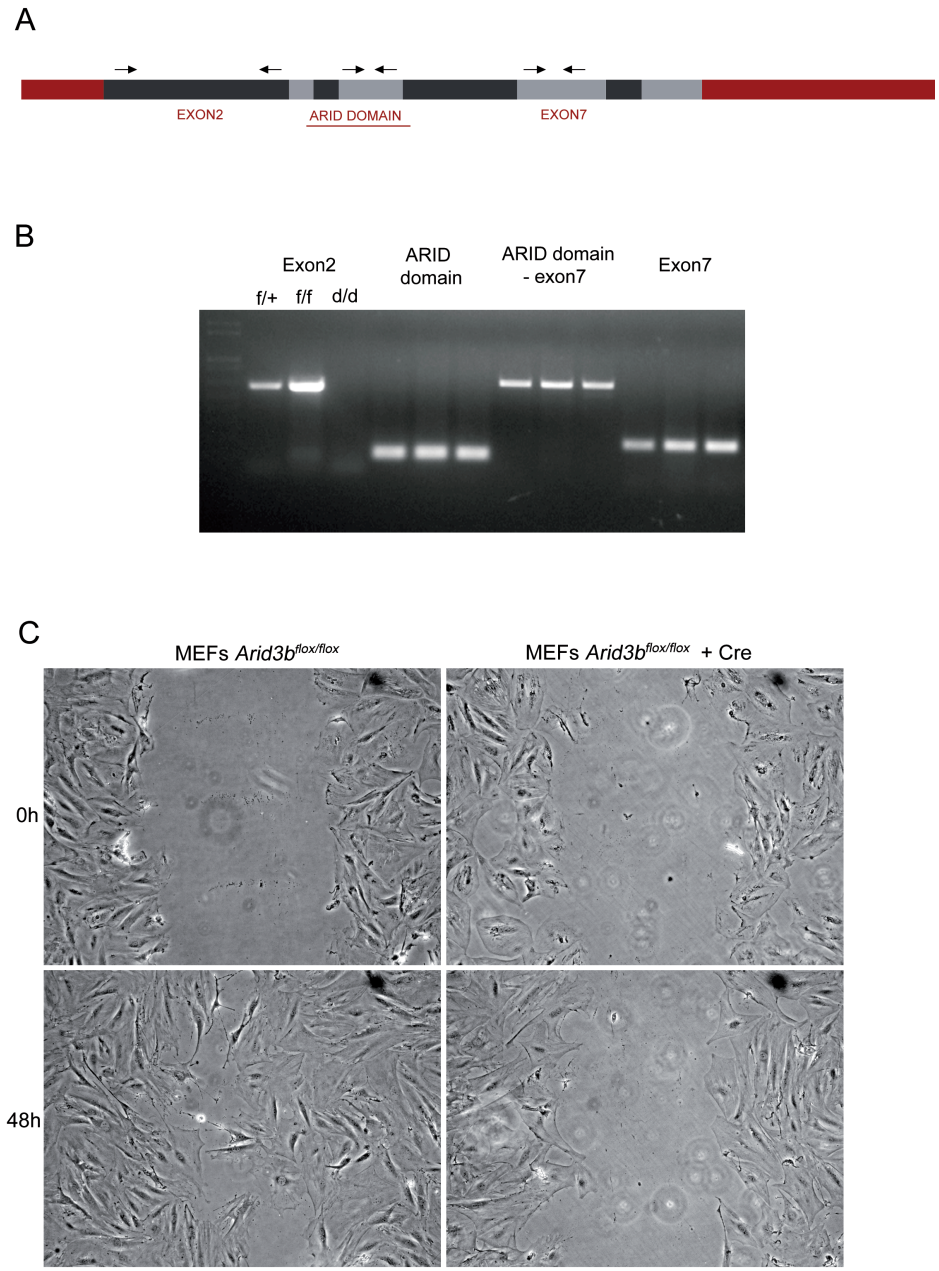

Figure 39. MEFs derived from *Arid3b*$^{flox/flox}$ embryos show a phenotype similar to *Arid3b*$^{gt/gt}$ MEFs. A. Scheme of the *Arid3b* mRNA with the pairs of primers used to detect the its expression: pair1 – exon2 (460 pb); pair2 – ARID domain (98 pb); pair3 – exon7 (166 pb); pair4 – exon5 - exon7 (664 pb); β-actin was used as control **B.** RT-PCR with RNA extracted from *Arid3b*$^{flox/+}$, *Arid3b*$^{flox/flox}$ and *Arid3b*$^{flox/flox}$ + Cre MEFs with different pairs of primers as shown above. **C.** Wound-healing experiment in *Arid3b*$^{flox/flox;Neo\ cassette}$ MEFs. While in a control situation 48 hours after the experiment the wound is almost closed, when *Arid3b* is deleted from the cells the wound remains very similar to t=0.

Analysis of the phenotype of the *Arid3b*$^{flox/flox}$ /*Nkx2.5-Cre* line

Arid3b$^{flox/flox}$ females were crossed with *Arid3b*$^{flox/+}$/*Nkx2.5-Cre* males to obtain mice with a deletion of *Arid3b* in the Nkx2.5+ population. As can be seen in **Table 7**, only about half of the expected *Arid3b*$^{flox/flox}$/*Nkx2.5-Cre* mice were recovered at weaning. Those that survived reached adulthood (6 month) without any particular phenotype. The expected and obtained numbers of animals for each genotype were separated depending on the particular male used in the cross and the results are depicted in **Table 8**. Note that the recovery rate of *Arid3b*$^{flox/flox}$/*Nkx2.5-Cre* mice was essentially reduced only in some of the crosses, while others showed a proportion according to the one expected. To detect whether deletion of *Arid3b* had occurred, we performed an *in situ* hybridisation at E9.5 with the two probes against *Arid3b* and observed a similar result to the obtained with the *Arid3b*$^{flox/flox}$/*Sox2-Cre* line: no differences in the expression with the full-lenght *Arid3b* 1209 pb probe between wild type and mutant embryos (**Figure 40A**), but a complete absence of signal with the *Arid3b* exon2 probe in the regions of expression of Nkx2.5 (myocardium, pharyngeal mesoderm and ventral part of the pharyngeal endoderm) (**Figure 40B, arrows**). These results confirm that the deletion of the second exon was successful.

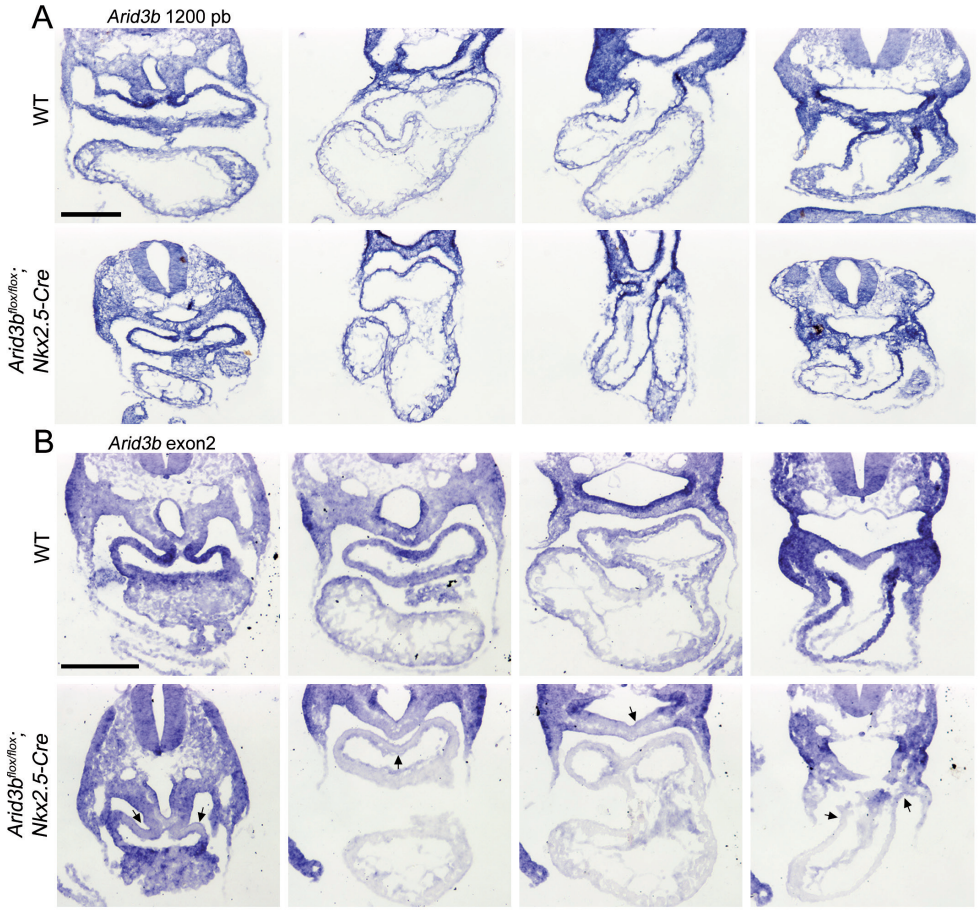

Figure 40. ***Arid3b*$^{flox/flox}$*/Nkx2.5-Cre* embryos show a successful deletion of *Arid3b* second exon. A.** RNA *in situ* hybridisation against the whole *Arid3b* mRNA. The expression is similar between wild type and *Arid3b*$^{flox/flox}$*/Nkx2.5-Cre* embryos **B.** RNA *in situ* hybridisation against *Arid3b* second exon; note the absence of signal in the region of expression of Nkx2.5 (arrows). Scale bar: 200 µm.

	Arid3b$^{flox/+}$/*Nkx2.5*$^{+}$	*Arid3b*$^{flox/+}$/*Nkx2.5*^{Cre}	*Arid3b*$^{flox/flox}$/*Nkx2.5*$^{+}$	*Arid3b*$^{flox/flox}$/*Nkx2.5*^{Cre}	TOTAL
Expected	25%	25%	25%	25%	258
Observed	28% (72)	30% (70)	27% (69)	15% (40)	258

Table 7. Total number of live adult mice of different genotypes obtained from distinct crosses between *Arid3b*$^{flox/+}$*/Nkx2.5-Cre* and *Arid3b*$^{flox/flox}$ mice.

MALE		*Arid3b*$^{flox/+}$/*Nkx2.5*$^{+}$	*Arid3b*$^{flox/+}$/*Nkx2.5*^{Cre}	*Arid3b*$^{flox/flox}$/*Nkx2.5*$^{+}$	*Arid3b*$^{flox/flox}$/*Nkx2.5*^{Cre}	TOTAL
BNA9	Observed	2	1	0	0	3
BNA1	Expected	25%	25%	25%	25%	123
	Observed	25% (31)	31% (38)	31% (38)	13% (16)	123
BNA4	Expected	25%	25%	25%	25%	40
	Observed	35% (14)	20% (8)	20% (8)	25% (10)	40
BNA5	Expected	25%	25%	25%	25%	43
	Observed	33% (14)	33% (14)	25% (11)	9% (4)	43
BNA74	Expected	25%	25%	25%	25%	29
	Observed	17% (5)	34% (10)	28% (8)	21% (6)	29
BNA75	Expected	25%	25%	25%	25%	20
	Observed	30% (6)	30% (6)	20% (4)	20% (4)	20

Table 8. Number of live adult mice obtained for each genotype per *Arid3b*$^{flox/+}$*/Nkx2.5-Cre* male; the red circles points to a reduced number of *Arid3b*$^{flox/flox}$*/Nkx2.5-Cre* live adult mice obtained in two of these crosses. In others the proportions were similar to the expected.

To determine whether mutant embryos show any cardiac phenotype, we collected embryos at different developmental stages, from E9.5 to E16.5. **Table 9** shows the proportions of the four genotypes obtained at E9.5 and at E16.5. Interestingly, while at E16.5 the number of embryos recovered for each genotype was similar to the expected, at E9.5 the number of *Arid3b*$^{flox/flox}$*/Nkx2.5-Cre* embryos was slightly reduced. When analysed in more detail, taking into account from which crosses each litter came, we observed that all the embryos collected at E9.5 were offsprings of the male that produced a reduced number of viable adult *Arid3b*$^{flox/flox}$*/Nkx2.5-Cre* mice. On the other hand, embryos collected at E16.5 came from different crosses, including those where normal proportions of the four genotypes were observed at weaning. Hence, the result seems to reflect the variability in the phenotype dependent on the male used to collect embryos. Also, we cannot exclude that increasing the number of litters at each stage, would let us observe a similar tendency in both groups.

Developmental stage		*Arid3b*$^{flox/+}$/*Nkx2.5*$^{+}$	*Arid3b*$^{flox/+}$/*Nkx2.5*^{Cre}	*Arid3b*$^{flox/flox}$/*Nkx2.5*$^{+}$	*Arid3b*$^{flox/flox}$/*Nkx2.5*^{Cre}	Reabsortions	TOTAL
E9.5	Expected	25%	25%	25%	25%	-	41
	Observed	32% (13)	32% (13)	19% (8)	17% (7)	2	41
E16.5	Expected	25%	25%	25%	25%	-	43
	Observed	23% (10)	26% (11)	28% (12)	23% (10)	-	43

Table 9. Number of embryos coming from *Arid3b*$^{flox/+}$*/Nkx2.5-Cre* x *Arid3b*$^{flox/flox}$ crosses of different genotype collected at E9.5 and E16.5.

Arid3b$^{flox/flox}$ */Nkx2.5-Cre* embryos show right ventricle and valve defects

At E16.5, *Arid3b*$^{flox/flox}$*/Nkx2.5-Cre* embryos looked grossly similar to their littermates (**Figure 41A**). To obtain detailed information on the possible cardiac defects, we performed haematoxylin and eosin staining on four different *Arid3b*$^{flox/flox}$*/Nkx2.5-Cre* embryos. Two of the mutant embryos showed mild defects in the affected regions of the heart. Interestingly, they came from the cross where the survival rate of the *Arid3b*$^{flox/flox}$*/Nkx2.5-Cre* mice was normal (**Table 8**). The other two embryos showed a number of more severe cardiac defects (**Figure 41B**). The heart looked less developed than in the wild type for the stage analysed. The compact myocardium of the right ventricle was thinner (**Figure 41B i,j, brackets**) and the ventricular septum was not properly formed and presented holes (**Figure 41B i,j, asterisk**). However, the defect of the septum was variable and in other embryos was not observed. The most severe and clear defects were related to the valves. They were much bigger than in the wild type embryos, with a higher content of fibrotic tissue and with low or no remodelling. The pulmonary and aortic valve defect was similar and consistent between the different mutants (**Figure 41B a-d, arrowheads**), while the phenotype on the tricuspid and mitral valves was more variable, ranging from very big fibrotic valves in one of the *Arid3b*$^{flox/flox}$*/Nkx2.5-Cre* embryos (**as shown in Figure 41B g,h, asterisk; i,j, arrowhead**), to a much milder defects observed in embryos with less severe phenotype.

Analysis of expression of mesenchymal and endocardial markers

To better characterise the observed valve defects, we checked for two molecules involved in normal valve development. Periostin is a secreted matricellular protein, which plays an important role in the differentiation and remodelling of cushion mesenchymal cells (Norris R.A. *et al*., 2008). On the other hand, Tbx20 is strongly expressed in the endocardial cushion mesenchyme and its up-regulation leads to increased cell proliferation and abnormal valve remodelling (Chakraborty S. *et al*., 2010). Both molecules were present in the *Arid3b*$^{flox/flox}$*/Nkx2.5-Cre* valves and their expression looked normal (**Figure 42 A,B**). Hence, the valvular phenotype observed in *Arid3b*$^{flox/flox}$*/Nkx2.5-Cre* embryos is dependent on other molecules.

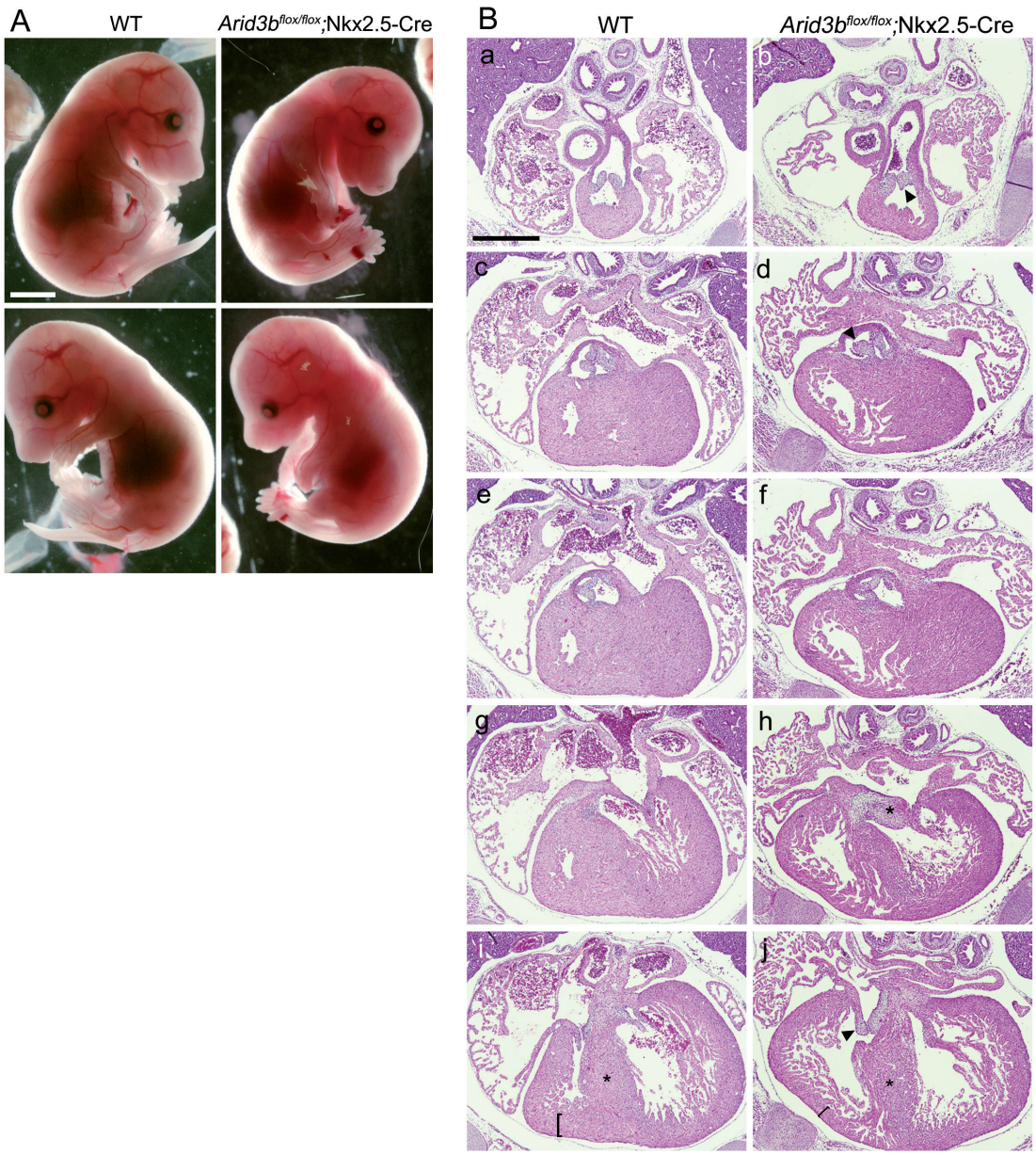

Figure 41. Histological analysis of *Arid3b*$^{flox/flox}$*/Nkx2.5-Cre* embryos revealed cardiac defects at E16.5. A. Whole-mount *Arid3b*$^{flox/flox}$*/Nkx2.5-Cre* embryos look grossly similar to their control littermates (right and left views are shown) **B.** Haematoxylin and eosin staining of wild type and *Arid3b*$^{flox/flox}$*/Nkx2.5-Cre* embryos. The myocardium of the right ventricle is thinner (**i,j,** brackets), the ventricular septum is abnormal (**i,j**, asterisk). Valves are bigger, not properly remodelled and with increased content of fibrotic tissue, both the great vessels valves (**a-d**, arrowheads), as well as tricuspid and mitral valves (**g,h**, asterisk; **i,j**, arrowhead) show this phenotype. Scale bar: panel A 3 mm; panel B 500 µm.

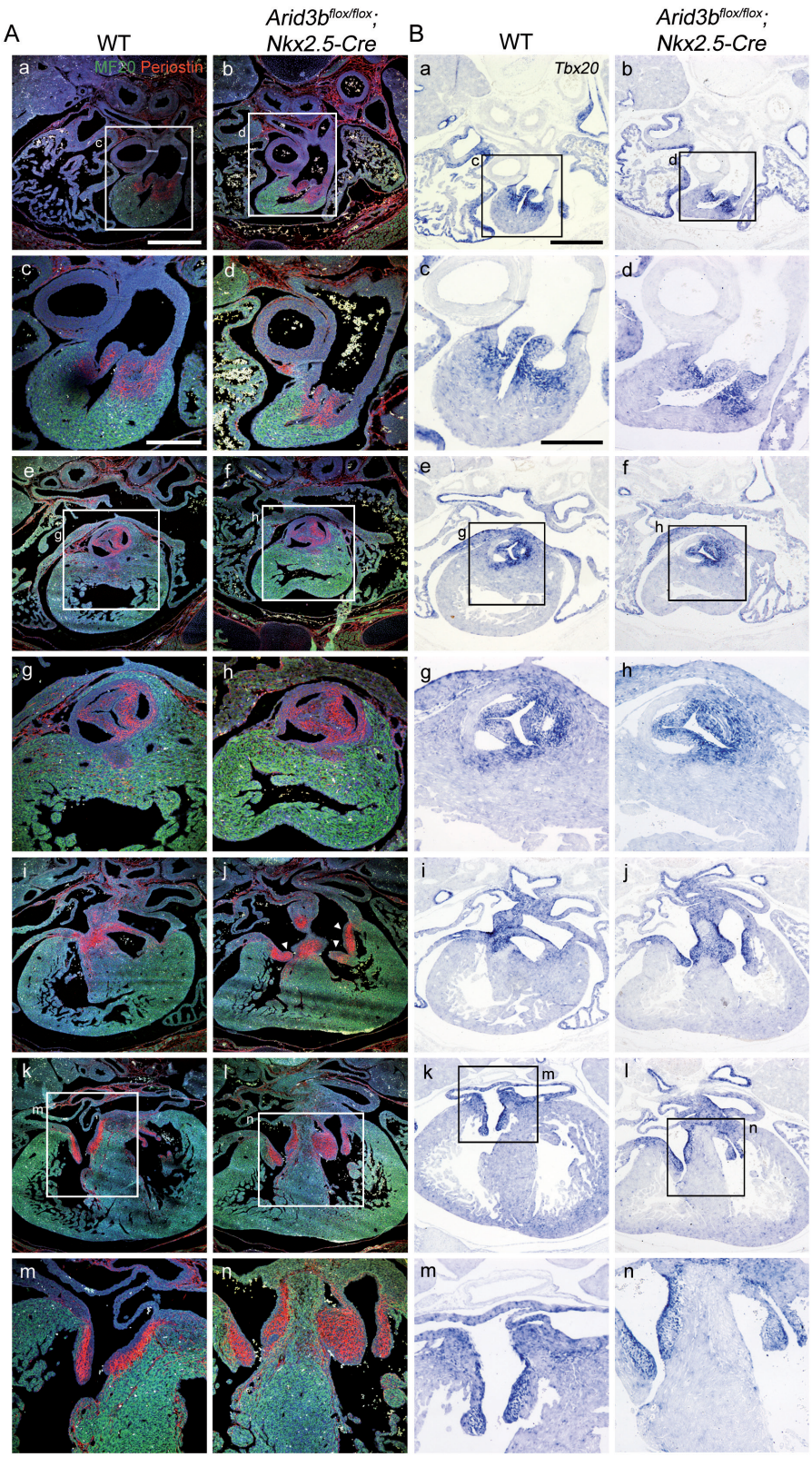

Figure 42. Periostin and *Tbx20* expression are normal in *Arid3b*$^{flox/flox}$*/Nkx2.5-Cre* embryos. A. Immunostaining against periostin (red) and myocardial marker MF20 (green) in wild type and mutant embryos at E16.5. Expression of periostin in the *Arid3b*$^{flox/flox}$*/Nkx2.5-Cre* embryos is grossly normal and reflects the increase of mesenchymal tissue in the valves. **B.** RNA *in situ* hybridisation against *Tbx20* in consecutive sections. No differences are observed in *Arid3b*$^{flox/flox}$*/Nkx2.5-Cre* embryos compared to wild type. Scale bars: 400 μm, magnifications 200 μm.

DISCUSSION

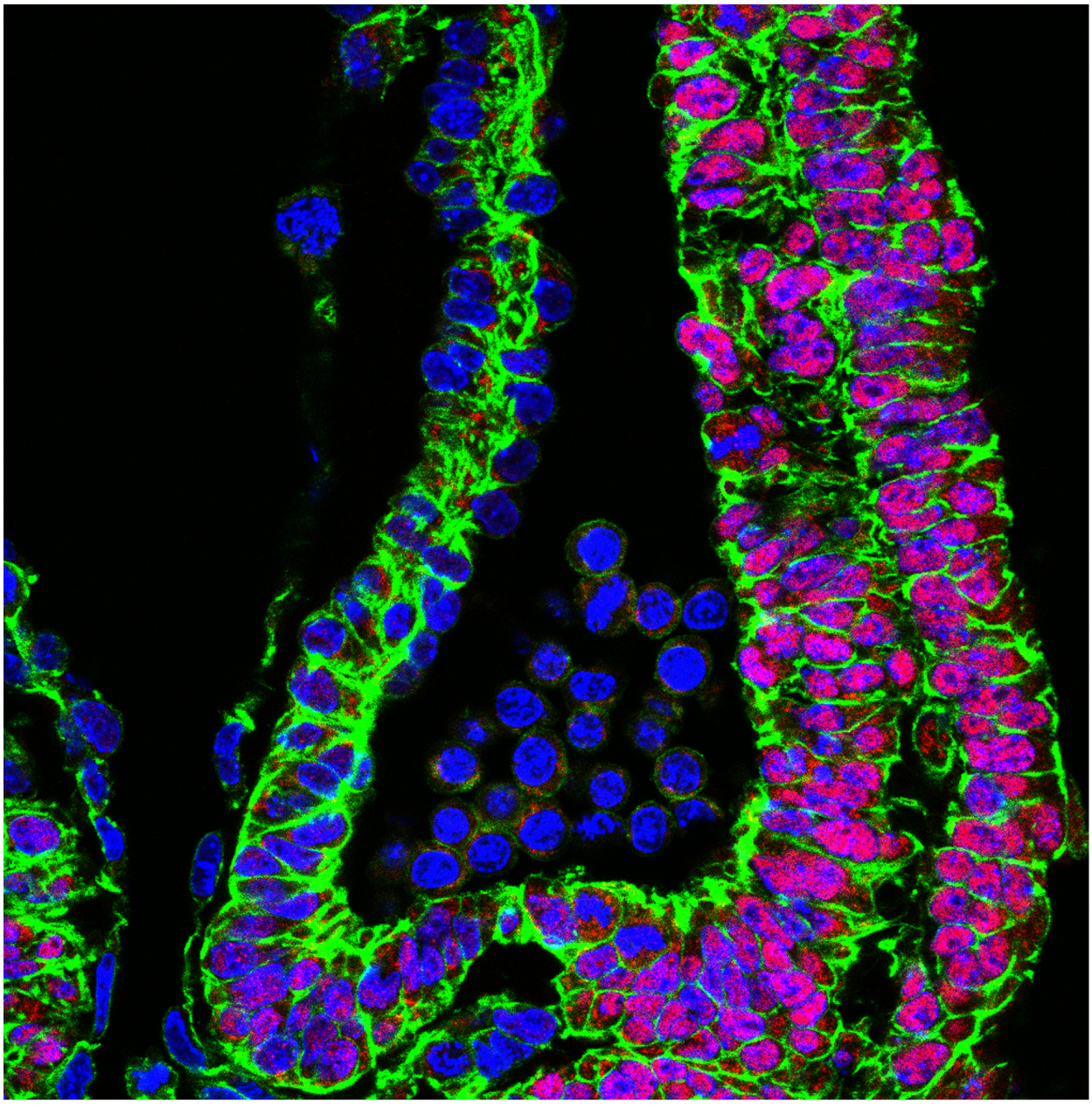

Arid3b is essential for mouse embryonic development, but its precise functions are not well characterised. In this thesis we analysed the role of Arid3b in heart development.

Arid3b is expressed in the heart in a dynamic fashion

A previous report (Takebe A. *et al*., 2006) dismissed a direct role for Arid3b in cardiac development on the basis that *Arid3b* expression was barely detected in the developing wild type heart. We reanalysed the expression of this gene by RNA *in situ* hybridisation. Our results, indeed, show a dynamic pattern of expression of *Arid3b* in different structures of the heart. At the stage of cardiac crescent strong expression could be detected in the myocardium and in heart precursors not yet added to the heart. The expression in the myocardium starts to vanish when the looping begins, but remains strong in the SHF and its derivatives, the poles of the heart. When the looping process finishes, *Arid3b* expression starts to be detected in the endocardium, being especially strong in the endocardium of the valve cushions. We could also detect expression of the gene in the epicardium. The failure to detect *Arid3b* signal in the heart by Takebe *et al*. might be explained by its dynamic expression and the fact that the strongest expression in the myocardium is detected only briefly at very early stages. Interestingly, the most severe heart defects observed are in accordance with the regions of strongest expression of *Arid3b*.

We could also confirm the expression of *Arid3b* in the heart by β-gal staining using our gene-trap line. While in general the pattern of expression is similar, important differences are observed between *Arid3b* RNA detection and β-gal staining. For instance, while *in situ* hybridisation at E10.5 shows almost no expression in the myocardium, a strong signal of β-gal activity can be detected through the whole myocardium. These differences could be the result of the different techniques used. While *in situ* hybridisation detects the levels of mRNA, a molecule that usually has a high turnover, β-gal staining shows the result of a enzymatic reaction where the levels of the product increase catalytically. Besides, β-gal is a stable protein with a low turnover, which enables it to remain in cells for longer time (Strange, 1966), even if it is not translated anymore. In this way, the high levels of staining observed in the heart at later stages reflect the earlier expression of *Arid3b* in the myocardium. Moreover, *in situ* hybridisation against the β-geo cassette revealed a similar pattern of expression to *Arid3b* RNA, confirming that the cassette reproduces the endogenous expression of *Arid3b*.

The observed vessel defect might be secondary to impaired heart function

Heart beating and circulation are present in mutant embryos, as was confirmed by ink injection in the heart. However, vasculature is abnormal in *Arid3b*$^{gt/gt}$ embryos: vessels are much smaller, remodelling of the primitive network in the yolk sac is not accomplished and bleeding is observed in the yolk sac. Vascular endothelial cells are formed but they fail to undergo remodelling. Interestingly, both in our study, as well as in the previous report (Takebe A. *et al*., 2006), no

expression of *Arid3b* could be detected in the endothelium at these early stages, when defects in vessel remodelling are observed. This result suggests that these defects are non-cell-autonomous. In fact, in the yolk sac, while no expression is detected in the endothelium of the vessels, Arid3b is indeed expressed in the endoderm. The yolk sac endoderm is an important signalling centre for hematopoietic and endothelial differentiation (Damert A. *et al*., 2002), and Arid3b might have an indirect role in vessel maturation through signalling from the yolk sac endoderm. The lack of normal vessel formation might also be partially due to impaired heart function. Hemodynamic forces are necessary for vessel remodelling and mutations that alter early cardiac function lead to a failure in normal vessel remodelling as a secondary consequence (Udan R.S. *et al*., 2013). Although heart beating is observed in *Arid3b*$^{gt/gt}$ embryos, the severe cardiac malformations observed, such as pole shortening and disrupted AVC patterning, might lead to defective beating, which affects normal blood circulation and, thus, vessels remodelling. We believe that defective circulation might contribute to the early lethality of the embryos.

Later on, from E9.5, *Arid3b* is indeed expressed in the endothelium, first appearing in the aorta and veins and later expanding to smaller vessels. This suggests that it may have additional roles in the maintenance or physiology of this tissue, once the early events are accomplished. The first disperse vascular plexus is gradually reorganized into a functional network. As vessels begin to be remodelled, they undergo localized proliferation and regression, branching and migration, as well as recruit supporting cells (smooth muscle cells and pericytes) involved in stabilization and maturation of the newly formed network (Coultas L. *et al*., 2005) (Herbert S.P. and Stainier, 2011). The early death of mutant embryos precludes study of these processes in our *Arid3b*$^{gt/gt}$ embryos, so a conditional deletion of *Arid3b* in the endothelium (using the *Tie2-Cre* driver (Kisanuki Y.Y. *et al*., 2001)) would be necessary to address its role in this tissue.

Differences in phenotype with the previously described mutant

The phenotype observed in *Arid3b*-null embryos confirms the important role of this gene in embryonic development. However, some important phenotypic differences exist between our null model and the knock-out described by Takebe *et al*. One of the possible explanations for the differences might be the mouse background, which differs from one model to the other. The null-mice described in Takebe's study (C57BL/6 strain) survive until E12.5, and 40% of the knock-out embryos showed no abnormality in their development, only a growth delay. Our null-mice (CD1 strain) never managed to survive later than E10.5 and all embryos displayed a severe phenotype. This might indicate that background differences between the two strains can alter the phenotype they show. The influence of the genetic background on the resulting phenotypes has been described previously (Threadgill D.W. *et al*., 1995) (Tanabe L.M. *et al*., 2012) (Montagutelli, 2000). We have generated *Arid3b*$^{gt/gt}$ embryos on a C57BL/6 background and evidence obtained from them supports this idea. We were able to recover embryos at E9.5 with apparently no defects, as well as mutant embryos at E12.5, similarly to what Takebe *et al*. observe. Hence, it looks that on

CD1 background *Arid3b* deletion gives a more severe phenotype that on C57BL/6 background. Interestingly, considering that CD1 is an outbred strain, while C57BL/6 is an inbred strain, more variability and a less penetrant phenotype would be expected on CD1 background, where the presence of genetic variations can modify the phenotype (Beck J.A. *et al*., 2000) (Chia R. *et al*., 2005). Our results suggest that on C57BL/6 background some modifier can partially compensates for the loss of Arid3b.

On the other hand, the genetic strategies by which the mutants were generated are different in each case and might also influence on the phenotypes observed. The mutant published by Takebe *et al*. presents a substitution of the first exon by a construction consistent on an IRES (internal ribosome entry site) and the LacZ gene. This strategy prevents the transcription of any region of Arid3b. In our case, a mutational insertion (gene-trap) in the $intron_{2\text{-}3}$ leads to the disruption of the gene transcript, but allows the expression of the second exon fused to β-geo. Although this exon has not been related to any function, no specific studies were done to address its possible roles. Hence, we cannot completely exclude the possible formation of a short truncated form of Arid3b fused to β-geo, which could act as a dominant negative form of the protein, bind other factors and disrupt their normal function, thus leading to a more severe phenotype.

Patterning defects in the heart

Despite the early Arid3b expression in the myocardium, the expression of genes involved in specification of chamber myocardium (*Nkx2*.5 and *Gata4*) and several chamber patterning markers (such as *Tbx5*, *Hand1/2*, *Hey1/2*) is normal in *Arid3b*$^{gt/gt}$ embryos. In fact, the defects observed are mostly related to SHF derivatives and precursor cells, where a more prolonged expression is observed. This is somehow reminiscent of the phenotype of *Islet1* mutants: despite an early brief expression of Islet1 in the heart tube, the mutant phenotype mainly reflects a defect in SHF contribution (Cai C.L. *et al*., 2003) (Vincent S.D. and Buckingham, 2010). However, the patterning of the AVC is affected in *Arid3b*$^{gt/gt}$ embryos: it seems to be properly specified, since early *Bmp2* expression is normal, but expression of transcription factors that define the AVC myocardium (*Tbx2*, *Tbx3*) is markedly impaired from E9.0, and this is accompanied by expansion of the chamber marker *Anf*. The AVC is partially derived from the SHF. In our DiI labelling experiments we mostly studied the contribution to the more posterior part of the heart, the IFT and the sinus horns, so we do not know whether the SHF contribution to the AVC is normal in *Arid3b*-null embryos or not. On the other hand, Tbx2+ cells fate tracing with *Tbx2*$^{Cre/+}$*;R26R* line shows that the E8.0 to E8.5 inflow tract population gives rise to the E9.0-9.5 AVC (Aanhaanen W.T.J. *et al*., 2009). In our mutants, *Tbx2* expression in the inflow region at E8.5 looks normal, suggesting that the precursors of AVC are present in *Arid3b*$^{gt/gt}$ embryos (**Supplementary Figure 1**). Also, normal levels of *Bmp2* at E9.0 as well as correct expression of *Hey1* and *Hey2*, which specify the atrioventricular boundary, further support normal early patterning of the AVC. However, because a clear signal of *Arid3b* is detected in the AVC myocardium at E9.0, it seems reasonable to suggest

that it might play an additional direct role in some steps of AVC patterning.

As mentioned above, *Tbx2* and *Tbx3* expression is reduced in the developing AVC of *Arid3b* mutants. BMP signal transduction appears to be normal in the myocardium, since pSmad1/5/8 is localised in the nucleus of myocardial cells. Tbx2 has been shown to be a direct target of Bmp2 in the AVC; an upstream 380 pb fragment enriched in pSmad binding sites is enough to drive *Tbx2* expression in the AVC and the OFT. Although such a direct regulation has not been shown for Tbx3, deletion of *Bmp2* leads to strong reduction of *Tbx3* in the AVC (Singh R. *et al*., 2012). Because we detect normal *Bmp2* and pSmad expression in the AVC myocardium of *Arid3b*$^{gt/gt}$ embryos, we suggest that Arid3b functions downstream pSmad in this tissue and that the defect in *Arid3b* mutants is due to improper function of transcriptional complexes that drive the expression of *Tbx2*. DNA-binding by pSmad proteins is sometimes dependent on stabilization by other sequence specific DNA-binding proteins to ensure successful activation of its targets (Blitz I.L. and Cho, 2009). Hence, one possibility is that Arid3b plays such a role, forming a complex with pSmad proteins. Although preliminary, our *in vitro* results of co-immunoprecipitation of Arid3b and pSmad1 do not seem to support this idea. However, Arid3b might still be forming a complex with pSmad proteins, although without binding directly to them. It might also have an indirect role that favours pSmad activity; for instance, it might bind or compete with Tbx20, which inhibits the formation of Smad1/5-Smad4 complexes and, thus, represses *Tbx2* expression. Further experiments would be necessary to address these questions.

Early EMT defects seem to be non-cell-autonomous

EMT disruption is one of the most noticeable defects observed in *Arid3b* mutant hearts. The EMT process is dependent on the crosstalk between the endocardium and myocardium with different pathways operating in each of the tissues (Notch pathway from the endocardium and Bmp pathway from the myocardium). We could not detect *Arid3b* expression in the endocardium at the stages when EMT starts, but it is expressed in the myocardium at E9.0, when the process of EMT begins, although no cells are yet detected in the endocardial cushions. This is the stage when we start to observe the AVC myocardium patterning defect (reduction of *Tbx2* and *Tbx3* and expansion of *Anf*). This defect is present at E9.5, when *Arid3b* expression has diminished greatly in the AVC. We think that one of the consequences of this abnormal patterning is the narrowing of the canal. Also, the expression of *Bmp2* is reduced at E9.5, possibly as a consequence of the reduction of *Tbx2* and *Tbx3* levels which act in a positive feedback loop with *Bmp2* (Singh R. *et al*., 2012). It is interesting that, while in the myocardium the number of pSmad positive nuclei is still similar between wild type and mutant embryos, their number is significantly reduced in the endocardium at E9.5 coinciding with the decrease in *Bmp2* expression. As could be expected from the histological EMT defects observed (great reduction of mesenchymal cells on the AVC), expression of several genes involved in this process (such as *Snail1*, *Twist1*, *Tgf*β2 and *Tbx20*) is reduced. *Snail1* and *Twist1* have been shown to be controlled by Bmp2 from the myocardium

(Luna-Zurita L. *et al*., 2010) (Ma L. *et al*., 2005). Because Bmp2 has been described as a key EMT-inducing factor (Sugi Y. *et al*., 2004), the low levels of this factor in *Arid3b*$^{gt/gt}$ myocardium could explain the defective EMT observed. This proposal is strongly supported by the rescue of EMT in AVC explants *in vitro* by application of Bmp2; this result suggests that the defective response of endocardial cells is not caused directly by the lack of *Arid3b* but is secondary to the patterning defect in the myocardium. Thus, Arid3b would play a non-cell-autonomous role in the early events of valve formation, although we cannot completely discard that a low level of expression in the endocardium not detected by *in situ* hybridisation could play an additional role.

While not detected early in the endocardium, we observe a robust expression of *Arid3b* in this layer from E10.5, including the endocardium of the valves. This expression might reflect a later role of *Arid3b* in valve formation. However, early lethality of *Arid3b*$^{gt/gt}$ embryos precludes the study of this possibility, making necessary the use of conditional mutants.

Microarray analysis reveals a large set of genes with altered expression in *Arid3b*$^{gt/gt}$ embryos

Our microarray experiments revealed a large number of genes differentially expressed in *Arid3b*$^{gt/gt}$ versus wild type embryos. When the standard filter of p value less than 0.05 and a fold change of +/-2 is applied, we observe that the number of genes differentially expressed after Arid3b deletion is higher in the microarray performed at E9.5 than at E9.0. One explanation is the fact that for the microarray at E9.0 whole embryos are used, and genes that are only up- or down-regulated in one particular region become diluted and might not reach the established threshold. At E9.5 the embryos are subdivided in three regions and genes specifically missregulated in the heart, head or trunk become apparent. On the other hand, the phenotype is more severe at E9.5 than at E9.0 and some genes that appear differentially expressed at this stage are probably not primary targets of Arid3b, but are secondary to the cardiovascular failure. For instance, expression of *HIF1*α is upregulated at E9.5 but not at E9.0; *HIF1*α encodes for one of the subunits of HIF1, a transcription factor which responds to hypoxia activating the transcription of genes involved in angiogenesis, energy metabolism and apoptosis (Majmundar A.J. *et al*., 2010). Immunostaining against pimonidazole, a marker of hypoxia, confirmed an increase in hypoxic regions in E9.5 mutant embryos (**Supplementary Figure 2**). We believe that upregulation of *HIF1*α and its targets is secondary to the cardiovascular failure. In this way, genes that appear misexpressed at E9.5 must be analysed carefully and their expression checked at earlier stages to make sure they respond directly to the absence of *Arid3b*.

A functional analysis with Ingenuity software of the filtered sets of genes enabled us to discover that the top highly overrepresented functions included cell morphology and cell movements. These results support a role for *Arid3b* in the control of cell motility and cellular rearrangements. However, the classification parameters used by the Ingenuity pathway, while proved to be very

useful for data analysis, must be considered critically. Some of the genes, although might have been described as being involved in cellular movement, might be playing a different role in our system. Moreover, some of the molecules included in the lists of genes involved in motility are related to movement of endothelial cells or leukocytes and might reflect some of the secondary effects of *Arid3b* deletions. One of the genes related to cell movement upregulated in the microarray that drew our attention was Lims2. *Lims2* expression appears upregulated only in the heart, and again very conspicuous at the heart poles. It is involved in signal transduction from integrins to their targets, including the actin cytoskeleton to control cell shape and motility; its upregulation in cells leads to decreased cell motility (Boudoukha S. *et al*., 2010). Because of these previously described functions, we suggest that Lims2 it as a good candidate mediator of Arid3b effects. We observed that increased expression of *Lims2* is especially strong in the atria and OFT, but do not detect increased levels in the SHF cells. It might be that the upregulation of *Lims2* impairs cell rearrangements or movements once they have ingressed into the heart tube, but does not seem to be responsible for the defect in their recruitment to the heart poles. A further detailed analysis of the expression of other genes related to cell motility or cell morphology is necessary to find more targets of *Arid3b* and determine its involvement in this cellular process.

An interesting result obtained from the microarray experiments is the possible effect on muscular differentiation, since several genes are downregulated in the somites. *Arid3b* is expressed in the caudal paraxial mesoderm and the newly formed somites and expression gradually diminishes as the somites mature. In *Arid3b* mutants, the expression of *Vggl2*, *Unc45b*, *Smyd1* and *Myf5* (**Supplementary Figure 3**) is reduced in the somites, suggesting that Arid3b is required for the expression of muscular markers. Not much is known about Arid3b implication in cell differentiation. Two reports have recently described a change in *Arid3b* expression upon ES and iPS cells differentiation. Interestingly, according to (Kobayashi K. *et al*., 2013) *Arid3b* is upregulated when neural cells are dedifferentiated, while (Wang J. *et al*., 2006) observe that *Arid3b* is among the genes most upregulated on ES cells differentiation. This would suggest that Arid3b does not have an exclusive role as repressor or activator of differentiation, but acts dependently on the cellular context, as has been shown for its *Drosophila* homologous (Häder T. *et al*., 2000). It might be also favouring differentiation towards a particular cellular fate, for instance, muscular cells. On the other hand, microarrays with RNA extracted from the head, also shows a large number of genes differentially expressed in this region. We observe alteration of genes related to neurogenesis and neuronal differentiation (such as Cend1, Neurog3 and Npcd), as well as genes related to neuronal morphogenesis (Nyap1, Nefh or Gprin1). Interestingly, *Arid3b* expression is upregulated in the midbrain of *RPB-Jk* mutants, which lack activity of the Notch pathway (Andersson E.R. *et al*., 2011) (**Supplementary Figure 4**). *RBP-jk* mutants show increased expression of some neuronal differentiation markers and excess of committed neuronal precursors (de la Pompa J.L. *et al*., 1997). Whether Arid3b is involved in neuronal differentiation and is repressed by the Notch pathway remains to be elucidated.

Upregulation of *Bhlhb2* and cardiomyocyte differentiation

Bhlhb2 drew our attention as it appeared as one of the most upregulated genes at both E9.0 and E9.5. Indeed, *in situ* hybridisation confirms high levels of expression in the somites, branchial arches, ventral region of the pharyngeal endoderm and in the forebrain. In the heart its expression is especially strong in the SHF, in the dorsal region of the sinus horns, in the atria and in the OFT, regions where higher levels of expression of *Arid3b* are observed. These results suggest that Arid3b might act as a repressor of *Bhlhb2*. Differentiation of the poles of the heart is impaired, as shown by the reduction of early myocardial markers, SMA and Troponin T. This is consistent with the impaired muscular differentiation observed in the somites. Also, *Smyd1* expression, which is necessary for cardiac differentiation and morphogenesis, is reduced throughout the myocardium and is absent in the inflow region, where the higher levels of *Bhlhb2* are observed. Since Bhlhb2 was shown to act as a repressor of *Smyd1* (Kwon Ch. *et al*., 2009), we propose that its upregulation is responsible for the impaired differentiation of the poles. *Bhlhb2* expression is directly regulated by Wnt/β-catenin pathway; although nuclear β-catenin expression is normal in $Arid3b^{gt/gt}$ embryos, we cannot exclude that Arid3b acts downstream β-catenin stabilization in the nucleus, for instance, blocking or modulating its binding to DNA to activate *Bhlhb2* expression. According to (Kwon C. et al., 2009), *Bhlhb2* is regulated through a Lef/Tcf consensus site located in the 5' UTR of *Bhlhb2* gene. Using the Jaspar database we could detect multiple putative Arid3b binding sites in this region; however, whether they are biologically relevant needs further investigation.

Pole defects in *Arid3b*-null embryos

A major defect in *Arid3b* mutant embryos is the shortening and abnormal morphology of the heart poles. This phenotype was not described in a previous article where *Arid3b* mutants were characterised. In that report, Takebe *et al*. explained the early lethality of *Arid3b*-null embryos by massive cranial neural crest cell death and proposed that Arid3b acts as surviving factor. In a later study, the same authors showed that Arid3b protects ES cells from MYCN induced apoptosis. Since the pool of precursors in the SHF is the main source of cells for heart growth at these stages, it seemed reasonable to think that progenitors' survival is compromised in *Arid3b*-null embryos and might be the cause of the shortening of the poles. However, cell death levels in SHF are similar in wild type and mutant embryos. The only increase is observed at E9.5, while the shortening of the poles starts to be detected already from E8.5. So increased apoptosis cannot be considered as the primary cause of the phenotype, although it might contribute to its severity at E9.5. Cell proliferation is also unaffected in $Arid3b^{gt/gt}$ SHF cells. In support of this data, the total number of precursors is similar in mutant and wild type embryos at all stages analysed, except at E9.5, when we observe the increase in cell death.

Since a difference in cell number does not seem to be the primary cause of the poles shortening, we wondered whether cell deployment might be affected by absence of *Arid3b*. Some previous

reports suggested that Arid3b might play a role in cell motility. In malignant ovarian cancer, Arid3b promotes mesenchymal transformation of the ovarian epithelium, while in breast cancer cells it is necessary for cell migration (Cowden Dahl K.D. *et al*., 2009) (Akhavantabasi S. *et al*., 2012). In *Arid3b*$^{gt/gt}$ embryos we have shown that defective cell rearrangements in the apical ectodermal ridge (AER) of the limb leads to aberrant maturation of this structure (Casanova J.C. *et al*., 2011); similar results are obtained in chick AER electroporated with dominant-negative forms of Arid3b which inhibit its function. Our *in vitro* studies with MEF cells derived from *Arid3b*$^{gt/gt}$ embryos further support the involvement of Arid3b in regulating normal cell movement. Mutant cells present increased levels of actin stress fibres, extensive membrane blebbing and breakage of cells upon detachment from substrate; moreover, they form less protrusions and show reduced cell motility. Based on this data we decided to address a possible role of Arid3b in SHF cell deployment.

At present, little is known about the cellular mechanisms by which cells leave the pharyngeal mesoderm and are added to the heart tube. One recent report suggests the existence of a caudal proliferative centre in the caudal coelomic wall from which cells move cranially via the dorsal pericardial mesoderm to contribute to the arterial pole (van den Berg G. *et al*., 2009). (Sinha T. *et al*., 2012) suggest that Wnt5a-activated planar cell polarity (PCP) signalling activates a protrusive behaviour in the caudal splachnic mesoderm to promote the incorporation of SHF into a cohesive epithelial-like sheet, which eventually pushes the sheet rostrally and favours the ingression of cells into the OFT. The proposed model would be similar to convergent extension movements that occur during gastrulation in zebrafish and *Xenopus*, which are regulated by PCP pathway (Wallingford J.B. *et al*., 2002). We observe that *Arid3b*$^{gt/gt}$ cells in the caudal splachnic mesoderm seem to form more compact clusters with less protrusions that in the wild type embryos, a phenotype reminiscent to the observed in *Wnt5a* and *Dvl1/2* mutants, where PCP signalling is disrupted. Interestingly, we proposed that Arid3b also somehow regulates a similar process of intercalation and compactation in the AER, as far as both in chick and mice loss of Arid3b function leads to an AER which is shorter in the AP axis and broader in the DV axis (Casanova J.C. *et al*., 2011). Whether Arid3b is involved in the non-canonical Wnt/PCP signalling needs further investigation, but we believe that the primary cause of shortening of the poles of the heart is related to Arid3b-regulated cell rearrangements and movements.

The DiI fate-mapping experiments confirm a defect in the contribution of SHF precursors to the heart in *Arid3b* mutant embryos. These experiments also show that the ingression of precursors into the heart tube is differently affected in the arterial and venous poles. When cells are labelled in the pSHF, only half of the mutant embryos display DiI staining in the heart IFT. On the contrary, we always see labelled cells in the OFT, although the contribution to its more proximal region and the right ventricle is impaired in *Arid3b*$^{gt/gt}$ embryos. One possible explanation is the difference in cell death rates between the two regions of the SHF. As mentioned above, an increase in apoptosis is observed in the SHF cells at E9.5; when analysed in more detail, we detect that most of the cells that undergo cell death are located in the proximity of the sinus horns. It might be that cells from

the pSHF that are not able to ingress into the IFT are eliminated by apoptosis. Consistent with that, we cannot find clear accumulation of cells near the IFT, as we do at the entrance of the OFT. There are several possible explanations for these different behaviours. One important point is the stage of labelling. The pSHF injections were done between 4-6 pairs of somites (ps) (although addition of cells to IFT is already occurring at 2 ps stage), while for AHF we used embryos between 8-10 ps. Another difference is the population that was marked. Our labelling of pSHF cells corresponds to a more caudal region, which contributes mostly to the sinus venosus and partially to the atria. We centred our attention in this population of cells because the more cranially derived region coming from the pSHF – the AVC – is present in mutant embryos according to Bmp2 expression. On the contrary, labelling of the OFT precursors is not so restricted and most likely includes a broader region of SHF cells in the anterio-posterior axis. In this case we can see contribution to all the AHF-derived regions, but in *Arid3b*$^{gt/gt}$ embryos cell progression towards the most distant zone (the right ventricle) is disrupted and cells accumulate closer to the entrance of the OFT. The lack of specific markers that distinguish the right ventricle from the OFT at these early stages limits our possibilities to address to what extent the right ventricle formation is affected, as we can do for the AVC. With our current approach we also do not know whether the cells, which are added later and will form the most distal OFT, are going to be added to the heart tube or undergo cell death before reaching it, similarly to what happens in the IFT. With these considerations in mind, we propose two possible hypothesis for the differences observed:

- The phenotype is similar between the two poles, with the most proximal cells being added to the heart tube and the most caudal failing and undergoing apoptosis. In this case, if we labelled a broader population of cells in the pSHF (more rostral), we should observe a decrease in DiI labelled cells in the AVC, similar to that observed in the right ventricle. On the other hand, DiI labelling of the AHF at later stages would result in a decreased proportion of mutant embryos with DiI+ cells in the distal OFT (as happens in the IFT) and to the observation of an important increase in cell death in the AHF.

- The absence of Arid3b in the pSHF only affects a subpopulation of cells, while in the AHF a broader group of cells is affected. In this case, labelling of a more cranial population of pSHF would result in normal contribution of cells to the AVC.

One unexpected observation made by Domínguez *et al*. is that cells from the pSHF contribute to the OFT. At 2 ps stage the posterior-most SHF has a predominantly OFT fate. Later, at 4-6 ps, the most cranial portion of the pSHF contributes partially to the arterial pole in a sequential pattern (cells labelled at earlier stages migrate to the boundary between the OFT and the right ventricle, while cells labelled at later stage migrate to the boundary between OFT and the aortic sac). These cells seem to move via the dorsal pericardial mesoderm (Domínguez J.N. *et al*., 2012). Whether this process is affected in *Arid3b*$^{gt/gt}$ embryos is not known, but we must bear in mind that part of the labelled AHF cells are in fact derived from the pSHF on their way to the OFT and these different populations might be affected differentially by the absence of *Arid3b*. This also

reflects the fact that we currently do not know whether the cellular mechanisms underlying cell deployment to the arterial and venous poles are the same. It might be that, for example, cells which contribute to the arterial pole from the pSHF must move by migration, while cells situated in the border of the inflow tract and the heart tube incorporate through cell intercalation. The requirement and implication of Arid3b could then vary in these different situations.

Three different MEFs types?

To investigate the function of Arid3b at the cellular level, we isolated embryonic fibroblasts from three genetically different mouse lines. The first MEFs type, from *Arid3b*$^{gt/gt}$ embryos display a series of defects related to cell movement and adhesion. These cells are also incapable of expanding and increase their number. It was previously described that overexpression of Arid3b in MEFs leads to their immortalization (Kobayashi K. *et al*., 2006), so most probably, our MEFs cells deficient for *Arid3b* suffer an impairment in proliferation or become prematurely senescent. Interestingly, Arid3a, the closest homologue of Arid3b in mammals, has a different effect on MEFs, as this factor was shown to repress the expression of pluripotency factors and MEFs deficient for *Arid3a* bypassed senescence and were enhanced for reprograming (Popowski M. *et al*., 2014). We also cannot exclude that some of the defects observed in *Arid3b*$^{gt/gt}$ MEFs appear as a consequence of the absence of *Arid3b* in other cell types, which may have compromised these fibroblasts in the embryo before their isolation.

The other two types of MEFs came from the *Arid3b*$^{flox/flox}$ line and, in that cases, *Arid3b* is deleted by infection with Cre-expressing viral vectors after MEFs are isolated and expanded. This system permits us to avoid the possible influence of other tissues deficient for *Arid3b* in the embryo. The genetic difference between these two types of MEFs is the presence of the NEO cassette in one of the MEFs lines (we refer to it as *Arid3b*$^{flox/flox;NEO\ cassette}$ MEFs), while in the other line the gene is directly flanked by loxP sites (*Arid3b*$^{flox/flox}$ MEFs). As we mentioned in the results, *Arid3b*$^{flox/flox;NEO\ cassette}$ embryos are not viable and show a reduction of *Arid3b* RNA expression even in the absence of any Cre. It has been described that the neo cassette might interfere with gene expression and in some conditional lines the presence of the neo cassette leads to embryonic lethality (Chen L. *et al*., 1999) (Rucker E.B. *et al*., 2000) (Xu X. *et al*., 2001). Consistent with that, removal of the NEO cassette by crosses with mice carrying Flp (the Neo cassette is flanked by FRT sites) enabled us to obtain viable and fertile *Arid3b*$^{flox/flox}$ mice. Interestingly, MEFs cells obtained from *Arid3b*$^{flox/flox;NEO\ cassette}$ embryos, which can be considered hypomorphs for *Arid3b*, do not show any obvious defective phenotype and behave similarly to wild type MEFs. This suggests that the reduced levels of *Arid3b* expression are sufficient for MEFs survival at this stage of development. Moreover, these MEFs display a milder phenotype than *Arid3b*$^{flox/flox}$ MEFs upon addition of Cre and total deletion of the gene. *Arid3b*$^{flox/flox;NEO\ cassette}$ MEFs are still able to grow, but show a motility defect similar to the one observed in *Arid3b*$^{gt/gt}$ derived MEFs, as we assayed by wound healing experiments. Contrary, *Arid3b*$^{flox/flox}$ MEFs stop growing after infection with adenovirus containing

Cre, and seem to acquire a senescent phenotype, similar to the one observed in *Arid3b*$^{gt/gt}$ MEFs. We speculate that MEFs derived from *Arid3b*$^{flox/flox;NEO\ cassette}$ embryos, which present reduced levels of *Arid3b* from the beginning, are more adapted to overcome the absence of this gene. It might be that from the beginning cells more resistant to low levels of Arid3b are selected and later, when *Arid3b* is totally deleted, are able to overcome the growth arrest, although not the motility defect. We do not know what is the role of Arid3b in cell proliferation in MEFs, but maybe another factor can compensate for its function, and this factor is overexpressed in *Arid3b*$^{flox/flox;NEO\ cassette}$ cells from the moment of their isolation to overcome the reduced levels of *Arid3b*. On the other hand, *Arid3b*$^{flox/flox}$ MEFs are not under stress of shortage of this factor and, thus, are more sensitive when the gene is totally deleted. However, we have not performed any specific experiments to determine to which extent cell proliferation is normal in *Arid3b*$^{flox/flox;NEO\ cassette}$ cells; we can only say that these MEFs, contrary to what happens in the other two types, are able to grow. Because cytoskeleton changes and cell adhesion also play very important roles in normal cell division, we cannot exclude that the defects, that lead to decreased motility and abnormal cellular shape in the absence of Arid3b, can also affect cell division. To which extent Arid3b is required for this process and what is the molecular basis for the disrupted cell migration in *Arid3b*-null cells, needs further studies.

Phenotypic differences between *Arid3b*$^{flox/flox}$*/Sox2-Cre* and *Arid3b*$^{gt/gt}$ lines

The *Sox2-Cre* line allows us to delete *Arid3b* in the whole embryo from the epiblast stage (Hayashi S. *et al*., 2002) and compare the obtained phenotype with the one observed in *Arid3b*$^{gt/gt}$ embryos. No viable *Arid3b*$^{flox/flox}$*/Sox2-Cre* embryos are found at E12.5 but the general phenotype observed is milder than in the case of *Arid3b*$^{gt/gt}$ embryos. The *Arid3b*$^{flox/flox}$*/Sox2-Cre* embryos resemble more the phenotype described in Takebe *et al*., 2006 and our own *Arid3b*$^{gt/gt}$ embryos on C57BL/6 background. Our *Arid3b*$^{flox/flox}$*/Sox2-Cre* line is on mixed background of C57BL/6 and 129 (R1) strains. As already discussed, it seems that the phenotype obtained after *Arid3b* deletion is sensible to genetic background differences between strains. We think this might explain the distinct defects we observe between the two mice lines.

Another important observation is that we could detect *Arid3b* RNA in our conditional mutant line after Cre-directed recombination. The conditional allele was designed to delete the second Arid3b exon, where the initiator ATG is located. However, we still observe transcription of part of the gene, as can be detected by *in situ* hybridisation with a probe against the whole mRNA and RT-PCR with primers located in exons 5 and 7, downstream of the deletion. We do not know exactly which regions are transcribed and whether this mRNA is translated. An ATG in the first non-coding exon of the gene exists and is preceded by a consensus Kozak sequence. Moreover, if this ATG was used, the *Arid3b* reading frame would be maintained from splicing with exon3 and a putative Arid3b protein lacking the second exon could in theory be translated. Since the Arid3b antibodies used do not recognize the mouse protein, we have not been able to experimentally test the presence

of Arid3b in the conditional deletion. However, based on the functional defects observed using the *Sox2-Cre* driver line, where the severe cardiovascular defects and lethality are comparable to the full knock out mice, we suggest that if translation occurs, an unstable protein is formed and rapidly degraded. In any case, with our current results we cannot exclude an alternative situation, where a truncated form of Arid3b is translated that could somehow influence the phenotypes observed.

Differences in cardiac phenotype between *Arid3b$^{flox/flox}$/Nkx2.5-Cre* and *Arid3b$^{gt/gt}$* lines

We generated an *Arid3b$^{flox/flox}$/Nkx2.5-Cre* line to determine the specific role of Arid3b in the Nkx2.5+ population. The *Nkx2.5-Cre* is a good driver to study the role of Arid3b in cardiac development and has been widely used for this purpose with other genes (Ma L. *et al*., 2005) (Luna-Zurita L. *et al*., 2010). *Nkx2.5-Cre* expression starts to be detected in the cardiac mesoderm already at E7.75, both in the heart tube, as well as in the SHF and efficient recombination was reported in the cardiac crescent and heart tube (Stanley E.G. *et al*., 2002). We checked for deletion of Arid3b exon2 and indeed observed its absence in the SHF and in the OFT at E9.5. The phenotype we obtain upon deletion of *Arid3b* in the Nkx2.5 population is variable. First, more than half of the conditionally deleted mice are viable, reach adulthood and do not present any noticeable phenotype. The rest of the animals die before weaning, but normal proportions of *Arid3b$^{flox/flox}$/Nkx2.5-Cre* embryos are still observed at E16.5. Several explanations exist for these data. As we mentioned above, the *Arid3b$^{flox/flox}$* mice line is on mixed C57BL/6 and 129 (R1) background. We have shown that *Arid3b$^{gt/gt}$* embryos on C57BL/6 background present a later lethality and apparently fewer defects in the poles of the heart, suggesting that some of the heart defects might be attenuated by modifier loci on this background. The influence of the genetically mixed background on the phenotype is further supported by the fact that embryonic or perinatal lethality is only observed in some of the *Arid3b$^{flox/flox}$/Nkx2.5-Cre* crosses, while in others normal proportions of homozygous mutant adult mice are obtained. The variability between different crosses makes it very difficult to determine the exact amplitude and penetrance of the heart defects. We propose that backcrossing the *Arid3b$^{flox/flox}$/Nkx2.5-Cre* line to C57BL/6 background, for instance, would be necessary to obtain more homogeneous and reproducible phenotypes and, thus, more reliable information on the roles of Arid3b in the Nkx2.5 population.

On the other hand, the *Nkx2.5-Cre* driver might not be the most suitable *Cre* line to study the role of Arid3b in all aspects of heart development. As already mentioned, *Nkx2.5-Cre* recombination starts to be observed in the cardiac crescent at E7.75 and later through the whole myocardium, the SHF and in the endocardium in a mosaic way (Stanley E.G. *et al*., 2002). We observe strong *Arid3b* expression in the myocardium from the cardiac crescent stage, but already from E8.5 expression in the myocardium starts to vanish. On the contrary, expression in the SHF is maintained at high levels through the looping process, while expression in the endocardium is not detected till E10.5, when septation starts. The temporal patterns of expression of the *Nkx2.5-Cre* transgene and of *Arid3b* suggest that recombination might be too late to detect the role of *Arid3b*

in the myocardium. It is also important to mention that it was observed that the Z/AP locus showed transient resistance to deletion in caudal heart progenitors with the Nkx2.5-Cre and the authors suggested that Cre-mediated deletion in myocardium might be locus-dependent (Stanley E.G. *et al*., 2002). Our results show an efficient deletion of *Arid3b* at E9.5, but we have not checked whether at earlier stages the deletion is complete or shows a similar transient resistance. The use of other drivers, such as *Mesp1-Cre*, which recombines already at the stage of the cardiac mesoderm and has been proposed as the earlier molecular marker for the myocardial and endocardial lineages (Saga Y. et al., 2000), might enable us to address more precisely the role of Arid3b in the developing myocardium. The use of other Cre lines, which recombine in a specific cardiac tissues, such as the *Islet1-Cre* (specific for the SHF lineage (Yang L. *et al*., 2006)) or *Tie2-Cre* (deletion in the endocardium and endothelium (Kisanuki Y.Y. *et al*., 2001)) could complete this study and dissect the diverse tissue-specific roles of Arid3b in heart development.

Deletion of *Arid3b* in the endocardium might be responsible for the defects observed in *Arid3b$^{flox/flox}$/Nkx2.5-Cre* embryos

The two most prominent defects observed in *Arid3b$^{flox/flox}$/Nkx2.5-Cre* E16.5 embryos are thinning of the compact myocardium of the right ventricle and disrupted valve remodelling. The defect on the right ventricle is consistent with the high levels of *Arid3b* in the SHF and might reflect the requirement for Arid3b in this population of precursors for later proper development of the right ventricle. However, another possibility is that myocardial thinning is due to deletion of *Arid3b* in the endocardium and the disruption of the normal crosstalk between the two tissues. Different molecules acting from the endocardium have been shown to be critical for normal ventricular myocardium development, such as Jumonji or the Notch pathway. Deletion of either Jumonji (Mysliwiec M.R. *et al*., 2001);| or Notch1 and Delta4 (Grego-Bessa J. *et al*., 2007) from the endocardium leads to myocardial thinning and disruption of normal trabeculation. If this is the case, we would expect a similar or even more severe phenotype on the ventricles when using *Tie2-Cre* or *Nfat-Cre* drivers (Wang Y. *et al*., 2013) to delete *Arid3b* only in the endocardium.

Another striking phenotype is the failure of valve remodelling. Curiously, while in the *Arid3b$^{gt/gt}$* we observe an early defect in valve formation with EMT disruption and decreased number of mesenchymal cells in the AVC cardiac cushions, deletion of *Arid3b* by *Nkx2.5-Cre* gives rise to a later phenotype, where valves appear bigger and the number of mesenchymal cells seems to be increased. As already discussed above, we believe that the early EMT defect in *Arid3b$^{gt/gt}$* embryos is due to disruption of myocardial patterning. The valve defects we observe in *Arid3b$^{flox/flox}$/Nkx2.5-Cre* embryos could be related to the deletion of *Arid3b* in the endocardium, similarly to what we observe in the right ventricle. *Arid3b* is detected in the endocardium from E10.5, suggesting that it might be involved in some of the post-EMT processes of valve remodelling and maturation. The valves look bigger and not properly remodelled in the mutant embryos suggesting an alteration of the proliferation and differentiation balance. So far, the mesenchymal markers analysed, periostin

and *Tbx20*, are expressed normally in the valves. It would be interesting to look at the expression of other molecules, for instance from the Notch and the Bmp pathways. Disruption of Notch signalling by deletion of its ligand *Jagged1* in the endothelium leads to a set of cardiac defects including hypertrophic, not remodelled valves (Hofmann J.J. *et al*., 2012). The Bmp pathway promotes proliferation of mesenchymal cells and deletion of the inhibitory Smad, *Smad6*, leads to hyperplasia of both AVC and OFT valves and pre-weaning death of some of the mutant mice (Galvin K.M. *et al*., 2000) (Combs M.D. and Yutzey, 2009). Whether Arid3b is involved in the normal function of these pathways or is affecting other molecules important for normal valve formation requires further research.

CONCLUSIONS/ CONCLUSIONES

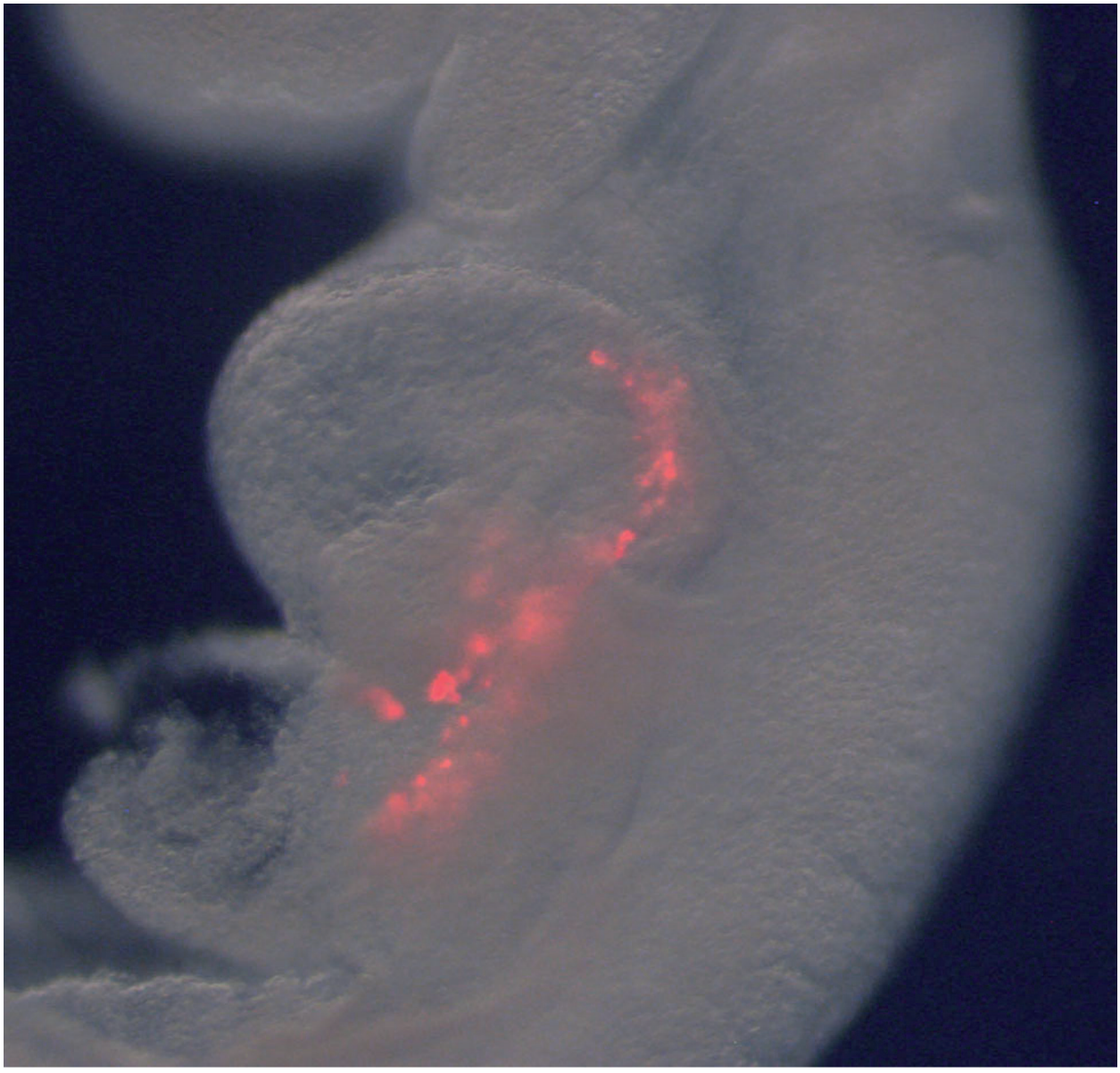

1. *Arid3b* is expressed in a dynamic way in the mouse heart, suggesting multiple roles at different stages of heart development.
   Arid3b *se expresa de manera dinámica en el corazón de ratón, sugiriendo múltiples funciones en diferentes estadios de desarrollo.*

2. Deletion of *Arid3b* in mouse embryos leads to early embryonic death with severe cardiovascular defects, including shortening of the poles of the heart and lack of EMT in the AVC.
   La eliminación del gen Arid3b *en embriones de ratón causa letalidad temprana con severos defectos cardiovasculares, que incluyen acortamiento de los polos cardiacos y ausencia de EMT en el canal atrioventricular.*

3. The phenotype of *Arid3b*-deficient animals is dependent on the mouse genetic background, suggesting the presence of modifier loci interacting with Arid3b functions.
   El fenotipo de embriones deficientes para Arid3b *depende del fondo genético del ratón, lo cual sugiere la presencia de loci modificadores que interfieren en la función del gen.*

4. Myocardial AVC patterning is disrupted in *Arid3b*$^{gt/gt}$ embryos and an expansion of chamber specific markers to the AVC is observed.
   El establecimiento de patrón del canal atrioventricular está alterado en los embriones Arid3b$^{gt/gt}$ *y se observa una expansión de los marcadores específicos de cámaras hacia aquel.*

5. The EMT defect in the AVC can be rescued *in vitro* by addition of Bmp2, suggesting that it is non-cell-autonomous and secondary to the patterning defect in the myocardium.
   El defecto en EMT puede ser rescatado in vitro *al añadir Bmp2, lo cual sugiere que el defecto de EMT es secundario al defecto de establecimiento de patrón del miocardio.*

6. An RNA microarray analysis of wild type versus mutant embryos at different developmental stages reveal a set of differentially expressed genes and top molecular functions related to cellular movement and cell morphology, which could mediate Arid3b function.
   El análisis de microarray de RNA, realizado en embriones salvajes y mutantes a diferentes estadios de desarrollo, ha revelado una serie de genes diferencialmente expresados, además de evidenciar que las funciones moleculares más representadas están relacionadas con motilidad y morfología celular, funciones que podrían estar mediadas por Arid3b.

7. The differentiation of the poles of the heart is impaired in *Arid3b*$^{gt/gt}$ embryos, and *Bhlhb2*, one of the genes upregulated in the microarray, might be involved in this process.
   La diferenciación de los polos del corazón está afectada en embriones Arid3b$^{gt/gt}$*, y*

Bhlhb2*, uno de los genes sobreexpresados en el microarray, podría estar involucrado en este proceso.*

8. Cell deployment of SHF cells to the heart poles is disrupted in *Arid3b* mutants, as shown by DiI labelling
   Marcajes de DiI de células de SHF en las regiones de salida y entrada muestran una deficiencia en el ingreso de las células al corazón en los embriones mutantes para Arid3b.

9. Mouse embryonic fibroblasts show reduced motility in the absence of *Arid3b.*
   Fibroblastos embrionarios de ratón muestran una motilidad reducida en ausencia de Arid3b.

10. Specific deletion of *Arid3b* in Nkx2.5+ cell population (with Nkx2.5-Cre) leads to cardiac defects including thinning of the right ventricle and failure in valve remodelling.
    La eliminación específica de Arid3b *en la población Nkx2.5+ (con Nkx2.5-Cre) da lugar a defectos cardiacos, incluyendo reducción del grosor del miocardio del ventrículo derecho y fallo en la remodelación de las válvulas.*

BIBLIOGRAPHY

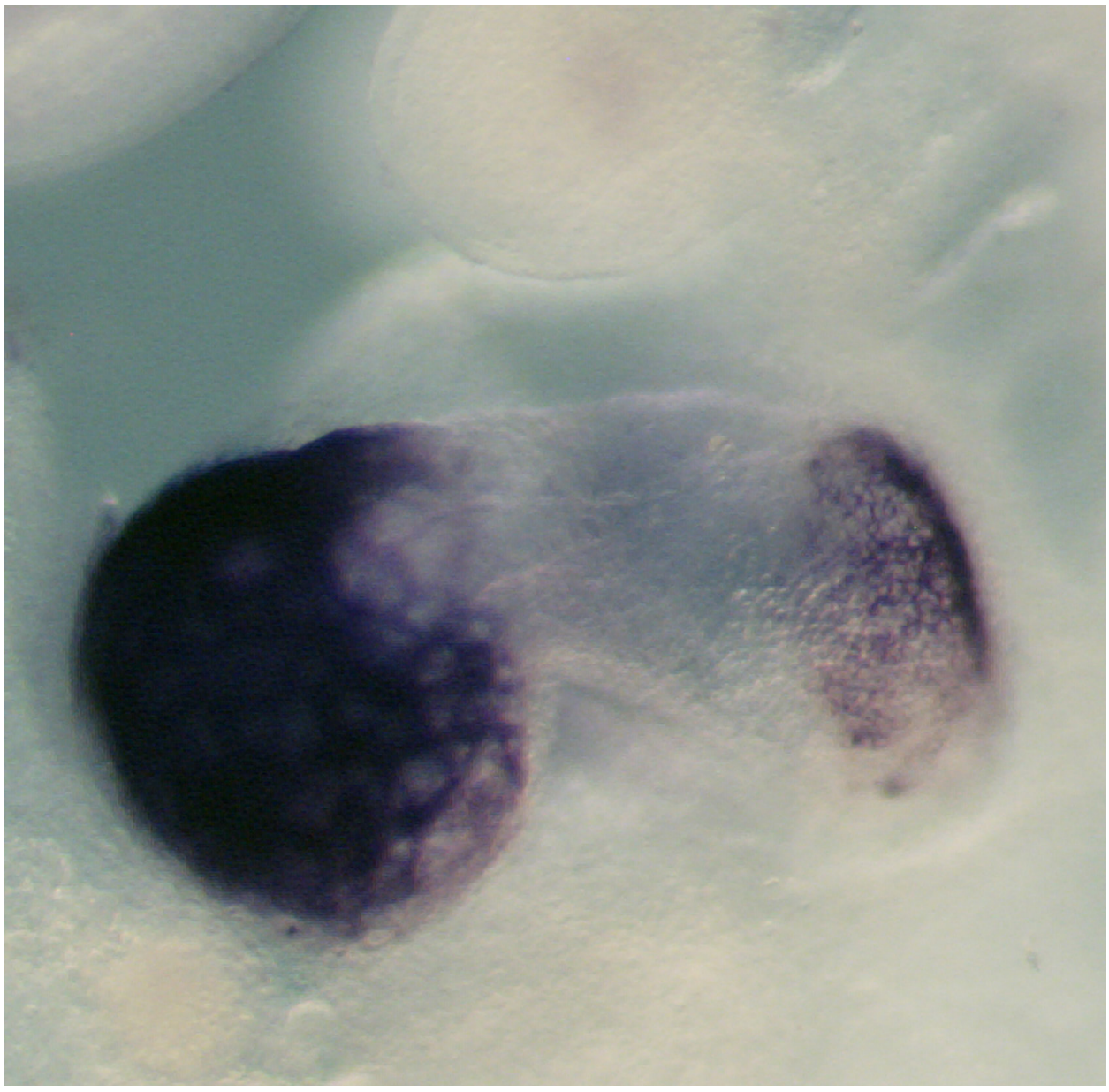

Aanhaanen W.T.J., Brons J.F., Domínguez J.N., Rana M.S., Norden J., Airik R., Wakker V., Gier-de Vries C. de, Brown N.A., Kispert A., et al. (2009). The Tbx2+ primary myocardium of the atrioventricular canal forms the atrioventricular node and the base of the left ventricle. *Circulation Research* **104**, 1267-1274.

Abu-Issa R., Smyth G., Smoak I., Yamamura K. and Meyers, E. N. (2002). Fgf8 is required for pharyngeal arch and cardiovascular development in the mouse. *Development* **129**, 4613-4625.

Ai D., Fu X., Wang J., Lu M.-F., Chen L., Baldini A., Klein W.H. and Martin, J. M. (2007). Canonical Wnt signaling functions in second heart field to promote right ventricular growth. *PNAS* **104**, 9319-9324.

Akhavantabasi S., Sapmaz A., Tuna S. and Erson-Bensan, A. E. (2012). miR-125b targets ARID3B in breast cancer cells. *Cell Structure and Function* **37**, 27-38.

An G., Miner C.A., Nixon J.C., Kincade P.W., Bryant J., Tucker P.W. and Webb, C. F. (2010). Loss of Bright/ARID3a function promotes developmental plasticity. *Stem Cells* **28**, 1560-1567.

Andersson E.R., Sandberg R. and Lendahl, U. (2011). Notch signaling: simplicity in design, versatility in function. *Development* **138**, 3593-3612.

Argüello C., de la Cruz M.V. and Gómez, C. S. (1975). Experimental study of the formation of the heart tube in the chick embryo. *J Embryol Exp Morphol* **33**, 1-11.

Azhar M., Brown K., Gard C., Chen H., Rajan S., Elliott D.A., Stevens M.V., Camenisch T.D., Conway S.J. and Doetschman, T. (2011). Transforming growth factor Beta2 is required for valve remodeling during heart development. *Developmental Dynamics* **240**, 2127-2141.

Azhar M., Runyan R.B., Gard C., Sanford L.P., Miller M.L., Andringa A., Pawlowski S., Rajan S. and Doetschman, T. (2009). Ligand-specific function of transforming growth factor beta in epithelial-mesenchymal transition in heart development. *Developmental Dynamics* **238**, 431-442.

Baba A., Ohtake F., Okuno Y., Yokota K., Okada M., Imai Y., Ni M., Meyer C.A., Igarashi K., Kanno J., et al. (2011). PKA-dependent regulation of the histone lysine demethylase complex PHF2-ARID5B. *Nature Cell Biology* **13**, 668-675.

Bakker M.L., Boukens B.J., Mommersteeg M.T., Brons J.F., Wakker V., Moorman A.F. and Christoffels, V. M. (2008). Transcription factor Tbx3 is required for the specification of the atrioventricular conduction system. *Circulation Research* **102**, 1340-1349.

Barth J.L., Clark C.D., Fresco V.M., Knoll E.P., Lee B., Argraves W.S. and Lee, K. H. (2010). Jarid2 is among a set of genes differentially regulated by Nkx2.5 during outflow tract morphogenesis. *Developmental Dynamics* **239**, 2024-2033.

Beck J.A., Lloyd S., Hafezparast M., Lennon-Pierce M., Eppig J.T., Festing M.F. and Fisher, E. M. (2000). Genealogies of mouse inbred strains. *Nature Genetics* **24**, 23-25.

Benevolenskaya E.V., Murray H.L., Branton P., Young R.A. and Kaelin, W. G. J. (2005). Binding of pRB to the PHD protein RBP2 promotes cellular differentiation. *Molecular Cell* **18**, 623-635.

Bertrand N., Roux M., Ryckebüsch L., Niederreither K., Dollé P., Moon A., Capecchi M. and Zaffran, S. (2011). Hox genes define distinct progenitor sub-domains within the second heart field. *Developmental Biology* **353**, 266-274.

Binda O., C Nassif C. and Branton, P. E. (2008). SIRT1 negatively regulates HDAC1-dependent transcriptional repression by the RBP1 family of proteins. *Oncogene* **27**, 3384-3392.

Blitz I.L. and Cho, K. W. Y. (2009). Finding partners: how BMPs select their targets. *Developmental Dynamics* **238**, 1321-1331.

Bondue A. and Blanpain, C. (2010). Mesp1: a key regulator of cardiovascular lineage commitment. *Circulation Research* **107**, 1414-1427.

Bondue A., Lapouge G., Paulissen C., Semeraro C., Iacovino M., Kyba M. and Blanpain, C. (2008). Mesp1 acts as a master regulator of multipotent cardiovascular progenitor specification. . *Cell Stem Cell* **3**, 69-84.

Bonnet A., Dai F., Brand-Saberi B. and Duprez, D. (2010). Vestigial-like 2 acts downstream of MyoD

activation and is associated with skeletal muscle differentiation in chick myogenesis. *Mechanism of Development* **127**, 120-136.

Boudoukha S., Cuvellier S. and Polesskaya, A. (2010). Role of the RNA-binding protein IMP-2 in muscle cell motility. *Molecular and Cellular Biology* **30**, 5710-5725.

Bressan M., Liu G. and Mikawa, T. (2013). Early mesodermal cues assign avian cardiac pacemaker fate potential in a tertiary heart field. *Science* **340**, 744-748.

Bruneau B.G., Nemer G., Schmitt J.P., Charron F., Robitaille L., Caron S., Conner D.A., Gessler M., Nemer M., Seidman C.E., et al. (2001). A murine model of Holt-Oram syndrome defines roles of the T-box transcription factor Tbx5 in cardiogenesis and disease. *Cell* **106**, 709-721.

Buckingham M., Meilhac S. and Zaffran, S. (2005). Building the mammalian heart from two sources of myocardial cells. *Nature Reviews Genetics* **6**, 826-835.

Cai C.L., Liang X., Shi Y., Chu P.H., Pfaff S.L., Chen J. and Evans, S. (2003). Isl1 identifies a cardiac progenitor population that proliferates prior to differentiation and contributes a majority of cells to the heart. *Developmental Cell* **5**, 877-889.

Cai S., Zhu L., Zhang Z. and Chen, Y. (2007). Determination of the three-dimensional structure of the Mrf2-DNA complex using paramagnetic spin labeling. *Biochemistry* **46**, 4943-4950.

Camenisch T.D., Spicer A.P., Brehm-Gibson T., Biesterfeldt J., Augustine M.L., Calabro A. Jr., Kubalak S., Klewer S.E. and McDonald, J. A. (2000). Disruption of hyaluronan synthase-2 abrogates normal cardiac morphogenesis and hyaluronan-mediated transformation of epithelium to mesenchyme. *Journal of Clinical Investigation* **106**, 349-360.

Carmena A., Murugasu-Oei B., Menon D., Jiménez F. and Chia, W. (1998). Inscuteable and numb mediate asymmetric muscle progenitor cell divisions during Drosophila myogenesis. *Genes&Development* **12**, 304-315.

Casanova J.C., Uribe V., Badía-Careaga C., Giovinazzo G., Torres M. and Sanz-Ezquerro, J. J. (2011). Apical ectodermal ridge morphogenesis in limb development is controlled by Arid3b-mediated regulation of cell movements. *Development* **138**, 1195-1205.

Catchpole S., Spencer-Dene B., Hall D., Santangelo S., Rosewell I., Guenatri M., Beatson R., Scibetta A.G., Burchell J.M. and Taylor-Papadimitriou, J. (2011). PLU-1/JARID1B/KDM5B is required for embryonic survival and contributes to cell proliferation in the mammary gland and in ER+ breast cancer cells. *Int. J. Oncol* **38**, 1267-1277.

Chakraborty S., Wirrig E.E., Hinton R.B., Merrill W.H., Spicer D.B. and Yutzey, K. E. (2010). Twist1 promotes heart valve cell proliferation and extracellular matrix gene expression during development in vivo and is expressed in human diseased aortic valves. *Developmental Biology* **347**, 167-179.

Chen L., Adar R., Yang X., Monsonego E.O., Li C., Hauschka P.V., Yayon A. and Deng, C. X. (1999). Gly369Cys mutation in mouse FGFR3 causes achondroplasia by affecting both chondrogenesis and osteogenesis. *Journal of Clinical Investigation* **104**, 1517-1525.

Chia R., Achilli F., Festing M.F. and Fisher, E. M. (2005). The origins and uses of mouse outbred stocks. *Nature Genetics* **37**, 1181-1186.

Christensen J., Agger K., Cloos P.A., Pasini D., Rose S., Sennels L., Rappsilber J., Hansen K.H., Salcini A.E. and Helin, K. (2007). RBP2 belongs to a family of demethylases, specific for tri-and dimethylated lysine 4 on histone 3. *Cell* **128**, 1063-1076.

Christoffels V.M., Habets P.E.M.H., Franco D., Campione M., Jong F. de, Lamers W.H., Bao Z.-Z., Palmer S., Biben Ch., Harvey R.P., et al. (2000). Chamber formation and morphogenesis in the developing mammalian heart. *Developmental Biology* **223**, 266-278.

Christoffels V.M., Hoogaars W.M.H., Tessari A., Clout D.E.W., Moorman A.F.M. and Campione, M. (2004). T-Box transcription factor Tbx2 represses differentiation and formation of the cardiac chambers. *Developmental Dynamics* **229**, 763-770.

Christoffels V.M., Mommersteeg M.T., Trowe M.O., Prall O.W., de Gier-de Vries C., Soufan A.T., Bussen M., Schuster-Gossler K., Harvey R.P., Moorman A.F., et al. (2006). Formation of the

venous pole of the heart from an Nkx2-5-negative precursor population requires Tbx18. *Circulation Research* **98**, 1555-1563.

Cohen E.D, Wang Z., Lepore J.L, Lu M.M., Taketo M.M., Epstein D.J. and Morrisey, E. E. (2007). Wnt/beta-catenin signaling promotes expansion of Islet-1 - positive cardiac progenitor cells through regulation of FGF signaling. *The Journal of Clinical Investigation* **117**, 1794-1804.

Cohen E.D., Miller M.F., Wang Z., Moon R.T. and Morrisey, E. E. (2012). Wnt5a and Wnt11 are essential for second heart field progenitor development. *Development* **139**, 1931-1940.

Combs M.D. and Yutzey, K. E. (2009). Heart valve development: regulatory networks in development and disease. *Circulation Research* **105**, 408-421.

Coultas L., Chawengsaksophak K. and Rossant, J. (2005). Endothelial cells and VEGF in vascular development. *Nature* **438**, 937-945.

Cowden Dahl K.D., Dahl R., Kruichak J.N. and Hudsonn, L. G. (2009). The epidermal growth factor receptor responsive miR-125a represses mesenchymal morphology in ovarian cancer cells. *Neoplasia* **11**, 1208-1215.

Damert A., Miquerol L., Gertsenstein M., Risau W. and Nagy, A. (2002). Insufficient VEGFA activity in yolk sac endoderm compromises haematopoietic and endothelial differentiation. *Development* **129**, 1881-1892.

de Boer B.A., Berg G., de Boer P.A.J., Moorman A.F.M. and Ruijter, J. M. (2012). Growth of the developing mouse heart: An interactive qualitative and quantitative 3D atlas. *Developmental Biology* **368**, 203-213.

de Castro M.P., Aránega A. and Franco, D. (2006). Protein distribution of Kcnq1, Kcnh2, and Kcne3 potassium channel subunits during mouse embryonic development. *Anat Rec A Discov Mol Cell Evol Biol* **288**, 304-315.

de la Cruz M.V., Sánchez Gómez C., Arteaga M.M. and C.Argüello (1977). Experimental study of the development of the truncus and the conus in the chick embryo. *J Anat.* **123**, 661-686.

de la Pompa J.L. and Epstein, J. A. (2012). Coordinating tissue interactions: Notch signaling in cardiac development and disease. *Developmental Cell* **22**, 244-254.

de la Pompa J.L., Wakeham A., Correia K.M., Samper E., Brown S., Aguilera R.J., Nakano T., Honjo T., Mak T.W., Rossant J., et al. (1997). Conservation of the Notch signalling pathway in mammalian neurogenesis. *Development* **124**, 1139-1148.

de Vlaming A., Sauls K., Hajdu Z., Visconti R.P., Mehesz A.N., Levine R.A., Slaugenhaupt S.A., Hagège A., Chester A.H., Markwald R.R., et al. (2012). Atrioventricular valve development: new perspectives on an old theme. *Differentiation* **84**, 103-116.

del Monte G., Grego-Bessa J., González-Rajal A., Bolós V. and de la Pompa, J. L. (2007). Monitoring Notch1 activity in development: evidence for a feedback regulatory loop. *Developmental Dynamics* **236**, 2594-2614.

Doetschman T. and Azhar, M. (2012). Cardiac-specific inducible and conditional gene targeting in mice. *Circulation Research* **110**, 1498-1512.

Domínguez J.N., Meilhac S.M., Bland Y.S., Buckingham M.E. and Brown, N. A. (2012). Asymmetric fate of the posterior part of the Second Heart Field results in unexpected left/right contributions to both poles of the heart. *Circulation Research* **26**, 1323-1335.

Eisenberg L.M. and Markwald, R. R. (1995). Molecular regulation of atrioventricular valvuloseptal morphogenesis. *Circulation Research* **77**, 1-6.

Fahed A.C., Gelb B.D., Seidman J.G. and Seidman, C. E. (2013). Genetics of congenital heart disease: the glass half empty. *Circulation Research* **112**, 707-720.

Fischer A., Steidl C., Wagner T.U., Lang E., Jakob P.M., Friedl P., Knobeloch K.P. and Gessler, M. (2007). Combined loss of Hey1 and HeyL causes congenital heart defects because of impaired epithelial to mesenchymal transition. *Circulation Research* **100**, 856-863.

Flores-Alcantar A., Gonzalez-Sandoval A., Escalante-Alcalde D. and Lomelí, H. (2011). Dynamics of

expression of ARID1A and ARID1B subunits in mouse embryos and in cells during the cell cycle. *Cell Tissue Res* **345**, 137-148.

Franco D., Kelly R., Moorman A.F., Lamers W.H., Buckingham M. and Brown, N. A. (2001). MLC3F transgene expression in iv mutant mice reveals the importance of left-right signalling pathways for the acquisition of left and right atrial but not ventricular compartment identity. *Developmental Dynamics* **221**, 206-215.

Galvin K.M., Donovan M.J., Lynch C.A., Meyer R.I., Paul R.J., Lorenz J.N., Fairchild-Huntress V., Dixon K.L., Dunmore J.H., Gimbrone M.A. Jr., et al. (2000). A role for smad6 in development and homeostasis of the cardiovascular system. *Nature Genetics* **24**, 171-174.

Garritano S., Inga A., Gemignani F. and Landi, S. (2013). More targets, more pathways and more clues for mutant p53. *Oncogenesis* **2**, 1-7.

Ghatak S., Misra S., Norris R.A., Rodriquez R.M., Hoffman S., Levine R.A., Hascall V.C. and Markwald, R. R. (2014). Periostin induces intracellular cross talk between kinases and hyaluronan in atrioventricular valvulogenesis. *Journal of Biological Chemistry*.

Goddeeris M.M., Schwartz R., Klingensmith J. and Meyers, E. N. (2007). Independent requirements for Hedgehog signaling by both the anterior heart field and neural crest cells for outflow tract development. *Development* **134**, 1593-1604.

Grego-Bessa J., Luna-Zurita L., del Monte G., Bolós V., Melgar P., Arandilla A., Garratt A.N., Zang H., Mukouyama Y.S., Chen H., et al. (2007). Notch signaling is essential for ventricular chamber development. *Developmental Cell* **12**, 415-429.

Gregory S.L., Kortschak R.D., Kalionis B. and Saint, R. (1996). Characterization of the dead ringer gene identifies a novel, highly conserved family of sequence-specific DNA-binding proteins. *Molecular and Cell Biology* **16**, 792-799.

Habets P.E.M.H., Moorman A.F.M., Clout D.E.W., van Roon M.A., Lingbeek M., van Lohuizen M., Campione M. and Christoffels, V. M. (2002). Cooperative action of Tbx2 and Nkx2.5 inhibits ANF expression in the atrioventricular canal: implications for cardiac chamber formation. *Genes&Development* **16**, 1234-1246.

Häder T., Wainwright D., Shandala T., Saint R., Taubert H., Brönner G. and Jäckle, H. (2000). Receptor tyrosine kinase signaling regulates different modes of Groucho-dependent control of Dorsal. *Current Biology* **10**, 51-54.

Hamburger V. and Hamilton, H. L. (1951). A series of normal stages in the development of the chick embryo. *J Morphology* **88**, 49-92.

Hansen F.T., Madsen C.K., Nordland A.M., Grasser M., Merkle T. and Grasser, K. D. (2008). A novel family of plant DNA-binding proteins containing both HMG-box and AT-rich interaction domains. *Biochemistry* **47**, 13207-13214.

Hata K., Takashima R., Amano K., Ono K., Nakanishi M., Yoshida M., Wakabayashi M., Matsuda A., Maeda Y., Suzuki Y., et al. (2013). Arid5b facilitates chondrogenesis by recruiting the histone demethylase Phf2 to Sox9-regulated genes. *Nature Communication* **4**, 2850.

Hayashi S., Lewis P., Pevny L. and McMahon, A. P. (2002). Efficient gene modulation in mouse epiblast using a Sox2Cre transgenic mouse strain. *Mechanism of Development* **119**.

Healy J., Richer C., Bourgey M., Kritikou E.A. and Sinnett, D. (2010). Replication analysis confirms the association of ARID5B with childhood B-cell acute lymphoblastic leukemia. *Haematologica* **95**, 1608-1611.

Herbert S.P. and Stainier, D. Y. R. (2011). Molecular control of endothelial cell behaviour during blood vessel morphogenesis. *Nature reviews Molecular Cell Biology* **12**, 551-564.

Herrscher R.F., Kaplan M.H., Lelsz D.L., Das C., Scheuermann R. and Tucker, P. W. (1995). The immunoglobulin heavy-chain matrix-associating regions are bound by Bright: a B cell-specific trans-activator that describes a new DNA-binding protein family. *Genes&Development* **9**, 3067-3082.

High F.A, Jain R., Stoller J.Z., Antonucci N.B., Lu M.M., Loomes K.M., Kaestner K.H., Pear W.S. and Epstein, J. A. (2009). Murine Jagged1/Notch signaling in the second heart field orchestrates Fgf8 expression and tissue-tissue interactions during outflow tract development. *The Journal of Clinical Investigation* **119**, 1986-1996.

Hiroi Y., Kudoh S., Monzen K., Ikeda Y., Yazaki Y., Nagai R. and Komuro, I. (2001). Tbx5 associates with Nkx2-5 and synergistically promotes cardiomyocyte differentiation. *Nature Genetics* **28**, 276-280.

Hoffmann A.D., Peterson M.A., Friedland-Little J.M., Anderson S.A. and Moskowitz, I. P. (2009). Sonic hedgehog is required in pulmonary endoderm for atrial septation. *Development* **136**, 1761-1770.

Honma S., Kawamoto T., Takagi Y., Fujimoto K., Sato F., Noshiro M., Kato Y. and Honma, K. (2002). Dec1 and Dec2 are regulators of the mammalian molecular clock. *Nature* **419**, 841-844.

Hoogaars W.M., Tessari A., Moorman A.F., de Boer P.A., Hagoort J., Soufan A.T., Campione M. and Christoffels, V. M. (2004). The transcriptional repressor Tbx3 delineates the developing central conduction system of the heart. *Cardiovascular Research* **62**, 489-499.

Hoogaars W.M.H., Engel A., Brons J.F., Verkerk A.O., Lange F. de, Wong L.Y.E., Bakker M.L., Clout D.E., Wakker V., Barnett P., et al. (2007). Tbx3 controls the sinoatrial node gene program and imposes pacemaker function on the atria. *Genes&Development* **21**, 1098-1112.

Hutson M.R., Zhang P., Stadt H.A., Sato A.K., Li Y.X., Burch J., Creazzo T.L. and Kirby, M. L. (2006). Cardiac arterial pole alignment is sensitive to FGF8 signaling in the pharynx. *Developmental Biology* **295**, 486-497.

Ilagan R., Abu-Issa R., Brown D., Yang Y.-P., Jiao K., Schwartz R.K., Klingensmith J. and Meyers, E. N. (2006). Fgf8 is required for anterior heart field development. *Development* **133**, 2435-2445.

Iwahara J. and Clubb, R. T. (1999). Solution structure of the DNA binding domain from Dead ringer, a sequence-specific AT-rich interaction domain (ARID). *EMBO J* **18**, 6084-6094.

Iwahara J., Iwahara M., Daughdrill G.W., Ford J. and Clubb, R. T. (2002). The structure of the Dead ringer-DNA complex reveals how AT-rich interaction domains (ARIDs) recognize DNA. *EMBO J* **21**, 1197-1209.

Iwase S., Lan F., Bayliss P., de la Torre-Ubieta L., Huarte M., Qi H.H., Whetstine J.R., Bonni A., Roberts T.M. and Shi, Y. (2007). The X-linked mental retardation gene SMCX/JARID1C defines a family of histone H3 lysine 4 demethylases. *Cell* **128**, 1077-1088.

Jensen L.R., Amende M., Gurok U., Moser B., Gimmel V., Tzschach A., Janecke A.R., Tariverdian G., Chelly J., Fryns J.P., et al. (2005). Mutations in the JARID1C gene, which is involved in transcriptional regulation and chromatin remodeling, cause X-linked mental retardation. *Am J Hum Genet* **76**, 227-236.

Jia Q., McDill B.W., Li S.Z., Deng C., C. C. P. and Chen, F. (2007). Smad signaling in the neural crest regulates cardiac outflow tract remodeling through cell autonomous and non-cell autonomous effects. *Developmental Biology* **311**, 172-184.

Joseph S., Deneke V.E. and Dahl, K. D. C. (2012). ARID3B induces tumor necrosis factor alpha mediated apoptosis while a novel ARID3B splice form does not induce cell death. *PLos One* **7**, 1-16.

Jostarndt K., Puntschart A., Hoppeler H. and Billeter, R. (1994). The use of 33P-labelled riboprobes for in situ hybridizations: localization of myosin alkali light-chain mRNAs in adult human skeletal muscle. *Histochem J.* **26**, 32-40.

Kamakura S., Nomura M., Hayase J., Iwakiri Y., Nishikimi A., Takayanagi R., Fukui Y. and Sumimoto, H. (2013). The cell polarity protein mInsc regulates neutrophil chemotaxis via a noncanonical G protein signaling pathway. *Developmental Cell* **26**, 292-302.

Kanzler B., Kuschert S.J., Liu Y.H. and Mallo, M. (1998). Hoxa-2 restricts the chondrogenic domain and inhibits bone formation during development of the branchial area. *Development* **125**, 2587-2597.

Kaplan M.H., Zong R.T., Herrscher R.F., Scheuermann R.H. and Tucker, P. W. (2001). Transcriptional

activation by a matrix associating region-binding protein. contextual requirements for the function of bright. *Journal of Biological Chemistry* **276**, 21325-21330.

Kelly R.G., Brown N.A. and Buckingham, M. E. (2001). The arterial pole of the mouse heart forms from Fgf10-expressing cells in pharyngeal mesoderm. *Developmental Cell* **1**, 435-440.

Kelly, R. G. (2012). The Second Heart Field. *Current Topics in Developmental Biology* **100**.

Kim D., Probst L., Das Ch. and Tucker, P. W. (2007). REKLES is an ARID3-restricted multifunctional domain. *The Journal of Biological Chemistry* **282**, 15768–15777.

Kim D. and Tucker, P. W. (2006). A regulated nucleocytoplasmic shuttle contributes to Bright's function as a transcriptional activator of immunoglobulin genes. *Molecular and Cell Biology* **26**, 2187-2201.

Kim R.Y., Robertson E.J. and Solloway, M. J. (2001). Bmp6 and Bmp7 are required for cushion formation and septation in the developing mouse heart. *Developmental Biology* **235**, 449-466.

Kim T.G., Chen J., Sadoshima J. and Lee, Y. (2004). Jumonji represses atrial natriuretic factor gene expression by inhibiting transcriptional activities of cardiac transcription factors. *Molecular and Cell Biology* **24**, 10151-10160.

Kisanuki Y.Y., Hammer R.E., Miyazaki J., Williams S.C., Richardson J.A. and Yanagisawa, M. (2001). Tie2-Cre transgenic mice: a new model for endothelial cell-lineage analysis in vivo. *Developmental Biology* **230**, 230-242.

Kitajima S., Takagi A., Inoue T. and Saga, Y. (2000). MesP1 and MesP2 are essential for the development of cardiac mesoderm. *Development* **127**, 3215-3226.

Kobayashi K., Era T., Takebe A., Jakt L.M. and Nishikawa, S. (2006). ARID3B induces malignant transformation of mouse embryonic fibroblasts and is strongly associated with malignant neuroblastoma. *Cancer Res* **66**, 8331-8336.

Kobayashi K., Jakt L.M. and Nishikawa, S. I. (2013). Epigenetic regulation of the neuroblastoma genes, Arid3b and Mycn. *Oncogene* **32**, 2640-2648.

Kokubo H., Tomita-Miyagawa S., Hamada Y. and Saga, Y. (2007). Hesr1 and Hesr2 regulate atrioventricular boundary formation in the developing heart through the repression of Tbx2. *Development* **134**, 747-755.

Kortschak R.D., Tucker P.W. and Saint, R. (2000). ARID proteins come in from the desert. *Trends Biochem Sci* **25**, 294-299.

Kovalevich J., Tracy B. and Langford, D. (2011). PINCH: more than just an adaptor protein in cellular response. *J Cell Physiol* **226**, 940-947.

Krohn K.A., Link J.M. and Mason, R. P. (2008). Molecular imaging of hypoxia. *J Nucl Med.* **49**, 129S-148S.

Kruithof B.P., Krawitz S.A. and Gaussin, V. (2007). Atrioventricular valve development during late embryonic and postnatal stages involves condensation and extracellular matrix remodeling. *Developmental Biology* **302**, 208-217.

Kwon C., Qian L., Cheng P., Nigam V., Arnold J. and Srivastava, D. (2009). A regulatory pathway involving Notch1/beta-catenin/Isl1 determines cardiac progenitor cell fate. *Nature Cell Biology* **11**, 951-957.

Kwon Ch., Qian L., Cheng P., Nigam V., Arnold J. and Srivastava, D. (2009). A regulatory pathway involving Notch1/beta-catenin/Isl1 determines cardiac progenitor cell fate. *Nature Cell Biology* **11**, 951-957.

Lahoud M.H., Ristevski S., Venter D.J., Jermiin L.S., Bertoncello I., Zavarsek S., Hasthorpe S., Drago J., Kretser D. de, Hertzog P.J., et al. (2001). Gene targeting of Desrt, a novel ARID class DNA-binding protein, causes growth retardation and abnormal development of reproductive organs. *Genome Research* **11**, 1327-1334.

Lai A., Kennedy B.K., Barbie D.A., Bertos N.R., Yang X.J., Theberge M.C., Tsai S.C., Seto E., Zhang Y., Kuzmichev A., et al. (2001). RBP1 recruits the mSIN3-histone deacetylase complex to the pocket of retinoblastoma tumor suppressor family proteins found in limited discrete regions of the

nucleus at growth arrest. *Molecular and Cellular Biology* **21**, 2918-2932.

Lai A., Lee J.M., Yang W.M., Decaprio J.A., Kaelin W.G.Jr., Seto E. and Branton, P. E. (1999). RBP1 recruits both histone deacetylase-dependent and -independent repression activities to retinoblastoma family proteins. *Molecular and Cellular Biology* **19**, 6632-6641.

Landeira D., Sauer S., Poot R., Dvorkina M., Mazzarella L., Jørgensen H.F., Pereira C.F., Leleu M., Piccolo F.M., Spivakov M., et al. (2010). Jarid2 is a PRC2 component in embryonic stem cells required for multi-lineage differentiation and recruitment of PRC1 and RNA Polymerase II to developmental regulators. *Nature Cell Biology* **12**, 618-625.

Lee Y., Song A.J., Baker R., Micales B., Conway S.J. and Lyons, G. E. (2000). Jumonji, a nuclear protein that is necessary for normal heart development. *Circulation Research* **86**, 932-938.

Lee Y.M., Jeong C.H., Koo S.Y., Son M.J., Song H.S., Bae S.K., Raleigh J.A., Chung H.Y., Yoo M.A. and Kim, K. W. (2001). Determination of hypoxic region by hypoxia marker in developing mouse embryos in vivo: a possible signal for vessel development. *Developmental Dynamics* **220**, 175-186.

Legate K.R., Montañez E., Kudlacek O. and Fässler, R. (2006). ILK, PINCH and parvin: the tIPP of integrin signalling. *Nature Molecular Cell Biology* **7**, 20-31.

Li G., Margueron R., Ku M., Chambon P., Bernstein B.E. and Reinberg, D. (2010). Jarid2 and PRC2, partners in regulating gene expression. *Genes&Development* **24**, 368-380.

Li J., Stouffs M., Serrander L., Banfi B., Bettiol E., Charnay Y., Steger K., Krause K.H. and Jaconi, M. E. (2006). The NADPH oxidase NOX4 drives cardiac differentiation: Role in regulating cardiac transcription factors and MAP kinase activation. *Mol Biol Cell* **17**, 3978-3988.

Liang X., Sun Y., Ye M., Scimia M.C., Cheng H., Martin J., Wang G., Rearden A., Wu C., Peterson K.L., et al. (2009). Targeted ablation of PINCH1 and PINCH2 from murine myocardium results in dilated cardiomyopathy and early postnatal lethality. *Circulation* **120**, 568-576.

Lin C.J., Lin C.Y., Chen C.H., B., Z. and Chang, C. P. (2012). Partitioning the heart: mechanisms of cardiac septation and valve development. *Development* **139**, 3277-3299.

Lindsley R.C., Gill J.G., Murphy T.L., Langer E.M., Cai M., Mashayekhi M., Wang W., Niwa N., Nerbonne J.M., Kyba M., et al. (2008). Mesp1 coordinately regulates cardiovascular fate restriction and epithelialmesenchymal transition in differentiating ESCs. . *Cell Stem Cell* **3**, 55-68.

Liu W., Selever J., Wang D., Lu M.F., Moses K.A., R.J., S. and Martin, J. F. (2004). Bmp4 signaling is required for outflow-tract septation and branchial-arch artery remodeling. *PNAS* **101**, 4489-4494.

Lockman K., Taylor J.M. and Mack, C. P. (2007). The histone demethylase, Jmjd1a, interacts with the myocardin factors to regulate SMC differentiation marker gene expression. *Circulation Research* **101**, 115-123.

Luna-Zurita L., Prados B., Grego-Bessa J., Luxán G., del Monte G., Benguría A., Adams R.H., Pérez-Pomares J.M. and de la Pompa, J. L. (2010). Integration of a Notch-dependent mesenchymal gene program and Bmp2-driven cell invasiveness regulates murine cardiac valve formation. *Journal of Clinical Investigation* **120**, 3493-3507.

Ma L., Lu M.F., Schwartz R.J. and Martin, J. F. (2005). Bmp2 is essential for cardiac cushion epithelial-mesenchymal transition and myocardial patterning. *Development* **135**, 5601–5611.

Ma Q., Zhou B. and Pu, W. T. (2008). Reassessment of Isl1 and Nkx2-5 cardiac fate maps using a Gata4-based reporter of Cre activity. *Developmental Biology* **323**, 98-104.

Madsen B., Spencer-Dene B., Poulsom R., Hall D., Lu P.J., Scott K., Shaw A.T., Burchell J.M., Freemont P. and Taylor-Papadimitriou, J. (2002). Characterisation and developmental expression of mouse Plu-1, a homologue of a human nuclear protein (PLU-1) which is specifically up-regulated in breast cancer. *Mechanism of Development* **119**, 239-246.

Majmundar A.J., Wong W.J. and Simon, M. C. (2010). Hypoxia-inducible factors and the response to hypoxic stress. *Molecular Cell* **40**, 294-309.

McCulley D.J., Kang J.O., Martin J.F. and Black, B. L. (2008). BMP4 is required in the anterior heart field and its derivatives for endocardial cushion remodeling, outflow tract septation, and semilunar

valve development. *Developmental Dynamics* **237**, 3200-3209.

Meilhac S.M., Esner M., Kelly R.G., Nicolas J.-F. and Buckingham, M. E. (2004). The clonal origin of myocardial cells in different regions of the embryonic mouse heart. *Developmental Cell* **6**, 685-698.

Mesbah K., Harrelson Z., Théveniau-Ruissy M., Papaioannou V.E. and Kelly, R. G. (2008). Tbx3 is required for outflow tract development. *Circulation Research* **103**, 743-750.

Miyazaki K., Kawamoto T., Tanimoto K., Nishiyama M., Honda H. and Kato, Y. (2002). Identification of functional hypoxia response elements in the promoter region of the DEC1 and DEC2 genes. *Journal of Biological Chemistry* **277**, 47014-47021.

Mjaatvedt C.H., Nakaoka T., Moreno-Rodriguez R., Norris R.A., Kern M.J., Eisenberg C.A., Turner D. and Markwald, R. R. (2001). The outflow tract of the heart is recruited from a novel heart-forming field. *Developmental Biology* **238**, 97-109.

Momose T., Tonegawa A., Takeuchi J., Ogawa H., Umesono K. and Yasuda, K. (1999). Efficient targeting of gene expression in chick embryos by microelectroporation. *Dev Growth Differ* **41**, 335-344.

Montagutelli, X. (2000). Effect of the genetic background on the phenotype of mouse mutations. *J Am Soc Nephrol.* **11**, S101-105.

Moorman A., Webb S., Brown N.A., Lamers W. and Anderson, R. H. (2003). Develoment of the heart: (1) Formation of the cardiac chambers and the arterial trunks. *Heart* **89**, 806–814.

Moorman A.F.M., Christoffels V.M., Anderson R.H. and van den Hoff, M. J. B. (2007). The heart-forming fields: one or multiple? *Phil. Trans. R. Soc. B* **362**, 1257-1265.

Moretti A., Caron L., Nakano A., Lam J.T., Bernshausen A., Chen Y., Qyang Y., Bu L., Sasaki M., Martin-Puig S., et al. (2006). Multipotent embryonic Isl1+ progenitor cells lead to cardiac, smooth muscle, and endothelial cell diversification. *Cell* **126**, 1151–1165.

Mysliwiec M.R., Bresnick E.H. and Lee, Y. (2001). Endothelial Jarid2/Jumonji is required for normal cardiac development and proper Notch1 expression. *Journal of Biological Chemistry* **286**, 17193-17204.

Nagl N.G.Jr., Wang X., Patsialou A., Van Scoy M. and Moran, E. (2007). Distinct mammalian SWI/SNF chromatin remodeling complexes with opposing roles in cell-cycle control. *EMBO J* **26**, 752-763.

Nijmeijer R.M., Leeuwis J.W., DeLisio A., Mummery C.L. and ChuvadeSousaLopes, S. M. (2009). Visceral endoderm induces specification of cardiomyocytes in mice. *Stem Cells Research* **3**, 170-178.

Nixon J.C., Rajaiya J.B., Ayers N., Evetts S. and Webb, C. F. (2004). The transcription factor, Bright, is not expressed in all human B lymphocyte subpopulations. *Cell Immunology* **228**, 42-53.

Norris R.A., Potts J.D., Yost M.J., Junor L., Brooks T., Tan H., Hoffman S., Hart M.M., Kern M.J., Damon B., et al. (2009). Periostin promotes a fibroblastic lineage pathway in atrioventricular valve progenitor cells. *Developmental Dynamics* **238**, 1052-1063.

Norris R.A., M.-R. R. A., Sugi Y., Hoffman S., Amos J., Hart M.M., Potts J.D., Goodwin R.L. and Markwald R.R. (2008). Periostin regulates atrioventricular valve maturation. *Developmental Biology* **316**, 200-213.

Numata S., Claudio P.P., Dean C., Giordano A. and Croce, C. M. (1999). Bdp, a new member of a family of DNA-binding proteins, associates with the retinoblastoma gene product. *Cancer Res* **59**, 3741-3747.

Palmer D.J. and Ng, P. (2008). Methods for the production of first generation adenoviral vectors. *Methods Mol Biol* **433**, 55-78.

Pardo M., Lang B., Yu L., Prosser H., Bradley A., Babu M.M. and Choudhary, J. (2010). An expanded Oct4 interaction network: implications for stem cell biology, development, and disease. *Cell Stem Cell* **6**, 382–395.

Park E.J., Ogden L.A., Talbot A., Evans S., Cai C.L., Black B.L., Frank D.U. and Moon, A. M. (2006).

Required, tissue-specific roles for Fgf8 in outflow tract formation and remodeling. *Development* **133**, 2419-2433.

Parker S.E., Mai C.T., Canfield M.A., Rickard R., Wang Y., Meyer R.E., Anderson P., Mason C.A., Collins J.S., Kirby R.S., et al. (2010). Updated National Birth Prevalence estimates for selected birth defects in the United States, 2004-2006. *Birth Defects Res A Clin Mol Teratol* **12**, 1008-1016.

Pasini D., Cloos P.A.C., Walfridsson J., Olsson L., Bukowski J.P., Johansen J.V., Bak M., Tommerup N., Rappsilber J. and Helin, K. (2010). JARID2 regulates binding of the Polycomb repressive complex 2 to target genes in ES cells. *Nature* **464**, 306-311.

Patsialou A., Wilsker D. and Moran, E. (2005). DNA-binding properties of ARID family proteins. *Nucleic Acids Research* **33**, 66-80.

Peng J.C., Valouev A., Swigut T., Zhang J., Zhao Y., Sidow A. and Wysocka, J. (2009). Jarid2/Jumonji coordinates control of PRC2 enzymatic activity and target gene occupancy in pluripotent cells. *Cell* **139**, 1290-1302.

Popowski M., Templeton T.D., Lee B.K., Rhee C., Li H., Miner C., Dekker J.D., Orlanski S., Bergman Y., Iyer V.R., et al. (2014). Bright/Arid3A acts as a barrier to somatic cell reprogramming through direct regulation of Oct4, Sox2, and Nanog. *Stem Cell Reports* **2**, 26-35.

Prall O.W.J., Menon M.K., Solloway M.J., Watanabe Y., Zaffran S., Bajolle F., Biben Ch., McBride J.J., Robertson B.R., Chaulet H., et al. (2007). An Nkx2-5/Bmp2/Smad1 negative feedback loop controls heart progenitor specification and proliferation. *Cell* **128**, 947-959.

Price M.G., Landsverk M.L., Barral J.M. and Epstein, H. F. (2002). Two mammalian UNC-45 isoforms are related to distinct cytoskeletal and muscle-specific functions. *J Cell Science* **115**, 4013-4023.

Qyang Y., Martin-Puig S., Chiravuri M., Chen S., Xu H., Bu L., Jiang X., Lin L., Granger A., Moretti A., et al. (2007). The renewal and differentiation of Isl1+ cardiovascular progenitors are controlled by a Wnt/b-catenin pathway. *Cell Stem Cell* **1**, 165-179.

Rivera-Feliciano J., Lee K.H., Kong S.W., Rajagopal S., Ma Q., Springer Z., Izumo S., Tabin C.J. and Pu, W. T. (2006). Development of heart valves requires Gata4 expression in endothelial-derived cells. *Development* **133**, 3607-3618.

Rucker E.B., Dierisseau P., Wagner K.U., Garrett L., Wynshaw-Boris A., Flaws J.A. and Hennighausen, L. (2000). Bcl-x and Bax regulate mouse primordial germ cell survival and apoptosis during embryogenesis. *Mol Endocrinol* **14**, 1038-1052.

Ryckebusch L., Wang Z., Bertrand N., Lin S.C., Chi X., Schwartz R., Zaffran S. and Niederreither, K. (2008). Retinoic acid deficiency alters second heart field formation. *PNAS* **105**, 2913-2918.

Saga Y., Kitajima S. and Miyagawa-Tomita, S. (2000a). Mesp1 expression is the earliest sign of cardiovascular development. *Trends Cardiovasc Med* **10**, 345-352.

Saga Y., Miyagawa-Tomita, Tagaki A., S. Kitajima S., Miyazaki J. and Inoue T. (2000b). MesP1 is expressed in the heart precursor cells and required for the formation of a single heart tube. *Trends Cardiovasc Med* **10**, 345-352.

Saga Y., Miyagawa-Tomita S., Takagi A., Kitajima S., Miyazaki J. and Inoue, T. (1999). MesP1 is expressed in the heart precursor cells and required for the formation of a single heart tube. *Development* **126**, 3437–3447.

Sakabe M., Kokubo H., Nakajima Y. and Saga, Y. (2012). Ectopic retinoic acid signaling affects outflow tract cushion development through suppression of the myocardial Tbx2-Tgfβ2 pathway. *Development* **139**, 385-395.

Satin J., Fujii S. and DeHaan, R. L. (1988). Development of cardiac beat rate in early chick embryos is regulated by regional cues. *Developmental Biology* **129**, 103-113.

Schaft J., Ashery-Padan R., van der Hoeven, F., Gruss P. and Stewart, A. F. (2001). Efficient FLP recombination in mouse ES cells and oocytes. *Genesis* **31**, 6-10.

Shandala T., Kortschak R.D., Gregory S. and Saint, R. (1999). The Drosophila dead ringer gene is required for early embryonic patterning through regulation of argos and buttonhead expression.

Development **126**, 4341-4349.

Shandala T., Kortschak R.D. and Saint, R. (2002). The Drosophila retained/dead ringer gene and ARID gene family function during development. *Int. J. Dev. Biol* **46**, 423-430.

Shandala T., Takizawa K. and Saint, R. (2003). The dead ringer/retained transcriptional regulatory gene is required for positioning of the longitudinal glia in the Drosophila embryonic CNS. *Development* **130**, 1505-1513.

Sharov A.A., Masui S., Sharova L.V., Piao Y., Aiba K., Matoba R., Xin L., Niwa H. and Ko, M. S. H. (2008). Identification of Pou5f1, Sox2, and Nanog downstream target genes with statistical confidence by applying a novel algorithm to time course microarray and genome-wide chromatin immunoprecipitation data. . *BMC Genomics* **9**, 1-19.

Shelton E.L. and Yutzey, K. E. (2007). Tbx20 regulation of endocardial cushion cell proliferation and extracellular matrix gene expression. *Developmental Biology* **302**, 376-388.

Shelton E.L. and Yutzey, K. E. (2008). Twist1 function in endocardial cushion cell proliferation, migration, and differentiation during heart valve development. *Developmental Biology* **317**, 282-295.

Shen M., Yoshida E., Yan W., Kawamoto T., Suardita K., Koyano Y., Fujimoto K., Noshiro M. and Kato, Y. (2002). Basic helix-loop-helix protein DEC1 promotes chondrocyte differentiation at the early and terminal stages. *Journal of Biological Chemistry* **277**, 50112-50120.

Shirai M., Imanaka-Yoshida K., Schneider M.D., Schwartz R.J. and Morisakie, T. (2009). T-box 2, a mediator of Bmp-Smad signaling, induced hyaluronan synthase 2 and Tgf2 expression and endocardial cushion formation. *PNAS* **106**, 18604-18609.

Singh M.K., Christoffels V.M., Dias J.M., Trowe M.O., Petry M., Schuster-Gossler K., Bürger A., Ericson J. and Kispert, A. (2005). Tbx20 is essential for cardiac chamber differentiation and repression of Tbx2. *Development* **132**, 2697-2707.

Singh R., Hoogaars W.M., Barnett P., Grieskamp T., Rana M.S., Buermans H., Farin H.F., Petry M., Heallen T., Martin J.F., et al. (2012). Tbx2 and Tbx3 induce atrioventricular myocardial development and endocardial cushion formation. *Cellular and Molecular Life Sciences* **69**, 1377–1389.

Singh R., Horsthuis T., Farin H.F., Grieskamp T., Norden J., Petry M., Wakker V., Moorman A.F.M., Christoffels V.M. and Kispert, A. (2009). Tbx20 interacts with Smads to confine Tbx2 expression to the atrioventricular canal. *Circulation Research* **105**, 442-452.

Sinha T., Wang B., Evans S., Wynshaw-Boris A. and Wang, J. (2012). Disheveled mediated planar cell polarity signaling is required in the second heart field lineage for outflow tract morphogenesis. *Developmental Biology* **370**, 135-144.

Sirbu I.O., Zhao X. and Duester, G. (2008). Retinoic acid controls heart anteroposterior patterning by down-regulating Isl1 through the Fgf8 pathway. *Developmental Dynamics* **237**, 1627-1635.

Soufan A.T., van den Berg G., Ruijter J.M., de Boer P.A.J., van den Hoff M.J.B. and Moorman, A. F. M. (2006). Regionalized sequence of myocardial cell growth and proliferation characterizes early chamber formation. *Circulation Research* **99**, 545-552.

Stanley E.G., Biben C., Elefanty A., Barnett L., Koentgen F., Robb L. and Harvey, R. P. (2002). Efficient Cre-mediated deletion in cardiac progenitor cells conferred by a 3'UTR-ires-Cre allele of the homeobox gene Nkx2-5. *Int. J. Dev. Biol* **46**, 431-439.

Strange, R. E. (1966). Stability of beta-galactosidase in starved Escherichia coli. *Nature* **209**, 428-429.

Sugi Y., Yamamura H., Okagawa H. and Markwald, R. R. (2004). Bone morphogenetic protein-2 can mediate myocardial regulation of atrioventricular cushion mesenchymal cell formation in mice. *Developmental Biology* **269**, 505-518.

Sun H., Li L., Vercherat C., Gulbagci N.T., Acharjee S., Li J., Chung T.K., Thin T.H. and Taneja, R. (2007). Stra13 regulates satellite cell activation by antagonizing Notch signaling. *J Cell Biology* **177**, 647-657.

Sun H. and Taneja, R. (2000). Stra13 expression is associated with growth arrest and represses transcription

through histone deacetylase (HDAC)-dependent and HDAC-independent mechanisms. *PNAS* **97**, 4058-4063.

Sun Y., Liang X., Najafi N., Cass M., Lin L., Cai C.L., Chen J. and Evans, S. M. (2007). Islet 1 is expressed in distinct cardiovascular lineages, including pacemaker and coronary vascular cells. *Developmental Biology* **304**, 286-296.

Takash W., Cañizares J., Bonneaud N., Poulat F., Mattéi M.G., Jay P. and Berta, P. (2001). SOX7 transcription factor: sequence, chromosomal localisation, expression, transactivation and interference with Wnt signalling. *Nucleic Acids Research* **29**, 4274-4283.

Takebe A., Era T., Okada M., Martin Jakt L., Kuroda Y. and Nishikawa, S. (2006). Microarray analysis of PDGFR alpha+ populations in ES cell differentiation culture identifies genes involved in differentiation of mesoderm and mesenchyme including ARID3b that is essential for development of embryonic mesenchymal cells. *Developmental Biology* **293**, 25-37.

Takeuchi J.K. and Bruneau, B. G. (2009). Directed transdifferentiation of mouse mesoderm to heart tissue by defined factors. *Nature* **459**, 708-712.

Takeuchi T., Watanabe Y., Takano-Shimizu T. and Kondo, S. (2006). Roles of jumonji and jumonji family genes in chromatin regulation and development. *Developmental Dynamics* **235**, 2449-2459.

Tanabe L.M., Martin C. and Dauer, W. T. (2012). Genetic background modulates the phenotype of a mouse model of DYT1 dystonia. *PLos One* **7**, 1-9.

Threadgill D.W., Dlugosz A.A., Hansen L.A., Tennenbaum T., Lichti U., Yee D., LaMantia C., Mourton T., Herrup K., Harris R.C., et al. (1995). Targeted disruption of mouse EGF receptor: effect of genetic background on mutant phenotype. *Science* **269**, 230-234.

Tian Y., Yuan L., Goss A.M., Wang T., Yang J., Lepore J.J., Zhou D., Schwartz R.J., Patel V., Cohen E.D., et al. (2010). Characterization and in vivo pharmacological rescue of a Wnt2-Gata6 pathway required for cardiac inflow tract development. *Developmental Cell* **18**, 275-287.

Tidwell J.A., Schmidt C., Heaton P., Wilson V. and Tucker, P. W. (2011). Characterization of a new ARID family transcription factor (Brightlike/ARID3C) that co-activates Bright/ARID3A-mediated immunoglobulin gene transcription. *Molecular Immunology* **49**, 260-272.

Timmerman L.A., Grego-Bessa J., Raya A., Bertrán E., Pérez-Pomares J.M., Díez J., Aranda S., Palomo S., McCormick F., Izpisúa-Belmonte J.C., et al. (2004). Notch promotes epithelial-mesenchymal transition during cardiac development and oncogenic transformation. *Genes&Development* **18**, 99-115.

Toyofuku T., Yoshida J., Sugimoto T., Yamamoto M., Makino N., Takamatsu H., Takegahara N., Suto F., Hori M., Fujisawa H., et al. (2008). Repulsive and attractive semaphorins cooperate to direct the navigation of cardiac neural crest cells. *Developmental Biology* **321**, 251-262.

Udan R.S., Vadakkan T.J. and Dickinson, M. E. (2013). Dynamic responses of endothelial cells to changes in blood flow during vascular remodeling of the mouse yolk sac. *Development* **140**, 4041-4050.

van den Berg D.L.C., Snoek T., Mullin N.P., Yates A., Bezstarosti K., Demmers J., Chambers I. and Poot, R. A. (2010). An Oct4-centered protein interaction network in embryonic stem cells. . *Cell Stem Cell* **6**, 369-381.

van den Berg G., Abu-Issa R., de Boer B.A., Hutson M.R., de Boer P.A.J., Soufan A.T., Ruijter J.M., Kirby M.L., van den Hoff M.J.B. and Moorman, A. F. M. (2009). A caudal proliferating growth center contributes to both poles of the forming heart tube. *Circulation Research* **104**, 179-188.

van den Berg G. and Moorman, A. F. M. (2009). Concepts of cardiac development in retrospect. *Pediatr Cardiol.*

Varona R., Cadenas V., Gómez L., Martínez-A. C. and Márquez, G. (2005). CCR6 regulates CD4+ T-cell-mediated acute graft-versus-host disease responses. *Blood* **106**, 18-26.

Vincent S.D. and Buckingham, M. E. (2010). How to make a heart: the origin and regulation of cardiac progenitor cells. *Curr Top Dev Biol* **90**, 1-41.

von Gise A. and Pu, W. T. (2012). Endocardial and epicardial epithelial to mesenchymal transitions in heart development and disease. *Circulation Research* **110**, 1628-1645.

Wagner M. and Siddiqui, M. A. Q. (2007). Signal transduction in early heart development (I): cardiogenic induction and heart tube formation. *Experimental Biology and Medicine* **232**, 852-865

Waldo K.L., Hutson M.R., Ward C.C., Zdanowicz M., Stadta H.A., Kumiskic D., Abu-Issa R. and Kirby, M. L. (2005). Secondary heart field contributes myocardium and smooth muscle to the arterial pole of the developing heart. *Developmental Biology* **281**, 78-90.

Waldo K.L., Kumiski D.H., Wallis K.T., Stadt H.A., Hutson M.R., Platt D.H. and Kirby, M. L. (2001). Conotruncal myocardium arises from a secondary heart field. *Development* **128**, 3179-3188.

Wallingford J.B., Fraser S.E. and Harland, R. M. (2002). Convergent extension: the molecular control of polarized cell movement during embryonic development. *Developmental Cell* **2**, 695-706.

Wang J., Greene S.B., Bonilla-Claudio M., Tao Y., Zhang J., Bai Y., Huang Z., Black B.L., Wang F. and Martin, J. F. (2010). Bmp signaling regulates myocardial differentiation from cardiac progenitors through a MicroRNA-mediated mechanism. *Developmental Cell* **19**, 903-912.

Wang J. and Orkin, S. H. (2008). A protein roadmap to pluripotency and faithful reprogramming. *Cells Tissues Organs* **188**, 23-30.

Wang J., Rao S., Chu J., Shen X., Levasseur D.N., Theunissen T.W. and Orkin, S. H. (2006). A protein interaction network for pluripotency of embryonic stem cells. *Nature* **444**, 364-368.

Wang Y., Wu B., Chamberlain A.A., Lui W., Koirala P., Susztak K., Klein D., Taylor V. and Zhou, B. (2013). Endocardial to myocardial notch-wnt-bmp axis regulates early heart valve development. *PLoS One* **8**, 1-8.

Watanabe M., Layne M.D., Hsieh C.M., Maemura K., Gray S., Lee M.E. and Jain, M. K. (2002). Regulation of smooth muscle cell differentiation by AT-rich interaction domain transcription factors Mrf2alpha and Mrf2beta. *Circulation Research* **91**, 382-389.

Webb C.F., Bryant J., Popowski M., Allred L., Kim D., Harriss J., Schmidt C., Miner C.A., Rose K., Cheng H.L., et al. (2011). The ARID family transcription factor bright is required for both hematopoietic stem cell and B lineage development. *Molecular and Cell Biology* **31**, 1041-1053.

Webb C.F., Yamashita Y., Ayers N., Evetts S., Paulin Y., Conley M.E. and Smith, E. A. (2000). The transcription factor Bright associates with Bruton's tyrosine kinase, the defective protein in immunodeficiency disease. *Journal of Immunology* **165**, 6956-6965.

Wilkinson D.G. and Nieto, M. A. (1993). Detection of messenger RNA by in situ hybridization to tissue sections and whole mounts. *Methods Enzymol* **225**.

Wilsker D., Patsialou A., Dallas P.B. and Moran, E. (2002). ARID proteins: a diverse family of DNA binding proteins implicated in the control of cell growth, differentiation, and development. *Cell Growth Differentiation* **13**, 95-106.

Winnier G.E., Kume T., Deng K., Rogers R., Bundy J., Raines C., Walter M.A., Hogan B.L. and Conway, S. J. (1999). Roles for the winged helix transcription factors MF1 and MFH1 in cardiovascular development revealed by nonallelic noncomplementation of null alleles. *Developmental Biology* **213**, 418-431.

Witte F., Dokas J., Neuendorf F., Mundlos S. and Stricker, S. (2009). Comprehensive expression analysis of all Wnt genes and their major secreted antagonists during mouse limb development and cartilage differentiation. *Gene Expression Patterns* **9**, 215-223.

Xu H., Cheng C., Devidas M., Pei D., Fan Y., Yang W., Neale G., Scheet P., Burchard E.G., Torgerson D.G., et al. (2012). ARID5B genetic polymorphisms contribute to racial disparities in the incidence and treatment outcome of childhood acute lymphoblastic leukemia. *Journal of Clinical Oncology* **30**, 751-757.

Xu X., Li C., Garrett-Beal L., Larson D., Wynshaw-Boris A. and Deng, C. X. (2001). Direct removal in the mouse of a floxed neo gene from a three-loxP conditional knockout allele by two novel approaches. *Genesis* **30**, 1-6.

Yan Z., Cui K., Murray D.M., Ling C., Xue Y., Gerstein A., Parsons R., Zhao K. and Wang, W. (2005). PBAF chromatin-remodeling complex requires a novel specificity subunit, BAF200, to regulate expression of selective interferon-responsive genes. *Genes&Development* **19**, 1662-1667.

Yang L., Cai C.L., Lin L., Qyang Y., Chung C., Monteiro R.M., Mummery C.L., Fishman G.I., Cogen A. and Evans, S. (2006). Isl1Cre reveals a common Bmp pathway in heart and limb development. *Development* **133**, 1575-1585.

Zaffran S., Kelly R.G., Meilhac S.M., Buckingham M.E. and Brown, N. A. (2004). Right ventricular myocardium derives from the Anterior Heart Field. *Circulation Research* **95**, 261-268.

Zhang J., Chang J.Y., Huang Y., Lin X., Luo Y., Schwartz R.J., Martin J.F. and Wang, F. (2010). The FGF-BMP signaling axis regulates outflow tract valve primordium formation by promoting cushion neural crest cell differentiation. *Circulation Research* **107**, 1209-1219.

Zhang Y., Chen K., Guo L. and Wu, C. (2002). Characterization of PINCH-2, a new focal adhesion protein that regulates the PINCH-1-ILK interaction, cell spreading, and migration. *Journal of Biological Chemistry* **277**, 38328-38338.

Zhang Z., Huynh T. and Baldini, A. (2006). Mesodermal expression of Tbx1 is necessary and sufficient for pharyngeal arch and cardiac outflow tract development. *Development* **133**, 3587-3595.

Zhou W., Lin L., Majumdar A., Li X., Zhang X., Liu W., Etheridge L., Shi Y., Martin J., Van de Ven W., et al. (2007). Modulation of morphogenesis by noncanonical Wnt signaling requires ATF/CREB family-mediated transcriptional activation of TGFbeta2. *Nature Genetics* **39**, 1225-1234.

Zhu H., Chen T., Zhu M., Fang Q., Kang H., Hong Z. and Zhang, Z. (2008). A novel ARID DNA-binding protein interacts with SymRK and is expressed during early nodule development in Lotus japonicus. *Plant Physiology* **148**, 337-347.

SUPPLEMENTARY MATERIAL

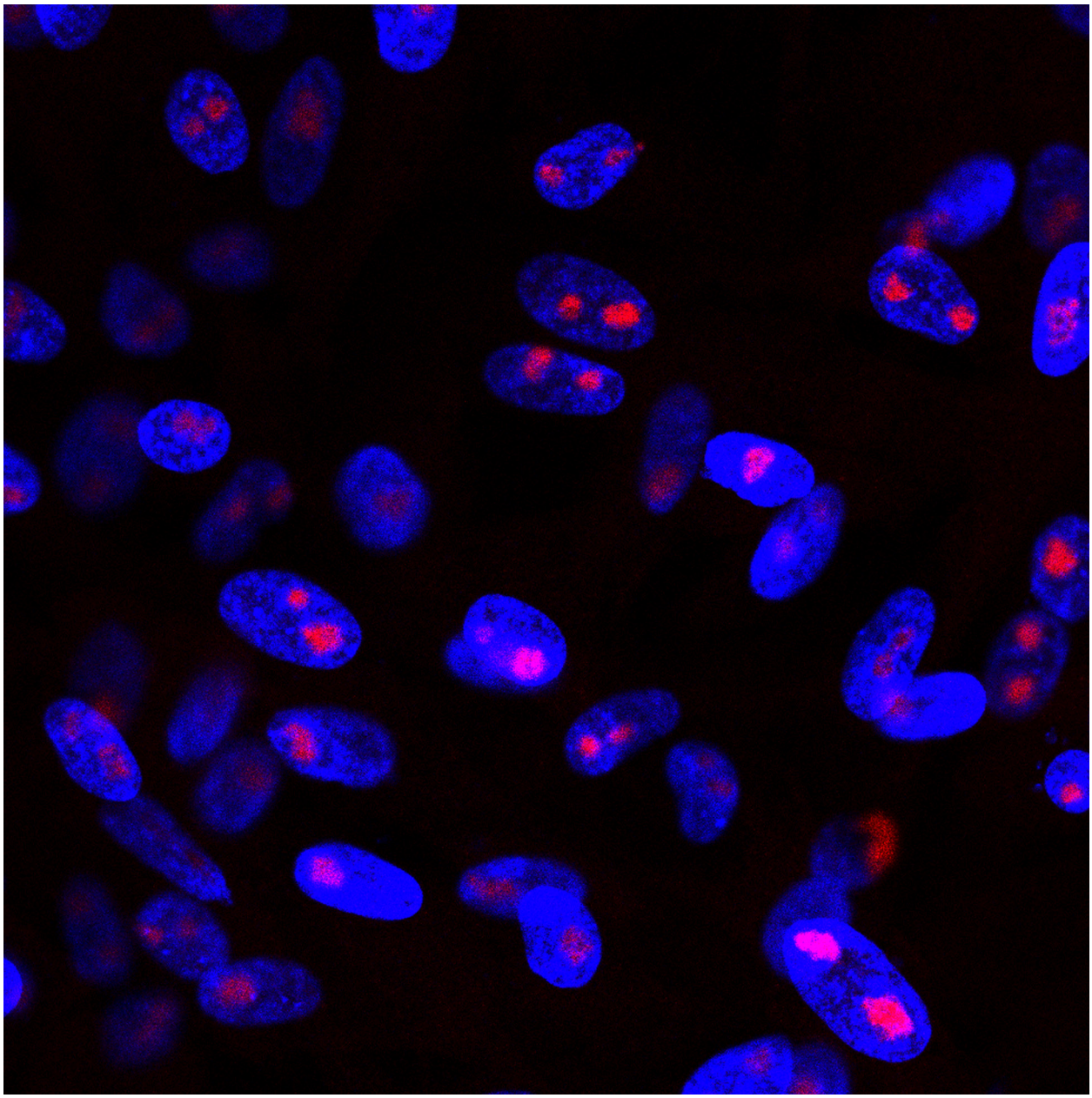

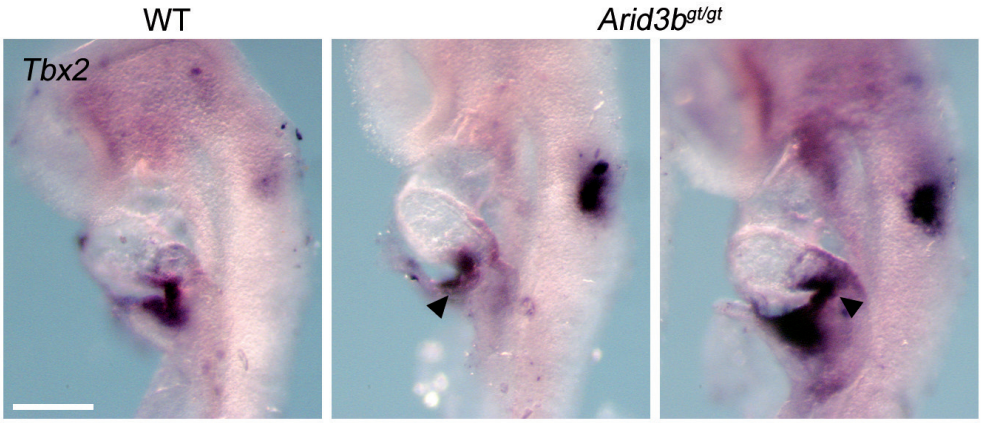

Supplementary figure 1. *Tbx2* expression is normal in the IFT at E8.5. *In situ* hybridisation against *Tbx2* shows similar expression in wild type and *Arid3b*$^{gt/gt}$ embryos in the heart IFT (arrowheads). Scale bar: 250 μm.

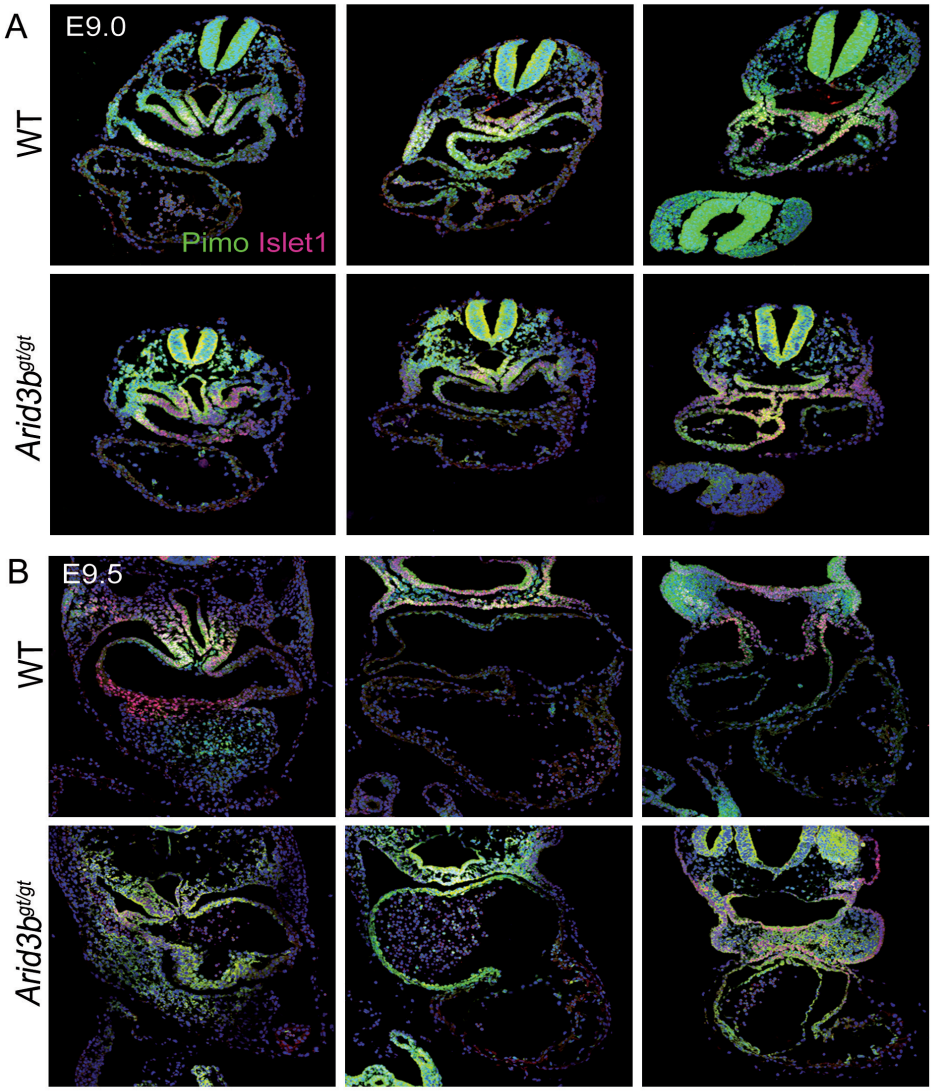

Supplementary figure 2. Immunostaining against pimonidazole (pimo, green), hypoxic marker and Islet1 (red) at E9.0 (**A**) and at E9.5 (**B**). Note the increase of hypoxic regions in *Arid3b*$^{gt/gt}$ embryos at E9.5.

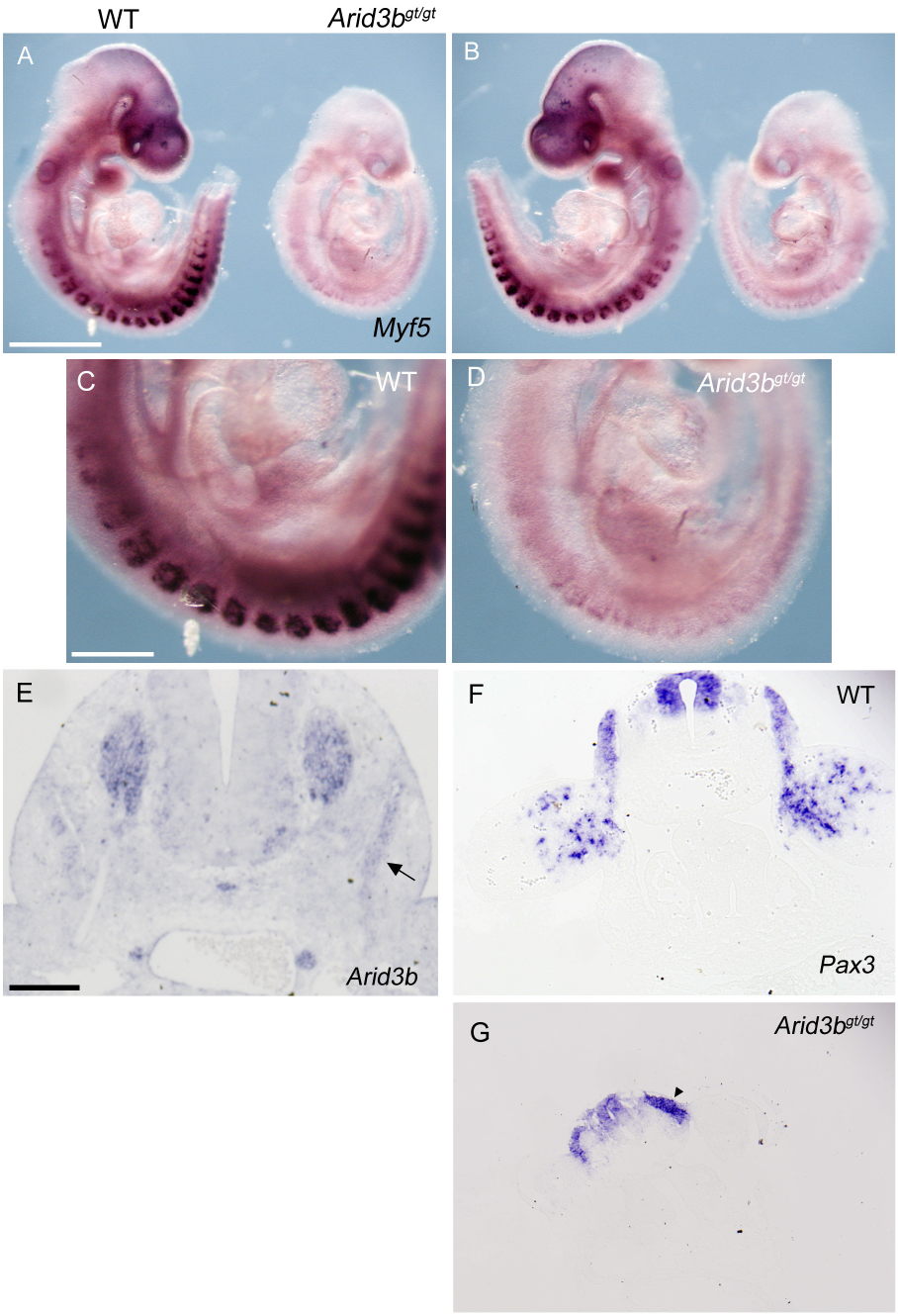

Supplementary figure 3. **A-D.** *In situ* hybridisation against *Myf5* in whole mount embryos. Note the reduction of the signal in the somites in *Arid3b*$^{gt/gt}$ embryos (compare **C to D**). **E.** *In situ* hybridisation on paraffin section of *Arid3b* on wild type embryo at E10.5; note the expression of the gene in the miotome (arrow). **F-G.** *In situ* hybridisation on paraffin section against Pax3 in wild type and *Arid3b*$^{gt/gt}$ embryos. Note that Pax3 positive cells in mutant embryos remain in the somite (arrowhead), while in the wild type situation these cells invade the limb. Scale bars: A,B 1 mm; C,D 400 μm; E 150 μm.

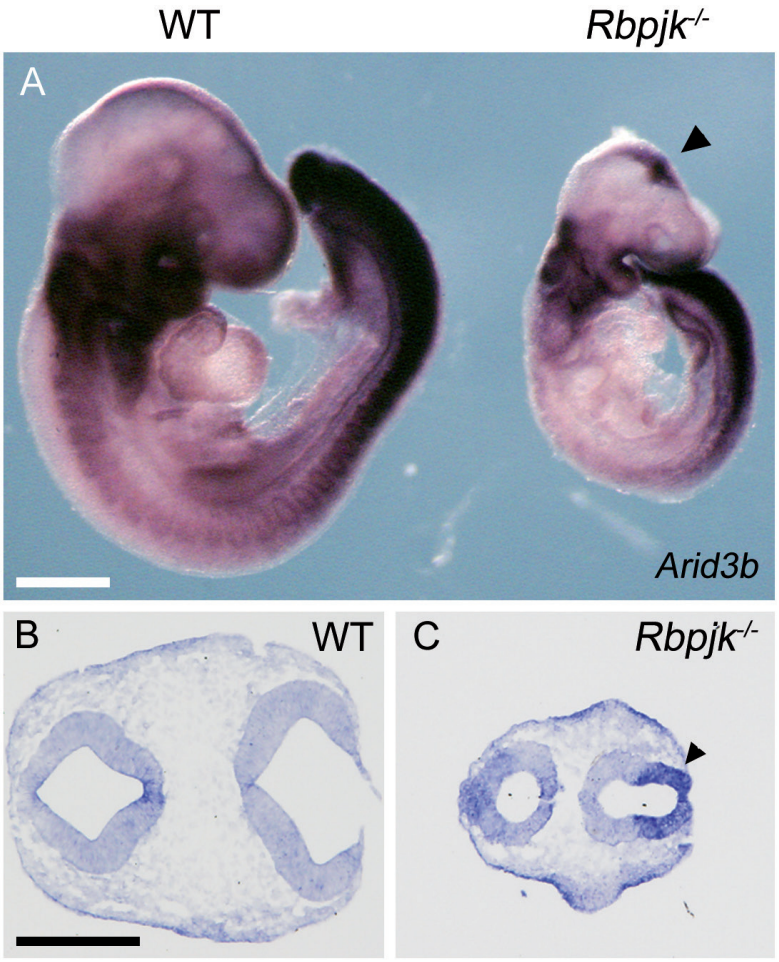

Supplementary figure 4. *In situ* hybridisation with *Arid3b* probe in whole-mount (**A**) and on paraffin sections (**B,C**) in wild type and *RPB-Jk* mutants. Note the ectopic expression of *Arid3b* in the midbrain of the mutant (arrowheads). Scale bars: A 500 μm; B,C 100 μm.

GENES UPREGULATED IN HEART AND WHOLE E9.0 EMBRYOS			
Symbol	ID	Entrez Gene Name	logFC Heart
5430434G16Rik	A_52_P1034794	RIKEN cDNA 5430434G16 gene	1,245
5830408C22Rik	A_52_P359257	RIKEN cDNA 5830408C22 gene	2,622
A2M	A_52_P455370	alpha-2-macroglobulin	3,656
ADM	A_51_P265571	adrenomedullin	2,081
ALDOC	A_51_P220681	aldolase C, fructose-bisphosphate	2,346
ANKRD37	A_52_P319438	ankyrin repeat domain 37	2,715
ANXA2	A_52_P1196772	annexin A2	1,506
ARHGEF4	A_51_P260504	Rho guanine nucleotide exchange factor (GEF) 4	1,428
ARRDC3	A_52_P164136	arrestin domain containing 3	1,401
ATR	A_52_P445778	ataxia telangiectasia and Rad3 related	1,090
BHLHE40	A_51_P272553	basic helix-loop-helix family, member e40	3,146
BHLHE41	A_51_P451176	basic helix-loop-helix family, member e41	2,370
BNIP3	A_51_P155234	BCL2/adenovirus E1B 19kDa interacting protein 3	2,408
C17orf58	A_51_P305213	chromosome 17 open reading frame 58	2,423
C3	A_51_P110301	complement component 3	3,318
C4orf29	A_52_P616229	chromosome 4 open reading frame 29	1,916
CCBP2	A_52_P222073	chemokine binding protein 2	1,484
CCL19	A_51_P458258	chemokine (C-C motif) ligand 19	1,544
CCNG2	A_51_P360165	cyclin G2	2,018
Cd55/Daf2	A_52_P199084	CD55 antigen	1,471
CHAC1	A_51_P134812	ChaC, cation transport regulator homolog 1 (E. coli)	4,578
CREG2	A_51_P227353	cellular repressor of E1A-stimulated genes 2	1,216
CYP2S1	A_51_P180091	cytochrome P450, family 2, subfamily S, polypeptide 1	3,217
DBP	A_51_P180492	D site of albumin promoter (albumin D-box) binding protein	1,674
DDIT3	A_52_P533146	DNA-damage-inducible transcript 3	1,944
DDIT4	A_51_P245796	DNA-damage-inducible transcript 4	3,097
DENND2D	A_52_P662796	DENN/MADD domain containing 2D	1,091
EBF4	A_52_P78975	early B-cell factor 4	1,333
EDIL3	A_52_P325527	EGF-like repeats and discoidin I-like domains 3	1,219
EGLN3	A_52_P387009	egl nine homolog 3 (C. elegans)	3,119
ENO2	A_52_P748882	enolase 2 (gamma, neuronal)	4,184
ERO1L	A_51_P481693	ERO1-like (S. cerevisiae)	1,965
ESM1	A_52_P257625	endothelial cell-specific molecule 1	1,871
ESPN	A_51_P451799	espin	2,484

FAM162A	A_52_P563694	family with sequence similarity 162, member A	1,102
FN3K	A_51_P398525	fructosamine 3 kinase	2,014
HEXB	A_51_P453111	hexosaminidase B (beta polypeptide)	1,699
HSPA1A/HSPA1B	A_52_P82741	heat shock 70kDa protein 1A	2,729
IER3	A_51_P286488	immediate early response 3	3,466
KBTBD11	A_52_P394448	kelch repeat and BTB (POZ) domain containing 11	4,523
KCNE3	A_52_P243425	potassium voltage-gated channel, Isk-related family, member 3	2,668
KRT19	A_51_P356642	keratin 19	3,015
LINGO3	A_51_P436491	leucine rich repeat and Ig domain containing 3	1,796
Lrrc51	A_52_P319137	leucine rich repeat containing 51	1,545
MACROD1	A_52_P559957	MACRO domain containing 1	1,084
MAFF	A_52_P608322	v-maf musculoaponeurotic fibrosarcoma oncogene homolog F (avian)	2,092
MEF2B	A_51_P330580	myocyte enhancer factor 2B	2,215
MGARP	A_51_P240501	mitochondria-localized glutamic acid-rich protein	2,390
MT1E	A_51_P294979	metallothionein 1E	2,410
MT1H	A_51_P246317	metallothionein 1H	2,324
NDRG1	A_51_P405606	N-myc downstream regulated 1	4,424
NDRG2	A_51_P176352	NDRG family member 2	1,852
NEK1	A_52_P818995	NIMA-related kinase 1	1,194
Nppb	A_52_P559955	natriuretic peptide type B	1,875
NRN1	A_51_P308844	neuritin 1	3,752
NUPR1	A_51_P519251	nuclear protein, transcriptional regulator, 1	3,553
P4HA1	A_52_P593723	prolyl 4-hydroxylase, alpha polypeptide I	1,939
PDK1	A_51_P406429	pyruvate dehydrogenase kinase, isozyme 1	1,522
PFKFB3	A_52_P138126	6-phosphofructo-2-kinase/fructose-2,6-biphosphatase 3	2,493
PFKP	A_52_P223083	phosphofructokinase, platelet	1,426
PGM1	A_51_P368074	phosphoglucomutase 1	1,191
PHYHD1	A_51_P357606	phytanoyl-CoA dioxygenase domain containing 1	1,909
PIK3IP1	A_51_P463428	phosphoinositide-3-kinase interacting protein 1	2,126
PLEKHA2	A_51_P280785	pleckstrin homology domain containing, family A (phosphoinositide binding specific) member 2	1,549
PPIL6	A_51_P224042	peptidylprolyl isomerase (cyclophilin)-like 6	1,260

PPP1R3C	A_51_P521010	protein phosphatase 1, regulatory subunit 3C	1,646
PRELID2	A_51_P480119	PRELI domain containing 2	1,691
PYGL	A_51_P452779	phosphorylase, glycogen, liver	1,616
RORA	A_51_P477779	RAR-related orphan receptor A	3,246
SESN2	A_52_P154710	sestrin 2	1,327
SLC38A3	A_51_P139030	solute carrier family 38, member 3	2,168
SLC7A3	A_51_P275016	solute carrier family 7 (cationic amino acid transporter, y+ system), member 3	4,430
ST3GAL1	A_51_P301804	ST3 beta-galactoside alpha-2,3-sialyltransferase 1	1,955
STAG3	A_51_P494822	stromal antigen 3	1,244
STC1	A_51_P233334	stanniocalcin 1	2,762
STC2	A_51_P208922	stanniocalcin 2	3,835
TET2	A_51_P478930	tet methylcytosine dioxygenase 2	1,346
TEX40	A_52_P357972	testis expressed 40	1,629
TMEM45A	A_51_P288876	transmembrane protein 45A	2,077
TRIB3	A_51_P331570	tribbles homolog 3 (Drosophila)	4,037
VLDLR	A_51_P278334	very low density lipoprotein receptor	3,054
Zbtb7b	A_51_P473229	zinc finger and BTB domain containing 7B	1,142
ZC3H6	A_52_P469956	zinc finger CCCH-type containing 6	2,164
ZMYM6NB	A_52_P70216	ZMYM6 neighbor	1,096

GENES DOWNREGULATED IN HEART AND WHOLE E9.0 EMBRYOS			
Symbol	ID	Entrez Gene Name	logFC Heart
AMICA1	A_52_P375312	adhesion molecule, interacts with CXADR antigen 1	-1,893
ARID3B	A_52_P454397	AT rich interactive domain 3B (BRIGHT-like)	-4,180
ATM	A_52_P369581	ataxia telangiectasia mutated	-1,318
Cryge	A_51_P289062	crystallin, gamma E	-1,844
HEYL	A_52_P337259	hairy/enhancer-of-split related with YRPW motif-like	-1,405
KLHL31	A_52_P90684	kelch-like family member 31	-1,876
LHX8	A_51_P298615	LIM homeobox 8	-1,475
PPCDC	A_52_P409457	phosphopantothenoylcysteine decarboxylase	-3,161
VGLL2	A_51_P491648	vestigial like 2 (Drosophila)	-2,031

GENES UPREGULATED IN HEART, HEAD AND TRUNK			
Symbol	ID	Entrez Gene Name	logFC Heart
1110035H17Rik	A_52_P185054	RIKEN cDNA 1110035H17 gene	1,039
1600014C23Rik	A_51_P147064	RIKEN cDNA 1600014C23 gene	2,510
1700001L05Rik	A_55_P2404484	RIKEN cDNA 1700001L05 gene	2,168
1700012L04Rik (includes others)	A_55_P1982494	predicted gene 4906	2,239
1700016J18Rik	A_66_P102628	RIKEN cDNA 1700016J18 gene	1,353
2310047D07Rik	A_55_P2182740	RIKEN cDNA 2310047D07 gene	1,524
2410006H16Rik	A_66_P111430	RIKEN cDNA 2410006H16 gene	1,577
2500002B13Rik	A_55_P2216561	RIKEN cDNA 2500002B13 gene	1,642
2610528A11Rik	A_66_P108468	RIKEN cDNA 2610528A11 gene	1,867
2700022O18Rik	A_55_P2233462	RIKEN cDNA 2700022O18 gene	1,553
2900055J20Rik	A_51_P471273	RIKEN cDNA 2900055J20 gene	4,760
4831440E17Rik	A_55_P2361647	RIKEN cDNA 4831440E17 gene	1,702
4930426I24Rik	A_55_P2387121	RIKEN cDNA 4930426I24 gene	1,750
4930466F19Rik	A_66_P108038	RIKEN cDNA 4930466F19 gene	1,593
4930579K19Rik	A_55_P2144701	RIKEN cDNA 4930579K19 gene	1,230
5033406O09Rik	A_55_P2324976	RIKEN cDNA 5033406O09 gene	1,171
5430402O13Rik	A_55_P2187829	RIKEN cDNA 5430402O13 gene	1,716
5830408C22Rik	A_52_P359257	RIKEN cDNA 5830408C22 gene	2,622
6720401G13Rik	A_55_P2181934	RIKEN cDNA 6720401G13 gene	1,005
6720407P12Rik	A_55_P2316612	RIKEN cDNA 6720407P12 gene	3,630
9330159N05Rik	A_55_P2349747	RIKEN cDNA 9330159N05 gene	1,153
9430065F17Rik	A_55_P2302848	RIKEN cDNA 9430065F17 gene	1,486
A2M	A_55_P2459897	alpha-2-macroglobulin	3,656
A530047J11Rik	A_55_P2234704	RIKEN cDNA A530047J11 gene	1,356
A830052D11Rik	A_55_P2412319	RIKEN cDNA A830052D11 gene	1,481
ABHD14B	A_55_P2059640	abhydrolase domain containing 14B	1,046
Acad12	A_51_P384113	acyl-Coenzyme A dehydrogenase family, member 12	1,015
ACVRL1	A_55_P2011380	activin A receptor type II-like 1	1,033
ADAMTS17	A_66_P124114	ADAM metallopeptidase with thrombospondin type 1 motif, 17	1,636
ADM	A_51_P265571	adrenomedullin	2,081
ADM2	A_55_P2181386	adrenomedullin 2	4,325
ADORA2A	A_55_P2109382	adenosine A2a receptor	1,734
AHNAK	A_55_P2153621	AHNAK nucleoprotein	1,596
ALDH1L2	A_52_P498193	aldehyde dehydrogenase 1 family, member L2	2,313
ALDOC	A_55_P2070992	aldolase C, fructose-bisphosphate	2,346
ALOX12	A_51_P520306	arachidonate 12-lipoxygenase	3,421
ALOXE3	A_55_P2023523	arachidonate lipoxygenase 3	1,366
AMY1A (includes others)	A_55_P1983418	amylase, alpha 1A (salivary)	2,044

ANKRD37	A_52_P319438	ankyrin repeat domain 37	2,715
ANKZF1	A_51_P365903	ankyrin repeat and zinc finger domain containing 1	1,045
ANXA2	A_55_P2110713	annexin A2	1,506
Apol7d	A_55_P2011557	apolipoprotein L 7d	1,936
ARHGEF4	A_51_P260504	Rho guanine nucleotide exchange factor (GEF) 4	1,428
ARRDC3	A_52_P164136	arrestin domain containing 3	1,401
ARSG	A_55_P2043122	arylsulfatase G	1,038
ASNS	A_55_P1959748	asparagine synthetase (glutamine-hydrolyzing)	1,562
ATF3	A_52_P452689	activating transcription factor 3	1,301
ATR	A_55_P2029176	ataxia telangiectasia and Rad3 related	1,090
B130046B21Rik	A_55_P2365710	RIKEN cDNA B130046B21 gene	2,129
BC048594	A_55_P2177498	cDNA sequence BC048594	1,012
BC062258	A_55_P2340101	cDNA sequence BC062258	1,215
BCL6	A_52_P161495	B-cell CLL/lymphoma 6	1,476
BHLHE40	A_51_P272553	basic helix-loop-helix family, member e40	3,146
BHLHE41	A_55_P2133001	basic helix-loop-helix family, member e41	2,370
BNIP3	A_55_P2091472	BCL2/adenovirus E1B 19kDa interacting protein 3	2,408
BNIP3L	A_55_P2073699	BCL2/adenovirus E1B 19kDa interacting protein 3-like	1,233
BSG	A_51_P329441	basigin (Ok blood group)	1,158
C130045F17Rik	A_55_P2311208	RIKEN cDNA C130045F17 gene	1,177
C17orf58	A_55_P2102095	chromosome 17 open reading frame 58	2,423
C20orf173	A_55_P2061934	chromosome 20 open reading frame 173	1,152
C4orf29	A_55_P2005808	chromosome 4 open reading frame 29	1,916
C4orf47	A_52_P641195	chromosome 4 open reading frame 47	1,287
C80012	A_55_P2212733	expressed sequence C80012	1,905
C8G	A_55_P2151556	complement component 8, gamma polypeptide	1,296
C920006O11Rik	A_51_P130447	RIKEN cDNA C920006O11 gene	1,970
C9orf9	A_55_P1979997	chromosome 9 open reading frame 9	1,171
CA12	A_55_P2019312	carbonic anhydrase XII	2,164
CA9	A_55_P2092750	carbonic anhydrase IX	4,447
CCBP2	A_52_P222073	chemokine binding protein 2	1,484
CCDC176	A_55_P1976494	coiled-coil domain containing 176	1,546
CCDC62	A_55_P1999556	coiled-coil domain containing 62	1,191

CCDC64	A_55_P2152991	coiled-coil domain containing 64	2,004
CCL19	A_55_P2099742	chemokine (C-C motif) ligand 19	1,544
CCNG2	A_55_P2068882	cyclin G2	2,018
CCT6B	A_55_P2050273	chaperonin containing TCP1, subunit 6B (zeta 2)	1,139
CDH13	A_51_P114826	cadherin 13, H-cadherin (heart)	1,103
CDKN1A	A_55_P1976204	cyclin-dependent kinase inhibitor 1A (p21, Cip1)	1,243
CHAC1	A_51_P134812	ChaC, cation transport regulator homolog 1 (E. coli)	4,578
CHADL	A_55_P2232325	chondroadherin-like	1,090
CHD5	A_55_P1978371	chromodomain helicase DNA binding protein 5	1,668
CLCN3	A_55_P2047842	chloride channel, voltage-sensitive 3	1,297
CNBD2	A_55_P2149144	cyclic nucleotide binding domain containing 2	1,019
CNNM1	A_52_P296913	cyclin M1	1,779
CNTD1	A_51_P467960	cyclin N-terminal domain containing 1	1,119
COL20A1	A_52_P474902	collagen, type XX, alpha 1	1,181
COX4I2	A_55_P2054663	cytochrome c oxidase subunit IV isoform 2 (lung)	2,687
CPEB1	A_55_P2074631	cytoplasmic polyadenylation element binding protein 1	1,495
CREBRF	A_52_P573290	CREB3 regulatory factor	2,605
CRLF1	A_52_P304720	cytokine receptor-like factor 1	1,357
CTSF	A_52_P660945	cathepsin F	1,220
CYB5R2	A_55_P2090214	cytochrome b5 reductase 2	2,524
CYP26C1	A_55_P2035407	cytochrome P450, family 26, subfamily C, polypeptide 1	1,880
CYP4B1	A_55_P2117959	cytochrome P450, family 4, subfamily B, polypeptide 1	1,494
D630032N06Rik	A_52_P400637	RIKEN cDNA D630032N06 gene	1,163
DAB1	A_51_P437135	Dab, reelin signal transducer, homolog 1 (Drosophila)	1,394
DBP	A_55_P2032081	D site of albumin promoter (albumin D-box) binding protein	1,674
DDIT3	A_52_P533146	DNA-damage-inducible transcript 3	1,944
DDIT4	A_51_P245796	DNA-damage-inducible transcript 4	3,097
DHRS3	A_55_P2020128	dehydrogenase/reductase (SDR family) member 3	1,163
Dnhd1	A_55_P2166703	dynein heavy chain domain 1	1,076
EBF4	A_55_P2011981	early B-cell factor 4	1,333
EDIL3	A_52_P325527	EGF-like repeats and discoidin I-like domains 3	1,219
EFHC1	A_51_P440327	EF-hand domain (C-terminal) containing 1	1,032

EGLN1	A_51_P186899	egl nine homolog 1 (C. elegans)	1,146
EGLN3	A_55_P1960916	egl nine homolog 3 (C. elegans)	3,119
EIF4B	A_52_P390114	eukaryotic translation initiation factor 4B	1,041
ENO2	A_55_P2019457	enolase 2 (gamma, neuronal)	4,184
ENPP5	A_55_P2021704	ectonucleotide pyrophosphatase/ phosphodiesterase 5 (putative)	1,648
EPM2A	A_55_P1992034	epilepsy, progressive myoclonus type 2A, Lafora disease (laforin)	2,488
ERO1L	A_51_P481693	ERO1-like (S. cerevisiae)	1,965
ESM1	A_52_P257625	endothelial cell-specific molecule 1	1,871
ESPN	A_55_P1997651	espin	2,484
EZH1	A_55_P2017086	enhancer of zeste homolog 1 (Drosophila)	1,349
F3	A_65_P08971	coagulation factor III (thromboplastin, tissue factor)	1,171
FAM163B	A_55_P2168441	family with sequence similarity 163, member B	1,306
FAM169A	A_52_P488623	family with sequence similarity 169, member A	1,271
FAM71F2	A_55_P2125613	family with sequence similarity 71, member F2	1,815
FBXL20	A_55_P1976859	F-box and leucine-rich repeat protein 20	1,190
FERMT3	A_52_P38639	fermitin family member 3	2,268
FGF12	A_52_P193161	fibroblast growth factor 12	1,606
FHAD1	A_55_P1956659	forkhead-associated (FHA) phosphopeptide binding domain 1	1,140
FLT1	A_55_P2166282	fms-related tyrosine kinase 1	1,908
FN3K	A_55_P2040090	fructosamine 3 kinase	2,014
FNDC1	A_51_P153423	fibronectin type III domain containing 1	1,280
FOXO3	A_55_P2150896	forkhead box O3	1,432
FST	A_55_P2394308	follistatin	1,361
FUT1	A_55_P1986247	fucosyltransferase 1 (galactoside 2-alpha-L-fucosyltransferase, H blood group)	2,957
FYB	A_55_P2006869	FYN binding protein	2,975
GAA	A_55_P2024429	glucosidase, alpha; acid	1,121
GAD1	A_52_P144310	glutamate decarboxylase 1 (brain, 67kDa)	3,430
GIPR	A_52_P238468	gastric inhibitory polypeptide receptor	3,238
GLS2	A_51_P169087	glutaminase 2 (liver, mitochondrial)	1,728
Gm10621	A_55_P2070262	predicted gene 10621	1,049
Gm10766	A_55_P2044488	predicted gene 10766	1,015
Gm12592	A_66_P103753	predicted gene 12592	2,351

Gm12758	A_55_P2329298	predicted gene 12758	1,441
Gm12866	A_66_P124728	predicted gene 12866	1,564
Gm14207	A_55_P2155848	predicted gene 14207	1,469
Gm15850	A_55_P2402577	predicted gene 15850	1,908
Gm2011	A_66_P129619	predicted gene 2011	2,162
Gm3367	A_66_P101261	predicted gene 3367	2,849
Gm4791	A_66_P133103	predicted gene 4791	1,578
GPR114	A_55_P2156638	G protein-coupled receptor 114	1,318
GPR146	A_55_P2027392	G protein-coupled receptor 146	1,600
GPT2	A_51_P493886	glutamic pyruvate transaminase (alanine aminotransferase) 2	1,248
GYS1	A_55_P2026315	glycogen synthase 1 (muscle)	1,541
HEXA	A_51_P282667	hexosaminidase A (alpha polypeptide)	1,025
HEXB	A_51_P453111	hexosaminidase B (beta polypeptide)	1,699
HIF3A	A_55_P2015541	hypoxia inducible factor 3, alpha subunit	1,057
HK2	A_51_P204080	hexokinase 2	1,772
HLA-DMB	A_51_P278868	major histocompatibility complex, class II, DM beta	1,229
HMX2	A_55_P2099620	H6 family homeobox 2	3,443
HMX3	A_51_P413910	H6 family homeobox 3	2,865
HRK	A_55_P2083559	harakiri, BCL2 interacting protein (contains only BH3 domain)	2,821
HSPA1A/HSPA1B	A_55_P2068459	heat shock 70kDa protein 1A	2,729
IDUA	A_55_P2097178	iduronidase, alpha-L-	1,319
IER3	A_51_P286488	immediate early response 3	3,466
IGFBP2	A_55_P2056729	insulin-like growth factor binding protein 2, 36kDa	1,454
Il4i1/Nup62-il4i1	A_55_P2087622	interleukin 4 induced 1	1,598
Isoc2b	A_51_P343356	isochorismatase domain containing 2b	1,059
ITGA2B	A_52_P459564	integrin, alpha 2b (platelet glycoprotein IIb of IIb/IIIa complex, antigen CD41)	1,858
JAK3	A_51_P355360	Janus kinase 3	1,087
JDP2	A_51_P254646	Jun dimerization protein 2	1,146
JHDM1D	A_55_P1962675	jumonji C domain containing histone demethylase 1 homolog D (S. cerevisiae)	1,705
JPH1	A_55_P2163744	junctophilin 1	1,149
Jpx	A_55_P2253169	Jpx transcript, Xist activator (non-protein coding)	1,197
KBTBD11	A_55_P2075213	kelch repeat and BTB (POZ) domain containing 11	4,523

KCNE3	A_51_P336599	potassium voltage-gated channel, Isk-related family, member 3	2,668
KCNJ4	A_51_P166740	potassium inwardly-rectifying channel, subfamily J, member 4	1,469
KCNT2	A_55_P1961730	potassium channel, subfamily T, member 2	1,040
KCTD16	A_51_P266579	potassium channel tetramerisation domain containing 16	3,691
KDM3A	A_55_P1982578	lysine (K)-specific demethylase 3A	1,557
KHNYN	A_52_P641849	KH and NYN domain containing	1,175
KIT	A_66_P128434	v-kit Hardy-Zuckerman 4 feline sarcoma viral oncogene homolog	1,306
KLHL24	A_55_P1962284	kelch-like family member 24	1,273
KRT19	A_51_P356642	keratin 19	3,015
Krt42	A_55_P2013840	keratin 42	2,966
LAMA5	A_55_P2064321	laminin, alpha 5	1,242
LAMB3	A_55_P1967196	laminin, beta 3	1,664
LDHD	A_55_P2018697	lactate dehydrogenase D	1,633
LINGO3	A_51_P436491	leucine rich repeat and Ig domain containing 3	1,796
LOC106740	A_55_P2189571	uncharacterized LOC106740	1,252
LOX	A_55_P2032678	lysyl oxidase	2,304
LOXL2	A_52_P480351	lysyl oxidase-like 2	1,563
LRFN2	A_51_P229498	leucine rich repeat and fibronectin type III domain containing 2	1,380
LRP2	A_55_P2099677	low density lipoprotein receptor-related protein 2	1,543
Lrrc51	A_55_P1999760	leucine rich repeat containing 51	1,545
LUC7L2	A_55_P1953369	LUC7-like 2 (S. cerevisiae)	1,749
MACROD1	A_51_P213030	MACRO domain containing 1	1,084
MAFF	A_52_P608322	v-maf musculoaponeurotic fibrosarcoma oncogene homolog F (avian)	2,092
MAML3	A_52_P47126	mastermind-like 3 (Drosophila)	1,201
MAP3K1	A_55_P1961084	mitogen-activated protein kinase kinase kinase 1, E3 ubiquitin protein ligase	1,029
MEF2B	A_55_P1959784	myocyte enhancer factor 2B	2,215
METTL7A	A_55_P2172822	methyltransferase like 7A	3,235
MGARP	A_55_P2048759	mitochondria-localized glutamic acid-rich protein	2,390
MORN1	A_51_P423825	MORN repeat containing 1	1,107
MT1E	A_66_P111660	metallothionein 1E	2,410
MT1H	A_51_P246317	metallothionein 1H	2,324
Muc2	A_51_P128320	mucin 2	2,948

NAMPT	A_51_P387235	nicotinamide phosphoribosyltransferase	1,062
NDRG1	A_51_P405606	N-myc downstream regulated 1	4,424
NDRG2	A_51_P176352	NDRG family member 2	1,852
NDUFA4L2	A_55_P1971244	NADH dehydrogenase (ubiquinone) 1 alpha subcomplex, 4-like 2	5,046
NEFH	A_55_P2099790	neurofilament, heavy polypeptide	1,229
NEIL2	A_55_P2099418	nei endonuclease VIII-like 2 (E. coli)	1,712
NMRK2	A_51_P369762	nicotinamide riboside kinase 2	1,991
NR4A1	A_51_P239654	nuclear receptor subfamily 4, group A, member 1	1,079
NRCAM	A_55_P2003541	neuronal cell adhesion molecule	1,283
NRN1	A_51_P308844	neuritin 1	3,752
Nrxn3	A_55_P2054643	neurexin III	1,375
NUPR1	A_51_P519251	nuclear protein, transcriptional regulator, 1	3,553
NYAP1	A_55_P1999923	neuronal tyrosine-phosphorylated phosphoinositide-3-kinase adaptor 1	1,555
Olfr1383	A_55_P1987284	olfactory receptor 1383	1,923
P2RX4	A_55_P2183015	purinergic receptor P2X, ligand-gated ion channel, 4	1,094
P4HA1	A_55_P2097808	prolyl 4-hydroxylase, alpha polypeptide I	1,939
P4HA2	A_52_P663413	prolyl 4-hydroxylase, alpha polypeptide II	2,702
PBLD	A_51_P165451	phenazine biosynthesis-like protein domain containing	1,261
PCSK4	A_55_P2167269	proprotein convertase subtilisin/ kexin type 4	1,357
PDE4B	A_52_P423247	phosphodiesterase 4B, cAMP-specific	1,017
PDGFB	A_55_P1974441	platelet-derived growth factor beta polypeptide	2,022
PDK1	A_51_P406429	pyruvate dehydrogenase kinase, isozyme 1	1,522
PF4	A_51_P441426	platelet factor 4	3,625
PFKFB3	A_52_P362917	6-phosphofructo-2-kinase/fructose-2,6-biphosphatase 3	2,493
PFKP	A_51_P378856	phosphofructokinase, platelet	1,426
PGM1	A_55_P1987483	phosphoglucomutase 1	1,191
PHF15	A_55_P2139753	PHD finger protein 15	1,194
PHYHD1	A_55_P2094896	phytanoyl-CoA dioxygenase domain containing 1	1,909
PIK3IP1	A_51_P463428	phosphoinositide-3-kinase interacting protein 1	2,126
PIP5K1A	A_55_P1999902	phosphatidylinositol-4-phosphate 5-kinase, type I, alpha	2,055

PLEKHA2	A_55_P2156274	pleckstrin homology domain containing, family A (phosphoinositide binding specific) member 2	1,549
PLOD2	A_51_P396570	procollagen-lysine, 2-oxoglutarate 5-dioxygenase 2	1,812
PORCN	A_55_P2077666	porcupine homolog (Drosophila)	1,040
PPBP	A_51_P428372	pro-platelet basic protein (chemokine (C-X-C motif) ligand 7)	4,268
PPIL6	A_51_P224042	peptidylprolyl isomerase (cyclophilin)-like 6	1,260
PPP1R16B	A_55_P2057040	protein phosphatase 1, regulatory subunit 16B	1,477
PPP1R3C	A_52_P30451	protein phosphatase 1, regulatory subunit 3C	1,646
PPP1R3G	A_51_P155873	protein phosphatase 1, regulatory subunit 3G	1,084
Ppp4r1l-ps	A_52_P91891	protein phosphatase 4, regulatory subunit 1-like, pseudogene	1,133
PRELID2	A_51_P480119	PRELI domain containing 2	1,691
PRKAR1B	A_55_P2176280	protein kinase, cAMP-dependent, regulatory, type I, beta	1,096
PROSER2	A_51_P474169	proline and serine-rich protein 2	1,549
PRSS35	A_55_P2111985	protease, serine, 35	1,715
PTPRZ1	A_55_P2173682	protein tyrosine phosphatase, receptor-type, Z polypeptide 1	2,114
Pvr	A_52_P628590	poliovirus receptor	1,113
PYCR1	A_51_P503896	pyrroline-5-carboxylate reductase 1	1,459
PYGL	A_51_P452779	phosphorylase, glycogen, liver	1,616
RAD9B	A_51_P513013	RAD9 homolog B (S. pombe)	1,461
RASD2	A_55_P2107155	RASD family, member 2	1,212
RDM1	A_51_P433127	RAD52 motif 1	1,028
RENBP	A_55_P2013357	renin binding protein	1,647
RGS11	A_55_P2000354	regulator of G-protein signaling 11	3,155
RGS9	A_55_P2032232	regulator of G-protein signaling 9	1,046
RNF19A	A_51_P277444	ring finger protein 19A, E3 ubiquitin protein ligase	1,281
ROBO2	A_52_P597791	roundabout, axon guidance receptor, homolog 2 (Drosophila)	1,187
RORA	A_55_P2078123	RAR-related orphan receptor A	3,246
RORC	A_55_P2051094	RAR-related orphan receptor C	1,450
RPP25	A_51_P104392	ribonuclease P/MRP 25kDa subunit	1,465
RPS6KC1	A_55_P2083664	ribosomal protein S6 kinase, 52kDa, polypeptide 1	1,372
RRAS	A_52_P635182	related RAS viral (r-ras) oncogene homolog	1,186
S100A1	A_55_P1979650	S100 calcium binding protein A1	1,401

SDC4	A_52_P93467	syndecan 4	1,855
SEMA3B	A_55_P1973868	sema domain, immunoglobulin domain (Ig), short basic domain, secreted, (semaphorin) 3B	1,259
SEMA4G	A_51_P331003	sema domain, immunoglobulin domain (Ig), transmembrane domain (TM) and short cytoplasmic domain, (semaphorin) 4G	1,473
SESN2	A_51_P161354	sestrin 2	1,327
SHMT2	A_51_P313761	serine hydroxymethyltransferase 2 (mitochondrial)	1,008
SLA	A_52_P513177	Src-like-adaptor	2,131
SLAMF9	A_51_P246066	SLAM family member 9	1,918
SLC16A6	A_52_P579933	solute carrier family 16, member 6 (monocarboxylic acid transporter 7)	1,264
SLC16A9	A_51_P493117	solute carrier family 16, member 9 (monocarboxylic acid transporter 9)	1,516
SLC1A6	A_51_P283016	solute carrier family 1 (high affinity aspartate/glutamate transporter), member 6	1,017
SLC22A7	A_51_P395856	solute carrier family 22 (organic anion transporter), member 7	1,202
Slc26a10	A_55_P2087067	solute carrier family 26, member 10	1,273
SLC2A1	A_51_P464738	solute carrier family 2 (facilitated glucose transporter), member 1	1,060
SLC2A3	A_52_P354744	solute carrier family 2 (facilitated glucose transporter), member 3	2,224
SLC35D3	A_52_P467488	solute carrier family 35, member D3	1,910
SLC38A3	A_51_P139030	solute carrier family 38, member 3	2,168
SLC39A5	A_51_P206235	solute carrier family 39 (metal ion transporter), member 5	1,180
SLC6A9	A_55_P1973838	solute carrier family 6 (neurotransmitter transporter, glycine), member 9	1,079
SLC7A3	A_55_P1988384	solute carrier family 7 (cationic amino acid transporter, y+ system), member 3	4,430
SLC7A5	A_55_P2017972	solute carrier family 7 (amino acid transporter light chain, L system), member 5	1,426
SNCB	A_51_P448971	synuclein, beta	4,016
SNX21	A_51_P323521	sorting nexin family member 21	1,030
SOX17	A_55_P2157023	SRY (sex determining region Y)-box 17	1,199
ST3GAL1	A_51_P301804	ST3 beta-galactoside alpha-2,3-sialyltransferase 1	1,955
STAB1	A_51_P232371	stabilin 1	1,094
STAG3	A_51_P494822	stromal antigen 3	1,244

STC1	A_51_P233334	stanniocalcin 1	2,762
STC2	A_51_P208922	stanniocalcin 2	3,835
Sts	A_51_P377526	steroid sulfatase	1,686
SULT6B1	A_51_P318577	sulfotransferase family, cytosolic, 6B, member 1	1,496
SYNGR1	A_52_P239320	synaptogyrin 1	1,832
SYT3	A_55_P2048441	synaptotagmin III	1,131
TAC1	A_55_P1954693	tachykinin, precursor 1	1,274
TBL2	A_52_P499206	transducin (beta)-like 2	1,061
TCHH	A_52_P468068	trichohyalin	1,481
TEF	A_55_P1979893	thyrotrophic embryonic factor	1,164
TEX40	A_51_P182257	testis expressed 40	1,629
Tmem191c	A_51_P165082	transmembrane protein 191C	1,271
TMEM217	A_55_P2153411	transmembrane protein 217	1,501
TMEM45A	A_51_P288876	transmembrane protein 45A	2,077
TMEM74B	A_55_P2002768	transmembrane protein 74B	2,996
TMPRSS13	A_55_P2177998	transmembrane protease, serine 13	1,481
TMTC1	A_55_P1975645	transmembrane and tetratricopeptide repeat containing 1	1,518
TNFAIP3	A_55_P2053838	tumor necrosis factor, alpha-induced protein 3	1,427
TRAPPC6A	A_55_P2106250	trafficking protein particle complex 6A	1,338
TRIB3	A_55_P2009988	tribbles homolog 3 (Drosophila)	4,037
TRIOBP	A_55_P1953353	TRIO and F-actin binding protein	1,858
UAP1L1	A_51_P509669	UDP-N-acteylglucosamine pyrophosphorylase 1-like 1	1,459
UPP1	A_51_P302738	uridine phosphorylase 1	1,805
USP35	A_55_P1970454	ubiquitin specific peptidase 35	1,588
VEGFA	A_52_P638895	vascular endothelial growth factor A	2,429
VLDLR	A_55_P2030524	very low density lipoprotein receptor	3,054
VSIG2	A_55_P2083879	V-set and immunoglobulin domain containing 2	1,265
VSIG8	A_55_P2124233	V-set and immunoglobulin domain containing 8	1,360
VSTM5	A_51_P220934	V-set and transmembrane domain containing 5	1,964
VWF	A_55_P2169659	von Willebrand factor	2,267
WDR64	A_51_P184991	WD repeat domain 64	2,399
WIPI1	A_55_P1968808	WD repeat domain, phosphoinositide interacting 1	1,025
YBX2	A_55_P1973447	Y box binding protein 2	1,325
ZAN	A_55_P2148809	zonadhesin	1,178
ZBTB4	A_55_P2165655	zinc finger and BTB domain containing 4	1,076

Zbtb7b	A_51_P473229	zinc finger and BTB domain containing 7B	1,142
ZC3H6	A_52_P139819	zinc finger CCCH-type containing 6	2,164
ZCWPW1	A_52_P154026	zinc finger, CW type with PWWP domain 1	1,066
ZFR2	A_55_P2053320	zinc finger RNA binding protein 2	1,608
ZMYM6	A_55_P2069525	zinc finger, MYM-type 6	1,011
ZMYM6NB	A_55_P2019909	ZMYM6 neighbor	1,096
ZNF383	A_55_P2059936	zinc finger protein 383	1,118
ZNF395	A_55_P2117590	zinc finger protein 395	1,473

GENES DOWNREGULATED IN HEART, HEAD AND TRUNK			
Symbol	ID	Entrez Gene Name	logFC Heart
1700121C10Rik	A_51_P313397	RIKEN cDNA 1700121C10 gene	-1,520
2310026L22Rik	A_66_P101427	RIKEN cDNA 2310026L22 gene	-1,393
4930524J08Rik	A_51_P415247	RIKEN cDNA 4930524J08 gene	-1,274
5930422O12Rik	A_55_P2115696	RIKEN cDNA 5930422O12 gene	-1,509
6030408B16Rik	A_66_P136813	RIKEN cDNA 6030408B16 gene	-1,602
6530403G13Rik	A_55_P2146389	RIKEN cDNA 6530403G13 gene	-1,189
A730089K16Rik	A_55_P2305010	RIKEN cDNA A730089K16 gene	-1,528
ACSBG1	A_52_P496956	acyl-CoA synthetase bubblegum family member 1	-1,953
ACYP2	A_55_P2005666	acylphosphatase 2, muscle type	-1,788
Adam4/Gm4787	A_66_P101707	a disintegrin and metallopeptidase domain 4	-1,687
AMICA1	A_52_P375312	adhesion molecule, interacts with CXADR antigen 1	-1,893
AMIGO3	A_51_P442933	adhesion molecule with Ig-like domain 3	-1,301
AP3B2	A_55_P1982229	adaptor-related protein complex 3, beta 2 subunit	-1,412
APH1B	A_52_P456750	anterior pharynx defective 1 homolog B (C. elegans)	-1,350
APOBEC3B	A_52_P308875	apolipoprotein B mRNA editing enzyme, catalytic polypeptide-like 3B	-1,862
ARID3B	A_55_P2123993	AT rich interactive domain 3B (BRIGHT-like)	-4,180
ASTN1	A_51_P143951	astrotactin 1	-1,103
ATM	A_52_P400509	ataxia telangiectasia mutated	-1,318
BRSK2	A_51_P160581	BR serine/threonine kinase 2	-2,034
C11orf1	A_55_P2023290	chromosome 11 open reading frame 1	-1,562
C5orf49	A_51_P234847	chromosome 5 open reading frame 49	-1,544
C9orf64	A_51_P224175	chromosome 9 open reading frame 64	-1,541
CBY1	A_51_P470311	chibby homolog 1 (Drosophila)	-1,186

Ccdc177	A_55_P1990200	coiled-coil domain containing 177	-1,215
CCDC30	A_66_P106421	coiled-coil domain containing 30	-1,547
CCL13	A_51_P286737	chemokine (C-C motif) ligand 13	-2,226
CLDN15	A_51_P306710	claudin 15	-1,042
CPA1	A_52_P161237	carboxypeptidase A1 (pancreatic)	-1,051
Cryge	A_55_P1975250	crystallin, gamma E	-1,844
CTU2	A_55_P2027634	cytosolic thiouridylase subunit 2 homolog (S. pombe)	-1,521
CYB5B	A_55_P1963712	cytochrome b5 type B (outer mitochondrial membrane)	-1,055
Cycs	A_55_P1968958	cytochrome c, somatic	-1,230
D630045M09Rik	A_55_P2335648	RIKEN cDNA D630045M09 gene	-1,718
DBH	A_55_P1974243	dopamine beta-hydroxylase (dopamine beta-monooxygenase)	-1,498
DIXDC1	A_52_P434279	DIX domain containing 1	-1,483
DNAH7	A_55_P2184023	dynein, axonemal, heavy chain 7	-1,507
DPYSL4	A_55_P1988413	dihydropyrimidinase-like 4	-1,965
E130201H02Rik	A_55_P2066568	Y box protein 1 pseudogene	-1,637
EHD2	A_55_P2076906	EH-domain containing 2	-1,111
FAM118B	A_55_P2462358	family with sequence similarity 118, member B	-1,072
FAM209B	A_51_P137184	family with sequence similarity 209, member B	-1,159
FBP1	A_51_P474701	fructose-1,6-bisphosphatase 1	-1,260
Fbxl22	A_51_P466685	F-box and leucine-rich repeat protein 22	-1,928
FDFT1	A_52_P136138	farnesyl-diphosphate farnesyltransferase 1	-1,076
Gm10099	A_66_P131406	predicted gene 10099	-1,659
Gm10548	A_66_P105771	ribosomal protein L29 pseudogene	-1,357
Gm10664	A_52_P1037027	predicted gene 10664	-1,052
Gm10751	A_55_P2121446	predicted gene 10751	-1,202
Gm13429	A_66_P126459	predicted gene 13429	-1,223
Gm4129	A_55_P2181665	predicted gene 4129	-1,536
Gm5868	A_55_P2034870	predicted gene 5868	-1,710
Gm7271	A_55_P2118234	predicted gene 7271	-1,018
GPD1	A_52_P16419	glycerol-3-phosphate dehydrogenase 1 (soluble)	-1,267
GPR17	A_51_P170463	G protein-coupled receptor 17	-1,255
GPR84	A_55_P2044932	G protein-coupled receptor 84	-1,832
GPRIN1	A_55_P1967010	G protein regulated inducer of neurite outgrowth 1	-1,316
GRK4	A_55_P2155347	G protein-coupled receptor kinase 4	-1,926
GUSB	A_52_P160936	glucuronidase, beta	-1,106
HDHD3	A_51_P465582	haloacid dehalogenase-like hydrolase domain containing 3	-1,031

HEYL	A_52_P337259	hairy/enhancer-of-split related with YRPW motif-like	-1,405
HPDL	A_51_P317214	4-hydroxyphenylpyruvate dioxygenase-like	-1,181
HSD17B7	A_55_P1964598	hydroxysteroid (17-beta) dehydrogenase 7	-1,541
HSPH1	A_55_P2003513	heat shock 105kDa/110kDa protein 1	-1,303
INSC	A_55_P2038183	inscuteable homolog (Drosophila)	-1,855
ITPKA	A_51_P273609	inositol-trisphosphate 3-kinase A	-1,240
KALRN	A_55_P2160623	kalirin, RhoGEF kinase	-1,322
KLHL25	A_51_P208121	kelch-like family member 25	-1,064
KRT15	A_55_P2006261	keratin 15	-1,158
KRT36	A_55_P2140036	keratin 36	-1,699
Lipo1/Lipo4	A_55_P2040777	lipase, member O1	-1,342
LRP8	A_55_P2014555	low density lipoprotein receptor-related protein 8, apolipoprotein e receptor	-1,321
LRRC4	A_55_P2176080	leucine rich repeat containing 4	-1,302
LRRC49	A_55_P2054967	leucine rich repeat containing 49	-1,324
LRTM1	A_51_P326685	leucine-rich repeats and transmembrane domains 1	-1,401
MRPS11	A_52_P582394	mitochondrial ribosomal protein S11	-1,005
MSRB2	A_51_P464911	methionine sulfoxide reductase B2	-1,400
MT-CO3	A_65_P07196	cytochrome c oxidase III	-1,628
MT-CYB	A_51_P315595	cytochrome b	-1,886
MT-ND1	A_65_P05358	NADH dehydrogenase, subunit 1 (complex I)	-2,110
MT-ND3	A_55_P2132147	NADH dehydrogenase, subunit 3 (complex I)	-1,689
MUC4	A_55_P2025687	mucin 4, cell surface associated	-2,333
MYB	A_55_P2017826	v-myb myeloblastosis viral oncogene homolog (avian)	-1,528
NDUFAF2	A_52_P2947	NADH dehydrogenase (ubiquinone) complex I, assembly factor 2	-1,291
NETO2	A_52_P381799	neuropilin (NRP) and tolloid (TLL)-like 2	-1,425
NHLH2	A_55_P2123902	nescient helix loop helix 2	-2,532
NMI	A_55_P2034705	N-myc (and STAT) interactor	-1,008
NOVA1	A_52_P204629	neuro-oncological ventral antigen 1	-1,354
NSDHL	A_66_P137462	NAD(P) dependent steroid dehydrogenase-like	-1,089
OSCP1	A_66_P121279	organic solute carrier partner 1	-1,228
P2RY6	A_51_P105124	pyrimidinergic receptor P2Y, G-protein coupled, 6	-1,306
PIH1D2	A_55_P2052048	PIH1 domain containing 2	-1,650

PIK3R3	A_55_P2000158	phosphoinositide-3-kinase, regulatory subunit 3 (gamma)	-1,666
PIN1	A_55_P2073268	peptidylprolyl cis/trans isomerase, NIMA-interacting 1	-1,018
PITPNA	A_51_P466371	phosphatidylinositol transfer protein, alpha	-1,059
PKIA	A_52_P314129	protein kinase (cAMP-dependent, catalytic) inhibitor alpha	-1,044
PPCDC	A_52_P409457	phosphopantothenoylcysteine decarboxylase	-3,161
PTS	A_52_P177021	6-pyruvoyltetrahydropterin synthase	-1,130
RAB19	A_51_P414126	RAB19, member RAS oncogene family	-1,509
RGS4	A_55_P2026734	regulator of G-protein signaling 4	-1,036
RPS25	A_52_P436318	ribosomal protein S25	-1,098
Rps27a	A_55_P2025173	ribosomal protein S27A	-1,738
SAA1	A_55_P1994807	serum amyloid A1	-2,150
SF3B4	A_55_P2056293	splicing factor 3b, subunit 4, 49kDa	-1,134
SLC25A35	A_52_P436447	solute carrier family 25, member 35	-1,937
SLFN13	A_55_P2135200	schlafen family member 13	-1,419
SNX11	A_55_P2120466	sorting nexin 11	-1,751
SPATA9	A_51_P212980	spermatogenesis associated 9	-1,561
SRRM4	A_52_P14456	serine/arginine repetitive matrix 4	-1,482
TAL2	A_52_P385594	T-cell acute lymphocytic leukemia 2	-1,457
TM4SF1	A_51_P240614	transmembrane 4 L six family member 1	-1,559
TMED5	A_55_P2105346	transmembrane emp24 protein transport domain containing 5	-1,336
TMEM25	A_55_P2126572	transmembrane protein 25	-1,766
TMEM251	A_52_P8903	transmembrane protein 251	-1,029
TMEM56	A_52_P54261	transmembrane protein 56	-1,442
TOMM40L	A_55_P2032363	translocase of outer mitochondrial membrane 40 homolog (yeast)-like	-1,212
TSSK6	A_55_P2107232	testis-specific serine kinase 6	-1,140
TTPA	A_66_P128446	tocopherol (alpha) transfer protein	-1,069
TTPAL	A_55_P2054435	tocopherol (alpha) transfer protein-like	-1,237
UTP6	A_52_P33927	UTP6, small subunit (SSU) processome component, homolog (yeast)	-1,412
WDR66	A_55_P2082096	WD repeat domain 66	-1,422
WSCD2	A_55_P2086455	WSC domain containing 2	-1,275

GENES UPREGULATED IN THE HEART BUT NOT IN OTHER STRUCTURES			
ATP2B2*	A_51_P256384	ATPase, Ca++ transporting, plasma membrane 2	1,524
CYP26B1**	A_51_P501844	cytochrome P450, family 26, subfamily B, polypeptide 1	1,406
ROBO3*	A_55_P2144886	roundabout, axon guidance receptor, homolog 3 (Drosophila)	1,557

AGRADECIMIENTOS

Не имей сто рублей, а имей сто друзей.

Русская пословица

Cuando te acercas al final de la tesis (y si, además, estás acabando un *paper* a la vez), el único deseo, entre las correcciones, los últimos experimentos, las becas, la búsqueda de postdoc…, es acabar todo lo antes posible. Y a uno se le olvida que junto con la tesis también termina el placer de compartir tu día a día en el laboratorio (y fuera de él) con gente que has conocido a lo largo de todo este tiempo y que realmente ha hecho posible que sea más llevadera, más divertida e incluso más productiva. Hay muchas personas que, bien con sus sabios consejos científicos o bien con su no menos valioso apoyo afectivo, hicieron que días negros de laboratorio parecieran menos oscuros y que días con más suerte mejoraran aún más. Yo me siento muy afortunada del lugar donde he podido desarrollar esta tesis, no sólo por su excelentes instalaciones y medios, sino porque me ha dado la oportunidad de conocer a personas únicas, de las que aprendí muchísimo –tanto científica como personalmente–, y de encontrarme en un ambiente cómodo y amistoso. Y sé que cuando me vaya voy a echar de menos muchas cosas; sólo espero que pueda conservar, independientemente de dónde esté en un bastante incierto futuro, algunas de las relaciones tan especiales que se han forjado aquí.

A lo largo de los siete años que he estado en el CNIC, he tenido la oportunidad de contar con la ayuda y el apoyo de muchos profesionales que lograron obtener lo mejor de mis experimentos. Muchas gracias a Ana Belén, que cuidó con tanto amor a mis ratones y que con su trabajo y dedicación evitó problemas mayores debidos a mis despistes. Gracias a Antonio y a Elvira, por la constante ayuda con los diferentes microscopios y por los consejos de análisis de imagen. Gracias también al equipo de Genómica y a Fátima, por los tres microarrays que se han hecho y analizado a lo largo de esta tesis, y en especial a Sergio, por la ayuda con las qPCRs. Gracias a Giovanna, por haberme enseñado a hacer MEFs y por habernos generado el mutante condicional. También gracias a Roisin, para la cual no existe misterio de histología que no pueda resolver.

Quería darle las gracias a Miguel Torres por haberme brindado la oportunidad de llevar a cabo mi tesis en el departamento de Desarrollo Cardiovascular, por todo su apoyo y por sus acertados consejos sobre el proyecto. También por haber aceptado ser mi tutor y por haber encontrado tiempo para escribirme unas cartas de recomendación que ya están siendo muy útiles. Igualmente, quería agradecerle a José Luis de la Pompa su ayuda y lo mucho que aprendí en los seminarios de su grupo.

Muchas gracias también a Jorge, mi gran maestro de marcajes y cultivos: tu contribución ha sido clave para esta tesis. Y, de paso, pude disfrutar de una divertida y enriquecedora estancia en Jaén.

Capítulo aparte merecen los agradecimientos a Juanjo, mi director de tesis. Hemos empezado una tesis complicada y la hemos llevado a buen puerto. Gracias por aguantar mi carácter a veces difícil y por ser paciente conmigo. Por darme buenos y sabios consejos científicos, teóricos y prácticos. Porque, si aprendí a ser rigurosa con los experimentos, fue gracias a ti y a que tú eras mi director. Por preocuparte por mi futuro y escribirme unas cartas de recomendación que me imagino que son exageradas. Por haber sido un jefe cercano y asequible.

Me llevo un recuerdo muy especial de mis primeros compañeros de laboratorio. Por supuesto, de mi pequeño maestro Jesús, gracias al cual aprendí no sólo a hacer sondas, sino también quién era Obi Wan Kenobi. En el laboratorio se echa de menos tu optimismo y sentido del humor. De Catiana, que siempre estaba dispuesta a resolverme cualquier duda de laboratorio (incluso 10 minutos antes de la defensa de su tesis…) y que ha sido una de las pocas personas con quien pude compartir aquí los placeres de la música barroca. ¿Y qué decir de las visitas que te hicimos Marina y yo a Malmö? De Alberto, tan sabio como trabajador, con una pasión abrumadora por la ciencia, y cuyos acertados consejos resolvieron dudas y problemas científicos existenciales tantas veces; gracias por poder compartir contigo mi lado más *freaky*, que tú, mejor que nadie, sabes que tengo. De Clara, por habernos regalado los *claraminutos* y una personalidad única e inolvidable.

También quería darle las gracias a Silvia por nuestras interesantes discusiones, tanto sobre temas científicos como sobre mi futuro profesional. A Laura Carramolino, por darme sabios consejos y compartir su amplia experiencia de laboratorio. A Ángel Ciprés, por ayudarme a arrancar la máquina de cultivos en el CNIC y por los buenos consejos sobre el postdoc. A Teresa Casaseca, por mantener el departamento en funcionamiento y a Beatriz Ferreiro, por los múltiples papeleos que ha tenido que hacer por mí.

No tengo más que palabras de agradecimiento para los chicos de José Luis, los *pomperos*. No sólo habéis compartido conmigo reactivos, conocimientos y trucos, sino que me habéis acogido en vuestro grupo, excepcionalmente generoso y unido, donde me sentí cómoda y donde aprendí tantas cosas. Gracias a Bea, una excelente y encantadora persona, que con tanta paciencia y arte me enseñó a hacer Western, IPs, transfecciones… A Julie, porque siempre se acordaba de mí a la hora de las comidas, por contarme cosas sobre zebrafish y porque no se puede ser mejor persona. A Gaetano, por robarme las cosas con tanta elegancia napolitana, pero también por ser un compañero único que alegra como nadie la vida en el laboratorio. A Marcos, porque intenta pasar por gamberro (igual siguiendo a algún compañero poco ejemplar), pero no puede disimular su cara de bueno. A Paola, por traer frescura y buen humor al labo. A Belén, que sabe de todo y siempre está dispuesta a echarle una mano a cualquiera. A Vane, por su simpatía y por ser la única que me devuelve mis gradillas. A Lao, compañero tenaz en difíciles momentos de explantes y que tanto se ha preocupado por mi *paper*. A Patri, que siempre tiene una sonrisa en la boca y palabras de ánimo para mí. A Guille, por ser tan Guille, pero también por los programas de Adobe, por mirar las válvulas de mis ratones y por lo bien que nos lo pasamos en Taos, NM. Thanks also to Dimitris, who looks so serious but in fact is the nicest guy you can imagine. A Tania, por ser tan simpática y sencilla. A Mauro, por ser tan majo y por ese tiramisú que sólo él sabe hacer.

Gracias también a las *manzanitas*. A Teresa, por ser una persona tan positiva y gran compañera de trabajo, y porque aprendí mucho de tu actitud frente a la tesis y la ciencia. A Melisa, porque siempre es una alegría verte y charlar contigo, porque no te enfadas cuando trato de parodiar el acento *choni* mejicano (bueno, igual un poco) y por el magnífico congreso en Cancún, que fue aún mejor porque estabas tú (y así es como los agradecimientos se convirtieron en una telenovela

mejicana ;P).

Gracias a Paloma, por ser una compañera tan dedicada y entusiasta, además de una persona excepcional; espero que el tiempo que hemos pasado trabajando juntas te haya resultado útil.

No puedo no acordarme de las chicas de enfrente, Esther y Dorota. Compartimos risas, salidas al cine, zapatilla en el *Melos* y bailes en el *retreat*. Tremendas compañeras de laboratorio y mejores personas y amigas. Esther, discreta y siempre atenta y dispuesta a ayudar. Dori, now I believe that not all Polish people hate Russians. In fact, they can get to be good friends ☺. No puedo olvidarme de lady Sandra, no tanto por su increíble eficiencia en el trabajo como por ese toque *British* de elegancia, seriedad e ironía que le da a todo; soy tu fan ☺. Y, por supuesto, Ghislaine, such a cheerful and nice person. I enjoyed so much sharing my time with you in the lab and our *Escapadas del CNIC/CNIO*. A Carlota la conocí no hace mucho, pero ya me ha conquistado con su simpatía. Muchas gracias por todo, chicas.

Y, claro, a Marina. Creo que esperas muchas páginas de agradecimiento, pero eso sale muy caro y mejor lo invertimos en una comida. Organizadora incansable de salidas, cenas y escapadas, lograste sacar mi lado más sociable y apartarme de la soledad a la que suelo tender. Y, aunque yo me resistía a veces, ahora sé que lo necesitaba y que me hizo mucho más feliz. Gracias por tu buen carácter, tu sentido del humor, tu gran ayuda en tantas cosas (como, por ejemplo, la maquetación de la primera versión de esta tesis hasta altas horas de la madrugada) y tu gran personalidad. Por nuestros viajes a Malmö, nuestras escapadas con María y Ghislaine, nuestras cenas improvisadas después del labo… Gracias por todo, AMIGA.

Y, por supuesto, a Claudio. Te voy a definir como Cervantes definió a Lope de Vega: *monstruo de naturaleza*, por la gran cantidad y calidad de sus obras. Las tuyas, compañero, se pueden admirar a lo largo de esta tesis. Pero eres más que un profesional increíble y un profesor que me ha enseñado tantísimas cosas. Eres un gran amigo. Saber que puedo contar contigo, pedirte tu sabio consejo o, simplemente, compartir penas y alegrías, no tiene precio. Muchas gracias, Clau.

Спасибо родителям и сестре Лёльке, пухлой щеке. Очень надеюсь, что не срывала на вас слишком часто усталость и раздражение от работы. Хорошо знать, что вы есть и, что на вас можно положиться. Что у нас дома так много свободы и терпимости. ☺

Gracias a Andrés, por su esfuerzo en que mi lado más humanista no perezca bajo el peso de la actividad científica, por su habilidad para distraerme de los problemas y por lo feliz que me hace.